Coupled-cluster Theory of Parity Nonconservation in Atoms

A thesis
Submitted for the degree of
Doctor of Philosophy

To
The Department of Physics
Mangalore University

By
Bijaya Kumar Sahoo

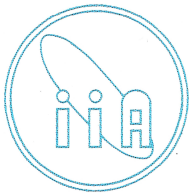

Indian Institute of Astrophysics
Non-accelerator Particle Physics Group
Bangalore - 560 034, India

September 2005

Declaration

I hearby declare that this thesis is the result of the investigations carried out by me at the Indian Institute of Astrophysics, Bangalore under the guidance and supervision of Prof. Bhanu Pratap Das. This thesis has not been submitted for the award of any degree, diploma, associateship, fellowship, etc. of any university or other institutes.

In keeping with the general practice of reporting scientific observations, due acknowledgment has been made whenever the work described is based on the findings of other investigators. Any omission which might have occurred by oversight or error in judgment is regretted.

Bangalore
September, 2005

Bijaya Kumar Sahoo
(Candidate)

Certificate

This is to certify that the thesis entitled 'Coupled-cluster Theory of Parity Non-conservation in Atoms' submitted to the Mangalore University by Mr Bijaya Kumar Sahoo for the award of the degree of Doctor of Philosophy in the faculty of science, is based on the results of the investigations carried out by him under my supervision and guidance, at the Indian Institute of Astrophysics. This thesis has not been submitted for the award of any degree, diploma, associateship, fellowship, etc., of any university or institute.

Bangalore
September, 2005

Prof. Bhanu Pratap Das
(Supervisor)

To my

Teachers
&
Parents

Acknowledgments

I consider it a privilege to express my sincere and deep gratitude to Prof. Bhanu Pratap Das, my supervisor, for his innovative ideas that are behind this thesis and for his constant support in carrying out this work. I have been very fortunate to have such an honest person and good teacher, who has taken care of me as a parent would and encouraged me and strengthened my morale at each stage enabling to pursue my work steadily. His valuable suggestions have made it possible for me to achieve the goal of carrying out a beautiful piece of research and to manage to finish this thesis in the alloted time.

My heartfelt thanks to Dr. Rajat Chaudhuri, for his initial help on many theoretical concepts in many-body physics, especially the coupled-cluster methods and providing input for handling complex codes in a systematic way.

I express my sincere gratitude to Prof. Debasish Mukherjee, Director of I.A.C.S., Kolkata, India, for his many valuable suggestions for this work. His constant support has helped me to carry out my research.

I express sincere thanks to all of my M.Sc. teachers from the Department of Physics, Utkal University, Bhubaneswar, India, for motivating me to pursue research after my M.Sc. My words may not be sufficient to acknowledge the help of both Prof. N. Barik and Prof. L. P. Singh during my Ph.D. period. Prof. N. Barik has stood as a pillar for me and his valuable suggestions have motivated me to concentrate on research. Prof. L. P. Singh has encouraged and advised me when it was necessary.

I am very grateful to my parents for their constant support for my studies and their wishes for my well being. Although they do not understand exactly what I do, they are ever happier than me with my research work. Their blessings and deepest love for me and that of my brother and sisters have enabled me to achieve such a goal and to become a better human being. My thanks are insufficient to repay for what they have given me.

It was my pleasure to meet a gentle person like Prof. Günther Werth, Retired Professor, Mainz University, Germany, who is one of the people I respect most in the world. His suggestions and the many discussions I have had with him about my research work have helped me to understand many parts of experimental physics. I would also like to thank Prof. K. -J. Kluge, Head of Atomphysik, GSI, Darmstadt, Germany for providing me with the required research facilities and financial support for travel related to my research work during my stay at GSI.

It was my pleasure to work with Dr. Thomas Beier at GSI. His regard for my well being and innovative concepts related to my research work have been a kind of internal strength for me in carrying out successful research work at GSI.

I would like to thank all of my friends from IIA and my friends: Raghunath Sahoo, Hara Prasanna Lenka, Sandesh Gupta, Suvrant Tripathy, Dillip Ku. Satapathy, Bibhuti Sahu, Satya Ranjan Sahu, Salila Pradhan, M. Kathiravan, Shanmugha Sundaram and Reji M. C. Thomas, whose friendship and constant encouragement have been conclusive to living in a good atmosphere and to carrying out my Ph.D. work. A special relationship with Mr. Ebenezer at IIA was very helpful. Many supportive friends including Vijay, Rana, Ankur, Baliga, Thiri, Nataraj, Vigeesh and Blesson in IIA, made it a challenge for me to carry out my work at a constant pace! I also met some of my well wishers like Vidya, Sneha, Shyama and Maya during their short project at IIA and their encouragement for my research has been invaluable. I would also like to thank V. N. Pandey and Srikantha from RRI, Bangalore, India for their encouragement. I am lucky to have friends like Hembram, Bibhuti, Subhasis and Martha at IISc, Bangalore, who have helped me on many occasions which I will not forget. I would like to thank M. Block, Manas, Emma, Punita, Sophqat, Shyamal, Robert and Goran for their friendship and for creating a pleasant environment to work at GSI. I also thank my DAAD friends Hemanti Nandan, Soumitra, Gufran Khan, Mohammad Alam, Myint, Rehana, Anchalee, Camron and my German teacher Karin for their close friendship. I was lucky to meet Jai bhai from Marburg, Germany, who treated me as a younger brother and cared for me during my stay in Marburg for a German language course.

I have made a special relationship with my seniors Dr. Sonjoy Majumder and Dr. Chiranjib Sur and their families during my Ph.D. work and I thank for their well wishes. I have also got supportive suggestions from one of my seniors Dr. Holger Merlitz. I have also had invaluable moments, support and many discussions with the other group members, my thanks to them.

It is my desire to express my sincere thanks to the authorities of C-DAC, Bangalore for providing me with computational facilities. Without their help it would have been impossible for me to carry out most of my thesis work. I thank Dr. Sunderajan, C-DAC, Pune, for helping me to adapt some of my codes to run in parallel and his encouragement.

I want to thank the IIA authorities for providing me with space in their research facilities and for most of my scholarship during my stay at IIA. I would like to thank DAAD for providing me with a scholarship for a definite period and also for broadening my research career.

Abstract

The primary objective of this thesis is to conduct theoretical studies of parity non-conservation (PNC) in atomic systems in order to pave the way for testing the Standard Model (SM) of the elementary particle physics.

Our present understanding of elementary particle physics is encapsulated in the SM. Despite the remarkable success of this model, it is widely believed as being not the ultimate theory of the matter. PNC in atomic systems which arises primarily from the neutral weak interaction between the electrons and the nucleus has the potential to probe new physics beyond the SM. By combing the results of high precision measurements and many-body calculations of atomic PNC observables, it is possible to extract the nuclear weak charge (Q_W) and compare with the corresponding value in the SM. A discrepancy between these two values could reveal the possible existence of new physics beyond the SM. The most accurate data on atomic PNC currently comes from the $6s\ ^2S_{1/2} \rightarrow 7s\ ^2S_{1/2}$ transition in cesium (Cs), where the claimed experimental and theoretical accuracies are 0.35% [C. S. Wood *et al.*, Science **275**, 1759 (1997)] and 0.5% [V. A. Dzuba *et al.*, Phys. Rev. D **66**, 076013 (2002)], respectively, and the deviation from the SM is about 1σ. It would indeed be desirable to consider other candidates which could yield accurate values of Q_W. Fortson has proposed an experiment to measure PNC in $6s\ ^2S_{1/2} \rightarrow 5d\ ^2D_{3/2}$ transition of singly ionized barium ($^{137}Ba^+$) [Phys. Rev. Lett. **70**, 2383 (1993)] using the techniques of laser cooling and ion trapping. The observable measured in this experiment is a PNC induced light shift which depends on the electric dipole transition amplitude caused by the parity non-conserving neutral weak interaction ($E1_{PNC}$) and the electric quadrupole (E2) transition amplitude for the $6s\ ^2S_{1/2} \rightarrow 5d\ ^2D_{3/2}$ transition. One can determine the value of Q_W by combining the measured light shift and the values of the $E1_{PNC}$ and E2 amplitudes. From a theoretical point of view, an accurate calculation of $E1_{PNC}$ is of special importance. The RCC theory which is an all order theory and based on an exponential ansatz is known to produce high quality results for atomic and molecular properties. It has been successfully applied to a wide range of problems; prominent among

them are high precision calculations of transition probabilities and hyperfine interaction constants.

In this thesis we have applied the RCC theory to calculate $E1_{PNC}$ for the $6s\ ^2S_{1/2} \rightarrow 5d\ ^2D_{3/2}$ transition in Ba^+. It is the first application of this theory to the atomic PNC. Blundell [Phys. Rev. Lett. **65**, 1411 (1990)] had used this theory in the linear approximation to calculate $E1_{PNC}$ amplitude for the $6s\ ^2S_{1/2} \rightarrow\ 7s^2S_{1/2}$ transition in Cs by sum-over-states approach. Dzuba *et al.* [Phys. Rev. A **63**, 062101 (2001)] and Geetha [K. P. Geetha, Ph.D. Thesis, Bangalore University, India (2002)] have calculated this PNC amplitude for the $6s\ ^2S_{1/2} \rightarrow 5d\ ^2D_{3/2}$ transition in Ba^+. The former calculation is based on a variant of all order many-body perturbation theory and is carried out using a mixed parity approach as well as a sum-over-states approach, while the latter is based on a RCC sum-over-states approach. Our calculation of Ba^+ PNC is more rigorous than these two calculations and has an accuracy of less than 1%. If the accuracy of this result can be matched by that of experiment then PNC in Ba^+ can provide an independent atomic probe of physics beyond the SM.

We have also carried out preliminary studies of the $E1_{PNC}$ amplitude for the $6s\ ^2S_{1/2} \rightarrow 7s\ ^2S_{1/2}$ transition in Cs using the same RCC theory that had been applied to Ba^+ PNC. The results we obtained suggest that a sub one percent calculation for Cs PNC should be possible.

The ratios of the atomic electric dipole moment (D_a) to the scalar-pseudoscalar (S-PS) coupling constant (C_S) for cesium and thallium (Tl) have been calculated using RCC theory with accuracies of 0.5% and 3.3%, respectively. Electron correlation effects are found to be important, especially, for Tl. By combining our calculated result for Tl with the measured value of the electric dipole moment of that atom gives the most accurate limit of the scalar-pseudoscalar coupling constant to date.

Contents

Chapter 1

Introduction

1.1 Fundamental Particles and Symmetries

According to our present state of knowledge quarks and leptons are the fundamental constituents of matter [1, 2]. These particles interact through four forces: strong, electromagnetic, weak and gravitation forces [1, 2]. The properties of these particles are studied primarily by high energy accelerators, although some non-accelerator experiments are in progress in different laboratories in the world. A large body of experimentally verified properties of quarks and leptons and the forces between them forms the basis of the Standard Model (SM) of particle physics. This model was developed with the help of gauge theory [2].

Symmetries play a crucial role in physics [3, 4]. It was thought for a long time that *physical laws are invariant under symmetry transformations.* The notion of gauge symmetry based on group theory is at the heart of modern particle physics. Here, distinct elements are related to each other by means of symmetry transformations and form a regular unity. Through these symmetry properties, Glashow, Weinberg and Salam independently showed that three of the fundamental forces: strong, electromagnetic and weak are invariant under $SU(3) \times SU(2) \times U(1)$ transformation [5]. The SM is based on this symmetry, but it is unable to explain some basic issues concerning

the elementary particles and their interactions. These are discussed later in this chapter.

1.2 Symmetry Transformations

Symmetry transformation in physical systems has important implications [6, 7]. As it was stated by a German mathematician Emmy Nöther in her famous theorem known as 'Noether's theorem' [8, 9] that: *every symmetry leads to a conservation of physical quantity.* In other words, if a transformation caused by an operator is invariant then the eigenvalue which corresponds to a physical property associated with the operator remains constant. For example, it can be shown that spatial symmetry results in the conservation of linear momentum, rotational symmetry gives conservation of angular momentum etc. [3].

The symmetry transformation for any physical system can be classified as continuous or discrete. If the symmetry transformation is carried out by a unitary function then the expectation value of the operator remains unaltered. In the continuous transformation these unitary operators can be expressed as the exponential function of a hermitian operator, but this is not true in the case of a discrete transformation. Generally, there are three different types of discrete transformation: parity (P), time-reversal (T) and charge conjugation (C). Studies of these discrete transformations have interesting consequences [1].

1.3 Parity: a discrete symmetry transformation

The parity operation on a co-ordinate system changes a right-handed (RH) system into a left-handed (LH) system, i.e. reflection against the origin of the coordinates of the system. The position vector under this transformation changes as

$$\vec{\mathbf{r}} \xrightarrow{\Pi} -\vec{\mathbf{r}} \tag{1.1}$$

where Π is defined as parity operator.

The state vector under the operation of Π gives

$$\Pi|\Psi(r)\rangle = |\Psi(-r)\rangle. \tag{1.2}$$

Operating two times this operator on $|\Psi(r)\rangle$ brings back the state to itself, i.e.

$$\begin{aligned} \Pi\Pi|\Psi(r)\rangle &= \Pi|\Psi(-r)\rangle \\ &= |\Psi(r)\rangle \end{aligned} \tag{1.3}$$

which implies $\Pi^2 = \mathbf{I}$. Therefore, the eigenvalues of this operator can only be + 1 or -1. i.e.

$$\begin{aligned} \Pi|\Psi(r)\rangle &= |\Psi(-r)\rangle \\ &= \pm|\Psi(r)\rangle \end{aligned} \tag{1.4}$$

The wavefunction with positive sign is known as even parity state and the one with a sign negative is odd parity state.

Π is a Hermitian operator since it has real eigenvalues. Therefore, $\Pi = \Pi^\dagger$. Also $\Pi^2 = I$ implies $\Pi = \Pi^{-1}$. Therefore, $\Pi^\dagger = \Pi^{-1}$, i.e. Π is an unitary operator. Hence the transformation of an operator under the action of parity is given by

$$O \rightarrow \Pi O \Pi^{-1} \tag{1.5}$$

The invariance of a system under parity means

$$\Pi H \Pi^{-1} = H$$

i.e.

$$[H, \Pi] = 0 \tag{1.6}$$

Otherwise parity is not conserved in the system.

Since the electromagnetic force is the dominant force in nature and it conserves parity, in reality one assumes that this would be universally conserved. The Hamiltonian corresponding to weak interactions between elementary particles is not invariant under parity. Therefore, due to weak interactions in atomic systems one encounters parity non-conservation (PNC).

1.4 Premises of SM

In the SM, matter is said to be consist only of *quarks* and *leptons*. And there four fundamental forces act on these particles are *strong, electromagnetic, weak* and gravity. Each quark and lepton has its corresponding anti-quark and anti-lepton, respectively, with same mass, but opposite charge. Quarks and anti-quarks do not exist freely, but bound together and possess fractional charges [2, 3].

The SM of particle physics is based on the following premises:
(i) Matter is made up of six quarks and six leptons.
(ii) Quantum theories exist for strong, electromagnetic and weak interactions.
(iii) Electromagnetic and weak interactions are unified.

1.5 Limitations of SM

It is well known in elementary particle physics that SM provides many experimental verifications in the microscopic world of the elementary particles which are the basic building blocks of matter. But there is a general belief that the SM is an intermediate step in the unification of all the interactions in the nature. One of the most obvious limitations of this model is that a new particle known as Higgs boson has not yet been found. It does not satisfactorily explain some of the questions regarding why there are only three generations of fermions and what is the origin of CP violation. The other models explain the possibility of extra Z-boson, lepto-quarks, composite fermions etc [10, 11]. The theories like Grand Unification Theory (GUTs) [12], Super Symmetry (SUSY) [13] with strong underlying logic put forth different models for the elementary particles. Therefore, some new type of physics almost certainly exists beyond the SM.

The study of physics beyond the SM is carried out by accelerator as well as non-accelerator techniques.

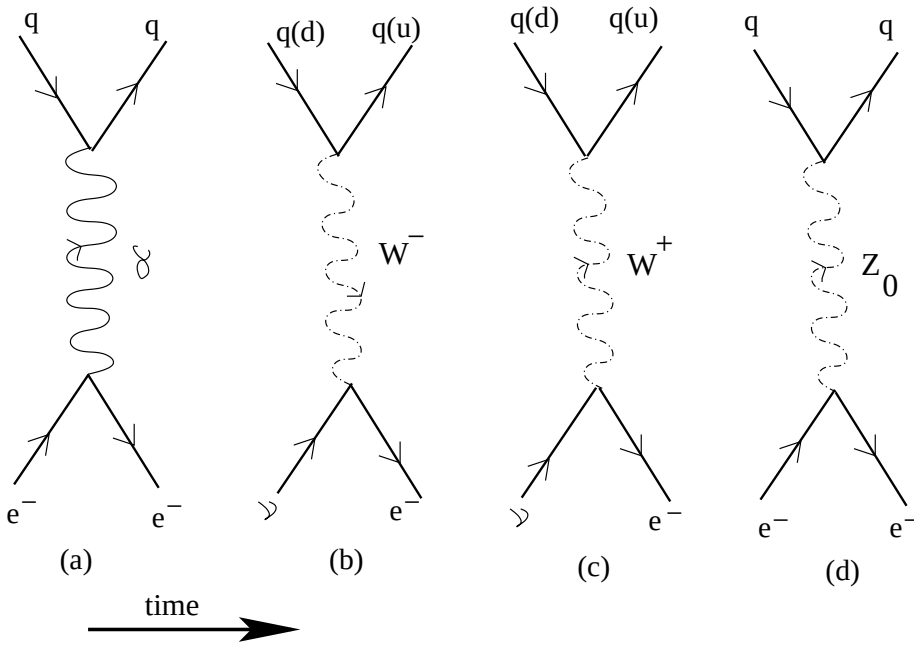

Figure 1.1: Diagrammatic representation of electro-weak interactions.

1.6 Origin of parity violation

As mentioned earlier there is parity non-conservation at the level of the fundamental particles due to weak interactions. Matter is made up of quarks and leptons. Interaction between quarks and leptons are due to the electromagnetic and weak interactions. The electromagnetic interaction is mediated by photons and is the pre-dominant interaction among these particles. The weak interaction is a tiny effect and occurs due to the exchange of heavy W^+, W^- and Z_0 intermediate particles. Since both W^+ and W^- are charged particles, the current associated with the weak interaction due to them also posses charge and there is a change in charge among the interacting particles. These interactions are represented diagrammatically using Feynman diagrams as shown by figure 1.1.

In atoms or molecules, there are electrons (leptons) and nucleons (con-

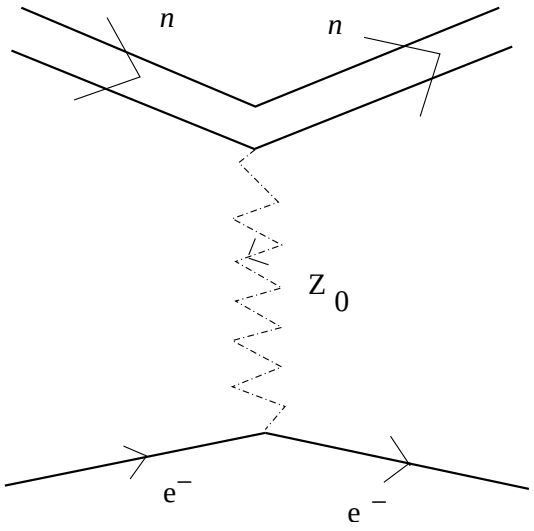

Figure 1.2: Diagrammatic representation of electro-weak interactions between nucleons and electrons inside an atomic system.

sisting of quarks) and they can interact via the weak interaction. The electromagnetic interactions due to photons are dominant and they conserve parity. The wavefunctions resulting from the electromagnetic interactions in an atom is represented by particular angular momentum and parity. However, the weak interaction mediated by the neutral boson Z_0 between the nucleus and the electrons can also arise in an atom. This is shown diagrammatically in figure 1.2. This interaction can cause mixing between opposite parity states. Since the magnitude of this effect is comparatively small, it can be treated perturbatively. Observing the experimental consequences of this effect is very challenging. After many years of intense effort, it has been observed by several groups [14, 15, 16, 17].

There is also an important electromagnetic moment which causes parity violation in atomic systems called the nuclear "*anapole moment*" (NAM). This arises due to the electromagnetic multipole moment expansions inside the nucleus. It is time-reversal invariant but odd in parity and interacts with the atomic electrons at regions close to the nucleus. Atomic parity non-

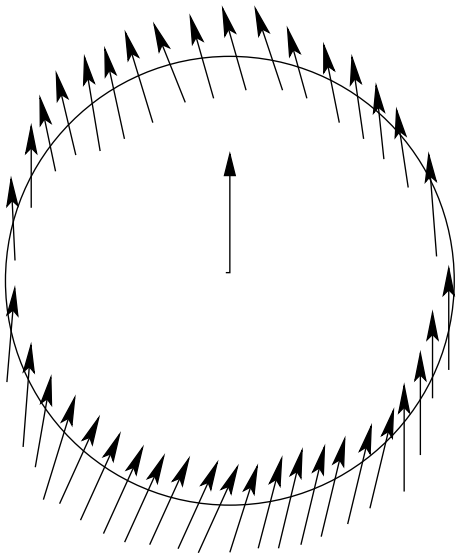

Figure 1.3: Spin helix corresponding to electromagnetic interaction which cause anapole moment due to unpaired nucleon.

conservation experiments are sensitive to both the neutral weak interaction and the nuclear anapole moment. The nuclear anapole moment has its origins in parity non-conserving interactions in the nucleus and is related to the electromagnetic current of unpaired nucleon caused by the spin helix, with a definite chirality, as shown in figure 1.3. This effect is not significant compared to the neutral weak interaction and it has therefore not been calculated in this thesis.

1.7 General principle of atomic PNC experiment

Due to the presence of PNC in an atomic system, states of opposite parity mix with each other. It is, therefore, possible to have finite transition amplitude between two atomic states of the same parity. The size of this transition

amplitude is typically of the order of 1 part 10^{11} in atomic unit [18]. The corresponding transition probability clearly cannot be measured. However, one can measure the interference of the parity non-conserving electric dipole ($E1_{PNC}$) transition amplitude with other electromagnetic transition amplitudes (E2, M1 etc.). For example, the Cs PNC experiment involves the interference of the $E1_{PNC}$ transition amplitude and E1 transition amplitude induced by a static external electric field [17] and in the Tl PNC experiment, the observable arises from the interference of the parity non-conserving E1 and M1 transition amplitudes [14, 19].

1.8 Parity non-conserving Atomic Hamiltonian from V-A current

Parity non-conserving interaction arises from combinations of vector and axial vector currents. In an atom such interactions can exist because of vector/axial vector currents associated with electron and nucleons and their total Hamiltonian can be written as

$$\begin{aligned} H_{PNC} &= \sum_N \frac{G_F}{2\sqrt{2}}[J^N_{\mu V} J^{\mu e}_A + J^N_{\mu A} J^{\mu e}_V] \\ &= H^{NSI}_{PNC} + H^{NSD}_{PNC} \end{aligned} \tag{1.7}$$

which has been further defined as nuclear spin independent PNC Hamiltonian (H^{NSI}_{PNC}) and nuclear spin dependent PNC Hamiltonian (H^{NSD}_{PNC}) due to the fact that the axial-vector currents of the nucleons depend explicitly on the total spin of the nucleus. The superscript 'N' and 'e' represent the nucleus and electron, respectively. Since H^{NSD}_{PNC} depends on the nuclear spin, the net interaction nullifies for even nuclei whereas in the case of an unpaired nucleon it contributes to the total interaction. Hence the effect due to this term is very small and has been neglected in our studies. The other term, H^{NSI}_{PNC}, which is the dominant source of atomic PNC is enhanced by total number of nucleons present in the system. It scales as Z^3, where Z is the number of protons [20]. Since this is a short range interaction, its magnitude depends on the density of the electronic wavefunctions in the nuclear region. With

the above discussions one can easily express possible form of the H_{PNC}^{NSI} as

$$H_{PNC}^{NSI} = \frac{G_F}{2\sqrt{2}} \int d^3r_e \int d^3r_N \sum_{i=p,n} 2[C_{1i}\bar{\psi}_N\gamma_\mu\psi_N \cdot \bar{\psi}_e\gamma_\mu\gamma_5\psi_e]\delta(r_i - r_e) \quad (1.8)$$

where C_{1i} are the electron-nucleon neutral weak coupling constants.

Since $\bar{\psi} = \psi^\dagger\gamma_0$, we get

$$H_{PNC}^{NSI} = \frac{G_F}{2\sqrt{2}} \int d^3r_e \int d^3r_N \sum_{i=p,n} 2[C_{1i}\psi_N^\dagger\gamma_0\gamma_\mu\psi_N \cdot \psi_e^\dagger\gamma_0\gamma_\mu\gamma_5\psi_e]\delta(r_i - r_e). \quad (1.9)$$

Neglecting the off-diagonal terms from the above summation whose contributions would be very small, we get

$$H_{PNC}^{NSI} = \frac{G_F}{2\sqrt{2}} \int d^3r_e\psi_e^\dagger\gamma_5\psi_e \int d^3r_N \sum_{i=p,n} 2C_{1i}\psi_i^\dagger\psi_i]\delta(r_i - r_e). \quad (1.10)$$

The summation over the nuclear wavefunctions yields the number densities of the protons and neutrons, which, in simple nuclear models are proportional to the nuclear density and is given by

$$\begin{aligned} \sum_p \psi_p^\dagger\psi_p &= Z\rho_N(r) \\ \sum_n \psi_n^\dagger\psi_n &= N\rho_N(r) \end{aligned} \quad (1.11)$$

where Z and N denote the number of protons and neutrons, respectively, and $\rho_N(r)$ is the nucleon number density normalized to

$$\int dr\ \rho_N 4\pi r^2 = 1. \quad (1.12)$$

In terms of individual terms, it yields

$$\begin{aligned} H_{PNC}^{NSI} = \frac{G_F}{2\sqrt{2}} \int d^3r_e\psi_e^\dagger\gamma_5\psi_e \int d^3r_N 2[C_{1p}\psi_p^\dagger\psi_p]\delta(r_p - r_e) \\ +C_{1n}\psi_n^\dagger\psi_n]\delta(r_n - r_e)] \end{aligned} \quad (1.13)$$

which over the nuclear region gives

$$\begin{aligned} H_{PNC}^{NSI} &= \frac{G_F}{2\sqrt{2}} \int d^3r_e \psi_e^\dagger \gamma_5 \psi_e 2[C_{1p}Z + C_{1n}N]\rho_N(r) \\ &= \frac{G_F}{2\sqrt{2}} Q_W \gamma_5 \rho_N(r) \end{aligned} \tag{1.14}$$

where we define $Q_W = 2[C_{1p}Z + C_{1n}N]$ and is known as nuclear weak charge.

Following similar procedure the operator form for H_{PNC}^{NSD} can also be defined as given below by considering the vector and axial vector currents from the electronic and nuclear parts, respectively.

Now we write

$$H_{PNC}^{NSD} = \frac{G_F}{2\sqrt{2}} \int d^3r_e \int d^3r_N \sum_{i=p,n} 2[C_{1i}\bar{\psi}_N \gamma_\mu \gamma_5 \psi_N \cdot \bar{\psi}_e \gamma_\mu \psi_e]\delta(r_i - r_e). \tag{1.15}$$

which leads to

$$\begin{aligned} H_{PNC}^{NSD} = \frac{G_F}{2\sqrt{2}} \int d^3r_e \int d^3r_N \sum_{i=p,n} 2C_{2i}[&\bar{\psi}_i \gamma_0 \gamma_5 \psi_i \cdot \bar{\psi}_e \gamma_0 \psi_e \\ &+ \sum_{r=1,2,3} \bar{\psi}_i \gamma_0 \gamma_5 \psi_i \cdot \bar{\psi}_e \gamma_r \psi_e] \;\; \delta(r_i - r_e). \end{aligned} \tag{1.16}$$

Substituting the value of $\bar{\psi}$, it leads to

$$\begin{aligned} H_{PNC}^{NSD} = \frac{G_F}{2\sqrt{2}} \int d^3r_e \int d^3r_N \sum_{i=p,n} 2C_{2i}[&\psi_i^\dagger \gamma_5 \psi_i \cdot \psi_e^\dagger \psi_e \\ &+ \psi_i^\dagger \alpha_r \gamma_5 \psi_i \cdot \psi_e^\dagger \alpha_r \psi_e] \;\; \delta(r_i - r_e). \end{aligned} \tag{1.17}$$

Since γ_5 is of the order of (v/c) and can be neglected from the above equation and then we get

$$H_{PNC}^{NSD} = \frac{G_F}{2\sqrt{2}} \int d^3r_e \int d^3r_N \sum_{i=p,n} 2C_{2i} \psi_i^\dagger \sigma \psi_i \cdot \psi_e^\dagger \alpha_r \psi_e \delta(r_i - r_e) \tag{1.18}$$

where the relation $\alpha_r \gamma_5 = \sigma$ has been substituted. Integration over the nuclear wavefunctions produce a quantity proportional to the spin of the

nucleus $\vec{\mathbf{I}}$ and the nuclear density $\rho_N(r)$. A constant of proportionality is defined such that

$$\sum_{i=p,n} 2C_{2i}\sigma_i\delta(r_i - r_e) = R_W\rho_N(r) = \frac{R_W}{I}\rho_N(r) \tag{1.19}$$

where R_W is called the weak magnetic moment of the nucleus, just as it is defined for Q_W. Therefore, the operator form of the nuclear spin dependent component of the parity violating interaction Hamiltonian for the atomic system yields the form

$$H_{PNC}^{NSD} = \frac{G_F}{2\sqrt{2}I}R_W\alpha_e \cdot \vec{\mathbf{I}}\rho_N(r) \tag{1.20}$$

which clearly shows the dependency of nuclear spin $\mathbf{I}$. This term has been neglected in the present study.

1.9 Nuclear anapole moment

The notion of the nuclear anapole moment was introduced by Zel'dovich [21]. A particle may have a parity violating electromagnetic form factor along with the usual electromagnetic form factors. Multipole moments arising from the expansion of the electrostatic and vector potentials as a series in R^{-1}, where R is the distance from the center of the charge or current distribution. Some of them obey discrete transformations under C, P and T while some others violate both P- and T- symmetries. There are also other electromagnetic multipole moments, which are not usually dealt with in multipole moment expansions as they give rise to contact potentials instead of long-range potentials. The anapole moment is one such example. It obeys time-reversal invariance but violates parity conservation and charge conjugation. This arises from the vector potential of the current distribution $\vec{\mathbf{j}}(r)$ inside the nucleus. The magnetic field corresponding to this vector potential can be expressed as

$$\vec{B}_l = \vec{\nabla} \times \vec{A}_l. \tag{1.21}$$

The electromagnetic interaction energy of an external current distribution with $\vec{A}_l$ is given by

$$W = \frac{1}{c}\int d^3r\vec{\mathbf{j}}'(r) \cdot \vec{A}_l. \tag{1.22}$$

Density of the external current distribution can be expanded as

$$\vec{\mathbf{j}}'(r) = \vec{\mathbf{j}}'(0) + (\vec{r}.\vec{\nabla})\vec{\mathbf{j}}'(0) + \cdots. \tag{1.23}$$

Considering just the first term, i.e. assuming that the extent of the external current distribution is small and that $\vec{\mathbf{j}}'(r)$ is essentially uniform, we get

$$W = -\frac{1}{c}\vec{\mathbf{j}}'(0)\int d^3r\vec{A}_l = -\frac{1}{c}\vec{\mathbf{j}}'(0)\cdot\vec{\mathbf{a}} \tag{1.24}$$

where $\vec{\mathbf{a}} = \int d^3r\vec{A}_l$ is known as the anapole moment of the current distribution. Again, expanding $\vec{A}_l = \int d^3r\frac{\vec{\mathbf{j}}(r)}{|\vec{\mathbf{R}}-\vec{\mathbf{r}}|}$ as a series of R^{-1}, the first term corresponds to the potential of the normal magnetic dipole moment. The second order term gives rise to,

$$\vec{A}^a_l(R) = \frac{1}{2}\int d^3r\vec{\mathbf{j}}(r)r_m r_n\partial_m\partial_n\frac{1}{R}. \tag{1.25}$$

Since $j_i r_m r_n$ is a reducible tensor whose trace is not zero, the vector potential contains two irreducible contributions of T- and P- odd magnetic quadrupole moment and that of the T-even, P- odd anapole moment. The vector potential due to the anapole moment is thus,

$$A^a(r) = \vec{\mathbf{a}}\ \delta(r) \tag{1.26}$$

where $\vec{\mathbf{a}} = -\pi\int d^3r\ r^2\ \vec{\mathbf{j}}(r)$ can be taken as the definition of anapole moment. The $\delta(r)$ is the result of $\partial_m\partial_n(\frac{1}{R}) = -4\pi\delta(r)$ and it is a rank one operator.

1.9.1 Parity non-conserving Hamiltonian from NAM

As it was shown before the expression for the anapole moment contains the current vector $\vec{\mathbf{j}}$, which changes sign under reflection of co-ordinates. Applying Wigner-Eckart theorem, we can say that the anapole moment vector must be directed along the nuclear spin $\mathbf{I}$: $< a >= -a\frac{\mathbf{I}}{I}$ and this does not change sign under coordinate transformation. The different behavior of the relation $< r^2\vec{\mathbf{j}} > \alpha\ \mathbf{I}$ under reflection of coordinates means that the existence of the anapole moment violates parity. General features of the anapole moment have been discussed by Flambaum and Khriplovich [22, 23]. They have

used the shell model and assume a nucleon-nucleon parity non-conserving interaction of the type

$$H^a_{PNC} = \frac{G_F g}{2\sqrt{2}m}[\vec{\sigma}.\vec{\mathbf{p}} + \vec{\mathbf{p}}.\vec{\sigma}]\rho_N(r) \tag{1.27}$$

where $\vec{\sigma}$ and $\vec{\mathbf{p}}$ are the spin and momentum operators of valence nucleon, m is the mass of the proton. The dimensionless constant g characterizes the parity odd interaction of the valence nucleon with the nucleon core. It is estimated that $g_p \approx 4$ for an external proton and $g_n \leq 1$ for a neutron.

Treating H^a_{PNC} as a first-order perturbation, it can be shown that the NAM arises only from the spin part of the current density and it can be expressed as

$$\vec{\mathbf{a}}_N = \frac{G_F}{2\sqrt{2}}\frac{1}{e}\frac{2\chi K_a \vec{\mathbf{I}}}{I(I+1)} \tag{1.28}$$

where $\chi = (I + \frac{1}{2})(-1)^{I+\frac{1}{2}-l}$ and $K_a = \frac{9}{10}(24\alpha^2\mu g A^{2/3})$.

Here l is the orbital angular momentum of the valence electron. The contribution of the core excitations to the NAM has been found to be small [22]. Note that the quantity K_a contains information about g, the parity non-conserving nucleon-meson coupling constant. Indeed, an accurate determination of K_a can lead to accurate values of g.

1.10 Parity non-conserving E1 transition amplitude

The presence of the above types of weak interaction Hamiltonian causes mixing of different parity states of Dirac-Coulomb (DC)/Dirac-Coulomb-Breit (DCB) Hamiltonian of the atomic systems. Therefore, an electric dipole transition between two same parity states is possible. Since the mixing of states is due to the weak interaction, the amplitude corresponding to such a transition is very small.

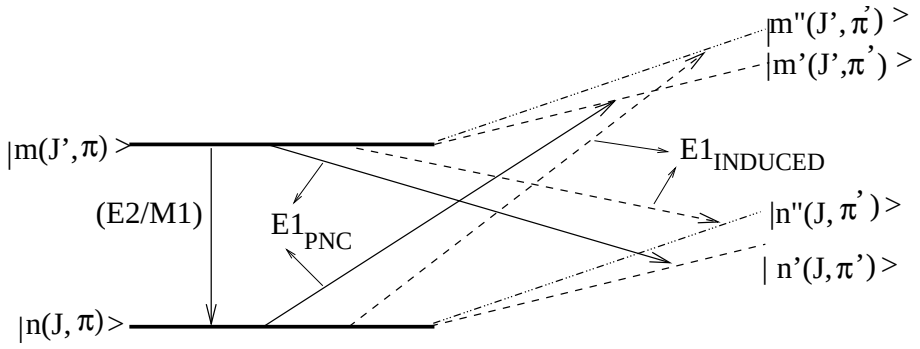

Figure 1.4: Diagrammatic representation of $E1_{PNC}$ transition

In figure 1.4, we have considered two same parity states $|n(J,\pi)\rangle$ and $|m(J',\pi)\rangle$, where π represents the parity eigenvalue. These two states mix with opposite parity states $|n'(J,\pi')\rangle$ and $|m'(J',\pi')\rangle$, respectively, of same angular momentum. Since the $E1_{PNC}$ matrix elements between $|n(J,\pi)\rangle$ and $|m'(J',\pi')\rangle$ or $|m(J',\pi)\rangle$ and $|n'(J,\pi')\rangle$ are very small, one has to measure the interference of $E1_{PNC}$ with other possible forbidden transition due to electromagnetic multipoles like (E2/M1) between $|n(J,\pi)\rangle$ and $|m(J',\pi)\rangle$ or an induced E1 transition amplitude due to a static electric field.

1.11 Theoretical procedure

From a theoretical point of view, it is important to calculate $E1_{PNC}$ accurately for the purpose of probing physics beyond the SM. We explain below the procedure for calculating this quantity.

The original atomic wavefunction ($|\Psi_i^{(0)}\rangle$) of the DC/DCB Hamiltonian given by

$$H_{DC(B)} = \sum_i [ic\vec{\alpha}_\mathbf{i} \cdot \vec{\mathbf{p}}_\mathbf{i} + (\beta_i - 1)c^2 + V_{nuc}(r_i)] + \sum_{i<j} V(r_{ij}), \qquad (1.29)$$

where $V(r_{ij})$ represents two-body interactions. α_i and β_i are the usual Dirac matrices and $V_{nuc}(r_i)$ is the potential at the site of the i^{th} electron due to the

atomic nucleus. The rest mass energy of the electron is subtracted from the energy eigenvalues. We use atomic units, electric charge $|e| = 1$ and mass of electron $m_e = 1$.

The modified atomic wavefunction can be written as

$$|\Psi_i\rangle = |\Psi_i^{(0)}\rangle + |\Psi_i^{(1)}\rangle. \tag{1.30}$$

where $|\Psi_i^{(1)}\rangle$ is the first order correction to the wavefunction $|\Psi_i^{(0)}\rangle$. Since this correction is sufficiently small, it is appropriate to evaluate it perturbatively. Considering the weak interaction only to first order, we can write

$$|\Psi_i^{(1)}\rangle = \sum_{I\neq i} |\Psi_I^{(0)}\rangle \frac{\langle\Psi_I^{(0)}|H_{PNC}|\Psi_i^{(0)}\rangle}{E_i^0 - E_I^0} \tag{1.31}$$

where H_{PNC} is the Hamiltonian of the appropriate weak interaction Hamiltonian, E_i^0 the eigenvalue of $H_{DC(B)}$ for i^{th} state wavefunction $|\Psi_i^{(0)}\rangle$. Since H_{PNC} does not conserve parity, the first order wavefunction $|\Psi_i^{(1)}\rangle$ are of different parity wavefunction than $|\Psi_i^{(0)}\rangle$. Considering the interaction Hamiltonian H_{PNC} from nuclear spin independent PNC effects, we can express the E1 matrix elements between states (f and i) originally of same parity given by

$$\begin{aligned} E1_{PNC} &= \langle\Psi_f|D|\Psi_i\rangle \\ &\approx \frac{\langle\Psi_f^{(0)}|D|\Psi_i^{(1)}\rangle + \langle\Psi_f^{(1)}|D|\Psi_i^{(0)}\rangle}{\sqrt{\langle\Psi_f^{(0)}|\Psi_f^{(0)}\rangle\langle\Psi_i^{(0)}|\Psi_i^{(0)}\rangle}} \end{aligned} \tag{1.32}$$

as other terms of the above expression after expansion will vanish due to the selection rule for E1 and higher order terms are neglected. Now substituting the explicit values of the first order perturbed wavefunctions, we have

$$\begin{aligned} E1_{PNC} = \frac{1}{\sqrt{\langle\Psi_f^{(0)}|\Psi_f^{(0)}\rangle\langle\Psi_i^{(0)}|\Psi_i^{(0)}\rangle}} \{ &\sum_{I\neq i} \frac{\langle\Psi_f^{(0)}|D|\Psi_I^{(0)}\rangle\langle\Psi_I^{(0)}|H_{PNC}|\Psi_i^{(0)}\rangle}{E_i^0 - E_I^0} \\ &+ \sum_{J\neq f} \frac{\langle\Psi_f^{(0)}|H_{PNC}|\Psi_J^{(0)}\rangle\langle\Psi_I^{(0)}|D|\Psi_i^{(0)}\rangle}{E_f^0 - E_J^0} \} \end{aligned} \tag{1.33}$$

where I and J represent intermediate states.

Many methods including semi-empirical and *ab initio* have been employed to determine the above expressions for various atomic systems with suitable transitions between atomic states on which experimental measurements have been carried out. Many-body perturbation theory (MBPT) is the widely used method for such calculations. It is not only necessary to calculate the correction to the atomic wavefunction, but also it is important to evaluate accurate atomic DC(B) wavefunctions ($|\Psi_i^{(0)}\rangle$) itself. A suitable and very powerful method is essential for carrying out these calculations in order to study atomic parity non-conservation. Relativistic coupled-cluster (RCC) method is known to be one of the most accurate methods for calculating atomic wavefunctions. It is an all order method [24, 25] with size-consistent and size-extensivity properties [26]. It can be easily shown that this method is related to relativistic many-body perturbation theory (RMBPT) and relativistic configuration interaction (RCI) method [24, 26]. But at a particular level of approximation, RCC theory has certain higher order excitations that are not present in RCI method.

1.12 Probing physics beyond SM

As mentioned earlier, it is only possible to measure the interference of $E1_{PNC}$ and some other forbidden electromagnetic transition amplitude. We can express the measured quantity as

$$X^{(expt.)} = Q_W \ \frac{E1_{PNC}^{(theory)}}{Y} \tag{1.34}$$

where X denotes a measured interference between $E1_{PNC}$ and one of the forbidden transition (Y) amplitudes due to electromagnetic potential (e.g. E2 or M1). Here Y can be obtained from either theoretical calculations or experiments. To extract Q_W from the equation (1.34), all the factors: X, $E1_{PNC}$ and Y have to be found very accurately which later can be compared with the SM given values.

As shown in figure 1.5, it is also possible to consider the induced stark effect due to DC electric field instead the electromagnetic forbidden transi-

tion (Y) for the above purpose. Experiments that have been successful so far are based on fluorescence and optical rotation in the neutral atoms. In the former case, the interference is between $E1_{PNC}$ and a Stark-induced electric dipole transition amplitude [17]. In the latter it is between $E1_{PNC}$ and an allowed magnetic dipole transition amplitude [14].

By combining the results of atomic parity non-conservation experiments and calculations, it is possible to extract Q_W, the nuclear weak charge. The extraction of Q_W has important implications for physics beyond the SM. One can express the deviation of this quantity from its SM value as

$$\Delta Q_W = Q_W - Q_W^{SM} \tag{1.35}$$

where the SM value of Q_W is given by

$$Q_W^{SM} = Z(1 - 4sin^2\theta_W) - N. \tag{1.36}$$

Here, Z is the atomic number, N is the number of neutrons and θ_W is the Weinberg mixing angle. After the inclusion of radiative corrections [27]

$$Q_W^{SM} = (0.9793 - 3.8968sin^2\theta_W)Z - 0.9793N. \tag{1.37}$$

It is possible to parameterize Q_W and hence ΔQ_W in terms of the isospin conserving and breaking parameters, S and T given by [28]

$$Q_W = (0.9857 \pm 0.0004)\rho(-N + Z[1 - 4.012 \pm (-0.010)\bar{x}]) \tag{1.38}$$

where

$$\rho = 1 + 0.00782T \tag{1.39}$$

and

$$\bar{x} = 0.2323 + 0.00365S - 0.00261T. \tag{1.40}$$

If $S \sim 1$ as predicted by certain model, then Q_W clearly must be determined to at least an accuracy of one percent. It may be shown that Q_W is sensitive to new physics where weak isospin is conserved. In other words the combined accuracy of atomic PNC experiment and the theory has to be at least a percent to test physics beyond the SM. Other related implications

to particle physics are given in the paper by Sandars [29]. The uncertainty arising from atomic calculations can be circumvented by measuring the fractional difference of Q_W, but that could lead to nuclear structure uncertainties [30]. The present status of PNC experiments and theories are given in the next section.

1.13 Status of NSI PNC in atoms/ions

Table 1.1: Present status of atomic PNC studies in various atomic systems

System	Transition	Accuracy of Experiments	Accuracy of Theory
Cesium	$[5p^6]6s_{1/2} \rightarrow [5p^6]7s_{1/2}$	0.35%	$\sim$ 0.5%
Cesium	$[5p^6]6s_{1/2} \rightarrow [4d^{10}]5d_{3/2}$	-	-
Thallium	$[6s^2]6p_{1/2} \rightarrow [6s^2]6p_{3/2}$	$\sim$ 1%	$\sim$ 3 %
Thallium	$[6s^2]6p_{1/2} \rightarrow [6s^2]7p_{1/2}$	$\sim$ 15%	$\sim$ 5%
Lead	$6p^2, J = 0 \rightarrow 6p^2, J = 1$	$\sim$ 1%	$\sim$ 10-15%
Bismuth	$6p^3, J = \frac{3}{2} \rightarrow 6p^3, J = \frac{3}{2}$	$\sim$ 2%	$\sim$ 10%
Bismuth	$6p^3, J = \frac{3}{2} \rightarrow 6p^3, J = \frac{5}{2}$	$\sim$ 2%	$\sim$ 10%
Barium$^+$	$[5p^6]6s_{1/2} \rightarrow [4d^{10}]5d_{3/2}$	-	$\sim$ 3 %
Ytterbium	$6s^2 \rightarrow 6s5d, J = 1$	-	$\sim$ 15%
Francium	$[6p^6]7s_{1/2} \rightarrow [6p^6]8s_{1/2}$	-	$\sim$ 1%

The present status of NSI atomic parity non-conservation is summarized in table 1.1. It is clear from this table that one can only use the results for cesium (Cs) at this stage to make predictions about physics beyond the SM. Using the results of $X^{(expt.)}$ and Y in equation (1.34) from the latest experimental and calculated $E1_{PNC}$ results in Cs, we get [31, 32]

$$Q_W = -72.57(29)_{expt}(36)_{th} \tag{1.41}$$

and for theoretical results of Y, we get [32, 33, 34]

$$Q_W = -73.09(39)_{expt}(37)_{th}. \tag{1.42}$$

Corrections from QED was found to be -0.27(3)% [35]. Oblique corrections have been formulated by Peskin and Takeuchi [27] in terms of weak isospin conserving and weak isospin breaking parameters S and T, respectively. For Cs, these oblique corrections for Q_W is given by [28]

$$-0.800S - 0.007T. \tag{1.43}$$

The constraint on S for Cs is recently given by [36]

$$S = -0.56(60). \tag{1.44}$$

A lower bound for the Z_x boson mass predicted in $SO(10)$ theories which can be obtained from the deviation of the measured weak charge from theory as [37]

$$\Delta Q_W \approx 0.4(2N + Z)(M_W/M_{Z_x})^2. \tag{1.45}$$

A lower bound on the mass M_{Z_x} from the parity non-conservation in Cs is derived as [36]

$$M_{Z_x} > 750 \;\; GeV. \tag{1.46}$$

The SM value for Q_W is given by [38]

$$Q_W = -73.09(3). \tag{1.47}$$

Therefore, it differs from the SM by 1.1σ. For all the quantities which have been extracted above, the first and second errors correspond to experimental and theoretical errors, respectively. The latter must clearly be improved in order to make definitive predictions about physics beyond the SM. In the next section, the proposed experiment on singly ionized barium ($^{137}Ba^{+}$) ion using laser cooling and trapping is discussed.

Constraints on the upper limit of different parameters from various studies at different energy scale are presented in table 1.2.

Table 1.2: Limits on new physics beyond the SM currently obtained from atomic PNC and directly from high-energy physics (HEP).

New Physics	Parameter	Constraints from atomic PNC	Direct constraints from HEP
Oblique radiative corections	$-0.008S - 0.007T$	-0.056 ± 1.0	$S = -0.28 \pm 0.19$ $T = -2.0 \pm 0.26$
Z_x boson in SO(10) model	$M(Z_x)$	> 750 GeV	> 425 GeV
Lepto-quarks	M_s	> 0.7 TeV	> 0.28 TeV
composite fermions	L	> 14 TeV	> 6 TeV

1.14 Motivation

As mentioned earlier, PNC in atomic systems arising from the neutral weak currents has the potential to test the SM of particle physics. By combining the results of high accuracy measurements and calculations of atomic PNC observables, it is possible to extract Q_W value and compare with its corresponding value in the SM [36].

The most accurate data on atomic PNC currently comes from the $6s\ ^2S_{1/2} \rightarrow 7s\ ^2S_{1/2}$ transition in Cs, where the claimed uncertainty in Q_W value from the SM value is $1.1\sigma\%$ [35]. It would indeed be desirable to consider other candidates which yield accurate values of Q_W. In this context an experiment to observe PNC in the $6s\ ^2S_{1/2} \rightarrow 5d\ ^2D_{3/2}$ transition in $^{137}Ba^+$ using the techniques of an ion trapping and laser cooling proposed by Fortson is of special importance [42].

This thesis is concerned with a high precision calculation of the amplitude of the $E1_{PNC}$ amplitude of $6s\ ^2S_{1/2} \rightarrow 5d\ ^2D_{3/2}$ transition in $^{137}Ba^+$ using

RCC theory. It is the first application of this theory to atomic PNC. Blundell *et al.* had used this theory in the linear approximation to calculate $E1_{PNC}$ amplitude for the $6s\ ^2S_{1/2} \rightarrow 7s\ ^2S_{1/2}$ transition in Cs [39]. Dzuba *et al.* [32] and Geetha [40] have calculated this PNC amplitude for $6s\ ^2S_{1/2} \rightarrow 5d\ ^2D_{3/2}$ transition in Ba^+ as discussed later in this thesis.

1.15 PNC in laser cooled ion

In the last two decades, remarkable advances have been made in trapping and laser-cooling of ions and atoms [41]. Application of strong electromagnetic fields have made the trapping of ions possible. Trapped ions can be cooled in various ways. A novel approach to the measurement of PNC in ions by exploiting some of these advances was proposed by Fortson in 1993 [42]. The accuracy of this approach would most likely be sufficient to test the SM.

The energy levels of low-lying states of Ba^+ are given in figure 1.6. Ba^+ has been trapped by a potential with 50 eV depth created by RF fields of frequency 25 MHz and cooled to an orbital radius , 0.1 μm by Dehmelt and co-workers. This ensures that the wavelength of the $6s_{1/2} \rightarrow 5d_{3/2}$ transition which has been proposed for observing parity non-conservation ($\lambda = 2.05\mu m$) is much larger than the radius of the ion after it has been trapped and cooled. This requirement is known as the Lamb-Dicke condition and is necessary to overcome the first-order Doppler shift. The physical quantity that has been proposed to be measured in the afore mentioned experiment is a parity non-conserving light shift (AC Stark Shift) arising from the interference of the parity non-conserving electric dipole transition amplitude ($E1_{PNC}$) and the electric quadrupole transition amplitude (E2).

The electric field of the laser inducing the parity non-conserving transition is given by

$$\vec{E}(\vec{r},t) = \frac{1}{2}[\vec{E}(\vec{r})e^{-i\omega t} + cc] \tag{1.48}$$

where ω is the frequency of laser and cc refers to complex conjugate.

Parity non-conserving and electric quadrupole Rabbi frequencies are

$$\Omega^{PNC}_{m',m} = -\frac{1}{2\hbar}\sum_i (E1_{PNC})_{m'mi} E_i(0) \tag{1.49}$$

and

$$\Omega^{quad}_{m',m} = -\frac{1}{2\hbar}\sum_{ij} (E2_{m'm})_i \frac{\partial E_i}{\partial x_j}|_0 \tag{1.50}$$

where m and m' are the magnetic quantum numbers of initial and final states, respectively. $E_i(0)$ and $\frac{\partial E_i}{\partial x_j}|_0$ are the components of the electric field of laser and its gradient at the position of the ion.

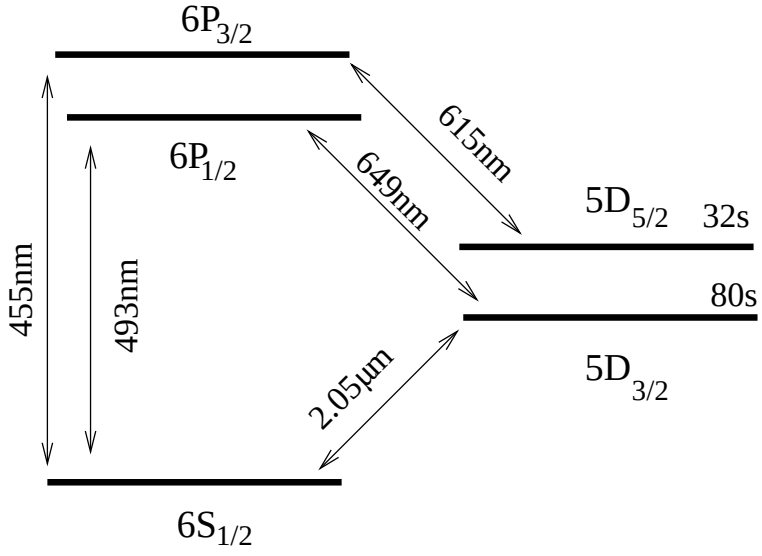

Figure 1.5: Energy levels in Ba^+ which are used to measure PNC effect.

The parity non-conserving effects are related to

$$\begin{aligned} |\Omega_{m'm}|^2 &= |\Omega^{quad}_{m'm} + \Omega^{PNC}_{m'm}|^2 \\ &\cong |\Omega^{quad}_{m'm}|^2 + 2Re(\Omega^{PNC*}_{m'm}\Omega^{quad}_{m'm}). \end{aligned} \tag{1.51}$$

Light shift of the m^{th} sub level of initial state is given by

$$\hbar\Delta\omega_m = \hbar[\frac{(\omega_0 - \omega)}{2} - \Omega_m], \tag{1.52}$$

where $\Omega_m = \sum_{m'} |\Omega_{m'm}|^2$ and ω_0 is the resonant frequency. Since contribution to the light shift comes from the parity non-conserving electric dipole and electric-quadrupole transitions, we get

$$\hbar\Delta\omega_m = \hbar\Delta\omega_m^{PNC} + \hbar\Delta\omega_m^{quad} \tag{1.53}$$

where

$$\omega_m^{PNC} \approx -Re\{\sum_{m'}(\Omega_{m'm}^{PNC*}\Omega_{m'm}^{quad})/\Omega_{m'm}^{quad}\} \tag{1.54}$$

and

$$\omega_m^{quad} \approx \frac{(\omega_0 - \omega)}{2}\Omega_m^{quad}. \tag{1.55}$$

Here, $(\Omega_m^{quad})^2 = \sum_{m'} |\Omega_{m'm}^{quad}|^2\Delta\omega_m^{PNC}$ changes sign when the sign of m changes, from $+\frac{1}{2}$ to $-\frac{1}{2}$, but $\Delta\omega_m^{quad}$ does not. This is exploited to measure the difference of the light shift for the magnetic quantum numbers $m = 1/2$ and $m = -1/2$, i.e.

$$\Delta\omega_{m=1/2} - \Delta\omega_{m=-1/2} = \Delta\omega_{m=1/2}^{PNC} - \Delta\omega_{m=-1/2}^{PNC}. \tag{1.56}$$

For the $6s_{1/2} \rightarrow 5d_{3/2}$ transition in Ba^+, this difference is approximately 1.2 Hz for an electric field equal to about $2 \times 10^4 V/cm$. Statistical accuracy of this kind of a PNC experiment is given by

$$\frac{E1_{PNC}}{\partial E1_{PNC}} = \frac{E1_{PNC}}{\hbar}Ef\sqrt{N}\tau t, \tag{1.57}$$

where f is the efficiency factor, τ is the coherence time determined by the decay of the final state, t is the total time available for the measurement and $N = 1$ is the number of ions. For $f = 0.2$, $E1_{PNC}$ can, in principle, be measured to 1 part in a 1000 in about a day. It is clear from the above expression that the competitive accuracy of the single ion experiment is due to the possibility of applying a large electric field to the ion and the long coherence time associated with the decay of the final state (the lifetime of the $5d_{3/2}$ is around 80sec).

1.16 Outline of the chapters

In the next chapter of this thesis, we discuss the basic tools in terms of algebraic and diagrammatic representations which are used in the RCC method. These algebraic and diagrammatic techniques simplify complicated atomic many-body formulations. We also discuss briefly the application of second quantization and Wick's theorem from quantum field theory in the context of atomic physics.

We discuss the general aspects and formulation of RCC theory in the third chapter. We also discuss there both the linearized and non-linearized CC theory. We present all possible Goldstone diagrams arising in these theories at a given level of approximation (LCCSD, CCSD and CCSD(T)). We also discuss the details of the various expectation values and transition matrix elements calculated in this thesis.

In chapter 4, we extend the RCC method to calculate PNC amplitudes. We present both working formulae and the procedure for this calculation. We also give all corresponding Goldstone diagrams used in our calculations and present the computational procedures for calculating PNC cluster amplitudes and a method for parallelizing the CC equations using Message Passing Interface (MPI).

We present all the results obtained using our theory in chapter 5. We compare these results with experimental results and discuss their dependence on different single particle orbitals. We also compare our results with previous calculated results. We compare our PNC amplitude with previous calculations. A detailed analysis of contributions from various intermediate states have been carried out.

We present preliminary results obtained for the Cs PNC in the sixth chapter. Since the PNC studies which we have carried out have similarities with atomic electric dipole moment (EDM) studies which again can be used to study physics beyond the SM, we present and discuss in chapter 6 scalar-pseudoscalar EDM calculations for both Cs and Tl.

In chapter 7, we conclude our thesis and give an outlook for future studies. We also discuss the importance of the present results and their implications.

Bibliography

[1] D. H. Perkins, *Introduction to High Energy Physics*, Addison-Wesley Publishing Company, London, UK (1972)

[2] F. Halzen and A. D. Martin, *Quarks and Leptons: An Introductory Course in Modern Particle Physics*, John Willey & Sons., New York (1984)

[3] For instance see: A. Hosaka and H. Toki, *Quarks, Baryons and Chiral Symmetry*, World Scientific, Singapore (2001)

[4] K. Huang, *Quarks, Leptons and Guge Fields*, 2nd edition, World Scientific, Singapore (1992)

[5] S. L. Glashow, Nucl. Phys. **22**, 579 (1961); S. Weinberg, Phys. Rev. Lett. **19**, 1264 (1964); A. Salam, *Elementary particle theory, relativistic groups and analyticity*, Edited by N. Svartholm (Almqvist and Wiksells, Stockholm, 1968) p. 367

[6] E. P. Wigner, *Symmetry Principles in Old and New Physics*, Bull. Am. Math. Soc. **74**, 793 (1968)

[7] A. Salem, *Theory of Groups and the Symmetry Physicist*, Lond. Math. Soc. J **41**, 49 (1966)

[8] E. L. Hill, Rev. Mod. Phys. **23**, 253 (1951)

[9] E. Noether, Nachr. Ges. Wiss., Göttingen **37**, 235 (1918)

[10] S. M. Barr, Phys. Rev. D **47**, 2025 (1993); Phys. Rev. Lett. **68**, 1822 (1992); Phys. Rev. D **45**, 4148 (1992)

[11] I. Bars, Phys. Lett. **106B**, 105 (1981)

[12] A. J. Buras, J. Ellis, M. K. Gaillard and D. V. Nanopoulos, Nuc. Phys. B, **135**, 66 (1978)

[13] S. Weinberg, Phys. Rev. D **19**, 1277 (1979)

[14] N. H. Edwards, S. J. Phipp, P. E. G. Baird and S. Nakayama, Phys. Rev. Lett. **74**, 2654 (1995)

[15] D. M. Meekhof, P. Vetter, P. K. Majumder, S. K. Lamoreaux and E. N. Fortson, Phys. Rev. Lett. **71**, 3442 (1993)

[16] M. J. D. Macpherson, K. P. Zetie, R. B. Warrington, D. N. Stacey and J. P. Hoare, Phys. Rev. Lett. **67**, 2784 (1991)

[17] C. S. Wood, S. C. Bennett, D. Cho, B. P. Masterson, J. L. Roberts, C. E. Tanner and C. E. Wieman, Science **275**, 1759 (1997)

[18] M. -A. Bouchiat and C. Bouchiat, Rep. Prog. Phys. **60**, 1351 (1997)

[19] P. A. Vetter, D. M. Meekhof, P. K. Majumder, S. K. Lamorcaux and E. N. Fortson, Phys. Rev. Lett. **74**, 2658 (1995)

[20] M. A. Bouchiat and C. Bouchiat, J. Phys. (Paris) **35**, 899 (1974); J. Phys. (Paris) **36**, 493 (1975)

[21] Y. B. Zel'dovich, Zh. Eksp. Theor. Fiz. **33**, 1531 (1957) [Sov. Phys. ZETP **6**, 1184 (1957)]

[22] I. B. Khriplovich, *Parity Nonconservation in Atomic Phenomena* (Gordon and Breach, Philadelphia, 1991)

[23] V. V. Flambaum and I. B. Khriplovich, Zh. Eksp. Teor. Fiz. **89**, 1505 (1985) [Sov. Phys. JETP **62**, 872 (1985)]

[24] I. Lindgren and J. Morrison, *Atomic Many-Body Theory*, Edited by G. Ecker, P. Lambropoulos, and H. Walther (Springer-Verlag, Berlin, 1985)

[25] Bijaya K. Sahoo, Rajat K. Chaudhuri, B. P. Das, Sonjoy Majumder, Holger Merlitz,Uttam Sinha Mahapatra and Debashis Mukherjee, J. Phys. B **36**, 1899-1906 (2003)

[26] A. Szabo and N. S. Ostlund, *Modern Quantum Chemistry: Introduction to Advanced Electronic structure theory*, Dover Publications Inc., *Mineola, New York*, First edition(revised), 1996

[27] M. Peskin and T. Taeichi, Phys. Rev. Lett. **65**, 964 (1990); Phys. Rev. D **46**, 381 (1992)

[28] J. L. Rosner, Phys. Rev. D **65**, 073026 (2002)

[29] P. G. H. Sandars, J. Phys. B **23**, L655 (1990); B. W. Lynn and P. G. H. Sandars, J. Phys. B **27**, 1469 (1994)

[30] P. K. Panda and B. P. Das, Phys. Rev. C **62**, 065501 (2000)

[31] S. C. Bennett and C. E. Wieman, Phys. Rev. Lett. **82**, 2484 (1999); **83**, 889 (1999)

[32] V. A. Dzuba, V. V. Flambaum and J. S. M. Ginges, Phys. Rev. D **66**, 076013 (2002)

[33] D. Cho, C. S. Wood, S. C. Bennett, J. L. Roberts and C. E. Wieman, Phys. Rev. A **55**, 1007 (1997)

[34] A. A. Vasilyev, I. M. Savukov, M. S. Sapronova and H. G. Berry, Phys. Rev. A **66**, 020101(R) (2002)

[35] V. M. Shabaev, K. Pachucki, I. I. Tupitsyn and V. A. Yerokhin, Phys. Rev. Lett. **94**, 213002 (2005)

[36] J. S. M. Ginges and V. V. Flambaum, Phys. Rep. **637**, 63 (2004)

[37] W. J. Marciano and J. L. Rosner, Phys. Rev. Lett. **65**, 2963 (1990)

[38] D. E. Groom *et al.*, Eur. Phys. J. C **15**, 1 (2000)

[39] S. A. Blundell, W. R. Johnson, J. Sapirstein, Phys. Rev. Lett. **65**, 1411 (1990); Phys. Rev. D **45**, 1602 (1992)

[40] K. P. Geetha, Ph. D. Thesis, Bangalore Univ., India (2002)

[41] P. K. Ghosh, *Oxford Science Publications*, Clarendon Press, Oxford (1995)

[42] N. Fortson, Phys. Rev. Lett. **70**, 2383 (1993)

Chapter 2

Basic Tools for Calculations

2.1 Introduction

In practice one needs basic tools to simplify the computational tasks for the calculation of properties in atomic systems. It is widely recognized in field theory that the second quantized formulation, normal order form, Wick's theorem etc. help calculations to be performed easily and enable to understand all the physical processes [1]. In fact one also uses Feynman-like diagrams to understand all the physical processes in simpler and realistic approach [1, 2]. In atomic physics we use these tools to consider different processes by modifying some of the above definitions in an appropriate and convenient manner [3, 4, 5], then we interpret the results in terms of the system's electrons. Different electron excitations and de-excitations can be well understood using these basic instruments. In this chapter we define these mathematical tools and a corresponding diagrammatic approach known as a Goldstone diagram [3, 4, 5] for both occupied and unoccupied electron states. Different interaction forces present inside atomic systems are expressed in terms of these mechanisms, we also discuss methods to construct single particle wavefunctions. The matrix elements of the interaction operators are then expressed separately in terms of radial integrals and angular factors of the single particle orbitals. We also use a diagrammatic approach to calculate the angular factors [3, 6, 7, 8] and simplify all the complicated products of the complex

Clebsch-Gordan coefficients.

2.2 Relativistic quantum numbers

The Dirac Hamiltonian of a relativistic atomic system without a two-body interaction can be written as

$$H = \sum_j c\ \vec{\alpha} \cdot \vec{p}_j + (\beta - 1)c^2 + V_{nuc}(r_j) \tag{2.1}$$

where α and β are the usual Dirac matrices and $V_{nuc}(r_j)$ is the potential at the position of the j^{th} electron due to the atomic nucleus. In our derivation, we have employed atomic units ($m_e = 1$, $|e| = 1$ and $\hbar = 1$). The rest-mass energy of the electron is subtracted from the energy eigenvalues.

The single particle (electron) orbitals can be expressed for the above Hamiltonian as [9]

$$|\phi(r)\rangle = \frac{1}{r} \begin{pmatrix} P(r) & \chi_{\kappa,m}(\theta,\phi) \\ iQ(r) & \chi_{-\kappa,m}(\theta,\phi) \end{pmatrix} \tag{2.2}$$

where $P(r)$ and $Q(r)$ are the large and small components of the wavefunction.

The angular functions are given by

$$\chi_{\kappa,m}(\theta,\phi) = \sum_{\sigma=\pm\frac{1}{2}} \langle lm - \sigma\frac{1}{2}\sigma | l\frac{1}{2}jm\rangle Y_l^{m-\sigma}(\theta,\phi)\phi_\sigma \tag{2.3}$$

where the $\langle lm - \sigma\frac{1}{2}\sigma | l\frac{1}{2}jm\rangle$ are Clebsch-Gordan coefficients, the $Y_l^{m-\sigma}(\theta,\phi)$ are normalized spherical harmonics and the ϕ_σ are the two-component spinors given by

$$\phi_{1/2} = \begin{pmatrix} 1 \\ 0 \end{pmatrix}, \quad \phi_{-1/2} = \begin{pmatrix} 0 \\ 1 \end{pmatrix}. \tag{2.4}$$

This function gives the simultaneous eigenfunctions of $\mathbf{L}$, $\mathbf{S}$, $\mathbf{J}$ and J_z [10, 11]:

$$\mathbf{J}^2\chi_{\kappa,m} \;=\; j(j+1)\chi_{\kappa,m}$$

$$\begin{aligned} \mathbf{L}^2\chi_{\kappa,m} &= l(l+1)\chi_{\kappa,m} \\ \mathbf{S}^2\chi_{\kappa,m} &= \frac{3}{4}\chi_{\kappa,m} \\ J_z\chi_{\kappa,m} &= m\chi_{\kappa,m} \end{aligned} \tag{2.5}$$

where the relativistic quantum numbers are defined as $\kappa = -(j+\frac{1}{2})a$ [9, 10] and $l = j - \frac{1}{2}a$, where $a = \pm 1$ [10, 11]. Note that wavefunctions with the same quantum number j but with different κ eigenvalues $(\kappa, -\kappa)$ belong to opposite parity states [9].

2.3 Atomic wavefunctions in second quantization form

An atomic system consist of many electrons, which satisfy Fermi-Dirac statistics. The wavefunctions for N electrons can be written in the general form [13, 14]

$$|\Phi\rangle = \sqrt{\frac{1}{N!}} \begin{vmatrix} |\phi_a(1)\rangle & |\phi_a(2)\rangle & \cdots & |\phi_a(N)\rangle \\ |\phi_b(1)\rangle & |\phi_b(2)\rangle & \cdots & |\phi_b(N)\rangle \\ .... & .... & .... & .... \\ |\phi_c(1)\rangle & |\phi_c(2)\rangle & \cdots & |\phi_c(N)\rangle \end{vmatrix} \tag{2.6}$$

where $|\phi_i(j)\rangle$ is the single particle wavefunction of the Dirac Hamiltonian given above for the i^{th} particle in the j^{th} position, the factor $\sqrt{\frac{1}{N!}}$ is the normalization factor. The above determinant is known as a Slater determinant. The above Slater determinant can also be denoted by the following curly bracket:

$$|\Phi\rangle = |\{abc\cdots N\}\rangle \tag{2.7}$$

and for any excited state it is defined as

$$\begin{aligned} |\Phi^{pq..}_{ab..}\rangle &= a_p^\dagger a_q^\dagger a_b a_a |\{abc\cdots N\}\rangle \\ &= |\{pqc\cdots N\}\rangle. \end{aligned} \tag{2.8}$$

$a_i^\dagger$ represents the creation of electron i, whereas a_i represents the annihilation of electron i. Therefore, the above notation of the excited state symbolizes

that electrons $a, b, c, \cdots$ are annihilated and electrons $p, q, \cdots$ are created.

We classify electrons, according to their locations in the atomic systems, as occupied (holes), unoccupied (particles) and general, due to the second quantization formalism and to differentiate their algebraic operations. In our notation we use $a, b, c, d \cdots$, $p, q, r, s \cdots$, and $i, j, k, l \cdots$ for occupied, virtual and general electrons, respectively.

2.4 Matrix representation of operators

From a computational point of view we express all physical operators on the atomic systems in terms of second quantized operators with a coefficient which is the matrix element of the electron orbitals. In this notation a general single-electron dependent (one-body) operator can be expressed as [3]

$$F = \sum_{i=1,N} f(i) = \sum_{i=1,N} \sum_{j,l} \langle j|f(i)|l\rangle a_j^\dagger a_l. \tag{2.9}$$

Now we can write the matrix element of the one-body operator in terms of atomic wavefunctions as

$$\langle\{ab\cdots\}|F|\{ab\cdots\}\rangle = \langle a|f(1)|a\rangle + \langle b|f(2)|b\rangle + \cdots\cdots \tag{2.10}$$

and

$$\begin{aligned} \langle\{ap\}|F|\{ab\}\rangle &= \langle p|f|b\rangle \\ \langle\{pq\}|F|\{ab\}\rangle &= 0 \end{aligned} \tag{2.11}$$

where the first matrix element represents the expectation value and the latter two transition matrix elements. Since the operator depends on only one particle, the two particle transitions are not achievable using this operator.

Similarly, a two-electron dependent operator can be written as [3]

$$G = \sum_{i<j=1,N} g(i,j) = \sum_{i<j=1,N} \sum_{k,l,m,n} \langle kl|g|mn\rangle a_k^\dagger a_l^\dagger a_m a_n \tag{2.12}$$

where the restriction is imposed to avoid double counting.

The matrix elements of this operator between atomic wavefunctions are then given by

$$\begin{aligned}\langle\{abc\cdots\}|G|\{abc\cdots\}\rangle &= \langle ab|g(1,2)|ab\rangle - \langle ba|g(1,2)|ab\rangle \\ &\quad +\langle ac|g(1,3)|ac\rangle - \langle ca|g(1,3)|ac\rangle + \cdots \quad (2.13)\end{aligned}$$

and

$$\begin{aligned}\langle\{ap\}|G|\{ab\}\rangle &= \sum_a [\langle ap|g|ab\rangle - \langle pa|g|ab\rangle \\ \langle\{pq\}|G|\{ab\}\rangle &= \langle pq|g|ab\rangle - \langle qp|g|ab\rangle \cdots \ . \quad (2.14)\end{aligned}$$

The transition matrix element will vanish if the wavefunctions differ by more than two occupied electrons.

2.5 Angular momentum calculation

The matrix elements of one-body and two-body operators contain both purely radial integrals and angular factors in terms of single particle orbitals. These angular factors are dealt with by applying simple formulae. From computational point of view it is difficult to handle the m_j components of the angular momentum j of an atomic system. Therefore, in the actual calculations one separates out m_j dependent factors and deals only with the remaining ones. A specific transition to any specific m_j state can be taken care of in the final calculations. This can be easily understood once we have discussed various matrix element calculations. First, let us discuss how to decompose the one-body and two-body matrix elements into m_j dependent and independent factors.

According to Wigner-Eckart theorem, a one-body operator of rank 'k' in a single particle representation can be expressed as [3, 6, 7]

$$\begin{aligned}\langle jm_j|f|j'm_j'\rangle &= \sum_q \langle jm_j|f_q^k|j'm_j'\rangle \\ &= (-1)^{j-m_j} \begin{pmatrix} j & k & j' \\ -m_j & q & m_j' \end{pmatrix} \langle j||f^k||j'\rangle \quad (2.15)\end{aligned}$$

where $\langle j||f^k||j'\rangle$ is called the reduced matrix element and is independent of m_j components. Generally one considers only the reduced matrix elements in computations of many-electron systems and uses the full operator only in special cases when it is important for a given m_j state.

One can similarly use the Wigner-Eckart theorem for two-body operators as a product of two individual matrix elements with a coupling factor [10, 12]. A two-particle dependent potential can be factorized as [3]

$$g(r_1, r_2) = \sum_k g_k(r_1, r_2)[U^{(k)}(1).V^{(k)}(2)] \tag{2.16}$$

where 'k' denotes the rank of the factorized operators and $g_k(r_1, r_2)$ is the radial part of the integral with k dependency. In terms of reduced matrix elements this can be written as [10, 11]

$$< ab|g(r_1, r_2)|cd >= \sum_{k,q}(-1)^{j_a-m_a+j_b-m_b+k-q} \begin{pmatrix} j_a & k & j_c \\ -m_a & q & m_c \end{pmatrix} \times \begin{pmatrix} j_b & k & j_d \\ -m_b & -q & m_d \end{pmatrix} R^k(abcd) \tag{2.17}$$

where the reduced matrix element (the strength of the interaction) is given by

$$R^k(abcd) = (-1)^k\langle a||U^{(k)}||c\rangle\langle b||V^{(k)}||d\rangle \tag{2.18}$$

where $\langle a||U^{(k)}||c\rangle$ and $\langle b||V^{(k)}||d\rangle$ are the reduced angular momentum matrix elements of the respective operators.

2.6 Angular momentum diagrams

To handle the angular factors for complex Clebsch-Gordan coefficients we use angular momentum diagrams. The one-body matrix element from the above Wigner-Eckart theorem can be expressed in terms of an angular momentum diagram as

$$\langle j_a m_a|f^k_q|j_b m_b\rangle = \langle j_a||f^k||j_b\rangle \ \times \ Ang1 \tag{2.19}$$

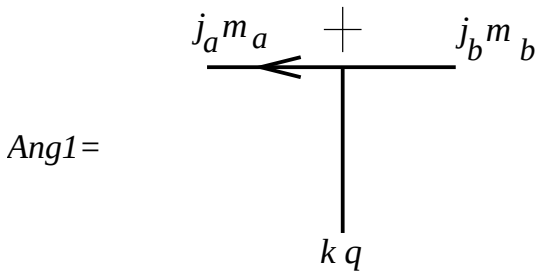

where the angular momentum diagram represents an m_j dependent 3-j factor. A detailed explanation for the representation of these diagrams can be found elsewhere [3, 6, 7].

The two-body operator in diagrammatic representation can be expressed as

$$< ab|G(r_1, r_2)|cd >= \sum_k R^k(abcd) \times Ang2 \tag{2.20}$$

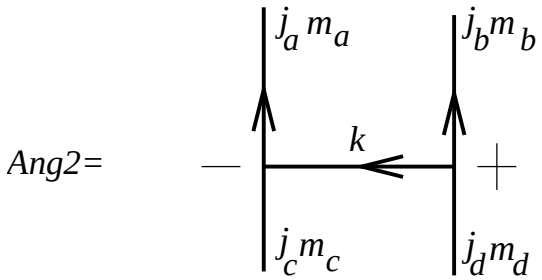

The interpretation of various parts of these angular diagrams including the arrows and signs are taken from Lindgren *et al* [3]. Angular factors with multiples of Clebsch-Gordan coefficients are solved using JLV theorems (see Appendix A).

2.7 Special two-body operators

The most crucial part to include in the atomic calculations are two-body interactions [3]. There are two such interactions possible to lowest order approximation. The Coulomb interaction due to the longitudinal photons (as opposed to the classical interpretation due to static charges) [1] is the dominant one, and the Breit interaction due to transverse photons [15] (where the classical interpretation is a current-current interaction of charges), which is a factor of α^2 smaller than former one. We discuss here the explicit expressions for both of the interaction which can be considered in the calculations.

2.7.1 The Coulomb interaction

A general matrix form of the Coulomb interaction ($V_C = \frac{1}{r_{12}}$) is given by [10, 11]

$$\begin{aligned}\langle ab|\frac{1}{r_{12}}|cd\rangle &= \int\int dr_1 dr_2 [P_a(r_1)P_c(r_1) + Q_a(r_1)Q_c(r_1)]\frac{r_<^k}{r_>^{k+1}} \\ &\quad [P_b(r_2)P_d(r_2) + Q_b(r_2)Q_d(r_2)] \times Ang. \qquad (2.21)\end{aligned}$$

this expression is derived using Legendre polynomials. In the above equation, $P_i(r_j)$ and $Q_i(r_j)$ are the large and small components of Dirac wavefunctions of the i^{th} orbital at the spatial distance r_j. The multi-pole k is given by $|j_a - j_c| \leq k \leq j_a + j_c$ and $|j_b - j_d| \leq k \leq j_b + j_d$. The angular momentum part is given by

$$\begin{aligned}Ang = \delta(m_a + m_c, m_b + m_d) \sum_k \Pi^e(\kappa_a, \kappa_c, k)\Pi^e(\kappa_b, \kappa_d, k) \\ d^k(j_c m_c, j_a m_a) d^k(j_b m_b, j_d m_d) \qquad (2.22)\end{aligned}$$

where the coefficient $d^k(jm, j'm')$ is defined as

$$d^k(jm, j'm') = (-1)^{m+\frac{1}{2}} \frac{[(2j+1)(2j'+1)]^{\frac{1}{2}}}{(2k+1)} C(jj'; \frac{1}{2} - \frac{1}{2}) C(jj'; -m, m') \qquad (2.23)$$

with $C(jj'; -m, m')$ is the Clebsch-Gordan or *vector-coupling* coefficient, $\kappa = j - \frac{1}{2}a$ and 'a' is the spatial relativistic quantum number as defined earlier.

The Π^e- function which decides the parity selection rule is defined as [12, 16]

$$\Pi^e(\kappa,\kappa',k) = \frac{1}{2}[1 - aa'(-1)^{j+j'+k}] \tag{2.24}$$

which in orbital angular momentum ensures that

$$l + l' + k = even \tag{2.25}$$

where l and l' are the orbital angular momentums for j and j' total angular momentums, respectively. The superscript 'e' in Π^e is used to denote the above even multipole (k) selection rules.

In terms of 3-j notation the above expression can be written as

$$Ang = \delta(m_a + m_c, m_b + m_d) \sum_{k,q} \Pi^e(\kappa_a,\kappa_c,k)\Pi^e(\kappa_b,\kappa_d,k)(-1)^{j_a - m_a + j_b - m_b + k - q}$$
$$\sqrt{(2j_a+1)(2j_b+1)(2j_c+1)(2j_d+1)} \begin{pmatrix} j_a & k & j_c \\ -m_a & q & m_c \end{pmatrix} \begin{pmatrix} j_b & k & j_d \\ -m_b & -q & m_d \end{pmatrix}$$
$$(-1)^{j_a+j_b+k+1} \begin{pmatrix} j_a & k & j_c \\ \frac{1}{2} & 0 & -\frac{1}{2} \end{pmatrix} \begin{pmatrix} j_b & k & j_d \\ \frac{1}{2} & 0 & -\frac{1}{2} \end{pmatrix}.$$

Therefore, the integral due to Coulomb operator can be expressed as

$$\langle ab|\frac{1}{r_{12}}|cd\rangle = \delta(m_a + m_c, m_b + m_d) \sum_{k,q} \Pi^e(\kappa_a,\kappa_c,k)\Pi^e(\kappa_b,\kappa_d,k)$$
$$(-1)^{j_a - m_a + j_b - m_b + k - q} \begin{pmatrix} j_a & k & j_c \\ -m_a & q & m_c \end{pmatrix} \begin{pmatrix} j_b & k & j_d \\ -m_b & -q & m_d \end{pmatrix} X^k(abcd), \tag{2.26}$$

where

$$\begin{aligned} X^k(abcd) \;=\; & \int\int dr_1 dr_2 [P_a(r_1)P_c(r_1) + Q_a(r_1)Q_c(r_1)] \frac{r_<^k}{r_>^{k+1}} \\ & [P_b(r_2)P_d(r_2) + Q_b(r_2)Q_d(r_2)] \\ & (-1)^{j_a+j_b+k+1} \begin{pmatrix} j_a & k & j_c \\ \frac{1}{2} & 0 & -\frac{1}{2} \end{pmatrix} \begin{pmatrix} j_b & k & j_d \\ \frac{1}{2} & 0 & -\frac{1}{2} \end{pmatrix} \end{aligned} \tag{2.27}$$

is the reduced angular momentum matrix element.

2.7.2 The Breit interaction

The general matrix element for the Breit interaction can also be expressed in a similar form as that of the Coulomb interaction. The Breit interaction is divided into two parts; namely the Gaunt or magnetic term and the retardation part [11, 12, 15]. The Gaunt term is given by

$$V_B^{mag} = -\frac{\vec{\alpha}_1.\vec{\alpha}_2}{r_{12}} \tag{2.28}$$

and the retardation term is given by

$$V_B^{ret} = \frac{1}{2}(\vec{\alpha}.\vec{\nabla})_1(\vec{\alpha}.\vec{\nabla})_2 r_{12}. \tag{2.29}$$

In terms of angular factors they are given by

$$\begin{aligned}\langle ab|V_B^{mag}|cd\rangle = \delta(m_a - m_c, m_b - m_d)(-1)^{j_a - m_a + j_b - m_b + k - q} \\ \begin{pmatrix} j_a & k & j_c \\ -m_a & q & m_c \end{pmatrix} \begin{pmatrix} j_b & k & j_d \\ -m_b & -q & m_d \end{pmatrix} Y^k(abcd)\end{aligned} \tag{2.30}$$

where

$$\begin{aligned}Y^k(abcd) = (-1)^{j_a + j_b + k + 1}\sqrt{(2j_a+1)(2j_b+1)(2j_c+1)(2j_d+1)} \\ \begin{pmatrix} j_a & k & j_c \\ \frac{1}{2} & 0 & -\frac{1}{2} \end{pmatrix} \begin{pmatrix} j_b & k & j_d \\ \frac{1}{2} & 0 & -\frac{1}{2} \end{pmatrix} \\ \Pi^o(\kappa_a, \kappa_c, k)\Pi^o(\kappa_b, \kappa_d, k) \sum_{\mu=1}^{4} r_\mu^{\nu,k}(abcd) R_\mu^\nu(abcd)\end{aligned} \tag{2.31}$$

$r_\mu^{\nu,k}$s are the angular factor as given in table 2.1 [12, 17, 18] and $R_\mu^\nu(abcd)$s are the radial integrals which are given in table 2.2 by defining [17, 19, 20]

$$R^k(abcd) = \int_0^\infty \int_0^\infty dr_1 dr_2 P_a(r_1) Q_c(r_1) \frac{r_<^k}{r_>^{k+1}} P_b(r_2) Q_d(r_2). \tag{2.32}$$

Similarly, we can express the integral for the retardation part as

$$\begin{aligned}\langle ab|V_B^{ret}|cd\rangle = \delta(m_a - m_c, m_b - m_d)(-1)^{j_a - m_a + j_b - m_b + k - q} \\ \begin{pmatrix} j_a & k & j_c \\ -m_a & q & m_c \end{pmatrix} \begin{pmatrix} j_b & k & j_d \\ -m_b & -q & m_d \end{pmatrix} Z^k(abcd)\end{aligned} \tag{2.33}$$

Table 2.1: Corresponding angular factors for $r_\mu^{\nu,k}(abcd)$.

	$\nu = k-1$	ν	$\nu = k+1$
$\mu = 1$	$A(K+k)(K'+k)$	A	$A(K-k-1)(K'-k-1)$
$\mu = 2$	$A(K-k)(K'-k)$	A	$A(K+k+1)(K'+k+1)$
$\mu = 3$	$A(K+k)(K'-k)$	A	$A(K-k-1)(K'+k+1)$
$\mu = 4$	$A(K-k)(K'+k)$	A	$A(K+k+1)(K'-k-1)$

Table 2.2: Corresponding radial integrals for $R_\mu^\nu(abcd)$.

$\mu = 1$	$R^\nu(abcd)$	$\mu = 3$	$R^\nu(acbd)$
$\mu = 2$	$R^\nu(cadb)$	$\mu = 4$	$R^\nu(cabd)$

where

$$Z^k(abcd) = (-1)^{j_a+j_b+k+1}\sqrt{(2j_a+1)(2j_b+1)(2j_c+1)(2j_d+1)} \begin{pmatrix} j_a & k & j_c \\ \frac{1}{2} & 0 & -\frac{1}{2} \end{pmatrix} \begin{pmatrix} j_b & k & j_d \\ \frac{1}{2} & 0 & -\frac{1}{2} \end{pmatrix}$$
$$\{\Pi^o(\kappa_a,\kappa_c,k)\Pi^o(\kappa_b,\kappa_d,k)\sum_{\mu=1}^{4} g_\mu^{\nu,k}(abcd)R_\mu^\nu(abcd)$$
$$+\Pi^o(\kappa_a,\kappa_c,k-1)\Pi^o(\kappa_b,\kappa_d,k+1)\sum_{\mu=1}^{8} s_\mu^k(abcd)S_\mu^k(abcd)\} \qquad (2.34)$$

where $g_\mu^{\nu,k}$s and $s_\mu^{\nu,k}$s are the angular factors as given in table 2.3 and 2.5, respectively [12, 17]. The radial integrals $S_\mu^\nu(abcd)$s are given by table 2.4, with the following definition

$$S^k(abcd) = \frac{(2k+1)}{2}\int_0^\infty dr_1 \int_{r_1}^\infty dr_2 [P_a(r_1)Q_c(r_1)\frac{r_<^{k+1}}{r_>^{k+2}}P_b(r_2)Q_d(r_2)$$

$$-P_a(r_1)Q_c(r_1)\frac{r_<^{k-1}}{r_>^k}P_b(r_2)Q_d(r_2)]. \quad (2.35)$$

Table 2.3: Corresponding angular factors for $g_\mu^{\nu,k}(abcd)$.

	$\nu = k-1$	ν	$\nu = k+1$
$\mu = 1$	$B(K+k)(K'+k)$	B	$B(K-k-1)(K'-k-1)$
$\mu = 2$	$B(K-k)(K'-k)$	B	$B(K+k+1)(K'+k+1)$
$\mu = 3$	$B(K+k)(K'-k)$	B	$B(K-k-1)(K'+k+1)$
$\mu = 4$	$B(K-k)(K'+k)$	B	$B(K+k+1)(K'-k-1)$

Table 2.4: Corresponding radial integrals for $S_\mu^k(abcd)$.

$\mu = 1$	$S^k(acbd)$	$\mu = 5$	$S^k(acdb)$
$\mu = 2$	$S^k(bdac)$	$\mu = 6$	$S^k(dbac)$
$\mu = 3$	$S^k(cadb)$	$\mu = 7$	$S^k(cabd)$
$\mu = 4$	$S^k(dbca)$	$\mu = 8$	$S^k(bdca)$

The parity selection rules are given by the function [12, 16]

$$\Pi^o(\kappa, \kappa', k) = \frac{1}{2}[1 + aa'(-1)^{j+j'+k}]. \quad (2.36)$$

We have also used the following constants for determining angular coefficients for Breit interactions given in the above tables

$$A = \frac{1}{k(2k-1)} \qquad for \quad \nu = k-1$$

Table 2.5: Corresponding angular factors for $s^k_\mu(abcd)$.

$\mu = 1$	$C(K+k)(K'-k-1)$	$\mu = 5$	$C(K+k)(K'+k+1)$
$\mu = 2$	$C(K'+k)(K-k-1)$	$\mu = 6$	$C(K'-k)(K-k-1)$
$\mu = 3$	$C(K-k)(K'+k+1)$	$\mu = 7$	$C(K-k)(K'-k-1)$
$\mu = 4$	$C(K'-k)(K+k+1)$	$\mu = 8$	$C(K'+k)(K+k+1)$

$$\begin{aligned} &= \frac{-(\kappa_a+\kappa_c)(\kappa_b+\kappa_d)}{(k+1)(2k+1)} && for \quad \nu = k \\ &= \frac{1}{(k+1)(2k+3)} && for \quad \nu = k+1 \end{aligned} \tag{2.37}$$

$$\begin{aligned} B &= \frac{-1}{(2k-1)(2k+1)} && for \quad \nu = k-1 \\ &= \frac{-1}{(2k+1)(2k+3)} && for \quad \nu = k+1 \end{aligned} \tag{2.38}$$

$$C = \frac{1}{(2k+1)^2} \tag{2.39}$$

and

$$K = \kappa_c - \kappa_a; \qquad K' = \kappa_d - \kappa_b. \tag{2.40}$$

2.8 The Dirac-Fock Model

Next, we consider the DC and DCB Hamiltonian for the atomic system. Due to the two-body term in the Hamiltonian representing the instantaneous Coulomb interaction and/or Breit interaction among the electrons, it is not possible to exactly solve the equation for this Hamiltonian. As a first step towards an approximate solution of this equation we can average out

the interactions between the electrons and construct an one-body potential that can replace the two-body term and produce a reasonable wavefunction as an initial solution. This assumption is referred to in many-body literature as the *independent particle model.*

The relativistic atomic Hamiltonian at Coulomb-Breit interaction level is given by

$$H = \sum_j c\ \vec{\alpha} \cdot \vec{p}_j + (\beta - 1)c^2 + V_{nuc}(r_j) + \sum_{j<l} V(r_{jl}) \tag{2.41}$$

where

$$V(r_{jl}) \ = \ V_C(r_{jl}) + V_B(r_{jl})$$

with

$$V_C(r_{jl}) \ = \ \frac{1}{r_{jl}}$$

is the Coulomb interaction and

$$V_B(r_{jl}) = -\frac{\alpha_1 \cdot \alpha_2}{r_{jl}} + \frac{1}{2}[\frac{1}{r_{jl}}\{\alpha_1 \cdot \alpha_2 - \frac{(\alpha_1 \cdot \vec{\mathbf{r}}_{jl})(\alpha_2 \cdot \vec{\mathbf{r}}_{jl})}{r_{jl}^2}\}]$$

is the Breit interaction.

We first solve the relativistic Hartree-Fock (Dirac-Fock (DF)) and/or Hartree-Fock-Breit (Dirac-Fock Breit (DFB)) equations to obtain the single particle orbitals and their energies. The corresponding DF(B) Hamiltonian is given by

$$H_{DF(B)} = \sum_j h_0(r_j) = \sum_j c\ \vec{\alpha} \cdot \vec{p}_j + (\beta - 1)c^2 + V_{nuc}(r_j) + U(r_j). \tag{2.42}$$

where h_0 is called the single particle Fock operator.

The residual interaction is given by

$$V_{es} = \sum_{j<l} V(r_{jl}) - \sum_j U(r_j). \tag{2.43}$$

The single particle orbitals are obtained by solving the following equation self-consistently

$$h_0(r_j)|\phi_j\rangle = (f(r_j) + U(r_j))|\phi_j\rangle = \epsilon_j|\phi_j\rangle, \tag{2.44}$$

where

$$f_j \;=\; c\,\vec{\alpha}\cdot\vec{p}_j + (\beta-1)c^2 + V_{nuc}(r_j) \tag{2.45}$$

and

$$U|\phi_j(\vec{r}_1)\rangle = \sum_{a=1}^{occ}\langle\phi_a(\vec{r}_2)|\frac{1}{r_{12}}|\phi_a(\vec{r}_2)\rangle|\phi_j(\vec{r}_1)\rangle - \langle\phi_a(\vec{r}_2)|\frac{1}{r_{12}}|\phi_j(\vec{r}_2)\rangle|\phi_a(\vec{r}_1)\rangle \tag{2.46}$$

and is known as the DF potential, wherein *occ* represents the total number of occupied orbitals.

Equation (2.44) is called the DF equation for a single particle and its solutions are the DF energy eigenvalues for the wavefunction $|\phi_j\rangle$. Combination of these solutions give the DF solution for the atomic system.

2.9 Dirac-Fock Theory of Closed-shell

For any closed system, equation (2.44) can be written as

$$h_0|\phi_a\rangle = \epsilon_a|\phi_a\rangle \tag{2.47}$$

where a represents occupied electron orbitals. The DF potential for this system is given by

$$U(r_a)|\phi_a\rangle = \sum_b[\langle\phi_b|V(r_{ab})|\phi_b\rangle|\phi_a\rangle - \langle\phi_b|V(r_{ab})|\phi_a\rangle|\phi_b\rangle] \tag{2.48}$$

Therefore, the single particle energy for the a^{th} orbital in Dirac-Fock theory is given by

$$\begin{aligned}\epsilon_a &= \langle\phi_a|[c\,\vec{\alpha}\cdot\vec{p}_a + (\beta_a-1)c^2 + V_{nuc}(r_a) + U(r_a)]|\phi_a\rangle \\ &= [\langle\phi_a|[c\,\vec{\alpha}\cdot\vec{p}_a + (\beta_a-1)c^2 + V_{nuc}(r_a)] \\ &\quad + \sum_b\{\langle\phi_a\phi_b|V(r_{ab})|\phi_a\phi_b\rangle - \langle\phi_a\phi_b|V(r_{ab})|\phi_b\phi_a\rangle\}\end{aligned} \tag{2.49}$$

The average energy of a closed-shell system is given by

$$\begin{aligned} E_{avg} &= \sum_a \epsilon_a \\ &= \sum_a \langle\phi_a|h_0|\phi_a\rangle \\ &= \sum_a (2j_a+1) f(a,a) + \sum_{a,b}(2j_a+1)\{\langle\phi_a\phi_b|V(r_{ab})|\phi_a\phi_b\rangle \\ &\quad -\langle\phi_a\phi_b|V(r_{ab})|\phi_b\phi_a\rangle\} \end{aligned} \tag{2.50}$$

where the matrix elements from the one-body operators take the form, in terms of Dirac wavefunctions;

$$\begin{aligned} \langle\phi_a|f|\phi_b\rangle &= \int_0^\infty dr\sqrt{(2j_a+1)(2j_b+1)} \\ &\quad [cQ_a(\frac{d}{dr}+\frac{\kappa}{r})P_b + cP_a(-\frac{d}{dr}+\frac{\kappa}{r})Q_b - 2c^2Q_aQ_b \\ &\quad -\frac{Z}{r}(P_aP_b+Q_aQ_b)] \end{aligned} \tag{2.51}$$

and

$$f(a,a) = \langle\phi_a|f|\phi_a\rangle. \tag{2.52}$$

2.10 General form of two-body integrals

It is clear from (2.26), (2.30) and (2.33) that it is difficult to calculate the two-body integrals along with m_j quantum numbers. Therefore, we simplify further the m_j dependent factors to solve (2.49) as follows. We can express the general two-body integrals as

$$< ab|V(r_1,r_2)|cd >= \sum_{k,q}(-1)^{j_a-m_a+j_b-m_b+k-q} \begin{pmatrix} j_a & k & j_c \\ -m_a & q & m_c \end{pmatrix} \times \begin{pmatrix} j_b & k & j_d \\ -m_b & -q & m_d \end{pmatrix} R^k(abcd) \tag{2.53}$$

As given in (2.49), we have two special cases, direct and exchange terms, to solve the Dirac-Fock solutions for the closed-shell system. We give below proscriptions to evaluate these integrals for both Coulomb and Breit terms.

2.10.1 Special cases

There are two terms in the two-body integrals in equation (2.49) to solve the DF equation for a closed system – (i) $a = c$, $b = d$ called the direct integral part and (ii) $a = d$, $b = c$ called the exchange integral term. Below, we discuss explicitly the simplified expressions for these integrals.

Before discussing the special cases of the integrals, we give the following two relationships which are used to get simplified angular factors in the closed-shell system [10, 11]:

$$\sum_{m_j}(-1)^{j-m_j}\begin{pmatrix} j & k & j \\ -m_j & 0 & m_j \end{pmatrix} = \frac{1}{\sqrt{2j+1}}\delta_{k,0} \tag{2.54}$$

and

$$\sum_{m_j,m'_j}\begin{pmatrix} j & k & j' \\ -m_j & m_k & m'_j \end{pmatrix}^2 = \frac{1}{2j'+1}. \tag{2.55}$$

A. **Coulomb interaction**

Case I. $a = c$, $b = d$

After summing over b for the Coulomb interaction, we get

$$\begin{aligned}\sum_b J_{ab} &= \sum_b \langle ab|\frac{1}{r_{12}}|ab\rangle \\ &= \sum_b (2j_b+1)\Pi^e(\kappa_a,\kappa_b,0)\int_0^\infty\int_0^\infty dr_1 dr_2[P_a(1)^2+Q_a(1)^2] \\ &\quad \frac{1}{r_>}[P_b(2)^2+Q_b(2)^2]\end{aligned} \tag{2.56}$$

Case II. $a = d$, $b = c$

After summing over b for the Coulomb interaction, we get

$$\sum_b K_{ab} = \sum_b \langle ab|\frac{1}{r_{12}}|ba\rangle$$

$$
\begin{aligned}
&= \sum_b (2j_b+1) \sum_k \Pi^e(\kappa_a,\kappa_b,k) \begin{pmatrix} j & k & j' \\ \frac{1}{2} & 0 & -\frac{1}{2} \end{pmatrix}^2 \\
&\int_0^\infty \int_0^\infty dr_1 dr_2 [P_a(1)P_b(1) + Q_a(1)Q_b(1)] \\
&\frac{r_<^k}{r_>^{k+1}} [P_a(2)P_b(2) + Q_a(2)Q_b(2)]. \qquad (2.57)
\end{aligned}
$$

B. **Breit interaction**

Case I. $a = c,\ b = d$

The direct integral vanishes for the Breit interaction in the closed-shell system [20, 21].

Case II. $a = d,\ b = c$

The expression for the magnetic part of the Breit interaction is

$$
\begin{aligned}
\sum_b L_{ab} &= \sum_b \langle ab|V_B^{mag}|ba\rangle \\
&= \sum_b (2j_b+1) \begin{pmatrix} j & k & j' \\ \frac{1}{2} & 0 & -\frac{1}{2} \end{pmatrix}^2 Y^k(abba) \qquad (2.58)
\end{aligned}
$$

and from the retardation part we get

$$
\begin{aligned}
\sum_b M_{ab} &= \sum_b \langle ab|V_B^{ret}|ba\rangle \\
&= \sum_b (2j_b+1) \sum_k \begin{pmatrix} j & k & j' \\ \frac{1}{2} & 0 & -\frac{1}{2} \end{pmatrix}^2 Z^k(abba) \qquad (2.59)
\end{aligned}
$$

Therefore, we can write the total average energy in the closed-shell system as

$$
E_{avg} = \sum_a (2j_a+1) f(a,a) + \frac{1}{2} \sum_{a,b} (2j_a+1)[J_{ab} - (K_{ab} + L_{ab} + M_{ab})]. \qquad (2.60)
$$

2.11 Basis functions

The DF single particle orbital $|\phi_i\rangle$ is constructed as linear combinations of Gaussian type orbitals (GTOs) as [22]

$$|\phi_i(r)\rangle = \sum_\nu c_{i\nu}|f_{i,\nu}(r)\rangle \tag{2.61}$$

where the GTOs are given by

$$f_{i,k}(r) = r^k e^{-\alpha_i r^2}, \tag{2.62}$$

where $k = 0, 1, \cdots$ for s, p, $\cdots$ type orbital symmetries, respectively. For the exponents, we have used [23]

$$\alpha_i = \alpha_0 \beta^{i-1}. \tag{2.63}$$

Therefore, we can express the DF orbitals as

$$\begin{aligned} |\phi_i(r)\rangle &= \sum_\nu c_{i\nu}|f_{i,\nu}(r)\rangle \\ \Rightarrow \frac{1}{r}\begin{pmatrix} P_i(r) & \chi_{\kappa,m} \\ iQ_i(r) & \chi_{-\kappa,m}\end{pmatrix} &= \frac{1}{r}\begin{pmatrix} \sum_\nu c^L_{i\nu} f_{i,\nu}(r) & \chi_{\kappa,m} \\ i\sum_\nu c^S_{i\nu} f_{i,\nu}(r) & \chi_{-\kappa,m}\end{pmatrix} \end{aligned} \tag{2.64}$$

where $c^L_{i\nu}$ and $c^S_{i\nu}$ are the coefficients for large (L) and small (S) components of the DF orbitals.

Substituting equation (2.61) into equation (2.44) and multiplying by $\langle f_{i,\mu}|$ from the left side, we can construct the following matrix equation for the DF orbitals:

$$\sum_\nu \langle f_{i,\mu}|h_0|f_{i,\nu}\rangle c_{i\nu} + \sum_\nu \sum_a \{\langle f_{i,\mu}\phi_a|V(r_{ia})|f_{i,\nu}\phi_b\rangle c_{i\nu} - \langle f_{i,\mu}\phi_a|V(r_{ia})|\phi_i f_{b,\nu}\rangle c_{i\nu} = \epsilon_i \sum_\nu \langle f_{i,\mu}|f_{i,\nu}\rangle c_{i\nu} \tag{2.65}$$

or

$$\sum_\nu F_{\mu\nu} c_{i\nu} = \epsilon_i \sum_{\mu\nu} \langle f_{i,\mu}|f_{i,\nu}\rangle c_{i\nu} \tag{2.66}$$

The definition of new operator ($F_{\mu\nu}$) can be easily understood from both the equations. For a closed atomic system they can be written in matrix notation as [23]

$$\tilde{F}\tilde{C} = \in \tilde{S}\tilde{C} \tag{2.67}$$

where $\tilde{S}$ is the orthogonal matrix with the element $\langle f_{i,\mu}|f_{i,\nu}\rangle$. To convert the above matrix into a symmetric form, we modify the above equation by multiplying by $\tilde{S}^{-1/2}\ \tilde{S}^{1/2}$ in the above equation as [22]

$$\begin{aligned} \tilde{F}\tilde{S}^{-1/2}\tilde{S}^{1/2}\tilde{C} &= \in \tilde{S}^{1/2}\tilde{S}^{1/2}\tilde{C} \\ \Rightarrow \tilde{S}^{-1/2}\tilde{F}\tilde{S}^{-1/2}\tilde{S}^{1/2}\tilde{C} &= \in \tilde{S}^{-1/2}\tilde{S}^{1/2}\ \tilde{S}^{1/2}\tilde{C} \\ \Rightarrow \widetilde{F'}\widetilde{C'} &= \in \widetilde{C'} \end{aligned} \tag{2.68}$$

where $\widetilde{F'} = \tilde{S}^{-1/2}\tilde{F}\tilde{S}^{-1/2}$ and $\widetilde{C'} = \tilde{S}^{1/2}\tilde{C}$. This matrix is symmetric and has been used to obtain the DF orbitals.

The kinetic balance condition [24, 25] has been imposed between the large and small components of the GTOs in order to avoid divergence of the self-consistent solution of the above DF equation.

For a finite nucleus all orbitals are generated on a grid using a two-parameter Fermi nuclear distribution approximation given by

$$\rho = \frac{\rho_0}{1 + e^{(r-c)/a}}, \tag{2.69}$$

where the parameter 'c' is the *half-charge radius,* and 'a' is related to the *skin thickness* which is defined as the interval of the nuclear thickness over which the nuclear charge density falls from near one to near zero. These values are tabulated by Vries *et al.* [26] for many atomic systems. We follow Mohanty and Parpia's method [27] to determine 'c' and 'a' for various atomic systems. The equations determining these parameters are

$$a = 2.3/4(ln3) \tag{2.70}$$

$$c = \sqrt{\frac{5}{3}r_{rms}^2 - \frac{7}{3}a^2\pi^2} \tag{2.71}$$

where r_{rms} is the root mean square radius of the nucleus.

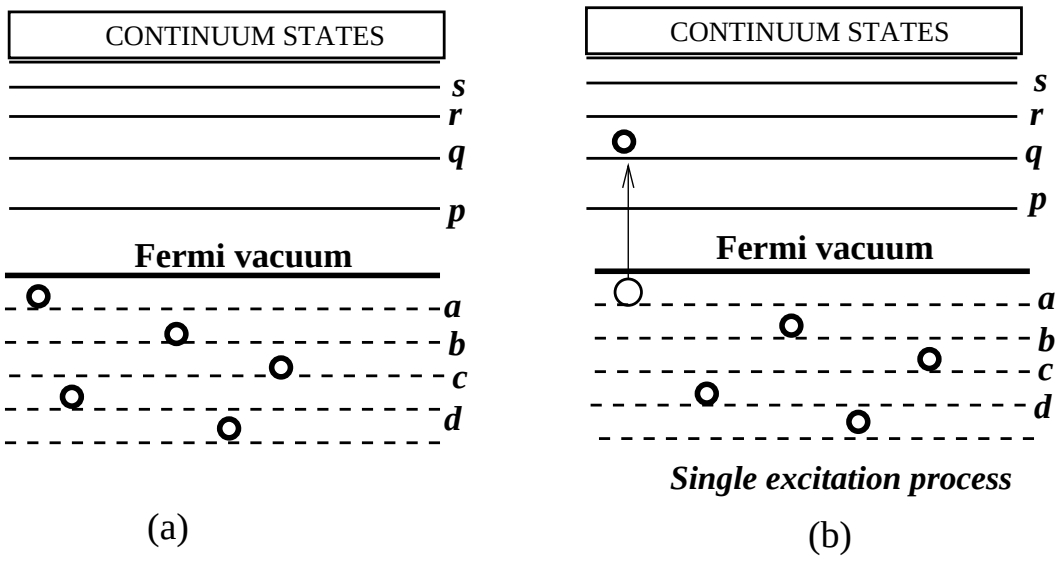

Figure 2.1: Representation of Fermi vacuum and single excitation process.

For point nuclei, we use

$$\rho = \rho_0 \tag{2.72}$$

where ρ_0 is the average nuclear density.

2.12 Fermi vacuum

The Fermi vacuum consists of certain occupied orbitals as shown in figure 2.1(a). This is also known as a reference state for a closed system, to define various excitations. An orbital excited out of the Fermi vacuum to an unoccupied or virtual orbital (e.g. $a \rightarrow q$) results in the creation of a hole as well as a particle which as shown in figure 2.1(b). This process is referred to as a single excitation. It is convenient to express these excitations through creation and annihilation operators. For example, a single excitation leads to the state $|\Phi_a^p\rangle = a_p^\dagger a_a |\Phi_0\rangle$, where $|\Phi_0\rangle$ is the DF wavefunction for an atomic system and is generally considered as a Fermi vacuum state. $a_p^\dagger$ and a_a are unoccupied orbital electron creation or particle creation and occupied orbital electron annihilation or hole creation operators, respectively.

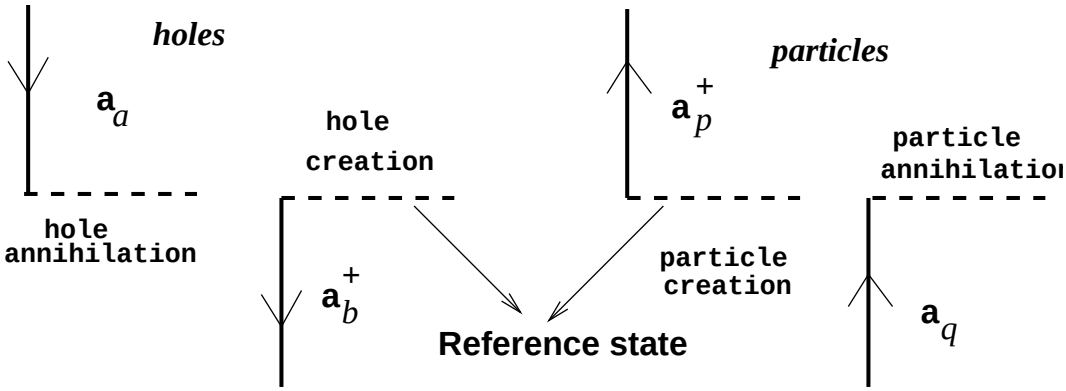

Figure 2.2: Diagrammatic representation of particle creation and annihilation processes.

2.13 Diagrammatic representation of orbital lines

To understand the actual process of excitations through electron orbitals we represent various annihilation and creation operators through diagrammatic convention. These representations are shown by figure 2.2.

As we explained earlier, all the physical operators can be expressed in terms of second quantized operators with the necessary matrix element. The products of such operators can be simplified by applying Wick's theorem (see Appendix B for the definition) which give us insight into various physical processes. In general, we express all the operators in normal order form (see Appendix B for the definition). When there are two normal order operators, we use generalized Wick's theorem (see Appendix B) and simplify the products.

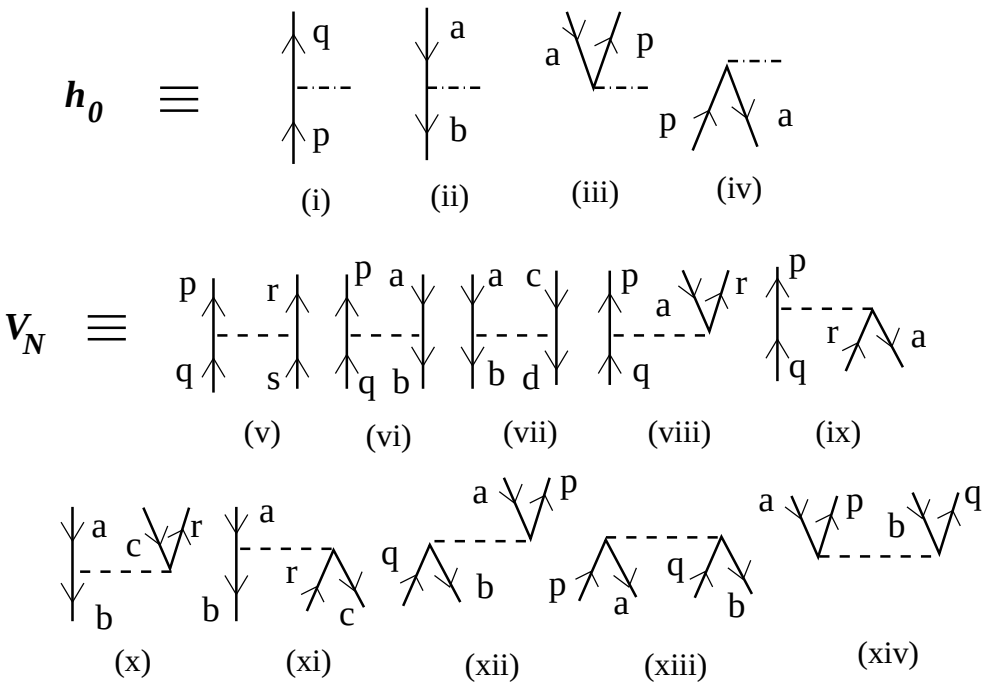

Figure 2.3: Diagrammatic representation of normal ordered one-body (h_0) and two-body (V_N) operators.

2.14 Diagrammatic representation of operators

We can express the second quantized operators, which represent electron orbitals, in a diagrammatic approach as shown in figure 2.2. Extending this representation we can also express all the normal order operators in terms of diagrams. Each second quantized operator is expressed and interpreted diagrammatically as shown in figure 2.2. We put one additional interaction line to one-body and two-body operators connecting various creation and annihilation lines. For example, we show a diagrammatic representation of a normal order Fock operator (h_0) and two-body (V_N) interaction terms in figure 2.3.

2.15 Important physical operators

In this subsection we present the single particle representation of important physical operators. These are used while calculating transition matrix elements and expectation values later.

2.15.1 Hyperfine structure

The relativistic hyperfine interaction Hamiltonian in the central potential form is given by [28]

$$H_{hf} = \sum_k \mathbf{M}^{(k)}.\mathbf{T}^{(k)} \tag{2.73}$$

where $\mathbf{M}^{(k)}$ and $\mathbf{T}^{(k)}$ are spherical tensor operators with rank 'k' in nuclear and electronic coordinates, respectively. In first order perturbation theory, the hyperfine energies for a given atomic state $|JM\rangle$ are given by

$$\begin{aligned} W(J) &= \langle IJ;F|\sum_k \mathbf{M}^{(k)}.\mathbf{T}^{(k)}|IJ;F\rangle \\ &= \sum_k (-1)^{I+J+F} \left\{ \begin{array}{ccc} J & I & F \\ I & J & k \end{array} \right\} \langle J||T^{(k)}||J\rangle\langle I||M^{(k)}||I\rangle \end{aligned} \tag{2.74}$$

where $\{\}$ represents 'six j' symbol notation, $\mathbf{I}$ is the nuclear spin momentum and $\mathbf{F} = \mathbf{I}+\mathbf{J}$ is the total angular momentum of the atomic system. Writing this in terms of multipole expansion, we have

$$W(J) = W_{M1} + W_{E2} + W_{M3} \tag{2.75}$$

where W_{M1} is the contribution due to the magnetic dipole (M1), W_{E2} is due to the electric quadrupole (E2) and W_{M3} is due to the magnetic octopole (M3) interactions. The explicit form of these terms are given by

$$W_{M1} = A\mathbf{I}.\mathbf{J} \tag{2.76}$$

$$W_{E2} = B\frac{3(\mathbf{I}.\mathbf{J})^2 + \frac{3}{2}(\mathbf{I}.\mathbf{J}) - I(I+1)J(J+1)}{2I(2I-1)J(2J-1)} \tag{2.77}$$

$$\begin{aligned} W_{M3} = {} & C\{10(\mathbf{I}.\mathbf{J})^3 + 20(\mathbf{I}.\mathbf{J})^2 + 2(\mathbf{I}.\mathbf{J})[-3I(I+1)J(J+1) + \\ & \frac{I(I+1) + J(J+1) + 3] - 5I(I+1)J(J+1)\}}{I(I-1)(2I-1)J(J-1)(2J-1)}. \end{aligned} \tag{2.78}$$

Where A, B and C are defined as hyperfine magnetic dipole, electric quadrupole and magnetic octopole constants which are given by [28, 29]

$$A = \mu_N[\frac{\mu_I}{I}]\frac{\langle J||T^{(1)}||J\rangle}{\sqrt{J(J+1)(2J+1)}} \tag{2.79}$$

$$B = 2eQ[\frac{2J(2J-1)}{(2J+1)(2J+2)(2J+3)}]^{1/2}\langle J||T^{(2)}||J\rangle \tag{2.80}$$

$$C = -\ \Omega\ \mu_N\ \frac{\langle J||T^{(3)}||J\rangle}{\sqrt{J(J+1)(2J+1)}} \tag{2.81}$$

where μ_N is the nuclear magnetic moment, $[\frac{\mu_I}{I}] = g_I$ is the nuclear Landé g- factor, Q is the nuclear electric quadrupole moment in *barns* and Ω is the nuclear magnetic moment in *barns*. These constants are derived from

$$\langle II|M^{(1)}|II\rangle = \mu_N\mu_I \tag{2.82}$$

$$\langle II|M^{(2)}|II\rangle = \frac{1}{2}Q \tag{2.83}$$

$$\langle II|M^{(3)}|II\rangle = -\ \Omega\ \mu_N \tag{2.84}$$

with

$$\langle II|M^{(k)}|II\rangle = \begin{bmatrix} I & k & I \\ -I & 0 & I \end{bmatrix}\langle II||M^{(k)}||II\rangle. \tag{2.85}$$

We use these quantities provided by Raghavan [30] and Harris [31] for our calculations of A and B.

The electronic parts of the operators are given by

$$\begin{aligned} T_q^{(1)} &= \sum t_q^{(1)} = \sum_j -ie\sqrt{8\pi/3}r_j^{-2}\alpha_{\mathbf{j}}.\mathbf{Y^{(0)}_{1q}}(\mathbf{r_j}) \\ T_q^{(2)} &= \sum t_q^{(2)} = \sum_j -ier_j^{-3}C_q^{(2)}(r_j) \\ T_q^{(3)} &= \sum t_q^{(3)} = \sum_j -ie\sqrt{8\pi/3}r_j^{-4}\alpha_{\mathbf{j}}.\mathbf{Y^{(0)}_{3q}}(\mathbf{r_j}) \end{aligned} \tag{2.86}$$

The single particle expressions for the above operators are given by [28, 29]

$$\langle\kappa m|t_q^{(1)}|\kappa' m'\rangle = -\langle -\kappa m|C_q^{(1)}|\kappa' m'\rangle(\kappa+\kappa')\int_0^\infty dr\frac{1}{r^2}(P_\kappa Q_{\kappa'} + P_\kappa Q_{\kappa'})$$

$$\begin{aligned}\langle\kappa m|t^{(2)}_q|\kappa' m'\rangle &= -\langle\kappa m|C^{(2)}_q|\kappa' m'\rangle\int_0^\infty drr^2(P_\kappa P_{\kappa'}+Q_\kappa Q_{\kappa'})\\ \langle\kappa m|t^{(3)}_q|\kappa' m'\rangle &= -\frac{1}{3}\langle -\kappa m|C^{(3)}_q|\kappa' m'\rangle(\kappa+\kappa')\int_0^\infty dr\frac{1}{r^4}(P_\kappa Q_{\kappa'}+P_\kappa Q_{\kappa'}).\end{aligned} \tag{2.87}$$

In these expressions [6, 7]

$$\langle\kappa m|C^{(k)}_q|\kappa' m'\rangle = (-1)^{j-m}\begin{pmatrix} j & k & j'\\ -m & q & m'\end{pmatrix}\langle\kappa||C^{(k)}||\kappa'\rangle \tag{2.88}$$

and

$$\langle\kappa||C^{(k)}||\kappa'\rangle = (-1)^{j+1/2}\sqrt{(2j+1)(2j'+1)}\begin{pmatrix} j & k & j'\\ 1/2 & 0 & -1/2\end{pmatrix}\pi(l,k,l') \tag{2.89}$$

with

$$\pi(l1,l2,l3)=1$$

for cases where $l1+l2+l3$ is even, and

$$\pi(l1,l2,l3)=0 \tag{2.90}$$

otherwise.

2.15.2 Transition operators

Below, we present the reduced matrix elements in terms of single particle orbitals for different electromagnetic transition operators both in length and velocity gauges [32, 33].

(I). E1 length:

$$\begin{aligned}\langle\kappa_i||d_l||\kappa_j\rangle &= \frac{3}{k}\langle\kappa_i||C^{(1)}||\kappa_j\rangle\int_0^\infty dr\{j_1(kr)[P_i(r)P_j(r)+Q_i(r)Q_j(r)]\\ &+j_2(kr)[\frac{\kappa_i-\kappa_j}{2}(P_i(r)Q_j(r)+Q_i(r)P_j(r))\\ &+(P_i(r)Q_j(r)-Q_i(r)P_j(r))]\}.\end{aligned} \tag{2.91}$$

(II). E1 velocity:

$$\begin{aligned}\langle\kappa_i||d_v||\kappa_j\rangle &= \frac{3}{k}\langle\kappa_i||C^{(1)}||\kappa_j\rangle\int_0^\infty dr\{-\frac{\kappa_i-\kappa_j}{2}\\ &[\frac{dj_1(kr)}{dkr}+\frac{j_1(kr)}{kr}][P_i(r)Q_j(r)+Q_i(r)P_j(r)]\\ &+\frac{j_1(kr)}{kr}(P_i(r)Q_j(r)-Q_i(r)P_j(r))\}. \qquad (2.92)\end{aligned}$$

(III). E2 length:

$$\begin{aligned}\langle\kappa_i||e_l||\kappa_j\rangle &= \frac{15}{k^2}\langle\kappa_i||C^{(2)}||\kappa_j\rangle\int_0^\infty dr\{j_2(kr)[P_i(r)P_j(r)+Q_i(r)Q_j(r)]\\ &+j_3(kr)[\frac{\kappa_i-\kappa_j}{3}(P_i(r)Q_j(r)+Q_i(r)P_j(r))\\ &+(P_i(r)Q_j(r)-Q_i(r)P_j(r))]\}. \qquad (2.93)\end{aligned}$$

(IV). E2 velocity:

$$\begin{aligned}\langle\kappa_i||e_v||\kappa_j\rangle &= \frac{15}{k^2}\langle\kappa_i||C^{(2)}||\kappa_j\rangle\int_0^\infty dr\{2\frac{j_2(kr)}{kr}[P_i(r)Q_j(r)-Q_i(r)P_j(r)]\\ &- \frac{\kappa_i-\kappa_j}{3}[-j_3(kr)+\frac{3}{kr}j_2(kr)](P_i(r)Q_j(r)+Q_i(r)P_j(r))\}. \qquad (2.94)\end{aligned}$$

(V). M1:

$$\begin{aligned}\langle\kappa_i||m1||\kappa_j\rangle &= \frac{6}{\alpha k}\langle-\kappa_i||C^{(1)}||\kappa_j\rangle\\ &\int_0^\infty dr\frac{\kappa_i+\kappa_j}{2}j_1(kr)(P_i(r)Q_j(r)+Q_i(r)P_j(r)). \qquad (2.95)\end{aligned}$$

(VI). M2:

$$\begin{aligned}\langle\kappa_i||m2||\kappa_j\rangle &= \frac{30}{\alpha k^2}\langle-\kappa_i||C^{(2)}||\kappa_j\rangle\\ &\int_0^\infty dr\frac{\kappa_i+\kappa_j}{3}j_2(kr)(P_i(r)Q_j(r)+Q_i(r)P_j(r)). \qquad (2.96)\end{aligned}$$

In the above expressions we define $k = w\alpha$, where $w = \epsilon_i - \epsilon_j$ is the excitation energy, α is the fine structure constant and $j_l(kr)$ is a spherical

Bessel function of order l. When kr is sufficiently small, one can apply the following approximation to calculate the above matrix elements:

$$z^{-n} j_n(z) \approx \frac{1}{1.3.5...(2n+1)}. \tag{2.97}$$

The E1, E2, M1 and M2 transition probabilities $A_{IJ}(s^{-1})$ are given in terms of line strengths S_{IF} (a.u.)

$$\begin{aligned} A_{IJ}^{E1} &= \frac{2.02613 \times 10^{18}}{[J_j]\lambda^3} S_{IJ}^{E1} \\ A_{IJ}^{E2} &= \frac{1.11995 \times 10^{18}}{[J_j]\lambda^5} S_{IJ}^{E2} \\ A_{IJ}^{M1} &= \frac{2.69735 \times 10^{13}}{[J_j]\lambda^3} S_{IJ}^{M1} \\ A_{IJ}^{M2} &= \frac{1.49097 \times 10^{13}}{[J_j]\lambda^5} S_{IJ}^{M2} \end{aligned} \tag{2.98}$$

Where $[J] = 2J+1$ is the degeneracy of the corresponding state and λ is the corresponding wavelength of the transition.

2.15.3 H_{PNC}^{NSI} matrix elements

Using Wigner-Eckart theorem, the single-particle matrix element of the nuclear spin independent PNC Hamiltonian (H_{PNC}^{NSI}) can be written as

$$\langle \phi_i | H_{PNC}^{NSI} | \phi_j \rangle = (-1)^{j_i - m_i} \begin{pmatrix} j_i & 0 & j_j \\ m_i & 0 & -m_j \end{pmatrix} \langle \phi_i || H_{PNC}^{NSI} || \phi_j \rangle \tag{2.99}$$

Writing the matrix element separately, we get

$$\begin{aligned} \langle \phi_i | H_{PNC}^{NSI} | \phi_j \rangle &= \frac{G_F}{2\sqrt{2}} Q_W \int_0^\infty dr (P_i(r)\chi^\dagger_{\kappa_i,m_i} - iQ_i\chi^\dagger_{-\kappa_i,m_i}) \begin{pmatrix} 0 & -I \\ -I & 0 \end{pmatrix} \\ &\quad \begin{pmatrix} P_j(r) & \chi_{\kappa_j,m_j} \\ iQ_j(r) & \chi_{-\kappa_j,m_j} \end{pmatrix} \rho_N(r) dr d\Omega \\ &= (-1)^{(j_i - m_i)} \delta(\kappa_i, -\kappa_j) \delta(m_i, m_j) i \frac{G_F}{2\sqrt{2}} Q_W \\ &\quad \int_0^\infty (P_i(r)Q_j(r) - Q_i(r)P_j(r)) \rho_N(r) dr, \end{aligned} \tag{2.100}$$

since

$$\int \chi^{\dagger}_{\kappa_a,m_a}\chi_{-\kappa_b,m_b}d\Omega = \delta(\kappa_a,-\kappa_b)\delta(m_a,m_b). \tag{2.101}$$

Therefore, the reduced matrix element can be written as

$$\begin{aligned}\langle\phi_i||H_{PNC}^{NSI}||\phi_j\rangle &= i\frac{G_F}{2\sqrt{2}}\ \frac{1}{\sqrt{2j_i+1}}\delta(\kappa_i,-\kappa_j)\\ &\quad \int_0^{\infty}(P_i(r)Q_j(r)-Q_i(r)P_j(r))\rho_N(r)dr. \end{aligned}\tag{2.102}$$

Bibliography

[1] F. Mandl and G. Shaw, *Quantum Field Theory*, A Wiley-Interscience Publication (1988)

[2] R. P. Feynman, *Quantum Electrodynamics*, Benjamin/Cummings Company, California USA (1961)

[3] I. Lindgren and J. Morrison, *Atomic Many-Body Theory*, edited by G. Ecker, P. Lambropoulos, and H. Walther, Springer-Verlag, Berlin (1985)

[4] A. Szabo and N. S. Ostlund, *Modern Quantum Chemistry: Introduction to Advanced Electronic structure theory*, Dover Publications Inc., *Mineola, New York*, First edition(revised), 1996

[5] R. J. Bartlett, *Modern Electronic Structure Theory*, vol-II, p.1047, Ed. D. R. Yarkony, World Scientific, Singapore (1995).

[6] M. E. Rose, *Elementary Theory of Angular Momentum*, John Wiley & Sons Inc., New York (1957)

[7] A.R. Edmonds, *Angular Momentum in Quantum Mechanics*, Princeton, New Jersey Princeton University Press, Second Edition (1960)

[8] D. M. Brink and G. R. Satchler, *Angular Momentum*, Clarendon Press, Oxford (1968)

[9] J. J. Sakurai, *Advance Quantum Mechanics*, Addison-Wesley Publishing Company, Inc., UK (1987)

[10] I. P. Grant, Relativistic self-consistent fields, Proc. R. Soc. London Ser. A **262**, 555 (1961)

[11] I. P. Grant, Adv. Phys. **19**, 747 (1970)

[12] I. P. Grant, *Relativistic Atomic Structure Calculations*, Methods in Computational Chemistry, Edt. by S. Wilson, Plenum Press (New York) (1988)

[13] L. I. Schiff, *Quantum Mechanics*, McGraw-Hill Book Company, New York (1968)

[14] B. H. Bransden and C. J. Joachain, *Physics of Atoms and Molecules*, Prentice Hall Publication (2003)

[15] G. Breit, Phys. Rev. **34**, 553 (1929)

[16] I. P. Grant and N. C. Pyper , J. Phys. B **9**, 761 (1976)

[17] I. P. Grant and B. J. McKenzie, J. Phys. B **13**, 2671 (1980)

[18] W. R. Johnson, S. A. Blundell, and J. Sapirstein, Phys. Rev. A **37**, 2764(1988)

[19] J. P. Desclaux, A Relativistic Multiconfiguration Dirac-Fock Package, Methods and Techniques in Computational Chemistry, Edited by E. Cleminti Cagliary, STEF. A (1993)

[20] J. P. Desclaux, Relativistic Multiconfiguration Package, *Private Communication* (2004); (Published elsewhere).

[21] Y. K. Kim, Phys. Rev. **154**, 17 (1967)

[22] R. K. Chaudhuri, P. K. Panda and B. P. Das, *Phys. Rev. A*, **59**, 1187 (1999)

[23] F. A. Parpia, Integral Generation for Relativistic Multiconfiguration Dirac-Fock Calculations using Gaussian Basis Sets, *Private Communication* (2004); (Published elsewhere).

[24] R.E. Stanton and S. Havriliak, J. Phys. B **81**, 1910(1984)

[25] A. K. Mohanty and E. Clementi, *Kinetically Balanced Geometric Gaussian Basis Set Calculations for Relativistic Many-Electron Atoms*, Chapter 4 of Modern Techniques in Computational Chemistry, Ed. E. Clementi (1989)

[26] H. De Vries *et al.*, *Nuclear Charge Density Distribution Parameters*, Atomic Data and Nuclear Tables, **36**, 502 (1987)

[27] F. A. Parpia and A. K. Mohanty, Phys. Rev. A **46**, 3735 (1992)

[28] Charles Schwartz, Phys. Rev. **97**, 380 (1955)

[29] K. T. Cheng and W. J. Childs, Phys. Rev. A **31**, 2775 (1985)

[30] P. Raghavan, Atomic Data and Nuclear Data Tables **42**, 189 (1989)

[31] R. K. Harris, *Encyclopedia of Nuclear Magnetic Resonance*, Edited by D. M. Granty and R. K. Harris **5**, John Wiley and Sons, Chichester, U.K. (1996)

[32] W. C. Martin and W. L. Wiese, p. 135, *Atomic, Mecular and Optical Physics Handbook*, ed. W. F. Drake Gordon, AIP Press, Woodburg, NY (1996).

[33] Igor I. Sobelman, *Introduction to the Theory of Atomic Spectra*, Pergamon Press, Oxford (1972)

Chapter 3

Relativistic Coupled-cluster Theory

3.1 Introduction

It is well known that the Schrödinger equation cannot be solved exactly for atoms having two or more electrons [1]. The calculation of parity non-conservation (PNC) observables, which are used for testing the SM of particle physics require very accurate atomic wavefunctions [2, 3, 4]. Furthermore, since atomic PNC scales as Z^3 [5], these calculations must be based on relativistic many-body theories. Although the Dirac-Coulomb Hamiltonian is not covariant, it incorporates the dominant relativistic effects and hence has been used in our calculations. Contributions from the Breit interaction [6, 7, 8, 9] have been verified, but a detailed analysis of these contributions are necessary. Quantum electrodynamics (QED) corrections [10, 11] in the bound electrons of the system have not been considered as their contributions to the physical effects of interest to us are rather small. The former arises from the exchange of transverse photons between electrons and is two orders of magnitude weaker than the Coulomb interaction [6].

Several relativistic many-body theories have been used in atomic structure calculations. Prominent among them are the relativistic multi-configuration

Dirac-Fock (RMCDF) method [12, 13], relativistic configuration interaction (RCI) method [14], relativistic many-body perturbation theory (RMBPT) [15, 16] and its all order generalization, relativistic coupled-cluster theory (RCC) [17, 18, 19].

The work carried out in this thesis is based on RCC theory as it has some distinct advantages over the RMCDF and the RCI methods. RCC theory takes into account a larger class of correlation effects than the other two theories at the same level of approximation [1, 20]. For example, at the singles and doubles level, nonlinear combinations of single and/or double excitations are included in RCC theory in contrast to the RMCDF and RCI methods. Unlikely the RMCDF and RCI methods, RCC theory is size extensive [1, 21].

3.2 Coupled-cluster wavefunction

Coupled-cluster (CC) theory has been used to study a wide range of many-body systems and has been referred to as the universal many-body theory [22, 23, 24]. It has recently been applied to calculate ground and excited-state properties of nuclei [25]. Although the non-relativistic version of this theory has been very successfully applied to a variety of light atoms and molecules [26, 27, 28], its extension to the relativistic regime is rather recent [2, 7, 29, 30]. There have been relatively few theoretical studies of the properties of heavy atomic systems based on the RCC theory.

The CC wavefunction for a many-electron atom incorporates the effects of electron correlation to all orders in many-body perturbation theory (MBPT) [1, 22]. To derive the explicit form of this wavefunction, we consider the electron-electron interactions beyond the *independent particle model*. These interactions will result in single, double and higher order excitations from the Fermi vacuum. In addition there will be excitations involving independent single and double excitations, one single and one double excitation et cetera.

3.2.1 Closed-shell system

Since the atomic wavefunction is the probability amplitude representing all the independent excitations, for the closed-shell system it can be written as [17, 21]

$$|\Psi\rangle = [1 + T_1 + \frac{1}{2}T_1^2 + T_2 + \frac{1}{3!}T_1^3 + T_1T_2 + \frac{1}{2}T_2^2 + \frac{1}{4!}T_1^4 + \cdots]|\Phi_0\rangle \quad (3.1)$$

where $|\Phi_0\rangle$ represents the independent particle model wavefunction also known as the reference function or Fermi vacuum. It is customary to take this is as the Hartree-Fock (HF)/Dirac-Fock (DF) wavefunction. T_1 and T_2 are single and double excitation operators producing one hole-one particle and two hole-two particle states.

The above equation can be expressed as

$$|\Psi\rangle = e^T|\Phi_0\rangle \quad (3.2)$$

where

$$T = T_1 + T_2 + \cdots. \quad (3.3)$$

In the second quantized notation these operators can be expressed as

$$\begin{aligned} T &= T_1 + T_2 + \cdots \\ &= \sum_{a,p} t_a^p a_p^\dagger a_a + \frac{1}{4}\sum_{ab,pq} t_{ab}^{pq} a_p^\dagger a_q^\dagger a_b a_a + \cdots \end{aligned} \quad (3.4)$$

where t_a^p and t_{ab}^{pq} represent amplitudes due to single excitation from core electron 'a' to virtual particle 'p' and double excitation from core electrons 'a and b' to virtual particles 'p and q', respectively.

It can be noted from the explicit form of the T operator that it is already expressed in the normal order form.

3.2.2 Single valence systems

The work described in this thesis deals only with the atomic systems having a single valence electron. For such systems the reference state can be

constructed as

$$|\Phi_v\rangle = a_v^\dagger |\Phi_0\rangle \tag{3.5}$$

where $|\Phi_0\rangle$, as defined earlier, is the DF closed-shell reference state and $a_v^\dagger$ is the creation operator for the valence electron.

The RCC wavefunction for a single valence system is given by [31]

$$|\Psi_v\rangle = e^T\{1 + S_v\}|\Phi_v\rangle \tag{3.6}$$

where the operator T is applied only to excite the occupied (core) electrons and S_v produces excitations from the valence sector and the core as well as for double and higher order excitations. The curly bracket around the operator S_v represents the normal order. The linearized form of the S_v operator is a consequence of the fact that the system has only a single valence electron. In the second quantized notation the single valence RCC operators can be written as

$$\begin{aligned} S_v &= S_{1v} + S_{2v} + \cdots \\ &= \sum_{p \neq v} s_v^p a_p^\dagger a_v + \frac{1}{2}\sum_{b,pq} s_{vb}^{pq} a_p^\dagger a_q^\dagger a_b a_v + \cdots \end{aligned} \tag{3.7}$$

where s_v^p is the amplitude for the excitation of the valence electron and s_{vb}^{pq} is the amplitude of the excitation involving the valence and a core electron.

The restriction over the summation for the single excitation ensures that the excitation from the valence electron 'v' to 'v', which does not correspond to any physical process, is not counted. A useful way of imagining the single excitation is by considering the valence electron v to be a spectator and allowing a hole to excite to any virtual state through the S_{2v} operator by allowing the virtual electrons denoted by 'p' or 'q' to be valence electron of the system.

3.2.3 Diagrammatic representation of CC operators

We represent the above CC operators for both closed-shell and open-shell systems in the diagrammatic approach as shown by figure 3.1 with their

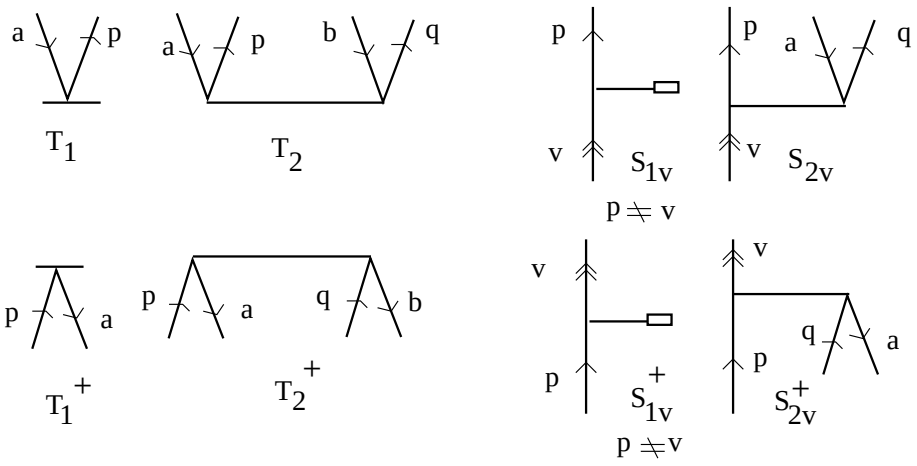

Figure 3.1: Diagrammatic representation of CC operators and their conjugates. Double arrow represents the valence electron v.

conjugates. They satisfy the time ordering property from bottom to top as Goldstone diagrams representing MBPT [1, 21].

The double arrow in a particle line represents a valence electron and cannot be contracted with any core or virtual electron.

3.3 Equivalence of All Order MBPT and CC

In order to establish the equivalence between all order MBPT and CC, we write the MBPT wavefunction as [1, 20]

$$\begin{aligned} |\Psi_{MBPT}\rangle &= |\Phi_v\rangle + |\Phi_v^{(1)}\rangle + |\Phi_v^{(2)}\rangle + \cdots \\ &= |\Phi_v\rangle + \sum_{I\neq v} C_I(1)|\Phi_I\rangle + \sum_{J\neq v} C_J(2)|\Phi_J\rangle + \cdots \end{aligned} \tag{3.8}$$

where $|\Phi_v^{(1)}\rangle$ and $|\Phi_v^{(2)}\rangle$ are the first and second order perturbed wavefunctions. Here $|\Phi_I\rangle$ and $|\Phi_J\rangle$ represent intermediate excited determinantal states and $C_I(1)$ and $C_J(2)$ are the coefficients for first order and second order perturbed wavefunctions, respectively. These corrected wavefunctions are linear combinations of different excited states. Therefore, one can collect all the

single, double etc. excitation amplitudes and put them together as

$$\begin{aligned}
|\Psi_{MBPT}\rangle &= |\Phi_v\rangle + \sum_{a,p}(C_a^p(1,1) + C_a^p(2,1) + \cdots)|\Phi_a^p\rangle \\
&\quad + \sum_{p\neq v}(C_v^p(1,1) + C_v^p(2,1) + \cdots)|\Phi_v^p\rangle \\
&\quad + \frac{1}{2}\sum_{abpq}(C_{ab}^{pq}(1,2) + C_{ab}^{pq}(2,2) + \cdots)|\Phi_{ab}^{pq}\rangle + \cdots \\
&\quad + \frac{1}{2}\sum_{bpq}(C_{vb}^{pq}(1,2) + C_{vb}^{pq}(2,2) + \cdots)|\Phi_{vb}^{pq}\rangle + \cdots
\end{aligned}$$

where C_i^j, $C_{ij}^{kl}\cdots$ represent the coefficients of the single, double etc. excitation states. The first index inside the parentheses represent the order of V_N included in the term and the second index represents the level of excitation from the reference state. Expanding in terms of second quantized operators, we get

$$\begin{aligned}
|\Psi_{MBPT}\rangle &= |\Phi_v\rangle + \sum_{ap}(C_a^p(1,1) + C_a^p(2,1) + \cdots)a_p^\dagger a_a|\Phi_0\rangle \\
&\quad + \sum_{p\neq v}(C_v^p(1,1) + C_v^p(2,1) + \cdots)a_p^\dagger a_v|\Phi_0\rangle \\
&\quad + \frac{1}{2}\sum_{abpq}(C_{ab}^{pq}(1,2) + C_{ab}^{pq}(2,2) + \cdots)a_p^\dagger a_q^\dagger a_b a_a|\Phi_0\rangle + \cdots \\
&\quad + \frac{1}{2}\sum_{bpq}(C_{vb}^{pq}(1,2) + C_{vb}^{pq}(2,2) + \cdots)a_p^\dagger a_q^\dagger a_b a_v|\Phi_v\rangle + \cdots \\
&= |\Phi_v\rangle + \sum_{ap} t_a^p a_p^\dagger a_a|\Phi_0\rangle + \frac{1}{2}\sum_{abpq} t_{ab}^{pq} a_p^\dagger a_q^\dagger a_b a_a|\Phi_0\rangle + \cdots \\
&\quad + \sum_{p\neq v} s_v^p a_p^\dagger a_v|\Phi_v\rangle + \frac{1}{2}\sum_{bpq} s_{vb}^{pq} a_p^\dagger a_q^\dagger a_b a_v|\Phi_v\rangle + \cdots \\
&\quad + \frac{1}{2}\sum_{abpq} t_a^p t_b^q a_p^\dagger a_q^\dagger a_b a_a \Phi_0\rangle + \cdots \\
&= (1 + T_1 + T_2 + \frac{1}{2}T_1^2 + \cdots)|\Phi_v\rangle + S_{1v}|\Phi_v\rangle + S_{2v}|\Phi_v\rangle + \cdots \\
&= e^T\{1 + S_v\}|\Phi_v\rangle \\
&\equiv |\Psi_{CC}\rangle
\end{aligned} \tag{3.9}$$

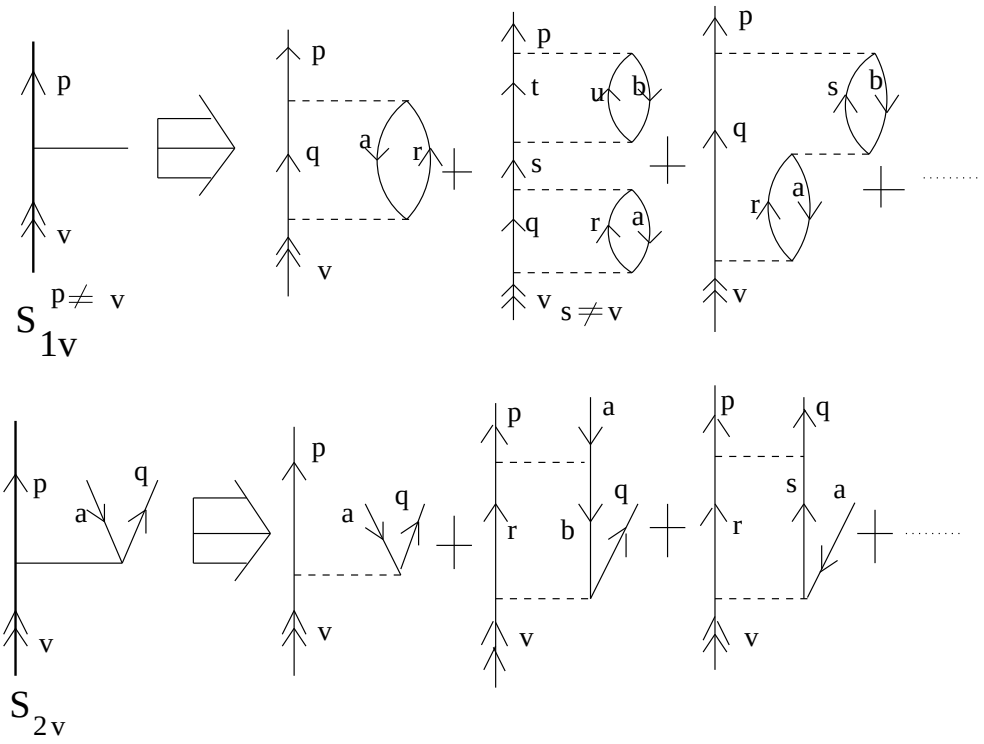

Figure 3.2: CC diagrams for S_{1v} and S_{2v} and some of their corresponding MBPT diagrams.

where

$$\begin{aligned} t_a^p &= C_a^p(1,1) + C_a^p(2,1) + \cdots \\ s_v^p &= C_v^p(1,1) + C_v^p(2,1) + \cdots \\ t_{ab}^{pq} + t_a^p t_b^q &= C_{ab}^{pq}(1,2) + C_{ab}^{pq}(2,2) + \cdots \\ s_{vb}^{pq} &= C_{vb}^{pq}(1,2) + C_{vb}^{pq}(2,2) + \cdots \end{aligned} \tag{3.10}$$

Therefore, ultimately we obtain the CC operators from the MBPT wavefunctions as

$$\begin{aligned} T_1 &= \sum_{ap} t_a^p a_p^\dagger a_a \\ S_{1v} &= \sum_{p \neq v} s_v^p a_p^\dagger a_v \end{aligned}$$

$$T_2 = \frac{1}{4}\sum_{abpq} t_{ab}^{pq} a_p^\dagger a_q^\dagger a_b a_a$$
$$S_{2v} = \frac{1}{2}\sum_{bpq} s_{vb}^{pq} a_p^\dagger a_q^\dagger a_b a_v.$$

This relationship can be expressed diagrammatically as shown by figure 3.2.

3.4 Equations for determining CC amplitudes

It is necessary to solve the coupled-cluster amplitudes both for closed-shell and a single valence system in order to obtain the atomic wavefunctions which can be used to determine various atomic properties. We solve the Dirac-Fock (DF) wavefunction for the closed-shell as discussed in the previous chapter. This DF function is considered as the reference state for the closed-shell and we express different cluster operators as described in the previous sections.

As the CC wavefunctions have an exponential structure, there are non-linear terms in the amplitude equations. It is clearly difficult to consider the non-linear terms as well as all core and valence excitations when solving for the wavefunctions of a heavy atomic system. In practice, one often approximates by considering only certain non-linear terms and only important excitations at a reasonable level of approximation depending on the problem of interest. For important problems single and double excitations give the largest contributions [1, 32]. Therefore, a large number of calculations are carried out using only single and double excitations and the method is known as CCSD.

Sometime it is very difficult, for large systems, to cope with the non-linear terms even in the CCSD approximations. Therefore, many calculations are carried out using only the linear terms of the exponential function of the CC wavefunction [2, 8] and the application of the non-linear formulation of CC is rather recent. We discuss the cluster amplitude equations for both the linearized and non-linearized CC method.

3.4.1 Linearized CC theory

Due to the enormous computational effort needed to solve the CC amplitude equations for heavy atomic systems, a linearized version of this theory has been used in the calculations of the properties of these systems. We present here the working equations for this method. We first solve the closed-shell system and obtain amplitudes for the T operators. Using these amplitudes we find the amplitudes for the S_v operators. This procedure simplifies some of the computational complexities, but the price to be paid is by storing the closed-shell amplitudes on the hard disk of the computer. Below we give a detailed description of the computational procedure.

3.4.1.1 Closed-shell equations

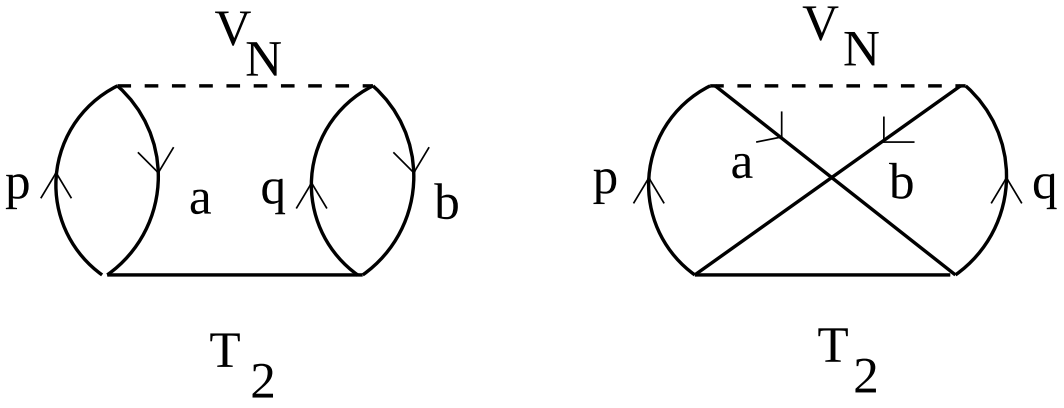

Figure 3.3: Diagrammatic representation of ΔE_{corr} for LCCSD.

The atomic wavefunction for a closed-shell system in the CC method is given by [1, 17]

$$|\Psi\rangle = e^T|\Phi_0\rangle. \tag{3.11}$$

Therefore, the eigenvalue equation for the state $|\Psi\rangle$ is given by

$$\begin{aligned} H|\Psi\rangle &= E|\Psi\rangle, \\ He^T|\Phi_0\rangle &= Ee^T|\Phi_0\rangle. \end{aligned}$$

Subtracting $\langle\Phi_0|H|\Phi_0\rangle$ and operating from the left by e^{-T} on both sides of the above equation, we get

$$e^{-T}(H - \langle\Phi_0|H|\Phi_0\rangle)e^{T}|\Phi_0\rangle \;=\; (E - E_{DF})|\Phi_0\rangle$$

where the DF energy is defined as $E_{DF} = \langle\Phi_0|H|\Phi_0\rangle$. From the definition of the normal order form we obtain

$$\begin{aligned} e^{-T}H_N e^{T}|\Phi_0\rangle &= \Delta E_{corr}|\Phi_0\rangle, \\ \overbrace{(H_N e^{T})}|\Phi_0\rangle &= \Delta E_{corr}|\Phi_0\rangle. \end{aligned} \tag{3.12}$$

The brace in the left hand side of the equation over the operators represents connected terms. H_N is the normal order form of the Hamiltonian and ΔE_{corr} is the correlation energy of the system over the DF energy. To evaluate the connected terms given in the left hand side of the above equation, we follow the generalized Wick's theorem (see Appendix B).

The correlation energy (ΔE_{corr}) can be obtained by operating by $\langle\Phi_0|$ in the above equation:

$$\langle\Phi_0|\overbrace{H_N e^{T}}|\Phi_0\rangle \;=\; \Delta E_{corr} \tag{3.13}$$

and in the linearized approximation this can be expressed as

$$\langle\Phi_0|H_N + \overbrace{H_N T}|\Phi_0\rangle \;=\; \Delta E_{corr} \tag{3.14}$$

where the first term vanishes in accordance with the definition of normal order. In the linearized CC theory with single and double excitations (LCCSD), the correlation energy diagrams are given by figure 3.3.

The T operator amplitudes are determined by projecting by $\langle\Phi_0^*|$ from the left side of equation (3.12), where $|\Phi_0^*\rangle$ denotes necessary single, double etc. excited states:

$$\langle\Phi_0^*|\overbrace{H_N e^{T}}|\Phi_0\rangle \;=\; 0. \tag{3.15}$$

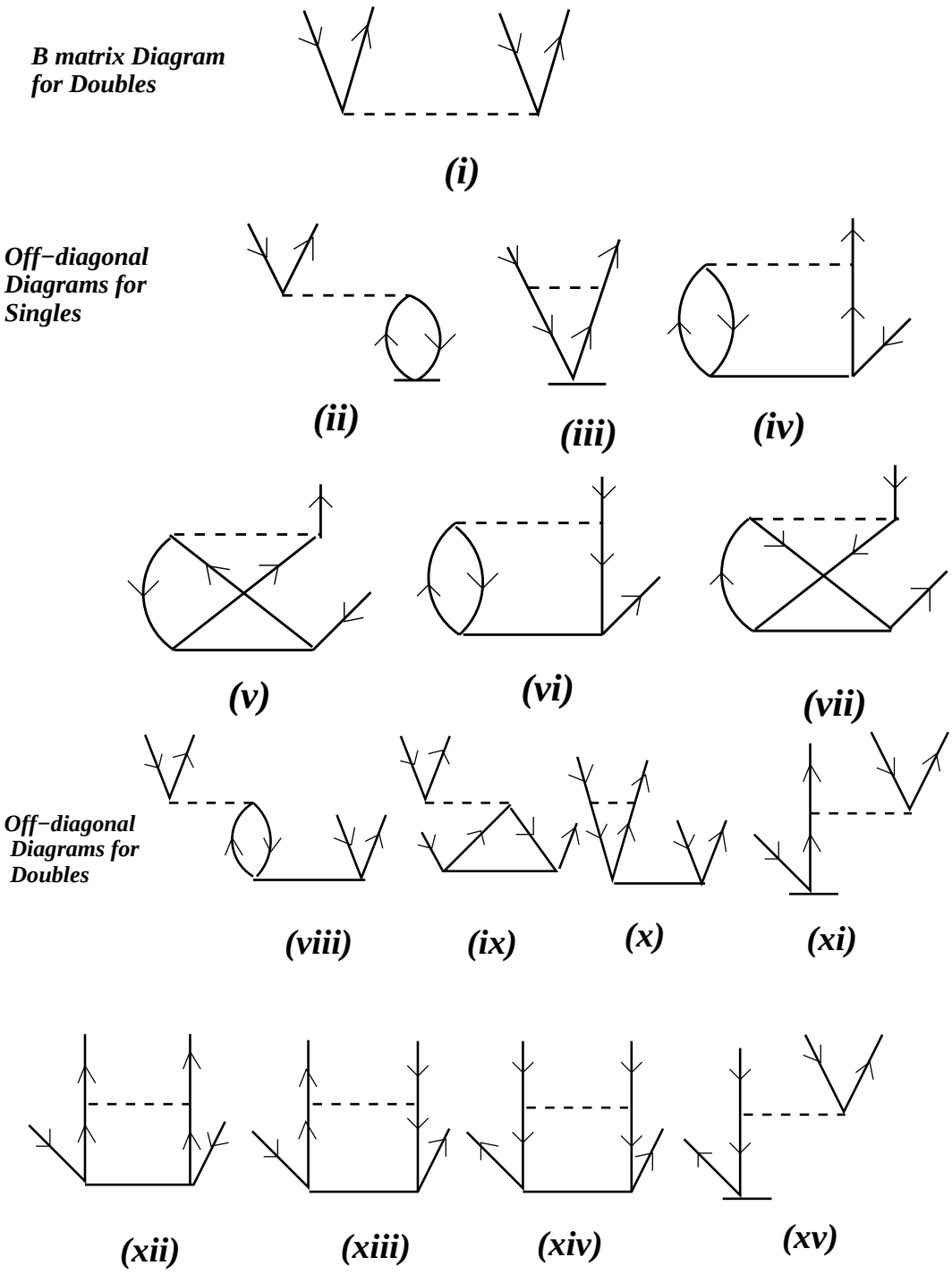

Figure 3.4: Diagrams connecting to T- amplitude calculation using LCCSD.

For linearized CC, the above equation yields

$$\langle \Phi_0^* | \widetilde{H_N T} | \Phi_0 \rangle \;=\; -\langle \Phi_0^* | H_N | \Phi_0 \rangle. \tag{3.16}$$

To solve the amplitude equation given by equation (3.16), we formulate the following matrix equation

$$\begin{pmatrix} \langle \Phi_a^p | H_N | \Phi_a^p \rangle & \langle \Phi_a^p | H_N | \Phi_{ab}^{pq} \rangle \\ \langle \Phi_{ab}^{pq} | H_N | \Phi_a^p \rangle & \langle \Phi_{ab}^{pq} | H_N | \Phi_{ab}^{pq} \rangle \end{pmatrix} \begin{pmatrix} t_a^p \\ t_{ab}^{pq} \end{pmatrix} = - \begin{pmatrix} \langle \Phi_a^p | H_N | \Phi_0 \rangle \\ \langle \Phi_{ab}^{pq} | H_N | \Phi_0 \rangle \end{pmatrix}$$

which can be written as

$$\mathbf{A} \cdot \mathbf{X} \;=\; -\mathbf{B}. \tag{3.17}$$

The j^{th} element of the vector $\mathbf{X}$, which represents the T operator, can be solved iteratively by

$$X_j^i \;=\; \frac{-B_j - \sum_{l \neq j} A_{jl} X_l^{(i-1)}}{A_{jj}} \tag{3.18}$$

where the 'i' represents the iteration number. A_{jl} and A_{jj} represent off diagonal and diagonal elements of the matrix $\mathbf{A}$, respectively. Obviously, the diagonal elements are nothing but the single particle orbital energies here.

The $\mathbf{B}$ matrix elements and off-diagonal elements of matrix $\mathbf{A}$ for the LCCSD method are given diagrammatically by figure 3.4. The T- amplitudes are solved by using the Jacobi iterative method where the initial value for the single and double excited amplitudes are given by

$$\begin{aligned} (t_a^p)^{(1)} &= 0 \\ (t_{ab}^{pq})^{(1)} &= -\frac{\langle pq | \frac{1}{r_{12}} | ab \rangle}{\epsilon_p + \epsilon_q - \epsilon_a - \epsilon_b}, \end{aligned} \tag{3.19}$$

respectively. The initial value for the $(t_a^p)^{(1)}$ is zero which follows from *Brillouin's condition* (See Appendix B) and ϵ's are the DF single particle orbital energies. Due to the coupling between single and double excited cluster amplitudes, the value of t_a^p becomes finite at higher order through the iterative process.

3.4.1.2 Open-shell CC equations

The open-shell atomic wavefunction with the valence electron 'v' in the CC method is given by [31]

$$|\Psi_v\rangle = e^T\{1+S_v\}|\Phi_v\rangle. \tag{3.20}$$

The equation of state is given by

$$\begin{aligned} H|\Psi_v\rangle &= E_v|\Psi_v\rangle \\ He^T\{1+S_v\}|\Phi_v\rangle &= E_v e^T\{1+S_v\}|\Phi_v\rangle. \end{aligned}$$

Operating by e^{-T} and using the definition of normal order form, we have

$$\begin{aligned} e^{-T}He^T\{1+S_v\}|\Phi_v\rangle &= E\{1+S_v\}|\Phi_v\rangle \\ ((e^{-T}H_Ne^T)_{op} + \langle\Phi_0|e^{-T}He^T|\Phi_0\rangle)\{1+S_v\}|\Phi_v\rangle &= E_v\{1+S_v\}|\Phi_v\rangle \\ (\overbrace{(He^T}^{})_{op} + E_g)\{1+S_v\}|\Phi_v\rangle &= E_v\{1+S_v\}|\Phi_v\rangle \\ \overbrace{(He^T}^{})_{op}\{1+S_v\}|\Phi_v\rangle &= (E_v - E_g)\{1+S_v\}|\Phi_v\rangle \\ \overbrace{(He^T}^{})_{op}\{1+S_v\}|\Phi_v\rangle &= \Delta E_v\{1+S_v\}|\Phi_v\rangle \end{aligned} \tag{3.21}$$

where the term $e^{-T}He^T$ has been decomposed into an open part ($(e^{-T}H_Ne^T)_{op}$), which can be contracted with the valence electron of the reference state by expanding it as $|\Phi_v\rangle = a_v^\dagger|\Phi_0\rangle$, and a completely contracted term giving rise to the ground state energy (E_g) for the closed-shell system. ΔE_v is the difference between the energy of the open-shell state with valence electron 'v' and the ground state energy of the closed-shell system, and is defined as the electron affinity energy or the negative of the ionization potential (IP) for the valence electron (v).

The IP and S_v operator amplitudes can be determined by applying $\langle\Phi_v|$ and $\langle\Phi_v^*|$, respectively, where $|\Phi_v^*\rangle$ denotes necessary single, double, etc. excited states from $|\Phi_v\rangle$, in the left side of the above equation:

$$\langle\Phi_v|\overbrace{(H_Ne^T}^{})_{op}\{1+S_v\}|\Phi_v\rangle = \Delta E_v \tag{3.22}$$

$$\langle\Phi_v^*|\overbrace{(H_Ne^T}^{})_{op}\{1+S_v\}|\Phi_v\rangle = \Delta E_v\langle\Phi_v^*|S_v|\Phi_v\rangle. \tag{3.23}$$

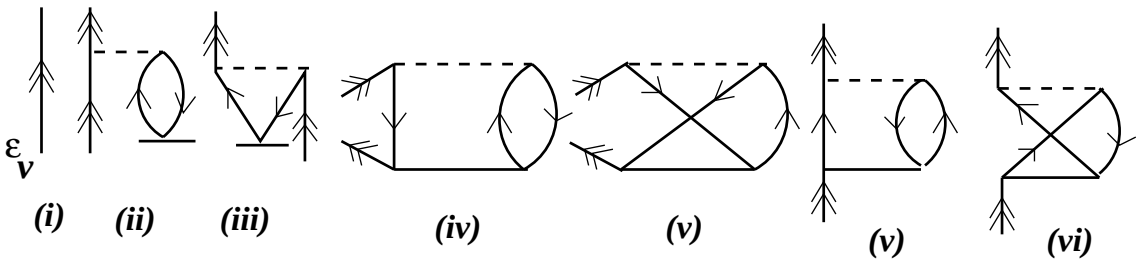

Figure 3.5: Ionization potential diagrams for LCCSD.

In the linearized CC, the above equations can be expressed as

$$\langle\Phi_v|H_N + \widetilde{(H_N T)}_{op} + \widetilde{(H_N S_v)}_{op}|\Phi_v\rangle = \Delta E_v, \qquad (3.24)$$

$$\langle\Phi_v^*|\widetilde{(H_N S_v)}_{op}|\Phi_v\rangle = -\langle\Phi_v^*|H_N + \widetilde{(H_N T)}_{op}|\Phi_v\rangle + \epsilon_v\langle\Phi_v^*|S_v|\Phi_v\rangle. \qquad (3.25)$$

We use only ϵ_v from ΔE_v, as other terms from equation (3.23) after taking the product with $\langle\Phi_v^*|S_v|\Phi_v\rangle$ will effectively be non-linear terms.

The IP diagrams using the LCCSD method are given by figure 3.5. To solve the amplitude equations we formulate matrix equations similar to these for the case of the closed-shell equations,

$$\begin{pmatrix} \langle\Phi_v^p|H_N - \epsilon_v|\Phi_a^p\rangle & \langle\Phi_v^p|H_N|\Phi_{vb}^{pq}\rangle \\ \langle\Phi_{vb}^{pq}|H_N|\Phi_v^p\rangle & \langle\Phi_{vb}^{pq}|H_N - \epsilon_v|\Phi_{vb}^{pq}\rangle \end{pmatrix} \begin{pmatrix} s_v^p \\ s_{vb}^{pq} \end{pmatrix} = - \begin{pmatrix} \langle\Phi_v^p|H_N + \widetilde{H_N T}|\Phi_v\rangle \\ \langle\Phi_{vb}^{pq}|H_N + \widetilde{H_N T}|\Phi_v\rangle \end{pmatrix}$$

or,

$$\begin{aligned} \mathbf{A}\cdot\mathbf{X} &= -\mathbf{B} \\ X_j^i &= \frac{-B_j - \sum_{l\neq j} A_{jl} X_l^{(i-1)}}{A_{jj}} \end{aligned} \qquad (3.26)$$

where 'i' represents the iteration number for the solution of element X_j which stands for the 'j^{th}' element of the S_v operator. A_{jl} and A_{jj} are the off diagonal and diagonal elements of the above **A** matrix. The diagonal elements are nothing but the single particle orbital energies. The above equation is solved

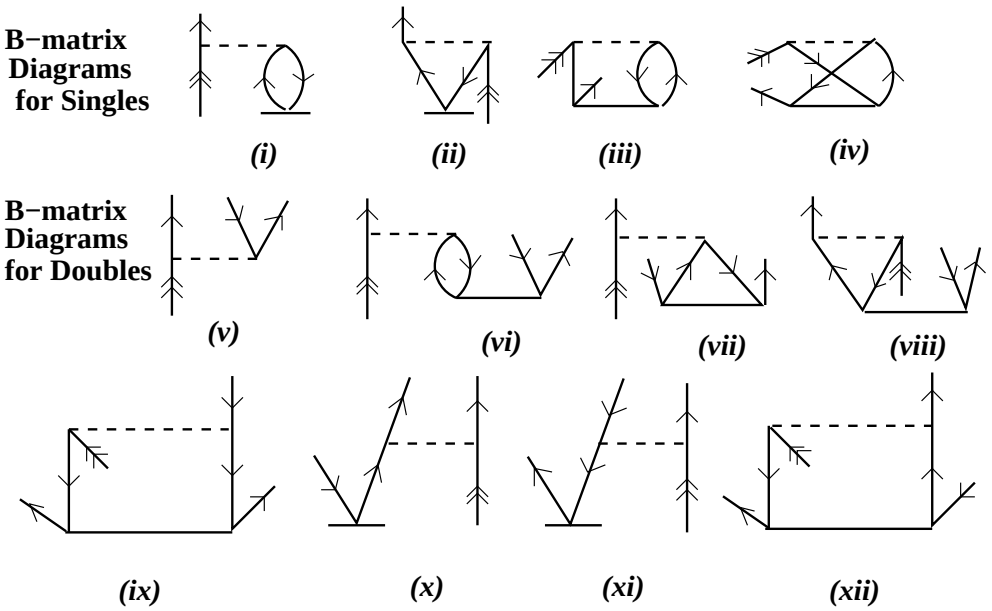

Figure 3.6: Diagrams connecting B- matrix of S_v- amplitudes using LCCSD.

using the Jacobi iterative method. The initial value for the single and double excited states are taken following the *Brillouin's condition* as

$$\begin{aligned} (s_v^p)^{(1)} &= 0 \\ (s_{vb}^{pq})^{(1)} &= -\frac{\langle pq|\frac{1}{r_{12}}|vb\rangle}{\epsilon_p + \epsilon_q - \epsilon_v - \epsilon_b}, \end{aligned} \tag{3.27}$$

respectively. The diagrammatic representation of **B** and the off diagonal matrix elements are shown by figures 3.6 and 3.7, respectively.

3.4.1.3 Matrix element of physical operator

The transition matrix elements of any general operator can be expressed using the CC method for a single valance system as

$$\langle O\rangle_{fi} = \frac{\langle\Psi_f|\{1+S_f^\dagger\}e^{T^\dagger}Oe^T\{1+S_i\}|\Psi_i\rangle}{\langle\Psi_f|\{1+S_f^\dagger\}e^{T^\dagger}e^T\{1+S_i\}|\Psi_i\rangle} \tag{3.28}$$

where i and f are the indices used to represent the initial and final states. For determining the expectation value one can use the special condition that

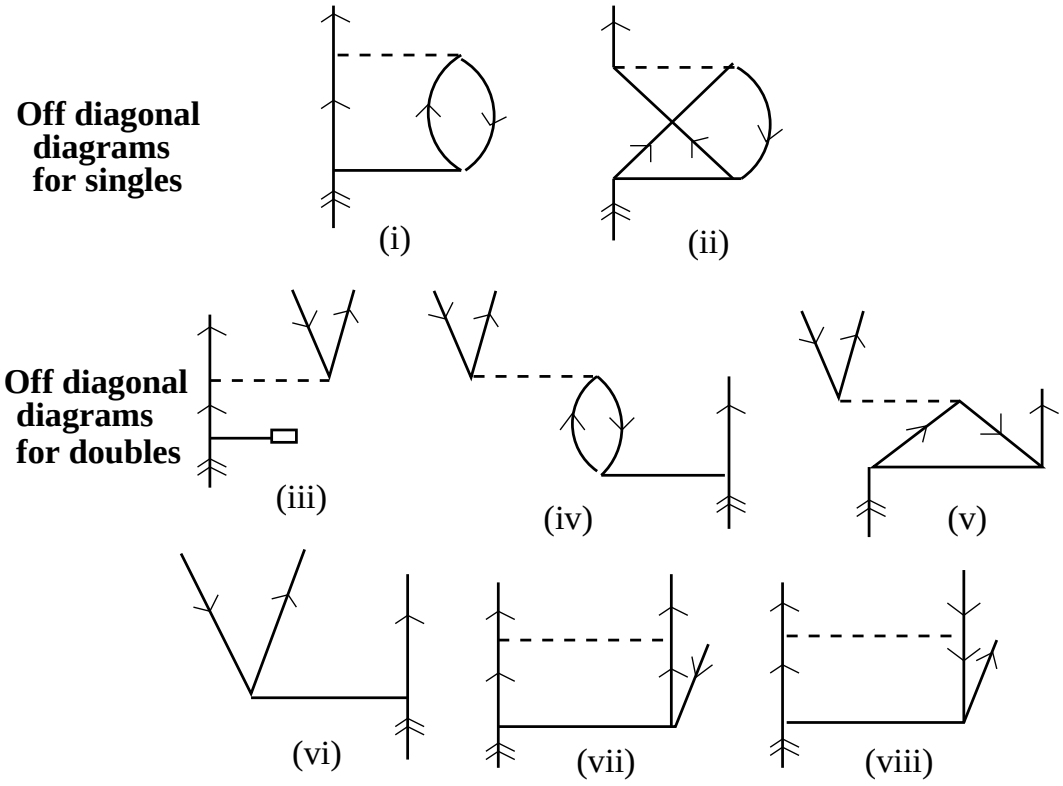

Figure 3.7: Diagrams connecting to off-diagonal elements of S_v- amplitude using LCCSD.

i is equal to f.

In particular for the linearized CC, the above expression yields

$$\langle D\rangle_{fi} = \frac{\langle\Psi_f|\{1+S_f^\dagger+T^\dagger\}D\{1+T+S_i\}|\Psi_i\rangle}{\langle\Psi_f|\{1+S_f^\dagger+T^\dagger\}\{1+T+S_i\}|\Psi_i\rangle}. \tag{3.29}$$

In the LCCSD approach, both $T^\dagger DT$ and $T^\dagger T$ truncate at $T_2^\dagger DT_2$ and $T_2^\dagger T_2$. But when applying Wick's theorem one can get a large number of possible diagrams in the property calculation. Therefore, we decompose these operators by effective one-body, two-body operators and so on. In principle, only terms up to effective three-body terms will contribute to the calculation, because these terms have to be contracted finally with S_v and/or its conjugate operators in order to determine the result. We consider only the effective one-body terms which are more important and then add the maximum contributing two-body terms. Other terms are of higher order and can be neglected. We have given all the property diagrams for the LCCSD method in figure 3.8.

3.4.2 Non-linear CC theory

As mentioned earlier, due to the computational complexity required in considering the non-linear terms in the coupled-cluster theory, many atomic properties are calculated at the linearized level. However, there are rare cases where these terms have to be included at the level of single and double excitations (CCSD). High precision calculations like PNC studies on heavy atomic systems require inclusion of these terms in order to achieve high accuracy. Considering non-linear terms may cause difficulties in constructing the matrix equations for solving CC amplitudes. We give here a prescription for handling such issues which have been applied in the present case.

It should be noted that computing each non-linear term itself directly may require an enormous amount of time. The total number of computational operations can be reduced by splitting all the non-linear terms into intermediate parts. There are many ways to construct such intermediate terms [32]. It is possible to break the non-linear terms in such a way that it take least

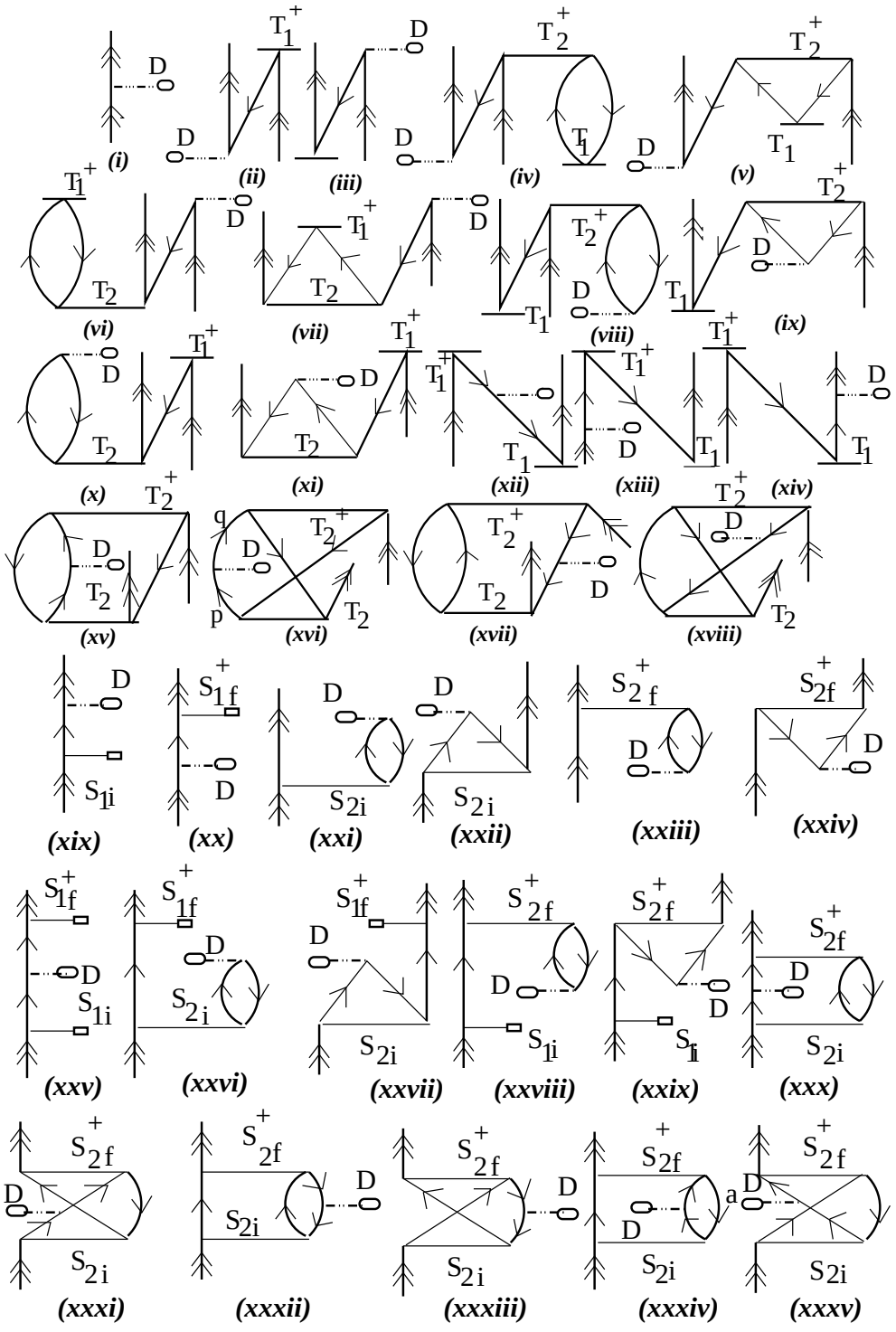
(i)
(ii)
(iii)
(iv)
(v)
(vi)
(vii)
(viii)
(ix)
(x)
(xi)
(xii)
(xiii)
(xiv)
(xv)
(xvi)
(xvii)
(xviii)
(xix)
(xx)
(xxi)
(xxii)
(xxiii)
(xxiv)
(xxv)
(xxvi)
(xxvii)
(xxviii)
(xxix)
(xxx)
(xxxi)
(xxxii)
(xxxiii)
(xxxiv)
(xxxv)

Cont.....

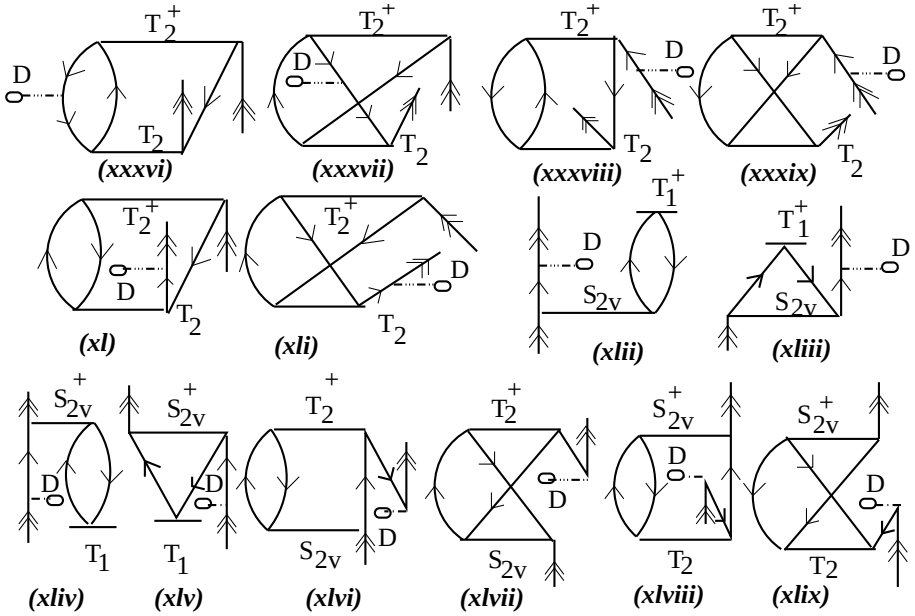

Figure 3.8: Property evaluation diagrams using LCCSD.

amount of time to compute in a program. But sometimes it is important to look on a longer time scale and appreciate that the non-linear terms can be broken up and stored in the computer hard disk and thereafter used several times in a sequence of programs. The second procedure may not be the least time consuming case for a single program but it will save more time when these terms are used repeatedly. Therefore, we follow this method which seems justified in our case and later this can be clearly understood when we discuss details of computational procedures in this and later chapters.

As usual we first start with the closed-shell CC equations to solve for the T amplitudes and using these amplitudes we calculate the S_v operator amplitudes followed by performing the matrix element calculations. Below, we discuss the detailed computational procedures.

3.4.2.1 Closed-shell equations

We consider the exact equations given by (3.14) and (3.15) for determining the correlation energy and CC amplitudes. Applying the Hausdorff expansion

(see Appendix D) one can expand $\overbrace{H_N e^T}$ as

$$\begin{aligned}
\overbrace{H_N e^T} &= H_N + [H_N, T] + \frac{1}{2!}[[H_N], T], T] + \frac{1}{3!}[[[H_N], T], T], T] \\
&\quad + \frac{1}{4!}[[[[H_N], T], T], T], T] \\
&= H_N + \{\overbrace{H_N T} - \overbrace{T H_N}\} + \frac{1}{2!}\{\overbrace{[H_N, T]T} - \overbrace{T[H_N, T]}\} \\
&\quad + \frac{1}{3!}\{\overbrace{[[H_N, T], T]T} - \overbrace{T[[H_N, T], T]}\} \\
&\quad + \frac{1}{4!}\{\overbrace{[[[H_N, T], T], T]T} - \overbrace{T[[[H_N, T], T], T]}\} \\
&= H_N + \overbrace{H_N T} + \frac{1}{2!}\overbrace{H_N T T} + \frac{1}{3!}\overbrace{H_N T T T} + \frac{1}{4!}\overbrace{H_N T T T T}
\end{aligned} \tag{3.30}$$

where the wide caps represent connected terms. Due to the fact that the atomic Hamiltonian has up to two-body operators (Coulomb or Breit interaction potential) maximum of four T_1 operators can connect with it and as a result the exponential function $H_N e^T$ naturally truncates at the fourth term as given by equation (3.30). Other terms will not satisfy the *Linked diagram theorem* (see Appendix C) and hence they are discarded from the calculations.

In the CCSD method, the extra diagrams contributing to the correlation energy calculations over and above the LCCSD method are given by figure 3.9.

The amplitudes are solved by the following non-linear matrix equations. These can be expressed in a way similar to linearized CC equations as

$$\begin{pmatrix} \langle \Phi_a^p | \overbrace{H_N(e^T - 1)} | \Phi_a^p \rangle & \langle \Phi_a^p | \overbrace{H_N(e^T - 1)} | \Phi_{ab}^{pq} \rangle \\ \langle \Phi_a^p | \overbrace{H_N(e^T - 1)} | \Phi_{ab}^{pq} \rangle & \langle \Phi_{ab}^{pq} | \overbrace{H_N(e^T - 1)} | \Phi_{ab}^{pq} \rangle \end{pmatrix} \begin{pmatrix} t_a^p \\ t_{ab}^{pq} \end{pmatrix} = - \begin{pmatrix} \langle \Phi_a^p | H_N | \Phi_0 \rangle \\ \langle \Phi_{ab}^{pq} | H_N | \Phi_0 \rangle \end{pmatrix}.$$

Or in vector form as:

$$\mathbf{A}(\mathbf{X}) \cdot \mathbf{X} = -\mathbf{B}.$$

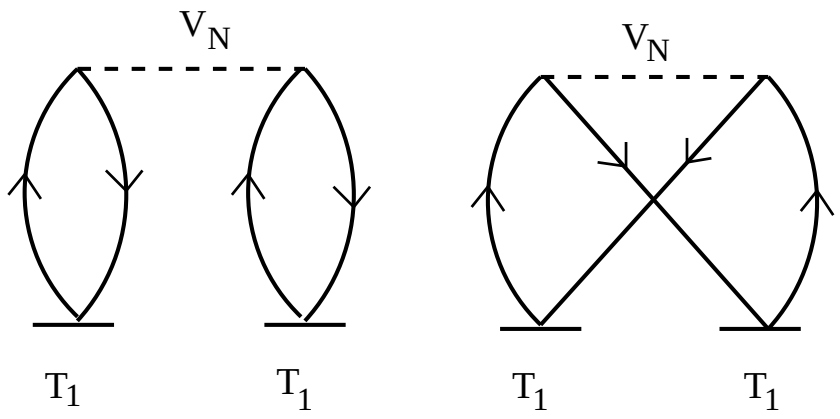

Figure 3.9: Extra diagrams for the calculation of ΔE_{corr} in CCSD.

(3.31)

The matrix **A** itself depends explicitly on the T operator amplitudes. The non-linear terms present in **A** can be split up as the product of T operators, some effective one-body terms and some intermediate parts with four open lines (two-body terms). First the effective one-body and intermediate two-body terms can be calculated and stored in RAM on the computer. These intermediate parts can be contracted with respective T operators to form the matrix elements of **A**. The solution of the above matrix equation can be expressed in the Jacobi iterative method as

$$X_j^i = \frac{-B_j - \sum_{l \neq j} A_{jl}(X) X_l^{(i-1)}}{A_{jj}}, \tag{3.32}$$

where the diagonal elements of the matrix **A** and **B** are same as for the linearized CC equations given in the earlier section. To construct the off-diagonal matrix elements $A_{jl}(X)$, we use the afore mentioned intermediate procedure. The T dependent intermediate terms are calculated using the solution from linearized CC amplitudes and the whole procedure has to be followed via the iterative way.

The effective one-body (HH, HP and PP) and two-body intermediate diagrams (aims1, aims2, aims3, aims4, aims5, aims6, aims7 and aims8) con-

structed for the CCSD method are shown by figures 3.10 and 3.11, respectively, and known as f-bar and v-bar diagrams. These terms are constructed by contracting V_N and T operators obtained from LCCSD. The off-diagonal elements of $\mathbf{A}$, constructed with these intermediate terms for T_1 and T_2 amplitudes, are shown by figures 3.12 and 3.13, respectively.

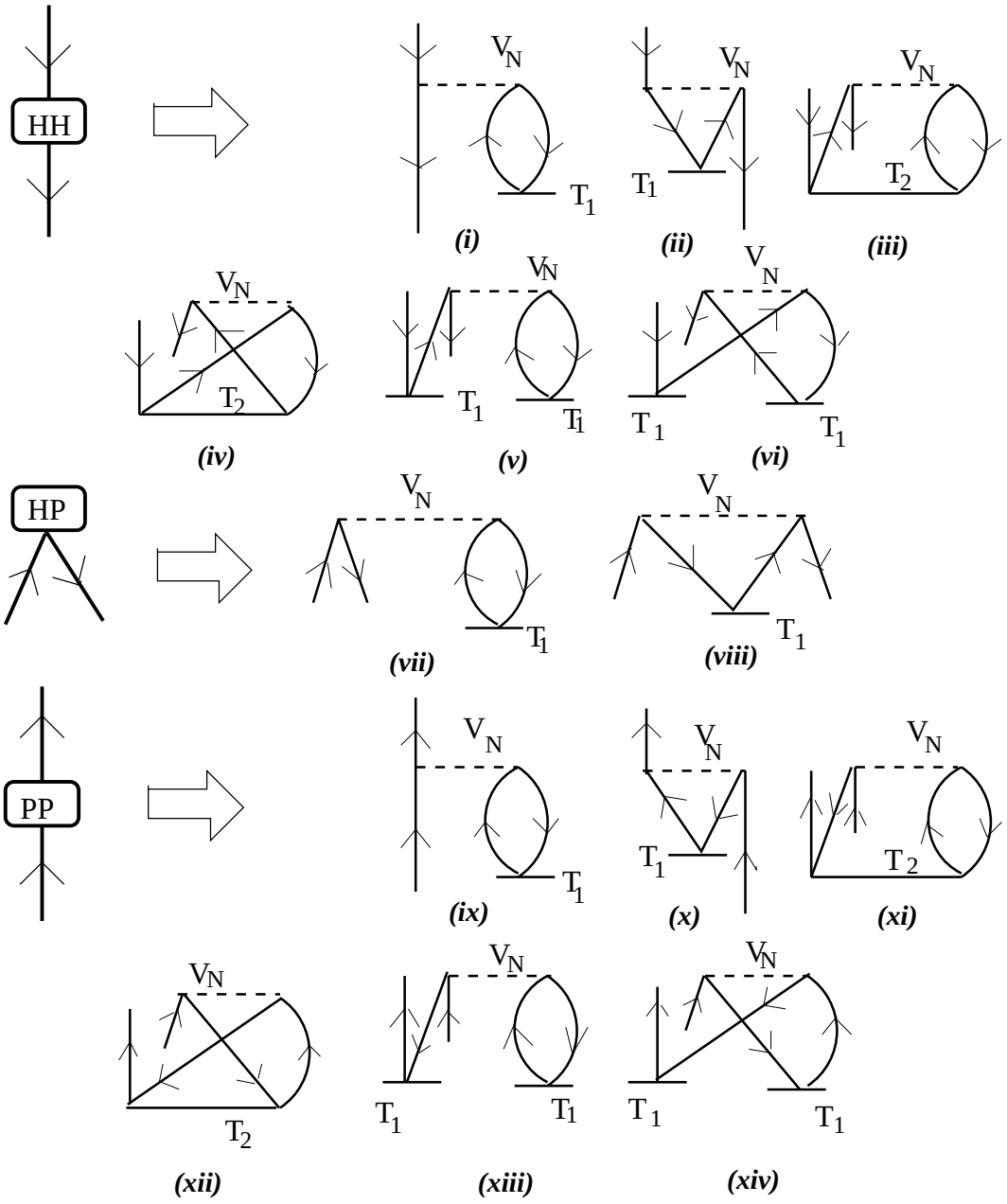

Figure 3.10: Diagrammatic representation of f-bar terms for closed-shell.

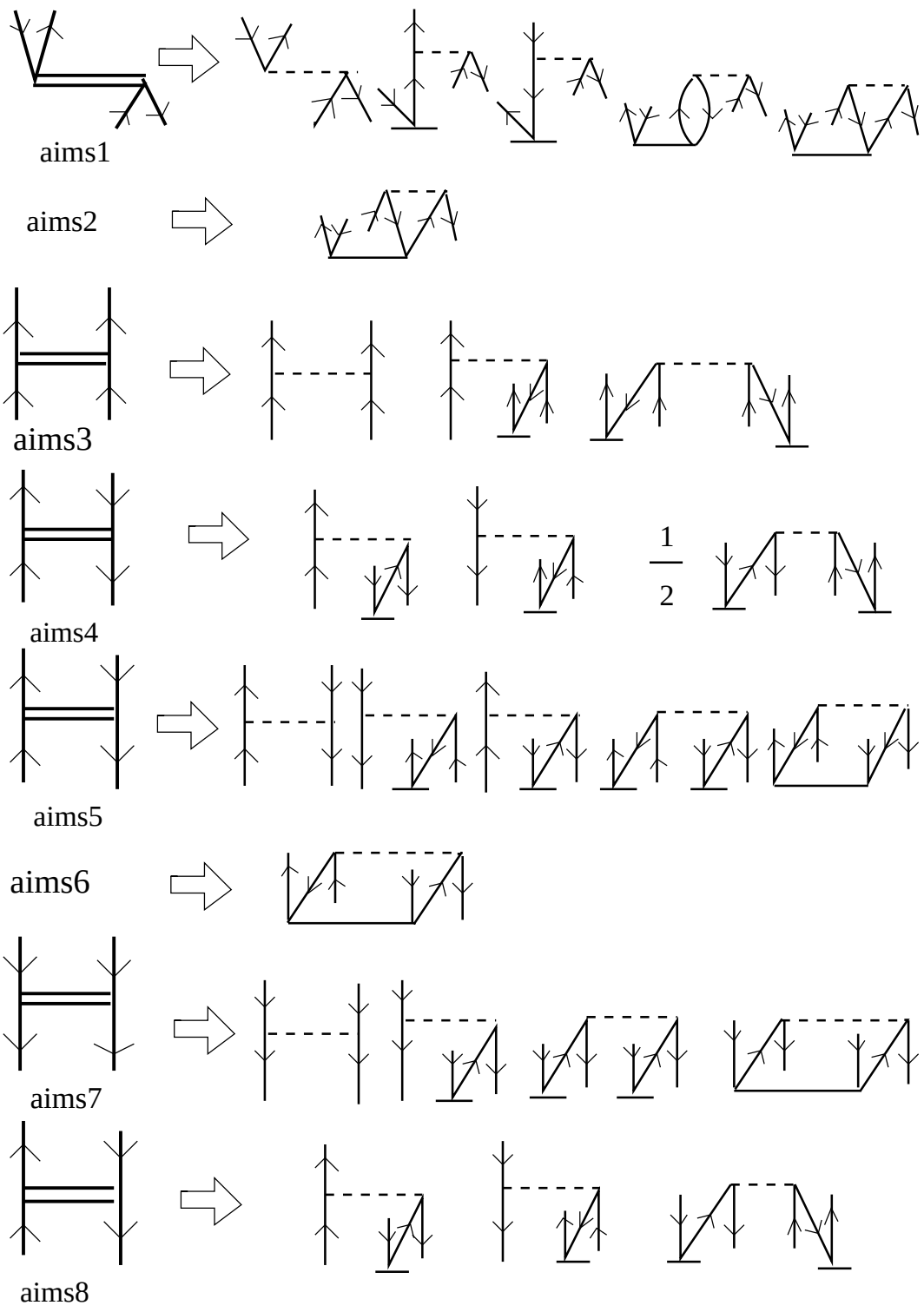

Figure 3.11: Diagrammatic representation of v-bar terms for closed-shell.

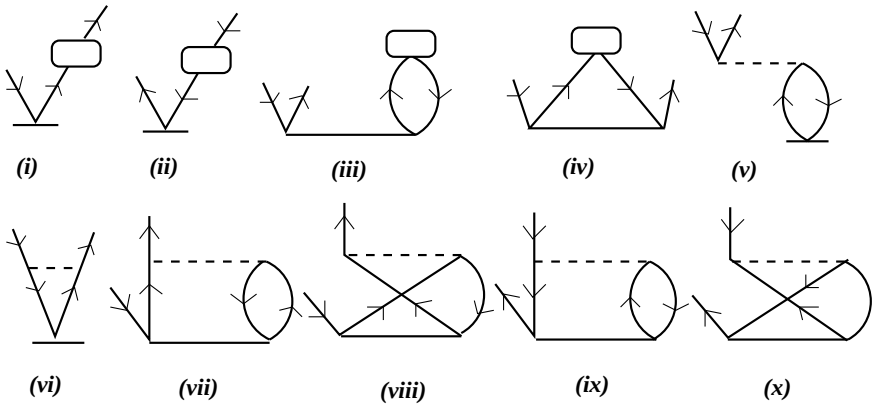

Figure 3.12: Diagrammatic representation of off-diagonal elements for singles.

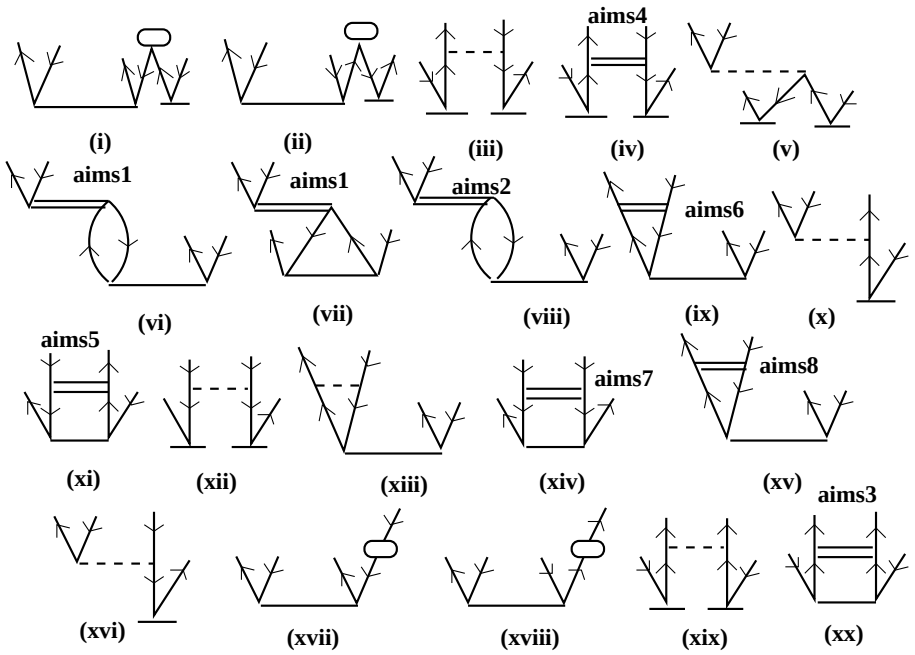

Figure 3.13: Diagrammatic representation of off-diagonal elements for doubles.

3.4.3 Open-shell equations

We follow a similar procedure of a non-linear closed-shell method to solve the amplitude determining equations for the single valence system. The exact form of equations (3.24) and (3.25) is considered in order to solve for the ionization potential and open-shell cluster amplitudes. The expansion of $H_N e^T$ will have linear terms up to the fourth power of T operators as explained in the closed-shell CC equations. The whole expression can be expressed as effective one-body and two-body terms which can contract with possible S_v operators in the above equations. The basic difference between such splitting up in the closed-shell and open-shell case is, in the closed-shell case the T operators are not known and the intermediate terms have to be followed by the iterative procedure with the amplitude determining equations. But in the case of open-shell, the T operators are already known and the effective one-body and two-body terms can be constructed and stored in RAM to use later. Again, since these operators have to be finally connected with S_v operators, all possible terms from $H_N e^T$ will contribute as opposed to closed-shell equations where only a certain set will contribute. So it is simple to construct all these diagrams by applying various rules such as the level of excitation procedure [32] or string algebra [26].

In principle, there will be four possible effective one-body terms: particle-particle (PP), hole-hole (HH), particle-hole (PH) and hole-particle (HP) types. But PH type one-body terms will not contribute to the calculation. We have shown all possible effective one-body terms in figure 3.14 which will contribute to the CCSD approximation. These diagrams are called f-bar diagrams.

Similarly, we can have ten possible types of effective two-body diagrams like V_N as shown in figure 2.3, but not all of them will contribute to the calculations. The contributing intermediate two-body diagrams at CCSD level are given in figure 3.15. These diagrams are called v-bar diagrams. However, sometimes a unique term has been considered here as a possible intermediate term, instead of, calculating this term directly with the S_v operator in the final form. We consider it in the intermediate part in order to store it in a common variable and make use of it arbitrarily by addressing its location when necessary.

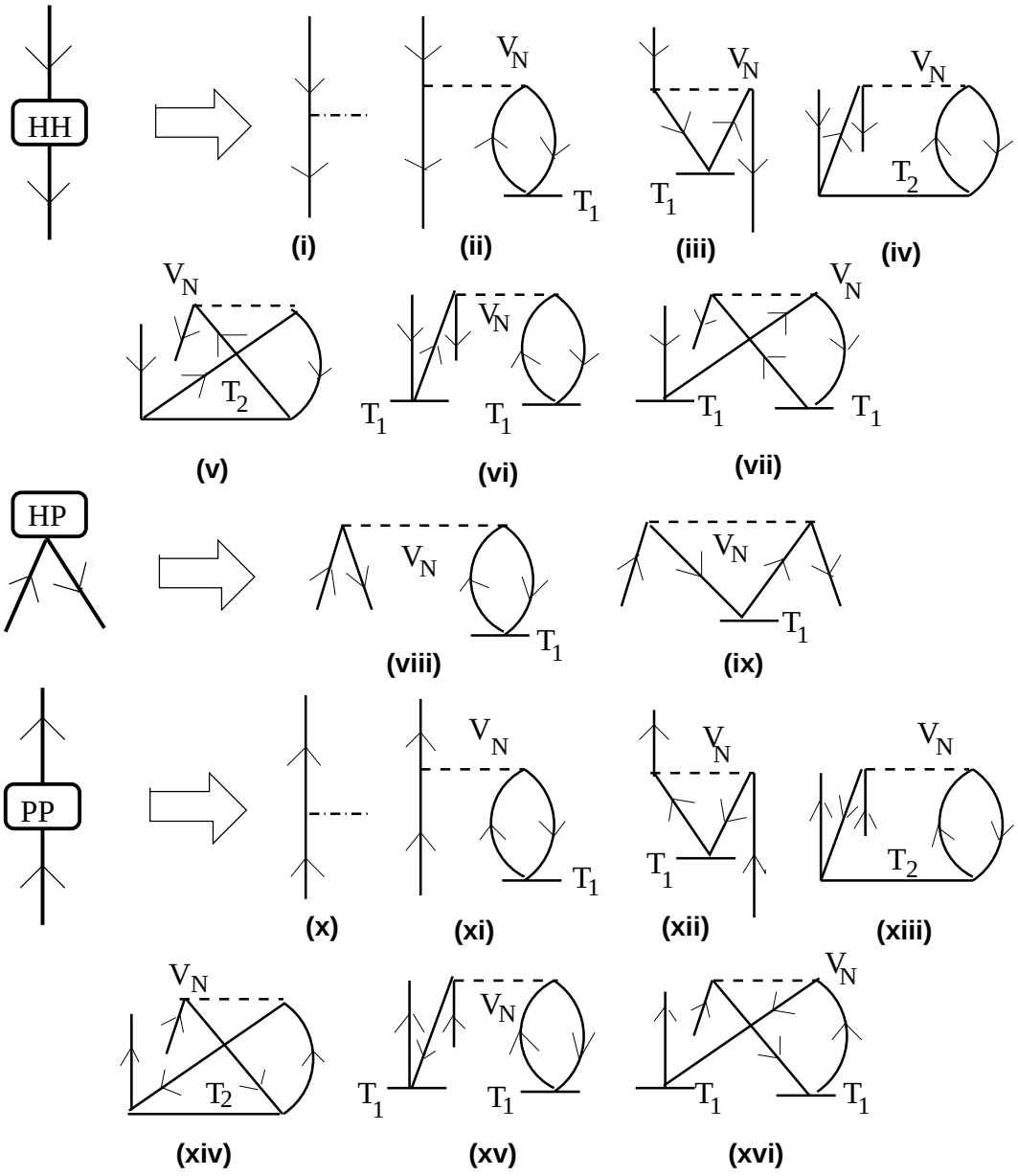

Figure 3.14: Diagrammatic representation for f-bar terms in open-shell CCSD calculation.

Diagrams corresponding to IP calculations using the non-linear CCSD method have been shown in figure 3.16.

The amplitude determining equation given by (3.23) can be expressed as

$$\begin{pmatrix} \langle \Phi_v^p | \widetilde{H_N e^T} - \Delta E_v | \Phi_a^p \rangle & \langle \Phi_v^p | \widetilde{H_N e^T} | \Phi_{vb}^{pq} \rangle \\ \langle \Phi_{vb}^{pq} | \widetilde{H_N e^T} | \Phi_v^p \rangle & \langle \Phi_{vb}^{pq} | \widetilde{H_N e^T} - \Delta E_v | \Phi_{vb}^{pq} \rangle \end{pmatrix} \begin{pmatrix} s_v^p \\ s_{vb}^{pq} \end{pmatrix} = - \begin{pmatrix} \langle \Phi_v^p | \widetilde{H_N e^T} | \Phi_v \rangle \\ \langle \Phi_{vb}^{pq} | \widetilde{H_N e^T} | \Phi_v \rangle \end{pmatrix}.$$

Or, in vector form

$$(\mathbf{A} - \mathbf{I}\Delta E_v) \cdot \mathbf{X} \;=\; -\mathbf{B} \tag{3.33}$$

where $\mathbf{I}$ is the identity operator. The matrix $\mathbf{A}$ and $\mathbf{B}$ depend explicitly on T operators and are known in this case. The above equation is non-linear because of the fact that the electron affinity energy (ΔE_v) itself depends on S_v operator amplitudes which can be observed from equations (3.22) and (3.23). Therefore, it has to be solved iteratively. In the Jacobi iterative method, the solution for the above equation can be expressed as

$$X_j^i \;=\; \frac{-B_j + (\Delta E_v - \epsilon_v) X_j^{(i-1)} - \sum_{l \neq j} A_{jl} X_l^{(i-1)}}{A_{jj}} \tag{3.34}$$

where different indices used here are defined in the earlier equations for the closed-shell. Here the single particle energy of the valence electron (ϵ_v) has been subtracted from ΔE_v, because it has been already considered in the diagonal elements of matrix $\mathbf{A}$. This can be clearly understood when we choose the initial values of the solutions for the above equations. The $\mathbf{B}$ matrix elements are P-P and PP-HP block diagrams of f-bar and v-bar terms for single and double excitation equations, respectively.

The initial values of the equation (3.34) have been considered as

$$\begin{aligned} (s_v^p)^{(1)} &= -\frac{f(p,v)}{f(p,p) - f(v,v)} \\ (s_{vb}^{pq})^{(1)} &= -\frac{\langle pq | V(pq,vb) | vb \rangle}{f(p,p) + f(q,q) - f(v,v) - f(b,b)} \end{aligned} \tag{3.35}$$

where $f(i,j)$ represent f-bar value with i and j matrix elements and $V(pq,vb)$ represent the v-bar values for PP-PH diagram with one of the particle equivalent to the valence electron.

Diagrams corresponding to the off-diagonal elements for calculating S_v amplitudes are given by figure 3.17.

3.4.4 Inclusion of effects from triple excitations

To improve the accuracy of the calculations we consider the leading triple excitation effects in the S_v amplitude determining equations of the CCSD method. This approximation is called the CCSD(T) method, where the T in the parenthesis represents partial triple excitations. In this approach, we construct the most important triple excitations by contracting the Coulomb operator (V_N) with T_2 and S_{2v} operators [30, 34] as follows:

$$S_{vbc}^{pqr} = \frac{\widetilde{V_N T_2} + \widetilde{V_N S_{2v}}}{\epsilon_v + \epsilon_b + \epsilon_c - \epsilon_p - \epsilon_q - \epsilon_r}. \tag{3.36}$$

Contributions from these excitations are included by contracting the above operator with the S_v operators and constructing diagrams for the ionization potential ($-\Delta E_v$) calculation, coupled with the solution of equation (3.35). Therefore, the equation (3.34) after the inclusion of partial triple excitations can be written as:

$$X_j^i = \frac{-B_j + (S_{vbc}^{pqr})_j^{(i-1)} X_j^{(i-1)} + (\Delta E_v - \epsilon_v) X_j^{(i-1)} - \sum_{l \neq j} A_{jl} X_l^{(i-1)}}{A_{jj}} \tag{3.37}$$

The diagrams corresponding to the ionization potential calculation from partial triple excitation terms are given in figure 3.18.

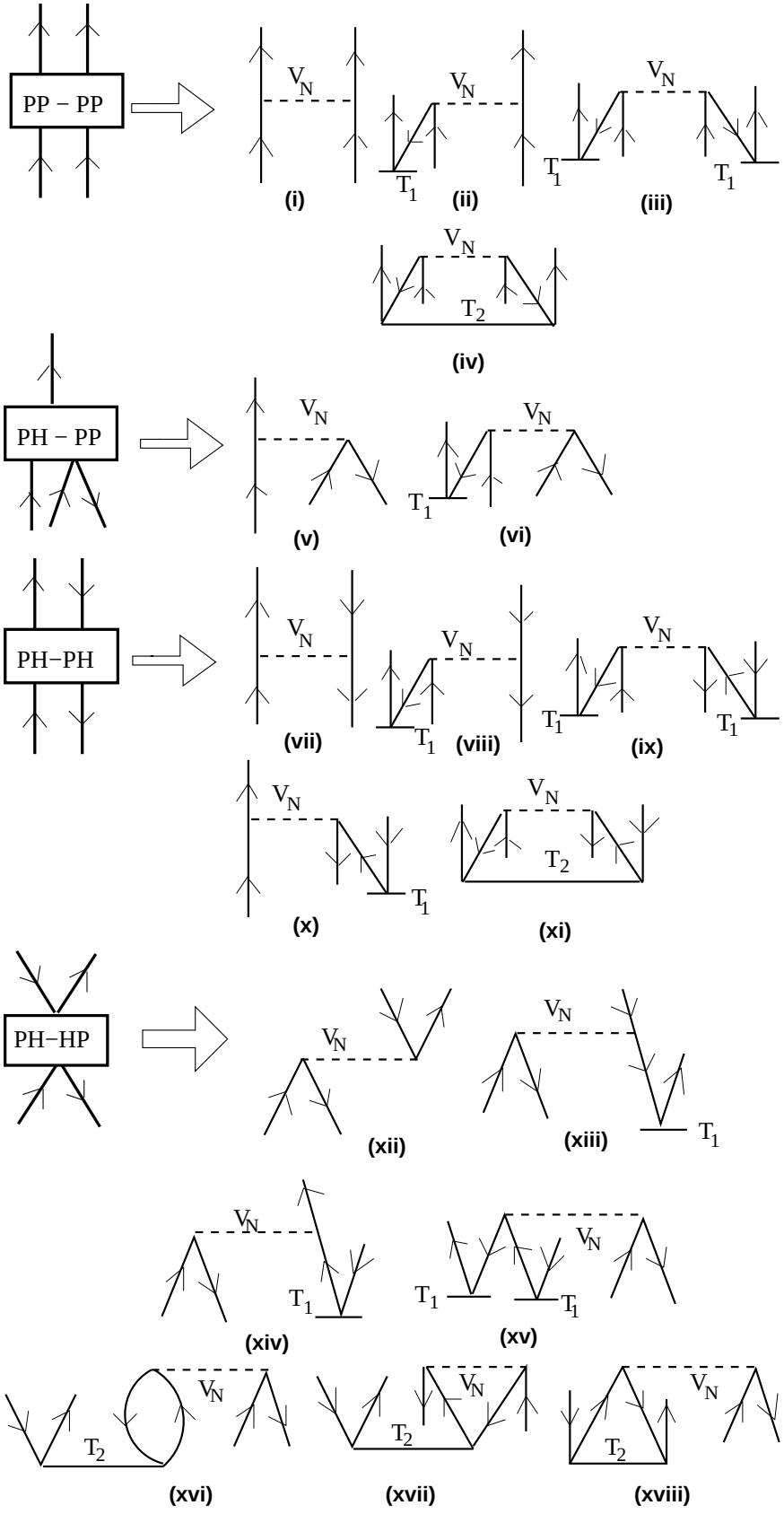
PP – PP
V_N
T_1
(i)
(ii)
(iii)
T_2
(iv)
PH – PP
(v)
(vi)
PH–PH
(vii)
(viii)
(ix)
(x)
(xi)
PH–HP
(xii)
(xiii)
(xiv)
(xv)
(xvi)
(xvii)
(xviii)

Cont.....

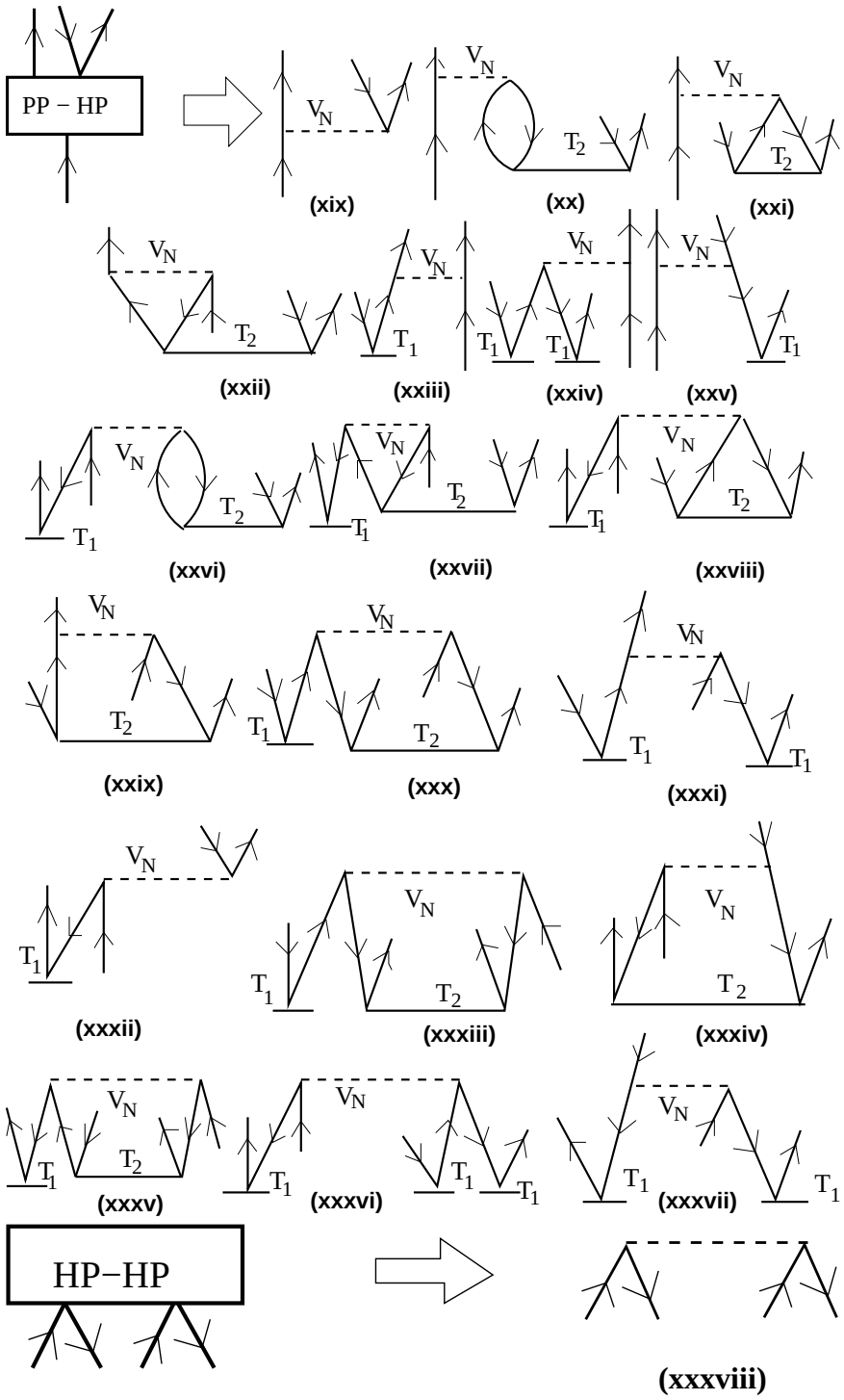

Figure 3.15: Diagrammatic representation of v-bar terms in an open-shell.

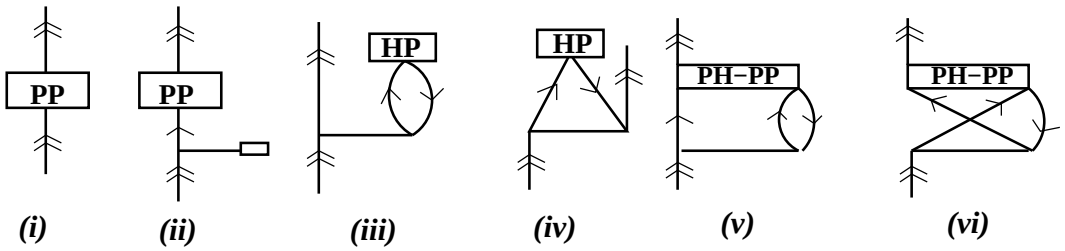

Figure 3.16: Diagrams corresponding to IP calculation using CCSD method.

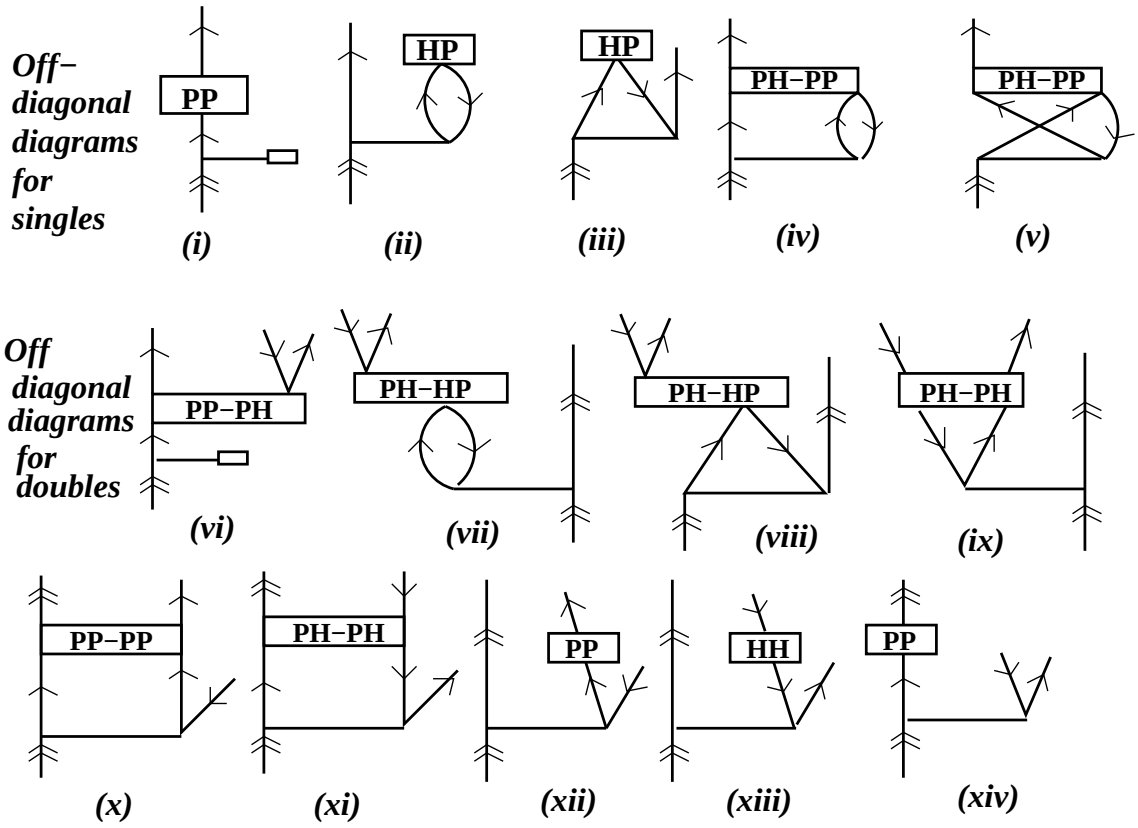

Figure 3.17: Diagrams for off-diagonal elements S_v determining equations.

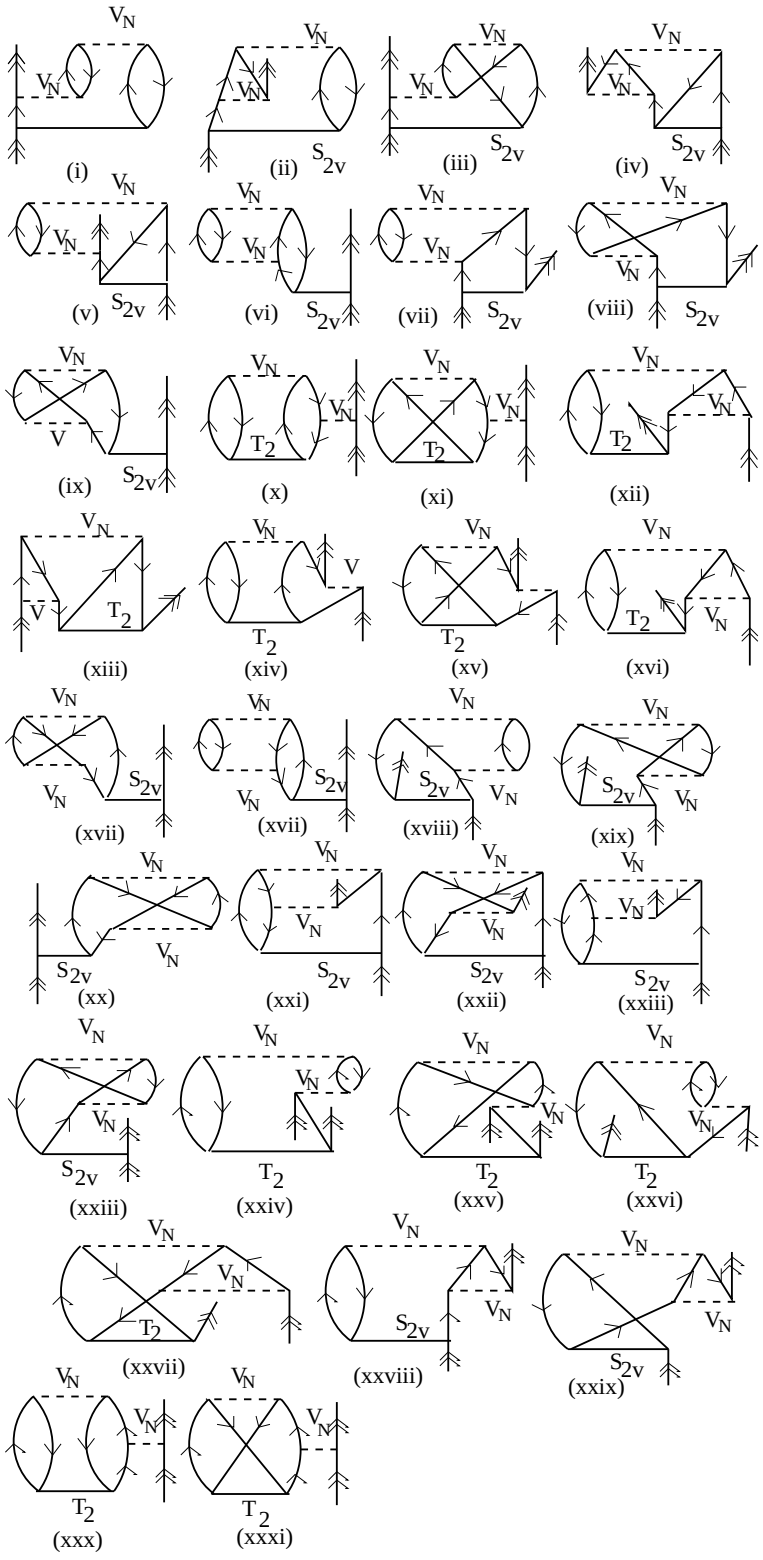

Figure 3.18: Diagrams for ionization potential (IP) calculations from the partial triples excitations.

3.4.5 Property evaluation

In many of the studies in quantum chemistry, only the energy of different states are verified using the CC method [17, 24, 32, 34]. In few atomic systems where the various atomic properties are calculated with the CC method [2, 8], the LCCSD approximation is mainly used. Here we discuss the working procedure using the CCSD method to calculate various properties and the calculated results are given in the following chapters.

We directly follow equation (3.29) in order to calculate either transition matrix elements or expectation values of any physical operator. In contrast to linearized CC, in the nonlinear case $e^{T^\dagger} D e^T$ will be a non-truncative series even at the level of the CCSD approximation. It is not possible to solve these matrix elements directly, but one can truncate the series by verifying the importance of immediate higher order terms with the required precision calculation of the results. We decompose the above non-truncative series as effective one-body, two-body etc. up to five-body terms for the CCSD method [35, 36, 37]. Since these terms again have to be contracted with appropriate S_v operators and their conjugates, only up to three-body terms will be valid in this expansion. We consider only effective one-body and two-body terms in our calculations as others correspond by to higher order terms and are computationally tedious to handle.

The effective one-body terms are classified as hole-hole (HH), hole-particle (HP), particle-particle (PP) and particle-hole (PH) types. The diagrams for each type in the CCSD method are shown in figure 3.19 which are called Dbar ($\overline{D}$) diagrams. Although we have given all possible diagrams, in practice these terms are calculated using the following procedure. We first calculate half of the HH and PP type diagrams and the other half are retrieved using the symmetric relationship. From that point of view HP and PH type diagrams are also symmetric to each other and hence, we calculate one type of these diagrams and using the aforementioned relationship we retrieve the other type. These matrix elements are stored in the hard disk after computation and finally, they are read in to another program where they are contracted with respective S_v and its conjugate operators to evaluate the final results. The final property diagrams obtained after sandwiching with effective one-body terms are shown in figure 3.20.

In fact, not all possible two-body terms are important in the property calculation. We have dropped terms (diagrams) corresponding to higher order terms whilst considering only important two-body terms. We have shown a schematic example of how the effective two-body terms are obtained diagrammatically in figure 3.21. These diagrams are directly computed for the property calculation. The diagrams corresponding to total effective two-body terms which are considered in our calculations are shown by figure 3.22.

We also follow the same procedure to compute the non-truncative series of $e^{T^\dagger} e^T$ from the denominator of equation (3.29).

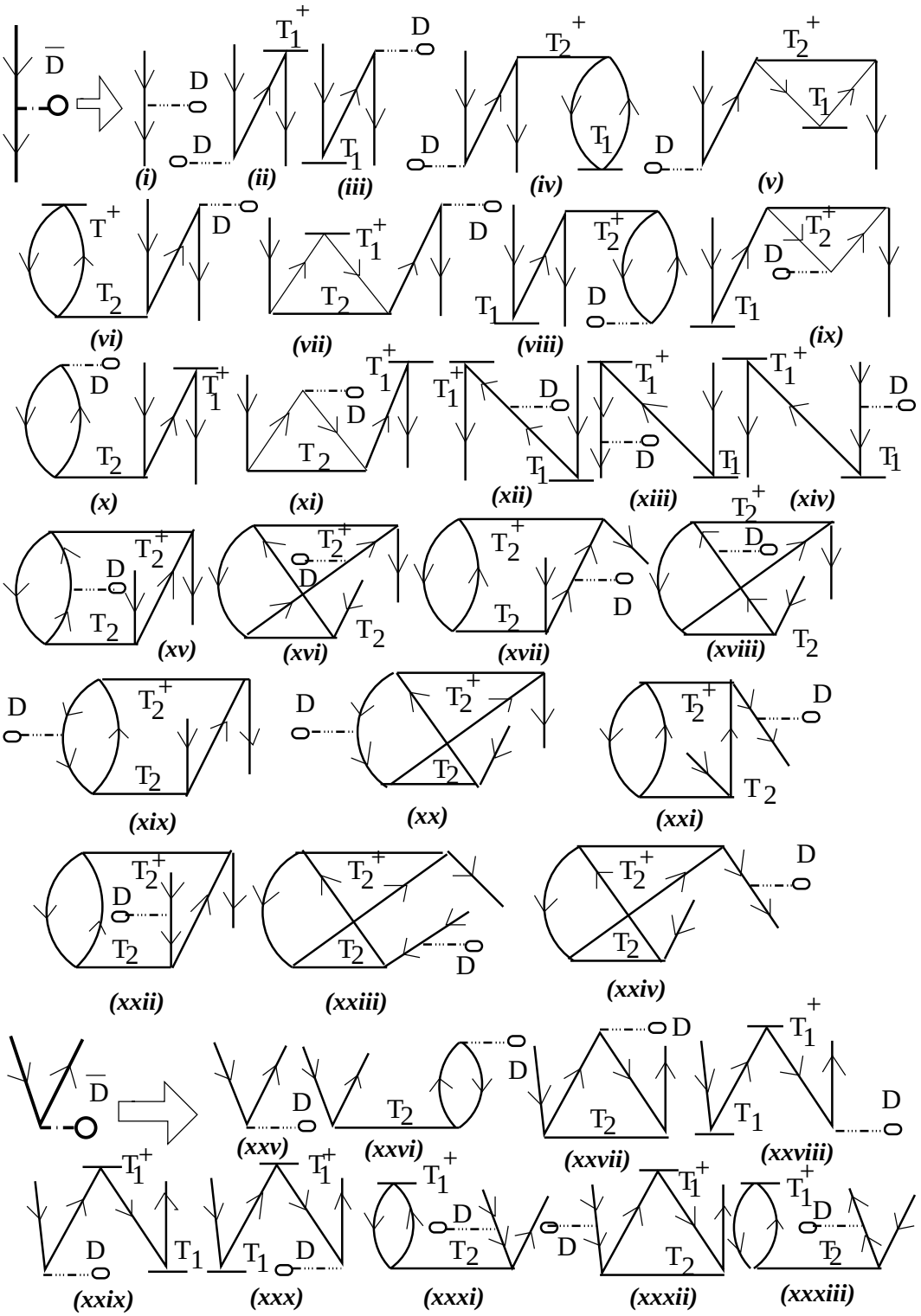
D
(i)
(ii)
(iii)
(iv)
(v)
(vi)
(vii)
(viii)
(ix)
(x)
(xi)
(xii)
(xiii)
(xiv)
(xv)
(xvi)
(xvii)
(xviii)
(xix)
(xx)
(xxi)
(xxii)
(xxiii)
(xxiv)
(xxv)
(xxvi)
(xxvii)
(xxviii)
(xxix)
(xxx)
(xxxi)
(xxxii)
(xxxiii)

Cont.....

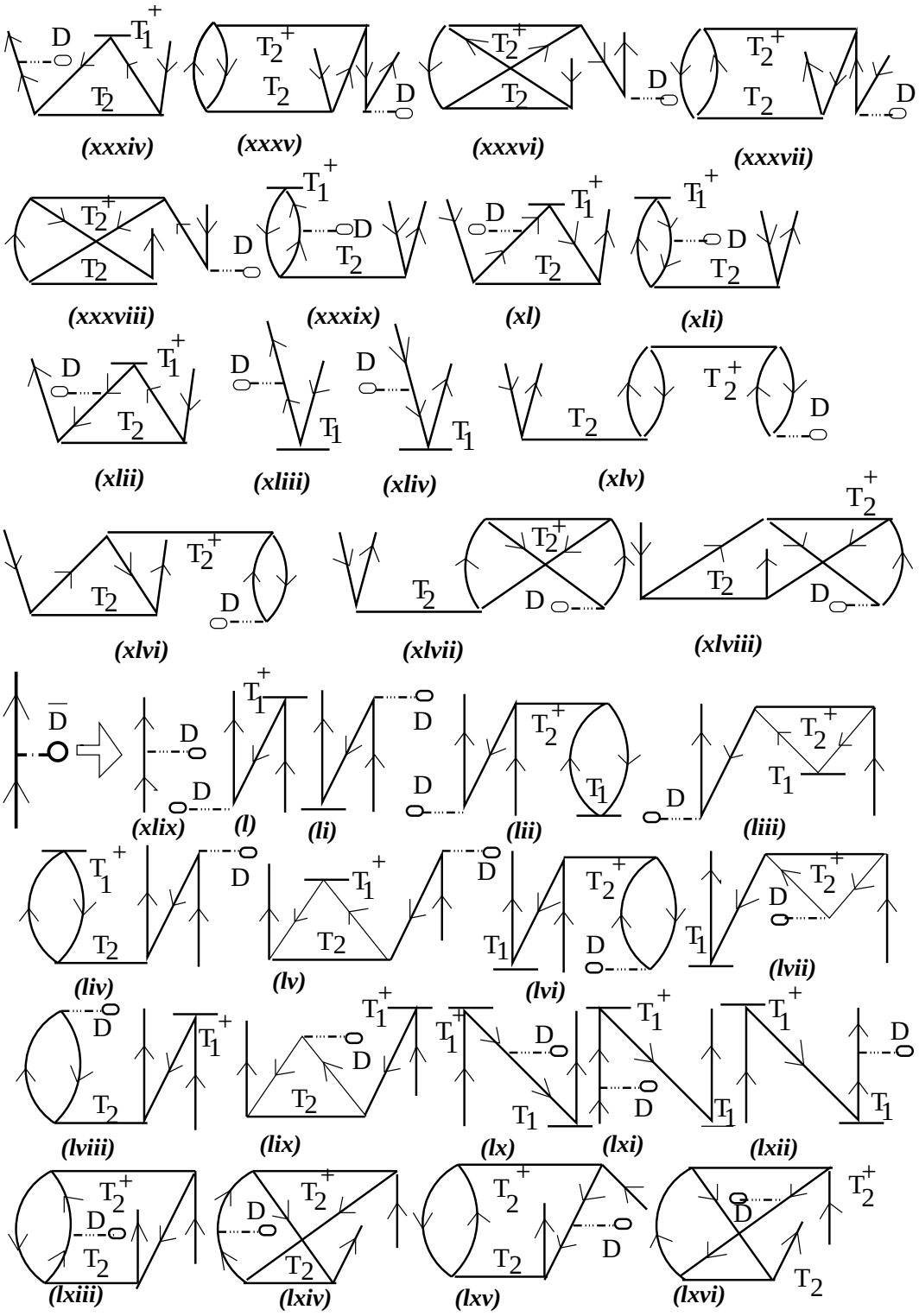
D
T1+
T2
T2+
T2
D
T2+
T2
D
T2+
T2
D
(xxxiv)
(xxxv)
(xxxvi)
(xxxvii)
T2+
T2
D
T1+
D
T2
D
T1+
T2
T1+
D
T2
(xxxviii)
(xxxix)
(xl)
(xli)
D
T1+
T2
D
T1
D
T1
T2
T2+
D
(xlii)
(xliii)
(xliv)
(xlv)
T2+
T2
D
T2+
T2
D
T2
T2+
D
(xlvi)
(xlvii)
(xlviii)
D
D
D
T1+
D
D
T2+
T1
D
T2+
T1
(xlix)
(l)
(li)
(lii)
(liii)
T1+
T2
D
T1+
T2
T2+
T1
D
T2+
D
T1
(liv)
(lv)
(lvi)
(lvii)
D
T1+
T2
T1+
D
T2
T1
T2+
D
T1
T1+
D
T1
T1+
D
T1
(lviii)
(lix)
(lx)
(lxi)
(lxii)
T2+
D
T2
T2+
D
T2
T2+
T2
D
D
T2+
T2
(lxiii)
(lxiv)
(lxv)
(lxvi)

Cont.....

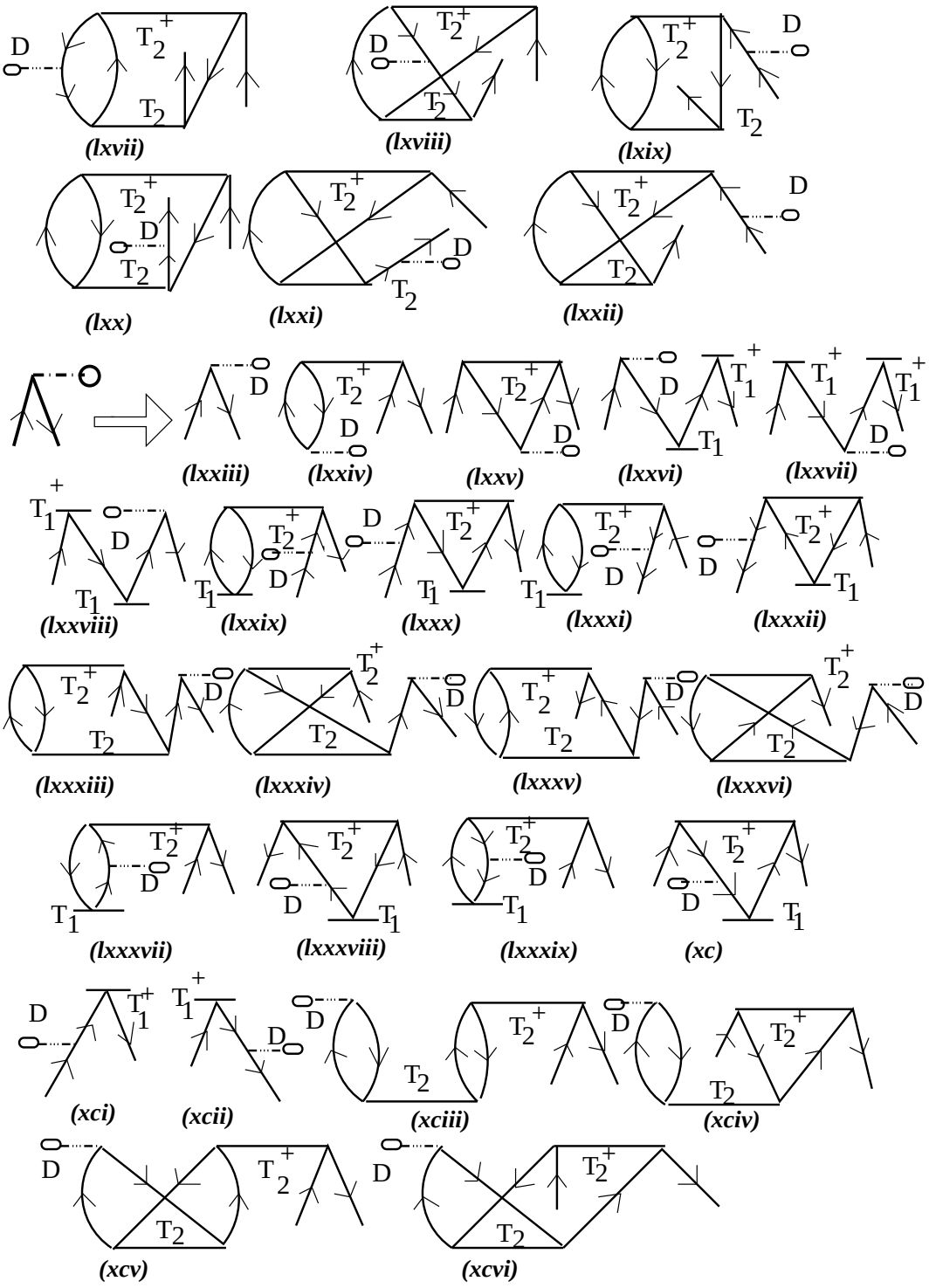

Figure 3.19: Dbar diagrams

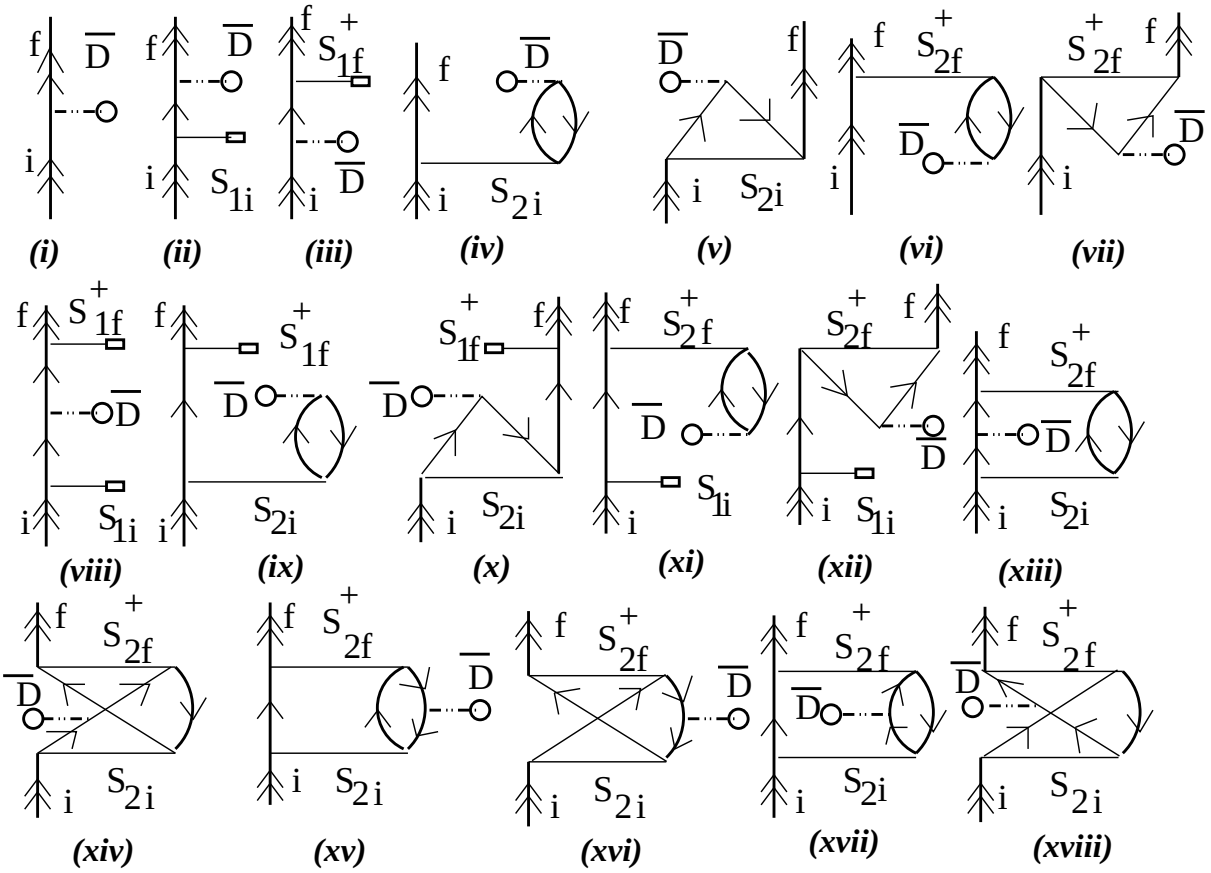

Figure 3.20: Final property evaluating diagrams from effective one-body terms.

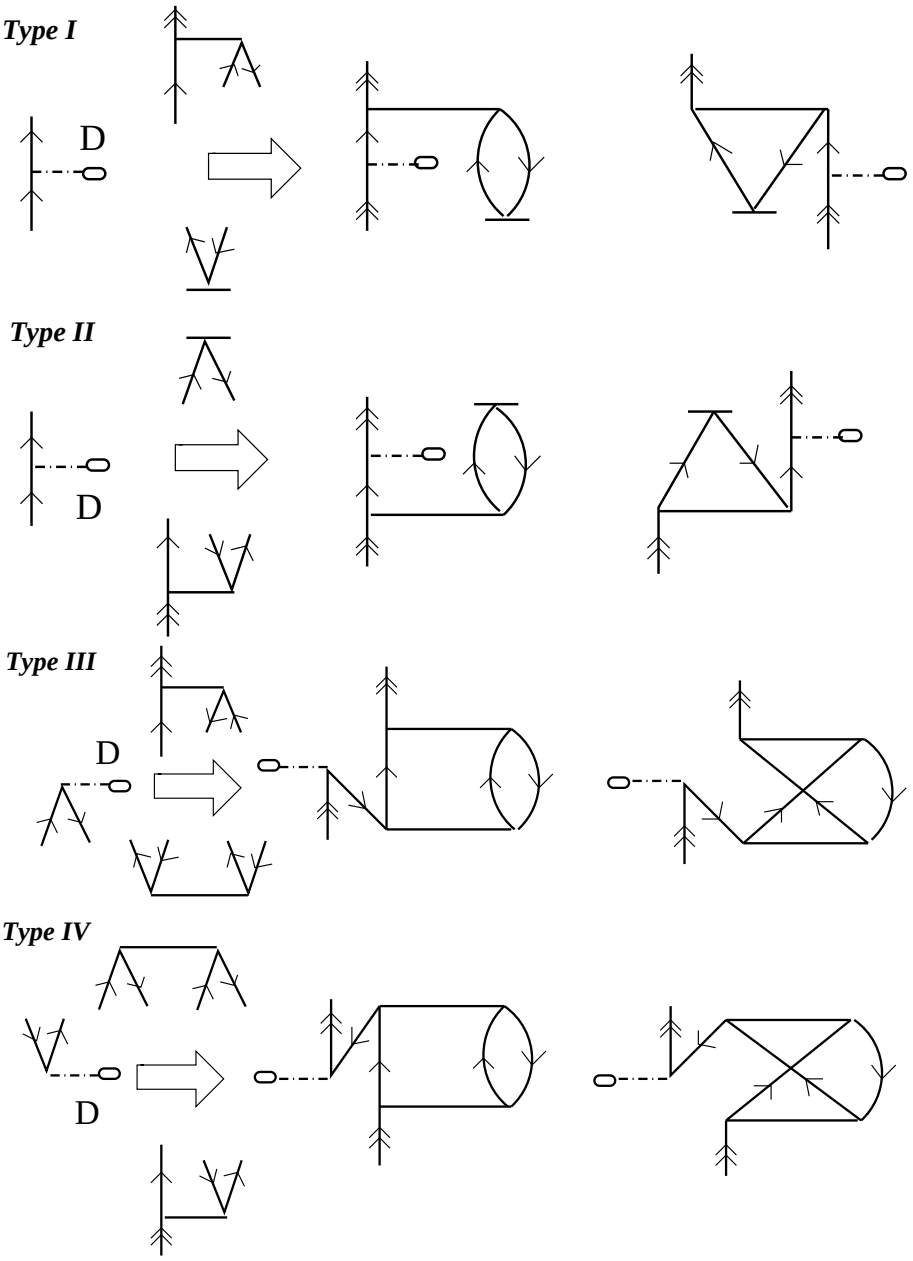

Figure 3.21: The effective two-body terms, which are calculated directly, constructed from $\bar{D}$ for the property calculation.

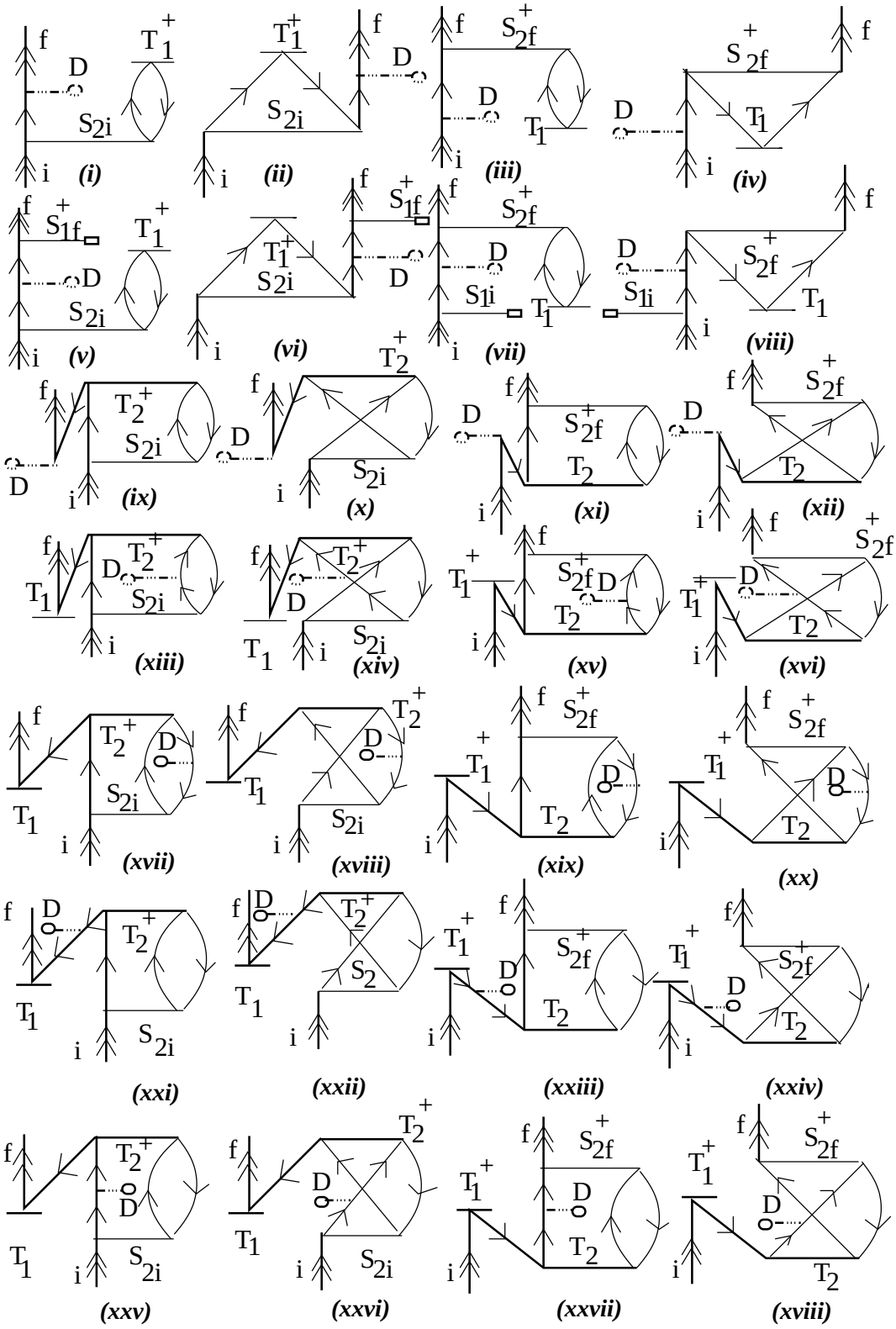

Figure 3.22: Final property evaluating diagrams from effective two-body terms.

3.5 Reduction of angular factors from Goldstone diagrams

The Goldstone diagrams given in this chapter can be expressed in terms of various radial integrals and complex Clebsch-Gordan coefficients. These factors are considered in terms of the reduced matrix elements of the related operators (expressions for these operators are given in the previous chapter) in the respective Goldstone diagrams and an azimuthal quantum number (m_j), of the angular momentum j- of the single particle orbital, dependent factor. These angular factors can be derived from the Goldstone diagrams using a set of rules given in Appendix C. The complex angular factors are further simplified using JLV theorems (see Appendix A).

For simplicity, one cancels m_j dependent factors from both sides of the different matrix equations of the amplitude determining CC equations. Therefore, one can deal with just the reduced matrix elements. It reduces the number of computational operations by a large amount and helps the JLV theorems to be used conveniently. It should be noted that the value of different CC amplitudes remains invariant in this procedure.

Again, in the calculation of matrix elements we need only the reduced matrix elements as we shall see in chapter 5 and therefore, it is not necessary to deal with the actual matrix elements of the operator. When we evaluate the expectation value of any physical operator, we deal with the reduced matrix element in the entire calculation and to obtain the final result, we multiply by the required m_j dependent factor which results in the net reduced matrix element.

Bibliography

[1] I. Lindgren and J. Morrison, *Atomic Many-Body Theory*, edited by G. Ecker, P. Lambropoulos, and H. Walther (Springer-Verlag, Berlin, 1985)

[2] S. A. Blundell, W. R. Johnson and J. Sapirstein, Phys. Rev. Lett. **65**, 1411 (1990)

[3] V. A. Dzuba, V. V. Flambaum, P. G. Silvestrov and O. P. Sushkov, Phys. Lett. A **141**, 147 (1989)

[4] A. C. Hartley, E. Lindroth and A. -M. Mårtensson-Pendrill, J. Phys. B **23**, 3417 (1990)

[5] M. A. Bouchiat and C. Bouchiat, J. Phys. (Paris) **35**, 899 (1974); J. Phys. (Paris) **36**, 493 (1975)

[6] G. Breit, Phys. Rev. **34**, 553 (1929)

[7] E. Eliav, U. Kaldor and Ishikawa, Phys. Rev. A **53**, 3050 (1996)

[8] A. Derevianko, Phys. Rev. Lett. **85**, 1618 (2000); Phys. Rev. A **65**, 012106 (2002)

[9] V. A. Dzuba, C. Harabati, W. R. Johnson and M. S. Safronova, Phys. Rev. A **61**, 044103 (2001)

[10] O. P. Sushkov, Phys. Rev. A **63**, 042504 (2001)

[11] V. M. Shabaev, K. Pachuki, I. I. Tupitsyn and V. A. Yerokhin, Phys. Rev. Letta. **94**, 213002 (2005)

[12] S. J. Rose, N. C. Pyper and I. P. Grant, J. Phys. B **11**, 755 (1978)

[13] I. P. Grant, Adv. Phys. **19**, 747 (1970)

[14] K. P. Geetha, Ph.D. Thesis, Bangalore Univ., India (2002)

[15] S. A. Blundell, W. R. Johnson and J. Sapirstein, Phys. Rev. A **37**, 2764 (1988); **38**, 2699 (1988); **42**, 1087 (1990)

[16] C. Guet and W. R. Johnson, Phys. Rev. A **44**, 1531 (1991)

[17] J. *Čížek*, J. Chem. Phys. **45**, 4256 (1966); Adv. Chem. Phys. **14**, 35 (1969)

[18] G. D. Purvis III and R. J. Bartlett, J. Chem. Phys. **86**, 7041 (1987)

[19] Y. S. Lee, S. A. Kucharski and R. J. Bartlett, Theor. Chim. Phys. **81**, 5906 (1984)

[20] B. K. Sahoo, S. Majumder, R. K. Chaudhuri, B. P. Das, D. Mukherjee, J. Phys B **37**, 3409 (2004)

[21] A. Szabo and N. S. Ostlund, *Modern Quantum Chemistry: Introduction to Advanced Electronic structure theory*, Dover Publications Inc., *Mineola, New York*, First edition (revised), 1996

[22] Raymond F. Bishop and Hermann G. Kuemmel, Physics Today **March** issue, 52-60 (1987)

[23] Raymond F. Bishop, *Microscopic Quantum Many-body Theories and their Applications*, Edited by J. Navarro and A. Polls, page. 1, Springer-Verlag Berlin Heidelberg (1998)

[24] U. Kaldor, *Microscopic Quantum Many-body Theories and their Applications*, Edited by J. Navarro and A. Polls, page. 71 (1998)

[25] K. Kowalski, D. J. Dean, M. Hjorth-Jensen, T. Papenbrock and P. Piecuch, Phys. Rev. Lett. **92**, 132501 (2004)

[26] Mihály Kállay and Péter R. Surján, J. Chem. Phys. **115**, 2945 (2001)

[27] Mihály Kállay, Jürgen Gauss and Péter Szalay, J. Chem. Phys. **120**, 6841 (2004)

[28] R. K. Chaudhuri, D. Mukhopadhyay Jr. and D. Mukherjee, Chem. Phys. Lett. **162**, 393 (1989)

[29] H. Merlitz, G. Gopakumar, R. K. Chaudhuri, B. P. Das, U. S. Mahapatra and D. Mukherjee, Phys. Rev. A **63**, 025507 (2001)

[30] Geetha Gopakumar, Holger Merlitz, Sonjoy Majumder, Rajat Chaudhuri, B.P. Das, U. S. Mahapatra, and D. Mukherjee, Phys. Rev. A **64**, 032502 (2001)

[31] D. Mukherjee and S. Pal, Adv. Quantum Chem. **20**, 281 (1989)

[32] R.J. Bartlett in *Modern Electronic Structure Theory*, edited by D.R. Yarkony, World Scientific, Vol. II, pp 1047 (1995)

[33] Geetha Gopakumar, Holger Merlitz, Rajat Chaudhuri, B.P. Das, U.S. Mahapatra, and D. Mukherjee, Phys. Rev. A **66**, 032502 (2002)

[34] U. Kaldor, J. Chem. Phys. **87**, 4676 (1987); **87**, 4693 (1987)

[35] S. A. Blundell, W. R. Johnson and J. Sapirstein, Phys. Rev. A **43**, 3407 (1991)

[36] E. Lindroth and A. Yennerman, Phys. Rev. A **47**, 961 (1993)

[37] Bijaya K. Sahoo, Geetha Gopakumar, Rajat K. Chaudhuri, B. P. Das, Holger Merlitz, Uttam Sinha Mahapatra and Debashis Mukherjee, Phys. Rev. A **68**, 040501(R) (2003)

Chapter 4

Application of Relativistic Coupled-cluster Theory to Parity Non-conservation in Atomic Systems

4.1 Introduction

The importance of accurate calculations of the electric dipole parity non-conserving amplitude ($E1_{PNC}$) in testing the Standard Model (SM) of particle physics has been mentioned earlier in this thesis. A number of calculations have been carried out on a variety of atomic systems [1, 2, 3, 4]. The most accurate calculation to date has been on $6s_{1/2} \rightarrow 7s_{1/2}$ transition in Cs [3, 4, 5]. Dzuba *et al.* have used a Green function-like approach based on a variant of relativistic many-body perturbation theory [4], while Blundell *et al.* have used linearized coupled-cluster (CC) theory [3].

In this thesis, we have developed a full fledged non-linear relativistic CC theory to calculate $E1_{PNC}$. This approach, which is discussed in detail in this chapter, is capable of treating the interplay of electromagnetic and weak interactions in a heavy atomic system to a high degree precision. This is

achieved by considering the electron correlation effects to all order in the residual Coulomb interaction for a given level of excitation and the neutral weak interaction to just one order. Unlike the approach of Blundell *et al.* [3], we do not calculate $E1_{PNC}$ by summing over intermediate states. These states are included implicitly in our approach.

4.2 Theoretical Approach

For atomic PNC studies, we consider only the nuclear spin independent interaction Hamiltonian (H_{PNC}^{NSI}) type, for the reasons mentioned in the chapter 1. Along with this interaction term the total atomic Hamiltonian can be written as

$$H = H^{(0)} + G_F H^{(1)} \tag{4.1}$$

where G_F is the Fermi constant and $H^{(0)}$ is the atomic Hamiltonian that has been considered in the previous chapter for atomic wavefunction calculation using relativistic coupled-cluster (RCC) method. $H^{(1)}$ is nothing but the H_{PNC}^{NSI} except the G_F factor given in chapter 1.

It is obvious from the properties of $H^{(1)}$ that it is responsible for mixing atomic states of opposite parities but with the same angular momentum. As its strength is sufficiently weak, we consider only up to first-order perturbation and the modified atomic state wavefunction is given by

$$|\Psi_v\rangle = |\Psi_v^{(0)}\rangle + G_F|\Psi_v^{(1)}\rangle \tag{4.2}$$

where 'v' represents the valence electron.

In RCC, the atomic wavefunction $|\Psi_v^{(0)}\rangle$ for a single valence open-shell system, as discussed in the last chapter is given by [6, 7]

$$|\Psi_v^{(0)}\rangle = e^{T^{(0)}}\{1 + S_v^{(0)}\}|\Phi_v\rangle \tag{4.3}$$

where $|\Phi_v\rangle$ is the reference state for the open-shell defined using the Dirac-Fock (DF) wavefunction of the closed-shell atomic system ($|\Phi_0\rangle$) as

$$|\Phi_v\rangle = a_v^\dagger|\Phi_0\rangle. \tag{4.4}$$

In the singles and doubles approximation, we have

$$\begin{aligned} T^{(0)} &= T_1^{(0)} + T_2^{(0)} \\ S_v^{(0)} &= S_{1v}^{(0)} + S_{2v}^{(0)} \end{aligned} \tag{4.5}$$

where $T_1^{(0)}$ and $T_2^{(0)}$ are the single and double particle-hole excitation operators for core electrons and $S_{1v}^{(0)}$ and $S_{2v}^{(0)}$ are the single and double excitation operators for the valence electron, respectively. The amplitudes corresponding to these operators are determined using the procedure explained in the earlier chapter.

Now, the expression for the $E1_{PNC}$ amplitude from the initial state (i) to the final state (f) is given by

$$E1_{PNC} = \frac{\langle \Psi_f | D | \Psi_i \rangle}{\sqrt{\langle \Psi_f | \Psi_f \rangle \langle \Psi_i | \Psi_i \rangle}}. \tag{4.6}$$

Substituting the wavefunctions from equation (4.2) and considering only up to linear terms in G_F terms we get

$$E_{PNC} = \frac{\langle \Psi_f^{(0)} | D | \Psi_i^{(1)} \rangle + \langle \Psi_f^{(1)} | D | \Psi_i^{(0)} \rangle}{\sqrt{\langle \Psi_f^{(0)} | \Psi_f^{(0)} \rangle \langle \Psi_i^{(0)} | \Psi_i^{(0)} \rangle}} \tag{4.7}$$

where $D(= e\vec{\mathbf{r}})$ is the electric dipole (E1) operator. Substituting the expression from the first order wavefunction in the sum-over-states approach, we get

$$\begin{aligned} E1_{PNC} = \frac{1}{\sqrt{\langle \Psi_f^{(0)} | \Psi_f^{(0)} \rangle \langle \Psi_i^{(0)} | \Psi_i^{(0)} \rangle}} \quad & \{ \sum_{I \neq i} \frac{\langle \Psi_f^{(0)} | D | \Psi_I^{(0)} \rangle \langle \Psi_I^{(0)} | H^{(1)} | \Psi_i^{(0)} \rangle}{E_i - E_I} \\ + \sum_{J \neq f} \quad & \frac{\langle \Psi_f^{(0)} | H^{(1)} | \Psi_J^{(0)} \rangle \langle \Psi_J^{(0)} | D | \Psi_i^{(0)} \rangle}{E_f - E_J} \} \end{aligned} \tag{4.8}$$

where I and J represent intermediate states.

Blundell *et al.* [3, 8] have used the above sum-over-states method to determine $E1_{PNC}$ for the $6s \rightarrow 7s$ transition in Cs, where most accurate

experimental results are available [5]. They have considered the important intermediate states. Dzuba *et al.* in one of their approaches [9] and Geetha [10] calculate the $E1_{PNC}$ amplitude for $6s\ ^2S_{1/2} \rightarrow 5d\ ^2D_{3/2}$ transition by following the approach of Blundell *et al.* [3]. The drawback of this approach is that the summation can be performed only over a finite set of intermediate states which limits the accuracy of the calculation.

The method we have used in the present work circumvents this problem by solving the first order perturbed equation for the corrected wavefunction of

$$(H^{(0)} - E^{(0)})|\Psi^{(1)}\rangle = (E^{(1)}_{PNC} - H^{(1)})|\Psi^{(0)}\rangle \tag{4.9}$$

where $E^{(1)}_{PNC} = 0$ since $H^{(1)}$ corresponds to the parity non-conserving weak interaction.

In RCC, the cluster operators for calculating the perturbed wavefunctions can be written as

$$\begin{aligned} T &= T^{(0)} + G_F T^{(1)} \\ S_v &= S_v^{(0)} + G_F S_v^{(1)} \end{aligned} \tag{4.10}$$

where $T^{(1)}$ and $S_v^{(1)}$ are the first order G_F corrections to the cluster operators $T^{(0)}$ and $S_v^{(0)}$ operators, respectively.

We discuss below the detailed procedure for determining the perturbed RCC amplitudes which are necessary to calculate the $E1_{PNC}$ amplitude. Like the previous procedure, we first solve the closed-shell cluster amplitudes followed by the open-shell amplitudes and then the PNC amplitude.

4.3 Closed-shell Theory

With the above modified wavefunction, the eigenvalue equation for the atomic systems can be written as

$$H|\Psi\rangle \;=\; E|\Psi\rangle.$$

Substituting the wavefunction from the closed-shell RCC method given in the previous chapter, we get

$$He^T|\Phi_0\rangle = Ee^T|\Phi_0\rangle. \tag{4.11}$$

Expanding the above equation using the relation (4.1), we get

$$\begin{aligned}(H^{(0)} + G_F H^{(1)})e^T|\Phi_0\rangle &= (E^{(0)} + G_F E^{(1)})e^T|\Phi_0\rangle \\ (H_N^{(0)} + G_F H^{(1)})e^T|\Phi_0\rangle &= (E^{(0)} - E_{DF}^{(0)} + G_F E^{(1)})e^T|\Phi_0\rangle\end{aligned}$$

where higher order corrections to the energy eigenvalues are neglected keeping only up to linear terms. Subscript N represents normal order form (see Appendix B for the definition). $E_{DF}^{(0)}$ is the DF energy.

Operating by e^{-T} on both sides from the left, we get

$$\begin{aligned}e^{-T}(H_N^{(0)} + G_F H^{(1)})e^T|\Phi_0\rangle &= (E^{(0)} - E_{DF}^{(0)})|\Phi_0\rangle \\ (\overbrace{(H_N^{(0)}e^T}^{} + G_F \overbrace{H^{(1)}e^T}^{}))|\Phi_0\rangle &= (E^{(0)} - E_{DF}^{(0)})|\Phi_0\rangle\end{aligned}$$

since $E^{(1)}$ is zero, where $e^{-T}He^T = \overbrace{He^T}^{}$ are the connected terms as given by Hausdorff expansion (see Appendix D).

Substituting expression for T from equation (4.10) and keeping only linear terms in G_F, we get

$$\begin{aligned}(\overline{H_N^{(0)}}(1 + G_F T^{(1)}) + G_F \overline{H^{(1)}}(1 + G_F T^{(1)})|\Phi_0\rangle &= (E^{(0)} - E_{DF}^{(0)})|\Phi_0\rangle \\ (\overline{H_N^{(0)}}T^{(1)} + \overline{H^{(1)}})|\Phi_0\rangle &= (E^{(0)} - E_{DF}^{(0)})|\Phi_0\rangle\end{aligned} \tag{4.12}$$

where we define $\overbrace{He^{T^{(0)}}}^{} = \overline{H}$ in the above equation. The final expression has been obtained by equating the first order terms in G_F on both sides.

The amplitudes for the $T^{(1)}$ operators are obtained by making the scalar products with the bra vector of excited states $|\Phi^*\rangle$ as

$$\langle\Phi^*|\overline{H_N^{(0)}}T^{(1)} + \overline{H^{(1)}}|\Phi_0\rangle = 0. \tag{4.13}$$

The computational procedure for solving this equation has been discussed later.

4.4 Open-shell Theory

We start with the equation for single valence system

$$H|\Psi_v\rangle = E|\Psi_v\rangle. \tag{4.14}$$

Substituting the relation given by equation (4.1) and the single valence RCC wavefunction formulation, we get

$$(H^{(0)} + G_F H^{(1)})e^T\{1+S_v\}|\Phi_v\rangle = (E^{(0)} + G_F E^{(1)})e^T\{1+S_v\}|\Phi_v\rangle$$

where higher order correction to the energy eigenvalues are neglected keeping only up to linear terms. Operating e^{-T} on both the sides yields

$$\begin{aligned} e^{-T}(H^{(0)} + G_F H^{(1)})e^T\{1+S_v\}|\Phi_v\rangle &= E^{(0)}|\{1+S_v\}\Phi_v\rangle \\ (\overbrace{H^{(0)}e^T} + G_F \overbrace{H^{(1)}e^T})\{1+S_v\}|\Phi_v\rangle &= E^{(0)}\{1+S_v\}|\Phi_v\rangle \end{aligned}$$

Substituting the value of T and S_v operators from equation (4.10) and keeping terms only up to linear order in G_F, we get

$$\begin{aligned} (\overline{H^{(0)}}\{1 + S_v^{(0)} + G_F(T^{(1)} + S_v^{(1)}\}) + G_F\overline{H^{(1)}}\{1 + S_v^{(0)} + G_F(T^{(1)} + S_v^{(1)})\})|\Phi_v\rangle \\ = E^{(0)}\{1 + S_v^{(0)} + G_F S_v^{(1)}\}|\Phi_v\rangle \\ (\overline{H^{(0)}}S_v^{(1)} + \overline{H^{(0)}}T^{(1)}\{1 + S_v^{(0)}\} + \overline{H^{(1)}}\{1 + S_v^{(0)}\})|\Phi_v\rangle = E^{(0)}\{1 + S_v^{(1)})|\Phi_v\rangle. \end{aligned} \tag{4.15}$$

The overline has been defined as $\overline{H^{(0)}} = e^{-T^{(0)}}He^{T^{(0)}}$ as in the case of the closed-shell equations. The open-shell perturbed amplitudes ($S_v^{(1)}$) are solved by projecting the excited states, ($|\Phi_v^*\rangle$) as

$$\langle\Phi_v^*|(\overline{H_N^{(0)}} - \Delta E_v)S_v^{(1)} + (\overline{H_N^{(0)}}T^{(1)} + \overline{H_{PNC}^{NSI}})\{1 + S_v^{(0)}\}|\Phi_v\rangle = 0 \tag{4.16}$$

where ΔE_v is the negative of ionization potential of the valence electron 'v'.

We discuss later the computational procedure for solving the above equation.

4.5 Evaluation of the $E1_{PNC}$ amplitude

The $E1_{PNC}$ amplitude between states $|\Psi_f\rangle$ and $|\Psi_i\rangle$ is given by

$$E1_{PNC} = \frac{\langle\Psi_f|D|\Psi_i\rangle}{\sqrt{\langle\Psi_f|\Psi_f\rangle\langle\Psi_i|\Psi_i\rangle}}.$$

Substituting the expressions for wavefunction in the RCC method and keeping terms only up to linear order in perturbed operators, we get

$$\begin{aligned} E1_{PNC} = G_F \quad & \frac{\underline{\langle\Phi_f|\{1+S_f^{(1)^\dagger}+S_f^{(0)^\dagger}T^{(1)^\dagger}+T^{(1)^\dagger}\}}}{\sqrt{(1+N_f^{(0)})(1+N_i^{(0)})}} \\ & \qquad e^{T^{(0)^\dagger}}De^{T^{(0)}}\{1+T^{(1)}+T^{(1)}S_i^{(0)}+S_i^{(1)}\}|\Phi_i\rangle \\ = G_F \quad & \frac{\underline{\langle\Phi_f|S_f^{(1)^\dagger}\overline{D^{(0)}}(1+S_i^{(0)})+(1+S_f^{(0)^\dagger})\overline{D^{(0)}}S_i^{(1)}}}{\sqrt{(1+N_f^{(0)})(1+N_i^{(0)})}} \\ & + S_f^{(0)^\dagger}(T^{(1)^\dagger}\overline{D^{(0)}}+\overline{D^{(0)}}T^{(1)})S_i^{(0)}+(T^{(1)^\dagger}\overline{D^{(0)}}+\overline{D^{(0)}}T^{(1)})S_i^{(0)}|\Phi_i\rangle \end{aligned} \tag{4.17}$$

where $\overline{D^{(0)}}$ is the effective one-body term of the expression $e^{T^{(0)^\dagger}}De^{T^{(0)}}$ and $N_v^{(0)} = S_v^{(0)^\dagger}e^{T^{(0)^\dagger}}De^{T^{(0)}}S_v^{(0)}$ for the valence electron 'v'.

We have shown all possible effective one-body terms arising from $\overline{D^{(0)}}$ in the previous chapter. These terms are used directly from the unperturbed part to evaluate the above $E1_{PNC}$ amplitude. We follow the strategy given by Lindroth *et al.* [11] and Blundell *et al.* [12] to calculate properties in the linearized RCC method by constructing effective one-body, two-body etc. operators. We assume $\overline{D^{(0)}}$ as an operator and construct effective one-body, two-body operators etc. by contracting this operator with $T^{(1)}$s and their adjoints. Then these terms are contracted with corresponding open-shell perturbed operators and their conjugates to compute the final result. We have given all possible diagrams to calculate the above $E1_{PNC}$ amplitude in figure 4.1.

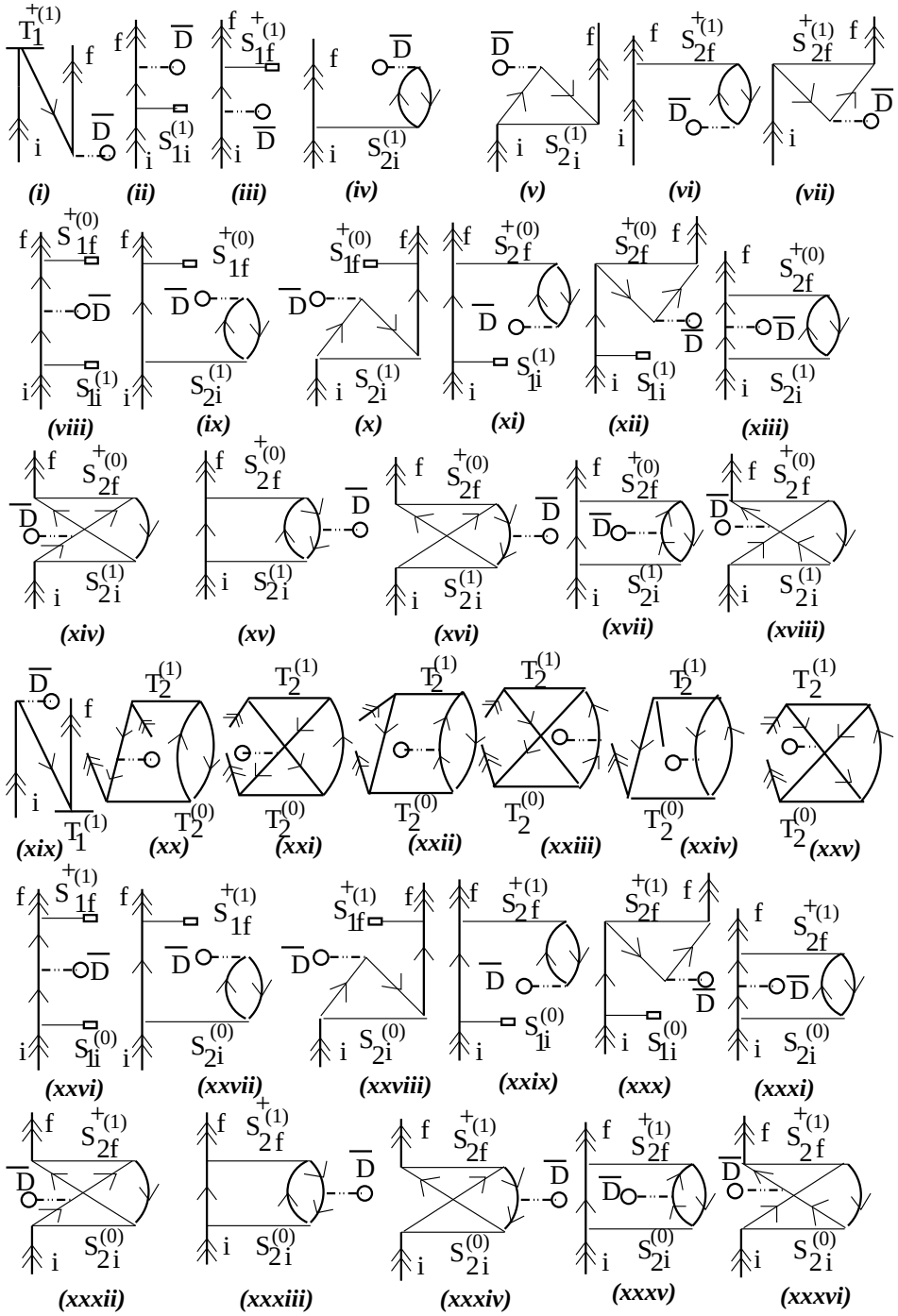
(i)
(ii)
(iii)
(iv)
(v)
(vi)
(vii)
(viii)
(ix)
(x)
(xi)
(xii)
(xiii)
(xiv)
(xv)
(xvi)
(xvii)
(xviii)
(xix)
(xx)
(xxi)
(xxii)
(xxiii)
(xxiv)
(xxv)
(xxvi)
(xxvii)
(xxviii)
(xxix)
(xxx)
(xxxi)
(xxxii)
(xxxiii)
(xxxiv)
(xxxv)
(xxxvi)

Cont.....

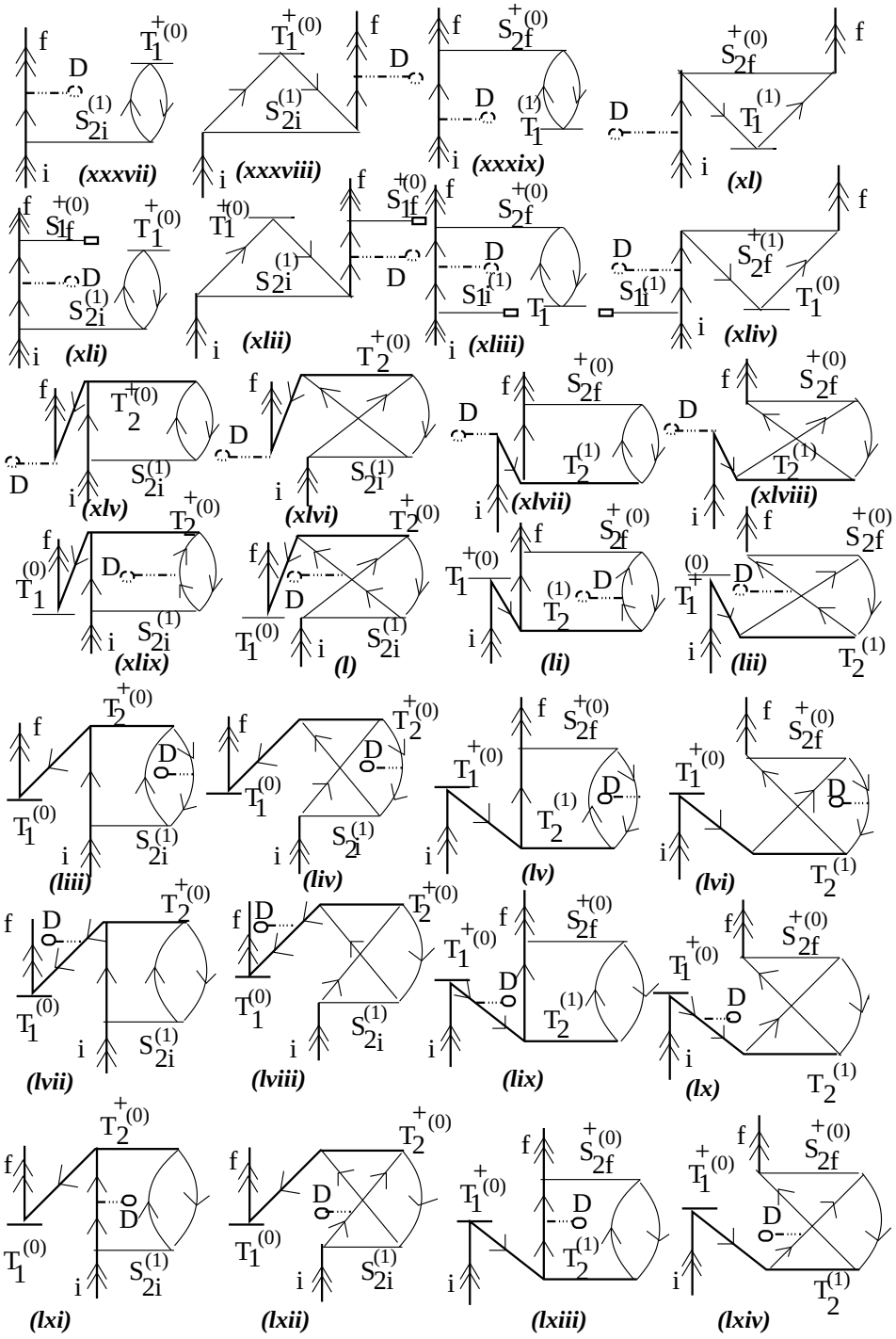

Figure 4.1: Diagrams for $E1_{PNC}$ evaluating terms.

4.6 Computational procedure and parallelization techniques

We present the procedure to evaluate the closed-shell and open-shell PNC cluster amplitudes in this section. We construct matrix equations similar to the unperturbed closed-shell and open-shell CC equations and solve them using the Jacobi iterative method. We make use of all the intermediate diagrams constructed for unperturbed open-shell CC amplitude equations which are given in the previous chapter.

Although we use the intermediate diagrams in both the unperturbed and perturbed amplitude determining equations, it still takes a long time to perform a single set of complete calculations to obtain the $E1_{PNC}$ amplitude and related quantities in heavy systems. Therefore, we have developed a method to compute our programs parallely by many processors using the Message Passing Interface (MPI) library routines [13]. We have explained the detailed procedure in the following subsections.

4.6.1 Computational method for closed-shell amplitudes

In the matrix representation, with the CCSD approximation, one can write the equation (4.13) as

$$\begin{pmatrix} \langle \Phi_a^p | \overline{H_N^{(0)}} | \Phi_a^p \rangle & \langle \Phi_a^p | \overline{H_N^{(0)}} | \Phi_{ab}^{pq} \rangle \\ \langle \Phi_{ab}^{pq} | \overline{H_N^{(0)}} | \Phi_a^p \rangle & \langle \Phi_{ab}^{pq} | \overline{H_N^{(0)}} | \Phi_{ab}^{pq} \rangle \end{pmatrix} \begin{pmatrix} t_a^{p(1)} \\ t_{ab}^{pq(1)} \end{pmatrix} = - \begin{pmatrix} \langle \Phi_a^p | \overline{H^{(1)}} | \Phi_0 \rangle \\ \langle \Phi_{ab}^{pq} | \overline{H^{(1)}} | \Phi_0 \rangle \end{pmatrix} \quad (4.18)$$

where $t_a^{p(1)}$ and $t_{ab}^{pq(1)}$ are the perturbed single and double excitation amplitudes, respectively.

Or, in vector form one writes

$$\mathbf{A} \cdot \mathbf{X} \;=\; -\mathbf{B}. \quad (4.19)$$

The j^{th} element of the vector $\mathbf{X}$, which represents $T^{(1)}$ operator, can be

solved using the Jacobi iterative method by expressing

$$X_j^i = \frac{-B_j - \sum_{l \neq j} A_{jl} X_l^{(i-1)}}{A_{jj}} \tag{4.20}$$

where i represents iteration number and j the element number. A_{jl} and A_{jj} are the off-diagonal and diagonal elements of the matrix $\mathbf{A}$. B_j is the j^{th} element of the matrix $\mathbf{B}$.

The initial values for these elements are considered as,

$$\begin{aligned} t_a^{p(1)}(1) &= -\frac{\langle \Phi_a^p | \overline{H^{(1)}} | \Phi_0 \rangle}{f(p,p) - f(a,a)} \\ t_{ab}^{pq(1)}(1) &= -\frac{\langle \Phi_{ab}^{pq} | \overline{H^{(1)}} | \Phi_0 \rangle}{f(p,p) + f(q,q) - f(a,a) - f(b,b)} \end{aligned} \tag{4.21}$$

where $f(i,j)$ represent the i and j element of f-bar terms given in the previous chapter. Here superscript (1) represents the perturbed operator and ordinary (1) stands for first iteration.

In equation (4.18), $\overline{H^{(0)}} = e^{-T^{(0)}} H e^{T^{(0)}}$ is same as the open-shell RCC equations given by equation (3.21) of the previous chapter. Therefore, the intermediate diagrams given by f-bar and v-bar in the previous chapter can be used here for solving the above perturbed amplitudes. Since the level of excitation for the open-shell and closed-shell excitation operators are different, therefore, it also requires some extra v-bar diagrams. These extra v-bar diagrams are presented in figure 4.2.

The $\mathbf{B}$ matrix diagrams are shown in figure 4.3. Off-diagonal diagrams for single and double excitation equations are shown in figures 4.4 and 4.5, respectively.

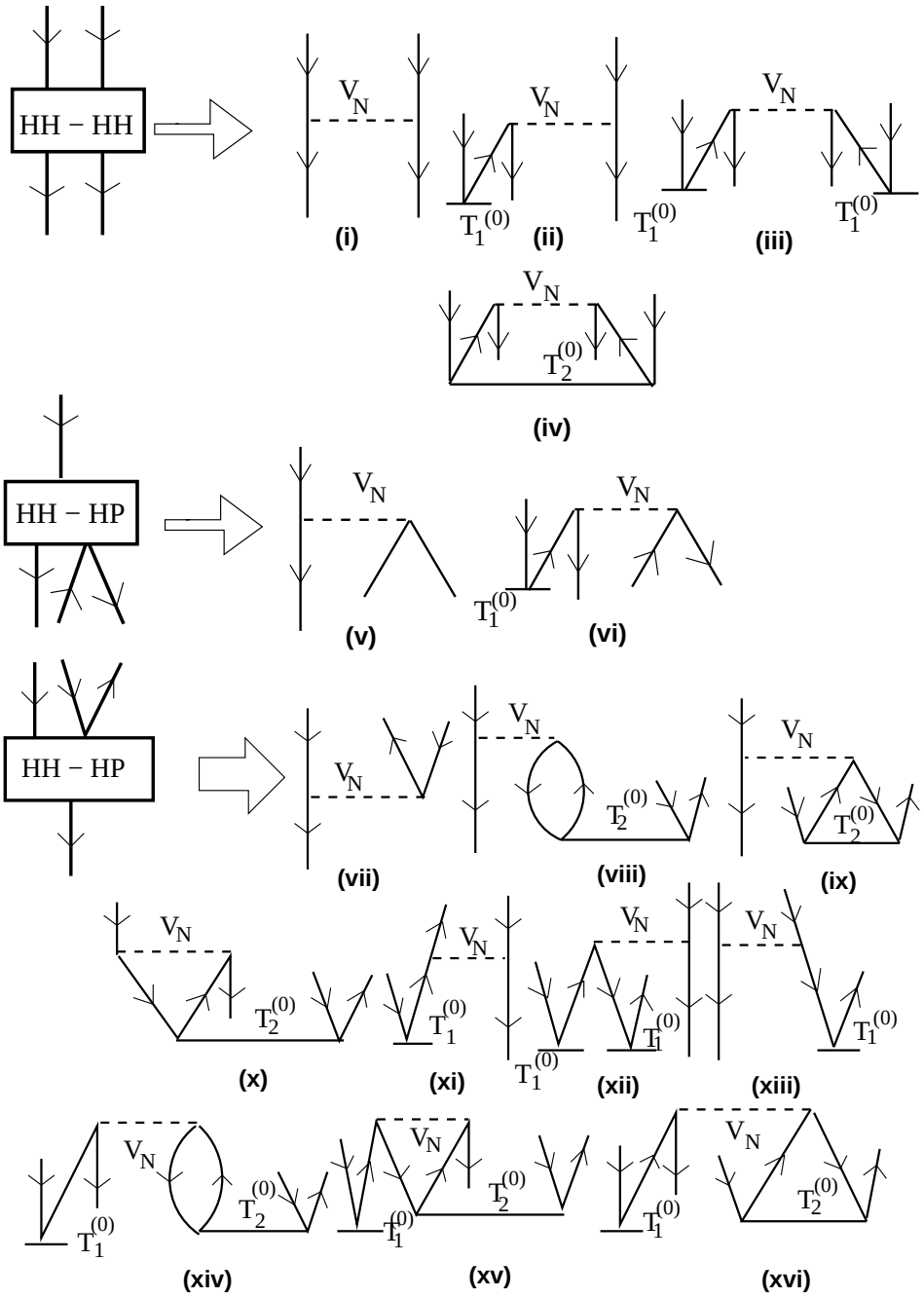
HH − HH
V_N
T_1^(0)
(i)
(ii)
(iii)
T_2^(0)
(iv)
HH − HP
(v)
(vi)
HH − HP
(vii)
(viii)
(ix)
(x)
(xi)
(xii)
(xiii)
(xiv)
(xv)
(xvi)

Cont.....

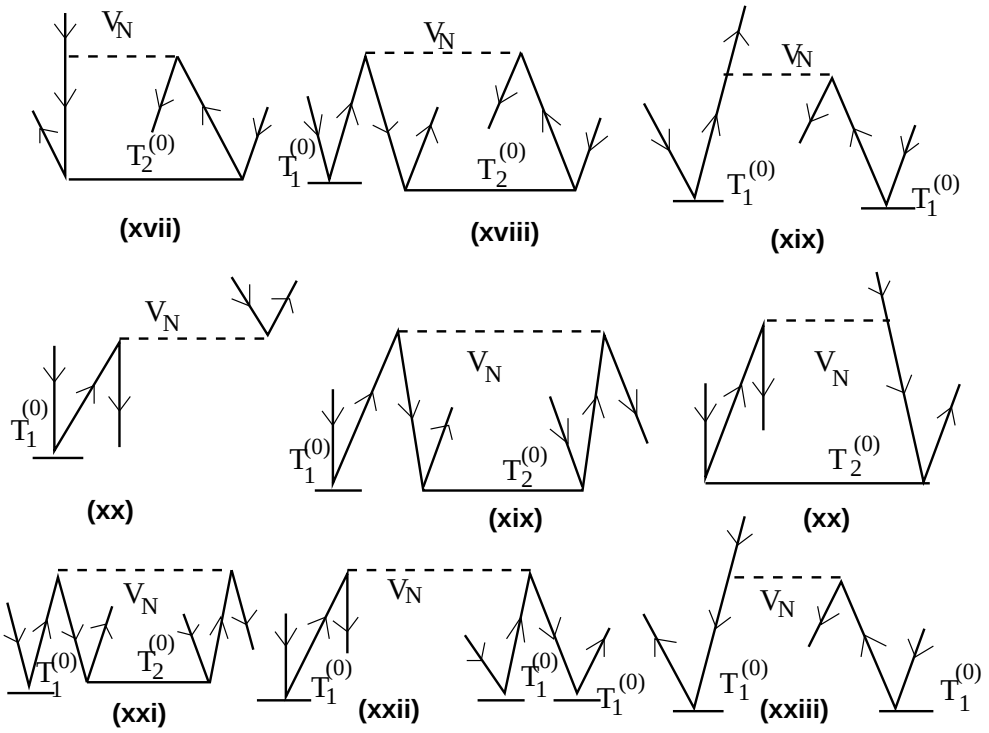

Figure 4.2: Diagrammatic representation of extra v-bar terms for $T^{(1)}$ amplitude calculation.

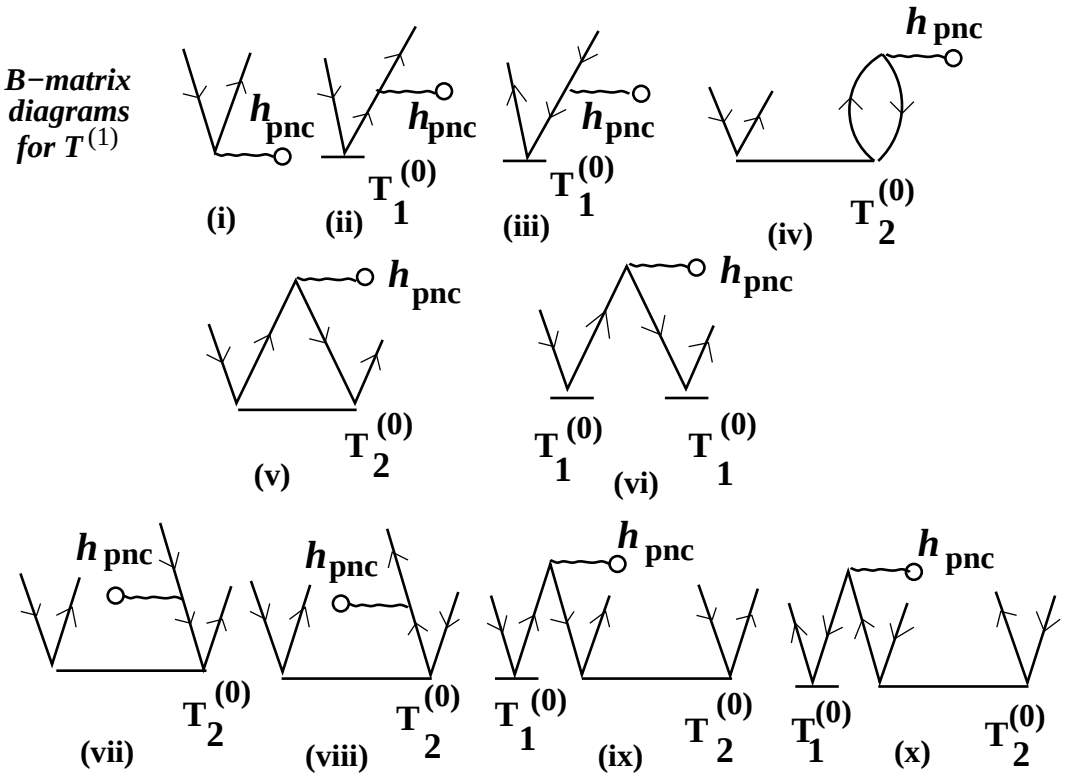

Figure 4.3: Diagrams of B- matrix elements for singles and doubles.

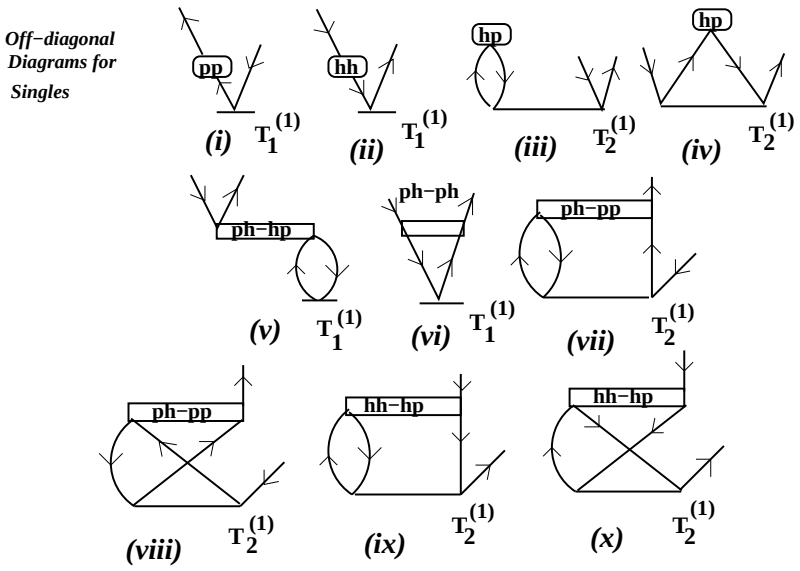

Figure 4.4: Diagrams for off-diagonal elements for $T^{(1)}$ with single excitations.

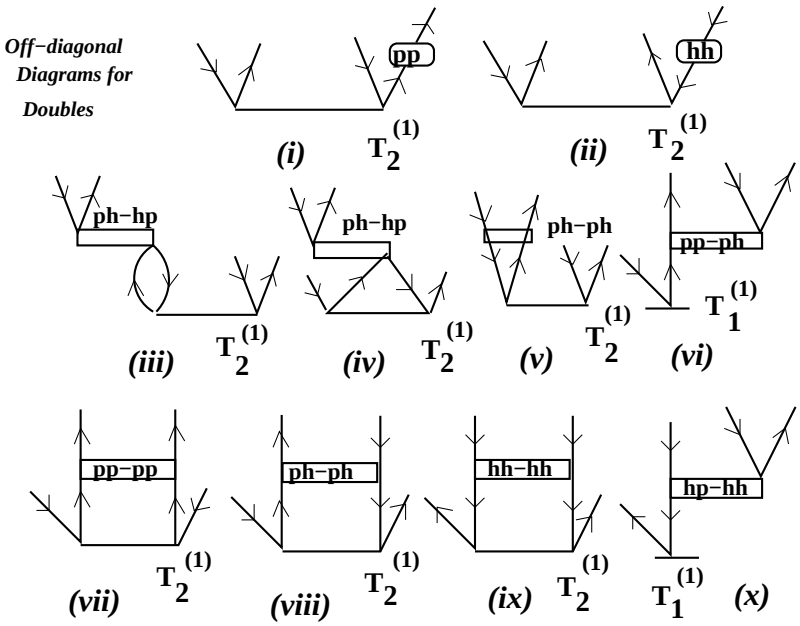

Figure 4.5: Diagrams for off-diagonal elements for $T^{(1)}$ with double excitations.

4.6.2 Computational method for open-shell amplitudes

Using CCSD approximation, the open-shell equation given by (4.16) can be represented by the following matrix form

$$\begin{pmatrix} \langle\Phi_v^p|\overline{H_N^{(0)}} - \Delta E_v|\Phi_v^p\rangle & \langle\Phi_v^p|\overline{H_N^{(0)}}|\Phi_{vb}^{pq}\rangle \\ \langle\Phi_{vb}^{pq}|\overline{H_N^{(0)}}|\Phi_v^p\rangle & \langle\Phi_{vb}^{pq}|\overline{H_N^{(0)}} - \Delta E_v|\Phi_{vb}^{pq}\rangle \end{pmatrix} \begin{pmatrix} s_v^{p(1)} \\ s_{vb}^{pq(1)} \end{pmatrix} = - \begin{pmatrix} \langle\Phi_v^p|\overline{H_N^{(0)}T^{(1)}} + \overline{H^{(1)}}|\Phi_v\rangle \\ \langle\Phi_{vb}^{pq}|\overline{H_N^{(0)}T^{(1)}} + \overline{H^{(1)}}|\Phi_v\rangle \end{pmatrix} \tag{4.22}$$

where $s_v^{p(1)}$ and $s_{vb}^{pq(1)}$ are the perturbed single and double excitation amplitudes, respectively, with the valence electron 'v'.

In vector notation, the above matrix can be expressed as

$$\mathbf{A} \cdot \mathbf{X} = -\mathbf{B}. \tag{4.23}$$

The j^{th} element of the vector $\mathbf{X}$, which represents $S_v^{(1)}$ operator, can be solved using the Jacobi iterative method by expressing

$$X_j^i = \frac{-B_j - \sum_{l \neq j} A_{jl} X_l^{(i-1)}}{A_{jj}} \tag{4.24}$$

where i stands for the iteration number and j for the element number. A_{jl} and A_{jj} are the off-diagonal and diagonal elements of the matrix $\mathbf{A}$. B_j is the j^{th} element of the matrix $\mathbf{B}$.

The initial values for these elements are considered as

$$\begin{aligned} s_v^{p(1)}(1) &= -\frac{\langle\Phi_v^p|\overline{H^{(0)}}T^{(1)} + \overline{H^{(1)}}|\Phi_0\rangle}{f(p,p) - \Delta E_v} \\ s_{vb}^{pq(1)}(1) &= -\frac{\langle\Phi_{vb}^{pq}|\overline{H^{(0)}}T^{(1)} + \overline{H^{(1)}}|\Phi_0\rangle}{f(p,p) + f(q,q) - f(b,b) - \Delta E_v} \end{aligned} \tag{4.25}$$

where $f(i,j)$ represent the i and j element of the f-bar diagrams as given in the previous section.

In equation (4.22), $\overline{H^{(0)}} = e^{-T^{(0)}} H e^{T^{(0)}}$ is same as the open-shell RCC equations given by equation (3.21) of the previous chapter. Therefore, the intermediate diagrams given by f-bar and v-bar there can be used here for solving the above perturbed amplitudes.

The B-matrix diagrams are shown in figures 4.6 and 4.7. The off-diagonal diagrams are shown in figure 4.8.

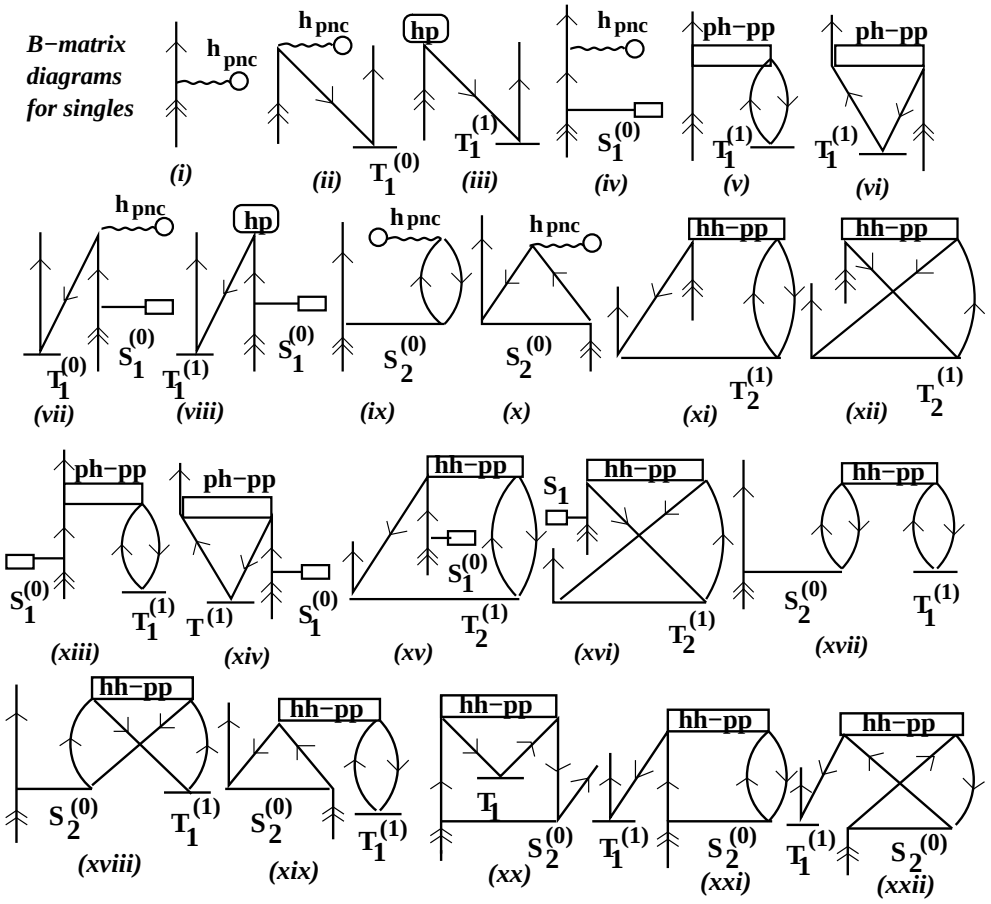

Figure 4.6: Diagrams for B-matrix element for single excitations.

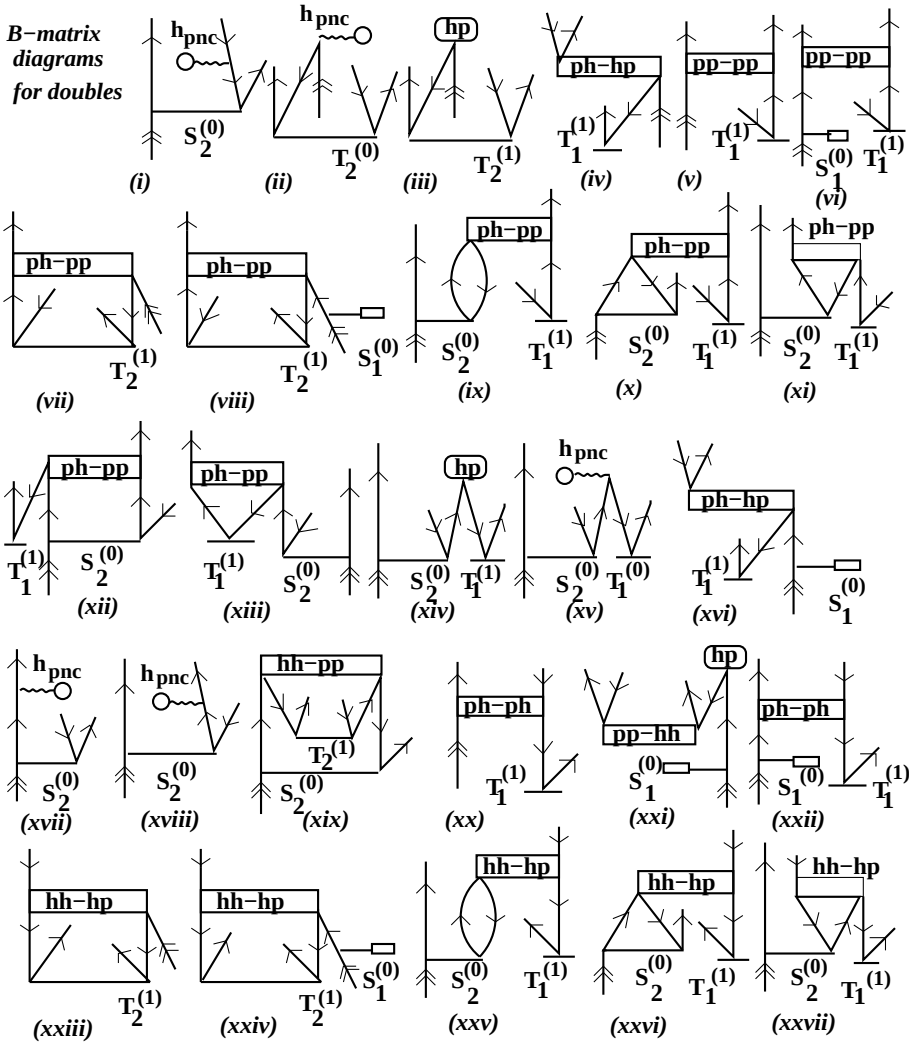
B−matrix diagrams for doubles
h pnc
hp
ph−hp
pp−pp
ph−pp
hh−pp
hh−hp
(i)
(ii)
(iii)
(iv)
(v)
(vi)
(vii)
(viii)
(ix)
(x)
(xi)
(xii)
(xiii)
(xiv)
(xv)
(xvi)
(xvii)
(xviii)
(xix)
(xx)
(xxi)
(xxii)
(xxiii)
(xxiv)
(xxv)
(xxvi)
(xxvii)

Cont.....

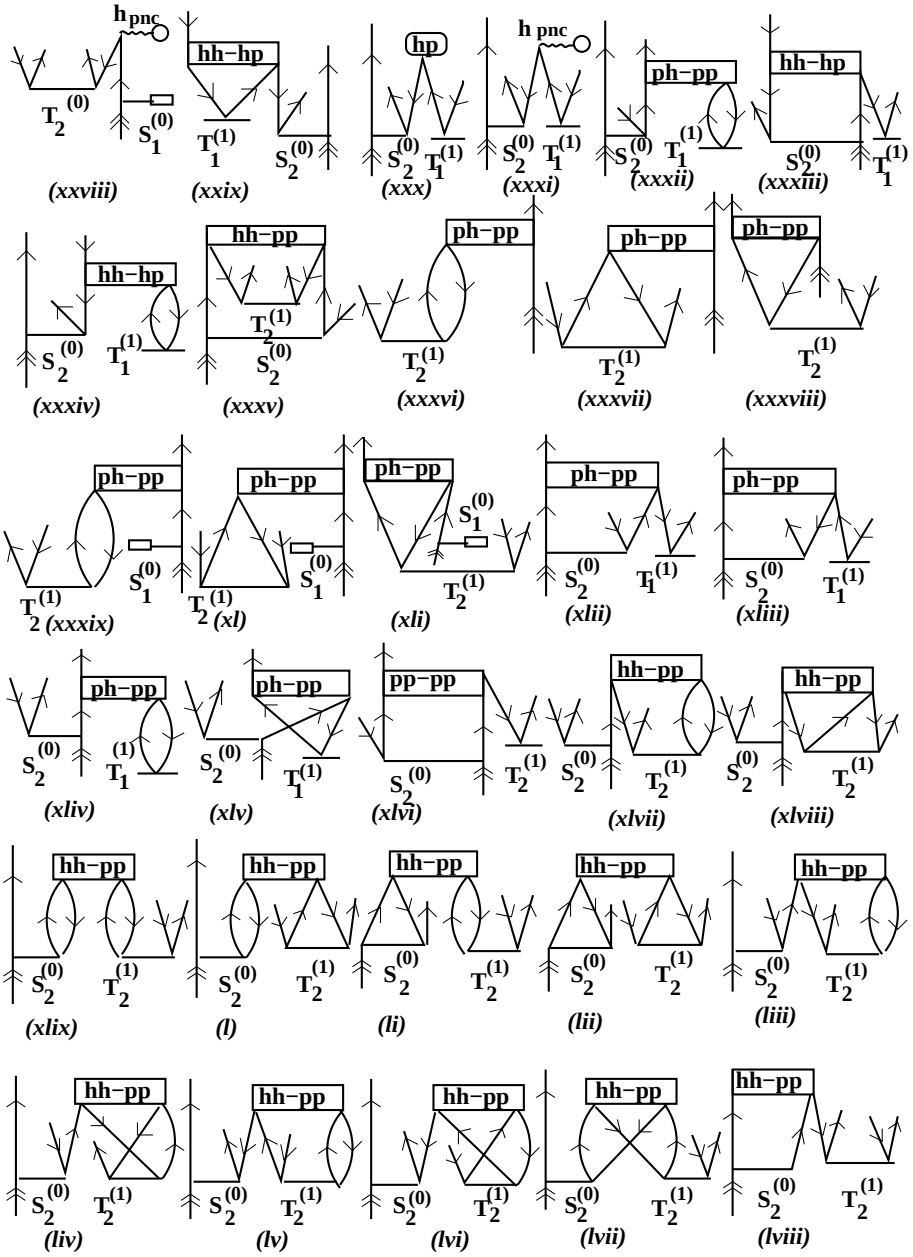

Figure 4.7: Diagrams for B-matrix element for double excitations.

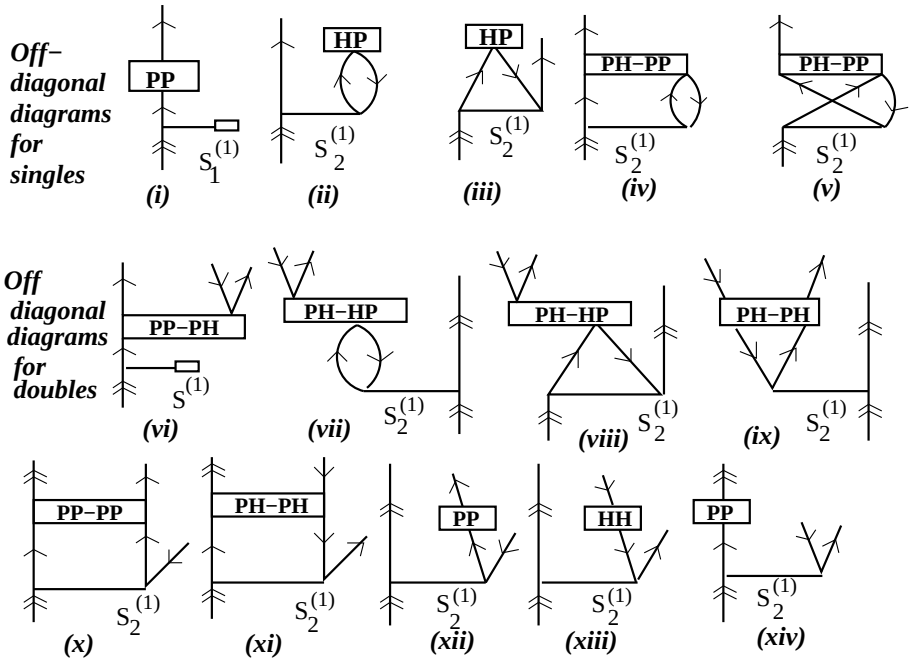

Figure 4.8: Diagrams for off-diagonal elements of S_v determining equations.

4.6.3 Parallelization of CCSD programs using MPI

It is clear from the last three chapters that the numerical computations for the present studies are of a very large scale. The $E1_{PNC}$ amplitude calculations are carried out only for the heavy systems because of the fact that the PNC matrix element depends on cubic power of the atomic number. Calculations on heavier systems means performing large computations. For example, if we examine the general formula for the Coulomb integrals, as given in the chapter 2, the computational procedure requires four outer loops for the total number of single particle orbitals along with an extra loop for the possible number of multipoles for each set of single particle orbitals. A sequential calculation of these integrals will consume lot of CPU time. In fact, all the intermediate steps and Jacobi iterative procedure will also take a lot of time. We have developed a parallelized method for computing the CCSD amplitudes using multiple processors. Although the actual procedure to parallelize these codes are somewhat subtle, we present here and outline of the parallelization structure for different parts of the CCSD code which take comparatively longer time than the other parts of the program.

4.6.4 Two-body integrals

In atomic properties one has to calculate integrals for Coulomb and/or Breit interactions. Their selection rules are such that the Coulomb integral allows either odd or even multipoles [15] and the Breit interaction allows both even and odd multipoles [16]. Therefore, inclusion of Breit interaction which could be important for heavier systems, will allow all possible multipoles and the amount of computation needed for these two-body integrations will be very large. Therefore, it is necessary to parallelize this part of the program. Again, these integrals have to be calculated repeatedly for closed-shell and open-shell systems in both the unperturbed and perturbed RCC amplitude determining equations.

A variable having any number of running indices can be calculated parallely by just dividing the outer loop into total number of processors, provided that the dimension of the outer index should be greater than or equal to the number of processors used, by expressing

```
Do I = 1 + IP, Imax, NP
  Do J = 1, Jmax
    Do K = 1, Kmax
          V(I, J, K, .....) = ···
          ···
    End do
  End do
End do
```

where $Imax$, $Jmax$, etc. are the dimensions of the I, J, etc running indices, respectively. NP is the total number of processors available and IP is the rank or address of each processor assigned by MPI_COMM_RANK using the MPI library package [13].

Direct implementation of this simple strategy in the two-body integrals will not be efficient, because these integrals we have an internal looping variable which depends on four outer indices representing angular momentum of the single particle orbitals. Again, they need to be stored in a specific sequence in order to use them later by calling their addresses. We present the following two steps to parallelise and store in a given sequence with any number of processors used for the parallelization

Step 1:

```
Ncount = 0
Do I_A = iproc, nproc
  Do I_B = 1, I_A
    Do I_C = 1, Nmax
      Do I_D = 1, Nmax
        Do K = |j_A − j_C|, j_B + j_D
          ···
          Ncount = Ncount + 1
          VP(Ncount) = X^K(ABCD)
          ···
        End do
      End do
    End do
  End do
```

End do

where $Nmax$ is the total number of basis used in the calculation, $X^K(ABCD)$ is the numerical value of the two-body integrals which depends on the multipole K and is derived from the angular momentum j of the orbitals. The restriction over the second loop is to overcome the double counting of the integrals. Here each processor is assigned an equal number of integrals from *iproc* to *nproc*, where $(nproc - iproc) = Nmax/NP$ with NP is the total number of processors used. It must be emphasized that the value of *iproc* and *nproc* are different for each processor. After calculation these integrals are stored as a variable VP and have been tracked by a counting index $Ncount$. These variables are then retrieved by the following procedure:

Step 2:

$Ncount1 = 0$
Do $I_A = iproc, nproc$
  Do $I_B = 1, I_A$
    Do $I_C = 1, Nmax$
      Do $I_D = 1, Nmax$
        Do $K = |j_A - j_C|, j_B + j_D$
          ...
          $Ncount1 = Ncount1 + 1$
          $V(I_A, I_B, I_C, I_D, K) = VP(Ncount1)$
          ...
        End do
      End do
    End do
  End do
End do.

Now all the integrals are stored in a specific format in a given variable 'V' which can be collected by a single processor (e.g. master processor). This variable can also be broadcasted using the command MPI_BCAST to all other processors and can be used by each processor at any time for further application wherever necessary.

4.6.5 Intermediate diagrams

As explained earlier, we construct our intermediate steps in terms of effective one-body terms (f-bar) and two-body terms (v-bar) for the RCC programs such that, we can use them repeatedly for both unperturbed and perturbed cluster amplitude equations and save an enormous amount of time instead of storing them in hard disk and reading them whenever required. Still it takes very large CPU time to compute them for heavy systems as it involves many non-linear terms. So we present briefly a parallel scheme to compute these intermediate terms. In case large hard disk space is not available, then the parallel computation is more helpful.

The f-bar terms depend only on two outer loops without any internal dependent index. Therefore, it can be parallelized using the general structure mentioned earlier. But the difficult part lies with the computation of the v-bar terms, because, again their structures are similar with the above two-body integrals with one internal dependent looping index. One can use the two-body integral strategy to parallelise them, but there is a possibility that it could cause problems while broadcasting a huge number of elements in a single variable array. Therefore, instead of following the above procedure, we parallelise the outer loop of the internal summation variables and compute them parallely. The price one has to pay in this case is that it is necessary to broadcast the parallelized variables. To compute them faster, in addition to the parallelization procedure one can also use string algebra to minimize internal looping structures as given by Kallay *et al.* [14] and save a large amount of computational time.

4.6.6 Jacobi iterative method

The parallelization procedure for the Jacobi iterative method for solving the RCC matrix equations are simpler compared to the above discussed parts of the program. One can simply divide total number of equations by total number of processors available to the user. Each set of equations can be calculated by an individual processor and then all the equations can be collected in a single array in a common variable and they can be broadcasted to all the other processors using MPI_ALL_GATHERV command. These

procedures have been followed in the present thesis work.

Bibliography

[1] B. P. Das, J. Andriessen, M. Vajed-Samii, S. N. Ray and T. P. Das, Phys. Rev. Lett. **49**, 32 (1982)

[2] V. A. Dzuba, V. V. Flambaum and O. P. Sushkov, Phys. Lett. A **141**, 147 (1989)

[3] S. A. Blundell, W. R. Johnson and J. Sapirstein, Phys. Rev. Lett. **65**, 1411 (1990)

[4] V. A. Dzuba, V. V. Flambaum, P. G. Silverstrov and O. P. Sushkov, Phys. Lett. A **141**, 147 (1987)

[5] C. S. Wood, S. C. Bennet, D. Cho, B. P. Masterson, J. L. Roberts, C. E. Tanner and C. E. Wieman, Science **275**, 1759 (1997)

[6] I. Lindgren and J. Morrison, *Atomic many-body Theory*, edited by J. P. Toennies Springer-Verlag, Berlin (1982)

[7] D. Mukherjee and S. Pal, Adv. Quant. Chem. **20**, 281 (1989)

[8] S. A. Blundell, J. Sapirstein and W. R. Johnson, Phys. Rev. D **45**, 1602 (1992)

[9] V. A. Dzuba, V. V. Flmbaum and J. S. M. Ginges, Phys. Rev. A **63**, 062101 (2001)

[10] K. P. Geetha, Ph. D. Thesis, Bangalore University, India (2002)

[11] E. Lindroth and Y. Yennerman, Phys. Rev. A **47**, 961 (1993)

[12] S. A. Blundell, W. R. Johnson and J. Sapirstein, Phys. Rev. A **43**, 3407 (1991)

[13] William Gropp, Ewing Lusk and Anthony Skjellum, MIT Press Publication (1999)

[14] Mihály Kállay and Péter R. Surján, J. Chem. Phys. **115**, 2945 (2001)

[15] I. P. Grant, Relativistic self-consistent fields, Proc. R. Soc. London Ser. A **262**, 555 (1961)

[16] I. P. Grant, *Relativistic Atomic Structure Calculations*, Methods in Computational Chemistry, Edt. by S. Wilson, Plenum Press (New York) (1988)

Chapter 5

Results and Discussions

5.1 Introduction

The main thrust of this thesis is to perform a high precision calculation of the parity non-conserving electric dipole transition amplitude ($E1_{PNC}$) for the $6s\ ^2S_{1/2} \rightarrow 5d\ ^2D_{3/2}$ transition in singly ionized barium ($^{137}Ba^+$) which could be used in testing new physics beyond the Standard Model (SM) [1, 2, 3, 4]. We employ the relativistic coupled-cluster (RCC) theory by considering all possible non-linear terms in the calculations at the level of single and double excitations (CCSD) arising from the residual Coulomb interaction. We have also included the leading triple excitations in our calculations, which is referred as CCSD(T) [6] and has been discussed in the chapter 3. The difference between the calculated results using the CCSD(T) and CCSD methods could be set as the error due to the higher order excitations in the present calculations.

As discussed earlier in section (1.11), the calculation of $E1_{PNC}$, depends on
(i) E1 transition amplitudes
(ii) Excitation energies
and
(iii) Matrix elements of the PNC interaction Hamiltonian.

Therefore, it is necessary to calculate these properties and ascertain their accuracies in order to determine the error associated with $E1_{PNC}$ for the above transition. The behavior of these quantities varies at different regions from the nucleus.

It is now well established that the RCC theory is one of the most powerful methods for the accurate calculations of atomic properties [7, 8, 9, 10]. This is further corroborated by the results obtained in this chapter. In order to obtain accurate atomic wavefunctions it is also necessary to use high quality single particle orbitals to construct the reference wavefunction in RCC theory as well as in considering excitations from this state. For atomic systems with few electrons, it is comparatively simple to obtain accurate numerical orbitals. However, this is not the case for heavy atoms and ions. Therefore, one adopts a different approach to construct the orbitals for these systems by considering a suitable analytical form [11]. A linear combination of certain types complete mathematical functions can be used for this purpose [12]. We use Gaussian type orbitals (GTOs) in the present study which were explained in chapter 2. The limitation of this approach is that it is difficult to construct single particle orbitals which can produce accurate atomic orbitals over all regions in space. However, an accurate over all average can be obtained for the aforementioned properties. It is also not always practical to consider a complete set of orbitals in the calculations due to computational limitations. To overcome these problems, we calculate the atomic properties related to PNC for different sets of GTOs. Then we calculate $E1_{PNC}$ with the basis which is able to produce the best over all results for these properties. Later, we also discuss estimation of possible errors associated with $E1_{PNC}$.

5.2 Property calculations

Singly ionized ^{137}Ba is a heavy system with the electronic configuration $[5p^6]\ 6s^1$. The electronic configuration is the same for Cs but they have different nuclear charges. Ba^+ is ionized and hence the electron orbitals are more contracted towards the nucleus than for neutral barium. We have used

GTOs to construct single particle orbitals. From their functional form mentioned in chapter 2, it is clear that they contain two parameters (α_0 and β). The appropriate choice of these parameters is necessary to obtain accurate orbitals which are suitable linear combinations of GTOs. We have performed several calculations to study how the atomic properties of interest to us depend on these parameters. Later we also show how the atomic properties depend on the number of GTOs chosen for a particular choice of α_0 and β.

We now turn to the details of our calculations. As mentioned in the previous section of this chapter, in order to obtain accurate atomic wavefunctions we require high quality single particle orbitals. The construction of such orbitals is the starting point of our calculations. This involves finding the best choices of α_0 and β for the GTOs used in our calculations. Here we have considered four different values of α_0 (0.00425, 0.00525, 0.00625, 0.00725), whilst keeping the value of $\beta = 2.73$ fixed. This makes it easier to understand the behavior of the single particle orbitals with respect to these two parameters. Comparison of the energies of the orbitals obtained from the GRASP2 code and those using GTOs with all α_0 values, are given in tables 5.1, 5.2, 5.3 and 5.4. The value of α_0 is listed at the top of each table. We have considered $38s_{1/2}$, $40p_{1/2}$, $40p_{3/2}$, $35d_{3/2}$, $35d_{5/2}$, $30f_{5/2}$, $30f_{7/2}$, $30g_{7/2}$ and $30g_{9/2}$ GTOs. These results show that values of $\alpha_0 = 0.00525$ and $\alpha_0 = 0.00625$ are able to produce good single particle energies. We have arrived at this conclusion by comparing our results with GRASP2 numerical orbitals. We have chosen $\alpha_0 = 0.00525$ in our calculations. To assess the accuracy of our single particle wavefunctions, we plot the differences of the large (P(r)) and small (Q(r)) components for our s, $p_{1/2}$ and $p_{3/2}$ orbitals and those from GRASP2 and shown in figures 5.1, 5.2 and 5.3.

I. With $\alpha_0 = 0.00425$ and $\beta = 2.73$.

Orbital	GRASP2	GTOs
$1s_{1/2}$	-1384.2767	-1385.0476
$2s_{1/2}$	-223.01881	-223.2783
$3s_{1/2}$	-49.0923	-49.2099
$4s_{1/2}$	-10.6961	-10.7309
$5s_{1/2}$	-2.0336	-2.0403
$6s_{1/2}$	-0.3432	-0.3440
$7s_{1/2}$	-0.1679	-0.1674
$8s_{1/2}$	-0.1003	-0.9776
$2p_{1/2}$	-209.5299	-209.6011
$3p_{1/2}$	-43.3980	-43.4316
$4p_{1/2}$	-8.5391	-8.5484
$5p_{1/2}$	-1.3877	-1.3870
$6p_{1/2}$	-0.2609	-0.2606
$7p_{1/2}$	-0.1377	-0.1371
$8p_{1/2}$	-0.0858	-0.0838
$2p_{3/2}$	-195.4521	-195.5409
$3p_{3/2}$	-40.6087	-40.6503
$4p_{3/2}$	-7.9532	-7.9639
$5p_{3/2}$	-1.3031	-1.3026
$6p_{3/2}$	-0.2545	-0.2543
$7p_{3/2}$	-0.1353	-0.1347
$8p_{3/2}$	-0.0846	-0.0829
$3d_{3/2}$	-30.7394	-30.7749
$4d_{3/2}$	-4.3530	-4.3632
$5d_{3/2}$	-0.3104	-0.3105
$6d_{3/2}$	-0.1515	-0.1513
$7d_{3/2}$	-0.0922	-0.0912
$3d_{5/2}$	-30.1534	-30.1916
$4d_{5/2}$	-4.2521	-4.2628
$5d_{5/2}$	-0.3083	-0.3084
$6d_{5/2}$	-0.1507	-0.1505
$7d_{5/2}$	-0.0919	-0.0907

Table 5.1: Comparison of single particle energies from GRASP2 and GTOs using $\alpha_0 = 0.00425$.

II. With $\alpha_0 = 0.00525$ and $\beta = 2.73$.

Orbital	GRASP2	GTOs
$1s_{1/2}$	-1384.2767	-1385.0341
$2s_{1/2}$	-223.01881	-223.2585
$3s_{1/2}$	-49.0923	-49.2112
$4s_{1/2}$	-10.6961	-10.7287
$5s_{1/2}$	-2.0336	-2.0384
$6s_{1/2}$	-0.3432	-0.3437
$7s_{1/2}$	-0.1679	-0.1679
$8s_{1/2}$	-0.1003	-0.9994
$2p_{1/2}$	-209.5299	-209.5894
$3p_{1/2}$	-43.3980	-43.4346
$4p_{1/2}$	-8.5391	-8.5510
$5p_{1/2}$	-1.3877	-1.3871
$6p_{1/2}$	-0.2609	-0.2607
$7p_{1/2}$	-0.1377	-0.1375
$8p_{1/2}$	-0.0858	-0.0856
$2p_{3/2}$	-195.4521	-195.5284
$3p_{3/2}$	-40.6087	-40.6527
$4p_{3/2}$	-7.9532	-7.9657
$5p_{3/2}$	-1.3031	-1.3029
$6p_{3/2}$	-0.2545	-0.2544
$7p_{3/2}$	-0.1353	-0.1352
$8p_{3/2}$	-0.0846	-0.0847
$3d_{3/2}$	-30.7394	-30.7705
$4d_{3/2}$	-4.3530	-4.3675
$5d_{3/2}$	-0.3104	-0.3110
$6d_{3/2}$	-0.1515	-0.1513
$7d_{3/2}$	-0.0922	-0.0905
$3d_{5/2}$	-30.1534	-30.1875
$4d_{5/2}$	-4.2521	-4.2670
$5d_{5/2}$	-0.3083	-0.3088
$6d_{5/2}$	-0.1507	-0.1505
$7d_{5/2}$	-0.0919	-0.0901

Table 5.2: Comparison of single particle energies from GRASP2 and GTOs using $\alpha_0 = 0.00525$.

III. With $\alpha_0 = 0.00625$ and $\beta = 2.73$.

Orbital	GRASP2	GTOs
$1s_{1/2}$	-1384.2767	-1385.0299
$2s_{1/2}$	-223.01881	-223.2558
$3s_{1/2}$	-49.0923	-49.2048
$4s_{1/2}$	-10.6961	-10.7286
$5s_{1/2}$	-2.0336	-2.0384
$6s_{1/2}$	-0.3432	-0.3437
$7s_{1/2}$	-0.1679	-0.1679
$8s_{1/2}$	-0.1003	-0.1001
$2p_{1/2}$	-209.5299	-209.5832
$3p_{1/2}$	-43.3980	-43.4370
$4p_{1/2}$	-8.5391	-8.5458
$5p_{1/2}$	-1.3877	-1.3871
$6p_{1/2}$	-0.2609	-0.2607
$7p_{1/2}$	-0.1377	-0.1373
$8p_{1/2}$	-0.0858	-0.0847
$2p_{3/2}$	-195.4521	-195.5223
$3p_{3/2}$	-40.6087	-40.6528
$4p_{3/2}$	-7.9532	-7.9607
$5p_{3/2}$	-1.3031	-1.3030
$6p_{3/2}$	-0.2545	-0.2544
$7p_{3/2}$	-0.1353	-0.1347
$7d_{3/2}$	-0.0922	-0.0905
$8p_{3/2}$	-0.0846	-0.0830
$3d_{3/2}$	-30.7394	-30.7714
$4d_{3/2}$	-4.3530	-4.3635
$5d_{3/2}$	-0.3104	-0.3109
$6d_{3/2}$	-0.1515	-0.1513
$7d_{3/2}$	-0.0922	-0.0909
$3d_{5/2}$	-30.1534	-30.1884
$4d_{5/2}$	-4.2521	-4.2629
$5d_{5/2}$	-0.3083	-0.3087
$6d_{5/2}$	-0.1507	-0.1505
$7d_{5/2}$	-0.0919	-0.0906

Table 5.3: Comparison of single particle energies from GRASP2 and GTOs using $\alpha_0 = 0.00625$.

IV. With $\alpha_0 = 0.00725$ and $\beta = 2.73$.

Orbital	GRASP2	GTOs
$1s_{1/2}$	-1384.2767	-1384.0357
$2s_{1/2}$	-223.01881	-223.2669
$3s_{1/2}$	-49.0923	-49.1993
$4s_{1/2}$	-10.6961	-10.7299
$5s_{1/2}$	-2.0336	-2.0396
$6s_{1/2}$	-0.3432	-0.3438
$7s_{1/2}$	-0.1679	-0.1674
$8s_{1/2}$	-0.1003	-0.9705
$2p_{1/2}$	-209.5299	-209.5863
$3p_{1/2}$	-43.3980	-43.4368
$4p_{1/2}$	-8.5391	-8.5402
$5p_{1/2}$	-1.3877	-1.3871
$6p_{1/2}$	-0.2609	-0.2607
$7d_{3/2}$	-0.0922	-0.0905
$7p_{1/2}$	-0.1377	-0.1367
$8p_{1/2}$	-0.0858	-0.0803
$2p_{3/2}$	-195.4521	-195.5259
$3p_{3/2}$	-40.6087	-40.6513
$4p_{3/2}$	-7.9532	-7.9559
$5p_{3/2}$	-1.3031	-1.3029
$6p_{3/2}$	-0.2545	-0.2544
$7p_{3/2}$	-0.1353	-0.1341
$8p_{3/2}$	-0.0846	-0.0775
$3d_{3/2}$	-30.7394	-30.7750
$4d_{3/2}$	-4.3530	-4.3577
$5d_{3/2}$	-0.3104	-0.3105
$6d_{3/2}$	-0.1515	-0.1513
$7d_{3/2}$	-0.0922	-0.0916
$3d_{5/2}$	-30.1534	-30.1918
$4d_{5/2}$	-4.2521	-4.3577
$5d_{5/2}$	-0.3083	-0.3105
$6d_{5/2}$	-0.1507	-0.1513
$7d_{5/2}$	-0.0919	-0.0916

Table 5.4: Comparison of single particle energies from GRASP2 and GTOs using $\alpha_0 = 0.00725$.

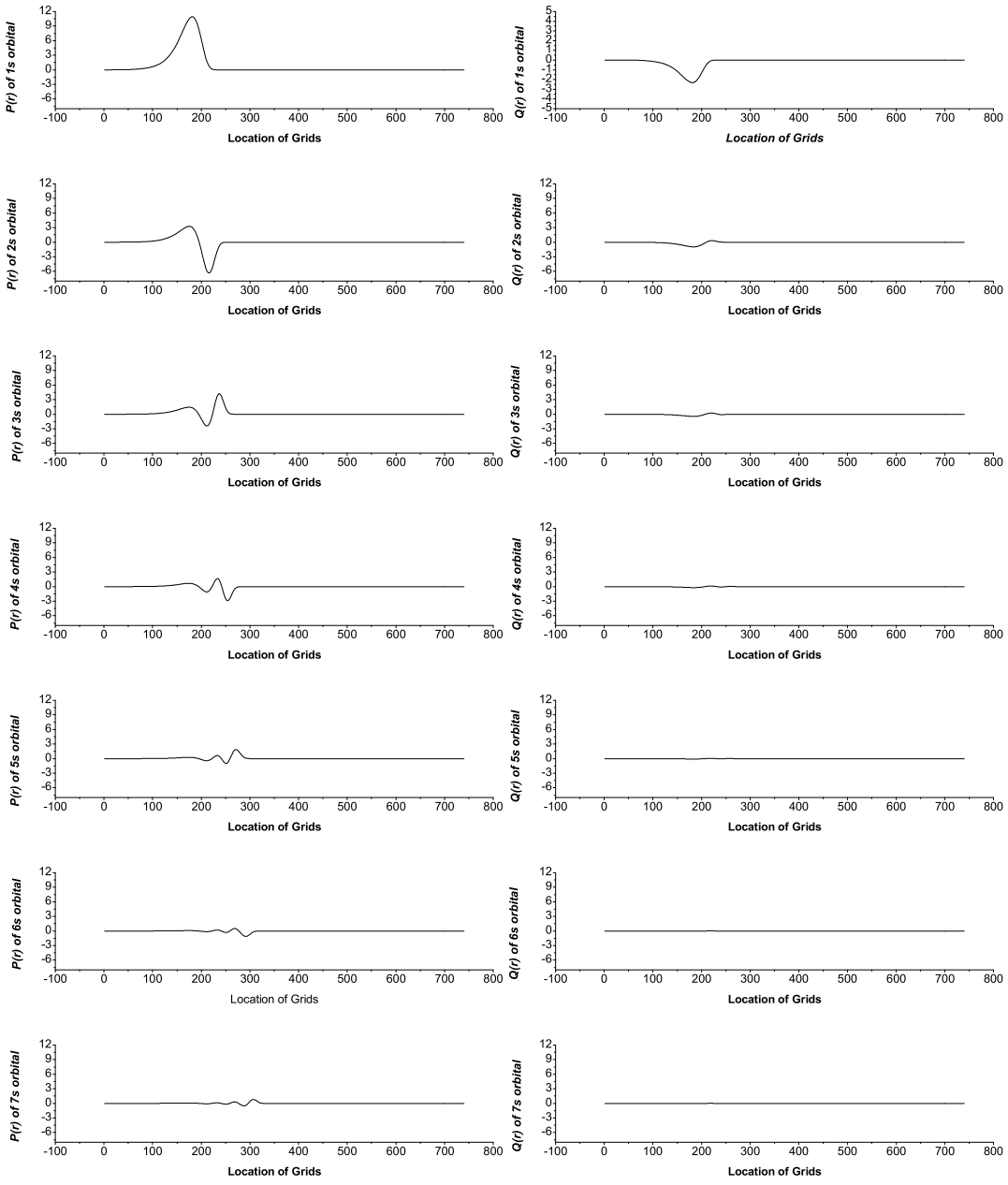

Figure 5.1: Difference between different s- orbital wavefunctions obtained using GRASP2 and GTOs.

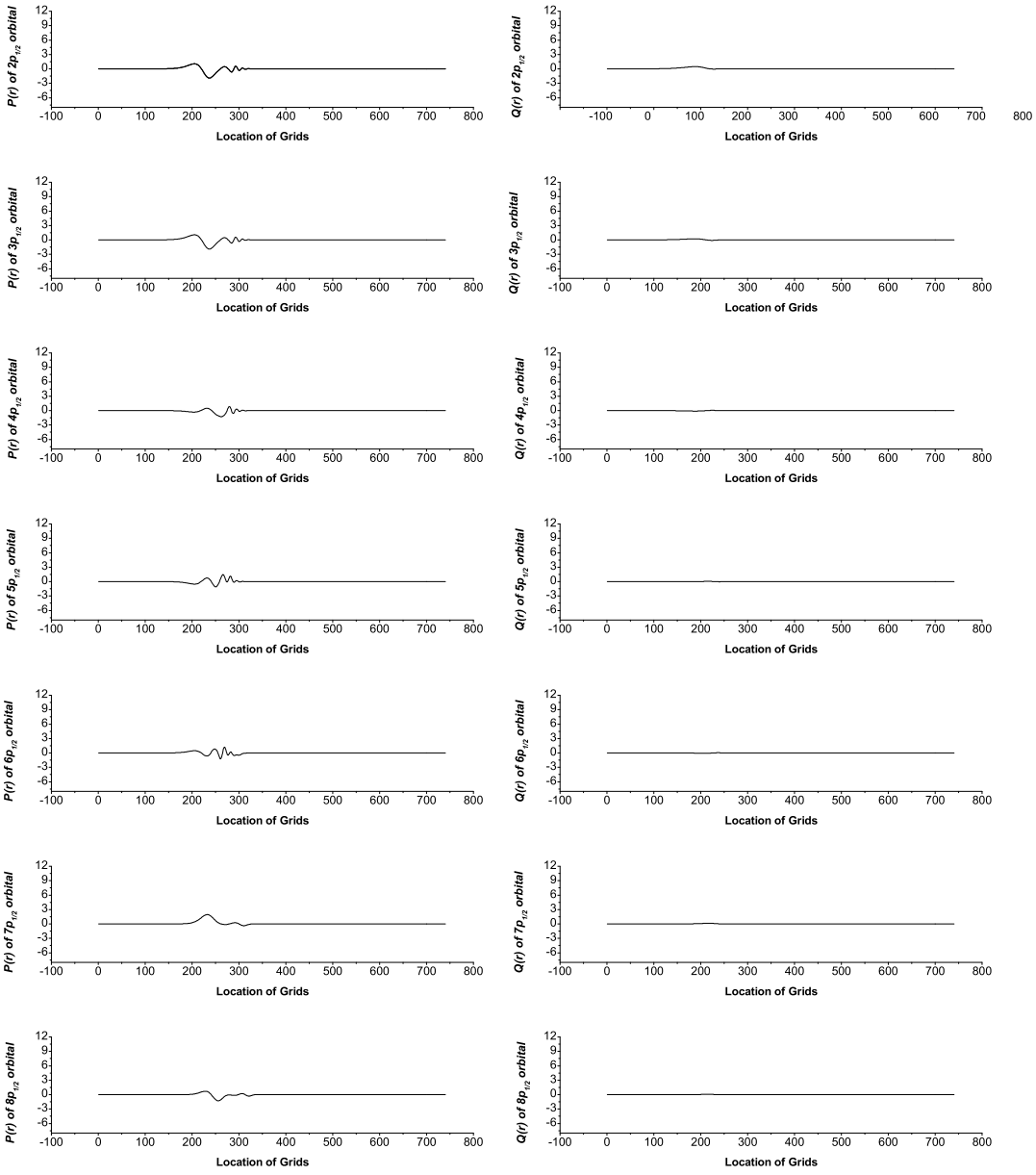

Figure 5.2: Difference between different $p_{1/2}$- orbital wavefunctions obtained using GRASP2 and GTOs.

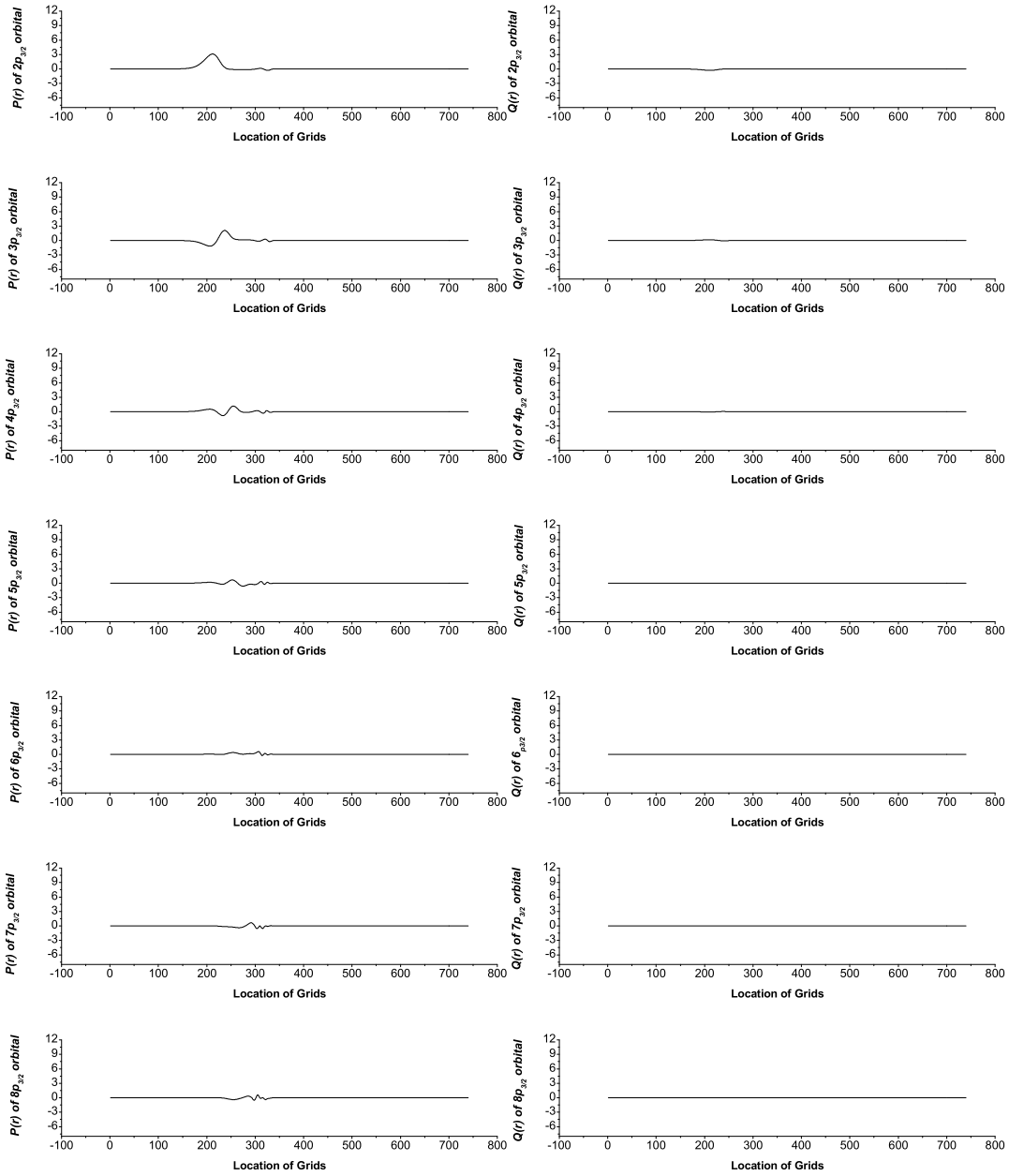

Figure 5.3: Difference between different $p_{3/2}$- orbital wavefunctions obtained using GRASP2 and GTOs.

5.2.1 Ionization Potentials and Excitation Energies

In table 5.5 we present the calculated ionization potentials obtained for different atomic states of Ba^+ and compare them with the experimental results given in the tables compiled by Moore [13] and Karlsson and Litzén [14]. We also compare these results with the previous calculations carried out by Guet and Johnson [15], Eliav *et al.* [16], Dzuba *et al.* [17] and Geetha *et al.* [7]. The uncertainties in the experimental results for the ground state is in the range of ± 0.001 cm^{-1} to ± 0.01 cm^{-1} in these two data tables. The improved energy levels used by Karlsson and Litzén yields the ionization limit as 80686.3(1) cm^{-1} for the ground state. For most states, we achieved an accuracy of around 1% in the calculations of the ionisation potentials for low lying states, but for higher states the deviations are comparatively larger from the experimental results. This is not surprising as an accurate description of excited atomic states requires the inclusion of a large number of orbitals of higher symmetries and this is often computationally prohibitive for RCC calculations with non-linear terms.

For the calculation of $E1_{PNC}$, $6p_{1/2}$, $7p_{1/2}$, $5d_{3/2}$, $6p_{3/2}$ and $7p_{3/2}$ excitation energies are important, whereas the excitation energies of other states contribute little. This will be evident later when we discuss the contributions to the total $E1_{PNC}$ from different states.

We obtain excitation energies by subtracting the calculated ionization potentials of the relevant states and they are presented in table 5.6. The errors associated with these calculations are the errors arising from both the states. From these results, it is clear that for the above states we obtain accurate excitation energies based on RCC theory and these can be used in the calculation of the $E1_{PNC}$ amplitude for the $6s\ ^2S_{1/2} \rightarrow 5d\ ^2D_{3/2}$ transition.

To understand how these calculations depend on the core and virtual orbitals of different symmetries, we study the trends of the ionization potentials of 6s, $6p_{1/2}$, $6p_{3/2}$ and $5d_{3/2}$ states in the next section.

Table 5.5: Ionization potentials (cm^{-1}) for different states of Ba^+.

	Ionization Potential					
State	Guet and Johnson [15] cm^{-1}	Eliav *et al.* [16] cm^{-1}	Dzuba *et al.* [17] cm^{-1}	Geetha *et al.* [7] cm^{-1}	This work cm^{-1} (a.u.)	Experiment cm^{-1}
$6s\ ^2S_{1/2}$	81882	80871	80813	80797	80794(0.36812)	80686.87[a]
						80686.3(1)[b]
$7s\ ^2S_{1/2}$			38333		38291(0.17447)	38331.688[a]
						38331.13[b]
$6p\ ^2P_{1/2}$	60887	60476	60581	60505	60384(0.27513)	60425.308[a]
						60424.74[b]
$7p\ ^2P_{1/2}$			31332		31216(0.14223)	31296.82[a]
						31296.48[b]
$8p\ ^2P_{1/2}$			19378		19213(0.08754)	19354.87[a]
$6p\ ^2P_{3/2}$	59140	58769	58860	58778	58690(0.26741)	58734.448[a]
						58733.90[b]
$7p\ ^2P_{3/2}$			30704		30597(0.13941)	30675.65[a]
						30674.96[b]
$5d\ ^2D_{3/2}$	77194	75605	76404	75989	75481(0.34392)	75813.02[a]
						75812.45[b]
$5d\ ^2D_{5/2}$	76263	74779	75525	75084	74346(0.33877)	75012.046[a]
						75011.49[b]
$4f\ ^2F_{5/2}$					32169(0.14657)	32428.28[a]
						32427.68[b]
$4f\ ^2F_{7/2}$					31272(0.14249)	32203.58[a]
						32202.97[b]

References: [a] [13], [b] [14].

Excitation Energy

Initial State	Final state	This work cm^{-1} (atomic unit)	Experiment cm^{-1} (atomic unit)
$6s\ ^2S_{1/2}$	$7s\ ^2S_{1/2}$	42502.58 (0.193656)	42355.182 (0.192985) [13]
			42355.175 (0.192984) [14]
$6s\ ^2S_{1/2}$	$6p\ ^2P_{1/2}$	20409.60 (0.092993)	20261.562 (0.092318) [13]
			20261.561 (0.092318) [14]
$6s\ ^2S_{1/2}$	$7p\ ^2P_{1/2}$	49577.78 (0.225893)	49390.05 (0.225038) [13]
			49389.822 (0.225037) [14]
$6s\ ^2S_{1/2}$	$6p\ ^2P_{3/2}$	22103.73 (0.100712)	21952.422 (0.100023) [13]
			21952.404 (0.100023) [14]
$6s\ ^2S_{1/2}$	$7p\ ^2P_{3/2}$	50196.26 (0.228711)	50011.22 (0.227867) [13]
			50011.340 (0.227868) [14]
$6s\ ^2S_{1/2}$	$8p\ ^2P_{3/2}$	61580.61 (0.280582)	61332.00 (0.279449) [13]
$6s\ ^2S_{1/2}$	$5d\ ^2D_{3/2}$	5312.38 (0.024205)	4873.850 (0.022207) [13]
			4873.852 (0.022207) [14]
$6s\ ^2S_{1/2}$	$5d\ ^2D_{5/2}$	6441.58 (0.029350)	5674.824 (0.025856) [13]
			5674.807 (0.025856) [14]
$6s\ ^2S_{1/2}$	$4f\ ^2F_{5/2}$	48624.82 (0.221551)	48258.59 (0.219882) [13]
			48258.617 (0.219882) [14]
$6s\ ^2S_{1/2}$	$4f\ ^2F_{7/2}$	49521.38 (0.225636)	48483.29 (0.220906) [13]
			48483.332 (0.220906) [14]
$5d\ ^2D_{3/2}$	$6p\ ^2P_{1/2}$	15097.22 (0.068788)	15387.712 (0.070112) [13]
			15387.71 (0.070112) [14]
$5d\ ^2D_{3/2}$	$6p\ ^2P_{3/2}$	16791.35 (0.076507)	17078.572 (0.077816) [13]
			17078.55 (0.077816) [14]
$5d\ ^2D_{3/2}$	$7p\ ^2P_{3/2}$	44883.88 (0.204506)	45137.37 (0.205661) [13]
			45137.49 (0.205662) [14]
$5d\ ^2D_{3/2}$	$4f\ ^2F_{5/2}$	43312.44 (0.197346)	43384.74 (0.197675) [13]
			43384.77 (0.197676) [14]
$5d\ ^2D_{3/2}$	$4f\ ^2F_{7/2}$	44208.99 (0.201431)	43609.44 (0.198699) [13]
			43609.48 (0.198699) [14]
$5d\ ^2D_{5/2}$	$6p\ ^2P_{3/2}$	15661.71 (0.071436)	16277.598 (0.74166) [13]
			16277.59 (0.074166) [14]
$5d\ ^2D_{5/2}$	$7p\ ^2P_{3/2}$	43754.46 (0.19936)	44336.396 (0.202011) [13]
			44336.53 (0.202012) [14]
$5d\ ^2D_{5/2}$	$4f\ ^2F_{5/2}$	42183.24 (0.192201)	42583.766 (0.194026) [13]
			42583.81 (0.194026) [14]
$5d\ ^2D_{5/2}$	$4f\ ^2F_{7/2}$	43079.80 (0.196286)	42808.52 (0.195050) [13]
			42808.52 (0.195050) [14]

Table 5.6: Excitation energies (cm^{-1}) for different states of Ba^+.

5.2.2 E1 transition amplitudes

Table 5.7: Transition probabilities A_{if}, where i is the initial and f is the final state, of E1 transition amplitudes from different works in 10^8 s^{-1}.

Transition States	Guet and Johnson[a]	Dzuba *et al.*[b]	Geetha *et al.*[c]	This work	Expt.
$6s\ ^2S_{1/2} \rightarrow 6p\ ^2P_{1/2}$	0.918	0.923	0.937	0.978	0.95(9)[d]
					0.955(10)[e]
					0.95(7)[f]
$6s\ ^2S_{1/2} \rightarrow 6p\ ^2P_{3/2}$	1.163	1.171	1.194	1.218	1.06(9)[d]
					1.17(4)[e]
					1.18(8)[f]
$5d\ ^2D_{3/2} \rightarrow 6p\ ^2P_{1/2}$	0.334	0.370	0.326	0.331	0.338(19)[d]
					0.33(8)[e]
					0.33(4)[f]
$5d\ ^2D_{3/2} \rightarrow 6p\ ^2P_{3/2}$	0.044	0.045	0.043	0.044	0.0469(29)[d]
					0.048(5)[e]
					0.048(6)[f]
$5d\ ^2D_{5/2} \rightarrow 6p\ ^2P_{3/2}$	0.360	0.345	0.349	0.342	0.377(24)[d]
					0.37(4)[e]
					0.37(4)[f]

References: [a] [15], [b] [17], [c] [8], [d] [18], [e] [19], [f] [20].

We present in table 5.7 the available experimental data for the probability coefficient (Einstein co-efficient A_{if}, where i and f represent initial and final states, respectively) between different atomic states from Kastberg *et al.* [18], Reader *et al.* [19] and Gallagher *et al.* [20]. In this table, we compare our calculated results using length gauge with experiments. These values are calculated using the expression given in the chapter 2 and employing RCC theory. We also present calculated results by other groups.

The calculated transition probabilities depend on two quantities. One is the excitation energy required to determine the wavelength of the transition and the other is the magnitude of the reduced matrix element of that transition. The excitation energies from different calculations have been given in the previous subsection and we present in table 5.8 the reduced matrix elements obtained by others. Our reduced matrix elements are in reasonable agreement with those of Dzuba *et al.* [17].

In table 5.7, we compare the A_{if} values from different calculations and experiments. It is clear from these results that the error bars in the experiments are rather large. Therefore, we consider experimental results with comparatively smaller error bars.

The calculated values of the reduced matrix elements of the E1 operator between different atomic states have been presented in table 5.8 and compared with the most accurate measured value which is derived from A_{if} with the smallest error (see table 5.7). The discrepancies between our results and those of other calculations are discussed in the next section.

Among all the transition amplitudes presented here, the 6s - $6p_{3/2}$ and $5d_{3/2}$ - $6p_{1/2}$ transitions are of particular interest for studying $E1_{PNC}$ in Ba^+. The dependence of the 6s - $6p_{1/2}$, 6s - $6p_{3/2}$, $5d_{3/2}$ - $6p_{1/2}$ and $5d_{3/2}$ - $6p_{3/2}$ transition amplitudes on different single particle basis is considered in the next section.

Table 5.8: Calculated absolute values of E1 reduced matrix elements in $a.u$ for different states.

Transition States	Guet and Johnson[a]	‡Dzuba *et al.*[b]	Geetha *et al.*[c]	This work	Expt.
$6s\ ^2S_{1/2} \rightarrow 6p\ ^2P_{1/2}$	3.30	4.05	3.33	3.37	3.37(2)[d]
$6s\ ^2S_{1/2} \rightarrow 7p\ ^2P_{1/2}$		0.12		0.09	
$6s\ ^2S_{1/2} \rightarrow 8p\ ^2P_{1/2}$		0.14		0.11	
$6s\ ^2S_{1/2} \rightarrow 6p\ ^2P_{3/2}$	4.66	4.05	4.70	4.72	4.67(8)[d]
$6s\ ^2S_{1/2} \rightarrow 7p\ ^2P_{3/2}$		0.03		0.17	
$7s\ ^2S_{1/2} \rightarrow 6p\ ^2P_{1/2}$		3.05		2.45	
$7s\ ^2S_{1/2} \rightarrow 7p\ ^2P_{1/2}$		8.58		7.11	
$7s\ ^2S_{1/2} \rightarrow 8p\ ^2P_{1/2}$		0.14		0.37	
$7s\ ^2S_{1/2} \rightarrow 6p\ ^2P_{3/2}$		3.36		3.80	
$7s\ ^2S_{1/2} \rightarrow 7p\ ^2P_{3/2}$		8.46		9.92	
$6p\ ^2P_{1/2} \rightarrow 5d\ ^2D_{3/2}$	3.01	2.65	2.94	3.08	3.03(8)[e]
$7p\ ^2P_{1/2} \rightarrow 5d\ ^2D_{3/2}$		0.23		0.28	
$8p\ ^2P_{1/2} \rightarrow 5d\ ^2D_{3/2}$		0.10		0.13	
$6p\ ^2P_{3/2} \rightarrow 5d\ ^2D_{3/2}$	1.31	0.89	1.28	1.36	1.36(4)[e]
$7p\ ^2P_{3/2} \rightarrow 5d\ ^2D_{3/2}$		0.29		0.16	
$6p\ ^2P_{3/2} \rightarrow 5d\ ^2D_{5/2}$	4.05	2.66	3.99	4.19	4.15(13)[e]
$7p\ ^2P_{3/2} \rightarrow 5d\ ^2D_{5/2}$		0.28		0.46	
$5d\ ^2D_{3/2} \rightarrow 4f\ ^2F_{5/2}$				3.73	
$5d\ ^2D_{5/2} \rightarrow 4f\ ^2F_{5/2}$				1.08	
$5d\ ^2D_{5/2} \rightarrow 4f\ ^2F_{7/2}$				4.59	

References: [a] [15], [b] [17], [c] [8], [d] [19], [e] [18].
‡ These values are not so reliable due to the fact that it is not clearly specified to which expressions they correspond.

5.2.3 Hyperfine constants

The high precision calculations of different hyperfine structure constants require accurate single particle wavefunctions in the nuclear region. They also provide a stringent test [21] of *ab initio* of atomic structure theory. For the last five decades many experimental techniques have been employed to measure the hyperfine structure of different low lying states of Ba^+. In table 5.9, we present different experimental results for this atomic system. The systematic errors have been carefully reduced on these experiments over the years and relatively precise results are currently available. We have underlined the results we used from this table which were chosen by considering the errors specified in the literature.

We have calculated the magnetic dipole (A) and electric quadrupole (B) hyperfine structure constants for these states using RCC theory. We have taken $g_I = 0.6238$ and $Q = 0.245$ *barn* for this system [22]. We have presented the theoretical results obtained by this work in table 5.10. Our earlier calculations and Geetha *et al.* were carried out using the same theory but with different basis functions, hence, these results differ. We discuss the discrepancy between these two sets of results and compare them with other theoretical studies in the next section.

We also present the Dirac-Fock (DF) values of the ratio of the octopole (C) hyperfine structure constant and the nuclear octopole moment (Ω) in *barns* in the same table and this can be used to extract an approximate value of Ω in *barns* by combining it with the measured C results as given in table 5.9.

The magnetic dipole (A) hyperfine structure constants of 6s, $6p_{1/2}$, $6p_{3/2}$ and $5d_{3/2}$ are used later to determine the error associated with the matrix elements of nuclear spin independent PNC interaction Hamiltonian. We discuss the influence of electron correlation on the hyperfine constants in the next section.

Table 5.9: Hyperfine structure constants for different states of Ba^+ in MHz.

	Experiment		
State	A	B	C
$6s\ ^2S_{1/2}$	4018.871(2)[a]		
	4018.8708(3)[l]		
	4018.8711(4)[m]		
	4015.42(3.3)[b]		
	4033.90(10.6)[d]		
	4062.38(15.0)[j]		
	4055.39(24.0)[k]		
$6p\ ^2P_{1/2}$	743.7(3)[n]		
	744.1(1.6)[o]		
	741.9(1.3)[b]		
	761(10)[d]		
	694.05[i]		
	697.05(21.0)[k]		
$6p\ ^2P_{3/2}$	127.1(6)[e]	89.7(15)	
	127.2(2)[n]	92.5(2)	
	126.44(2.44))[b]	97.15(1.39)	
	125.95(22)[l]	92.53(40)	
	126.2(4)[f]	93.3(6)	
	126.7(1.1)[o]	95.0(3.7)	
	125.8(5)[p]	91.6(1.2)	
$5d\ ^2D_{3/2}$	189.7288(6)[c]	44.5417(16)	-0.000058(54)
	191.2(6)[e,g]	47.5(13)	
	189.6(4)[h]	44.9(6)	
$5d\ ^2D_{5/2}$	-12.028(11)[i]	59.533(43)	
	-7.4(10)[e,g]	60.7(10)	
	-11.9(10)[h]	62.5(40)	

[a] [23], [b] [24], [c] [25], [d] [26], [e] [27], [f] [28], [g] [29], [h] [30], [i] [31], [j] [32], [k] [33], [l] [34], [m] [35], [n] [36], [o] [37], [p] [38]

State	Ahmad *et al.* [39] A	Geetha *el al.* [40] A	Ours [9] A	This work A	This work B	This work C (Dirac-Fock) ($\times 10^{-2}/\Omega$ *in barn*)
$6s\ ^2S_{1/2}$	4208(200)	4193.02	4072.83	4078.20		
$7s\ ^2S_{1/2}$				1196.30		
$6p\ ^2P_{1/2}$		783.34	736.98	740.77		
$7p\ ^2P_{1/2}$				264.92		
$8p\ ^2P_{1/2}$				109.93		
$6p\ ^2P_{3/2}$		134.94	130.94	128.27	92.87	-0.173223
$7p\ ^2P_{3/2}$				45.77	32.91	-0.069126
$5d\ ^2D_{3/2}$		198.759	188.76	189.92	46.23	-0.043025
$5d\ ^2D_{5/2}$				-11.67	62.17	-0.015177

Table 5.10: Hyperfine structure constants for different states of Ba^+ in MHz.

Table 5.11: Reduced matrix element of E2 transition of $5d\ ^2D_{5/2}$ state.

Transition States	Guet and Johnson[a]	Geetha *et al.*[b]	This work	Experiment
$5d\ ^2D_{3/2} \rightarrow 6s\ ^2S_{1/2}$	~ 13.7	12.63	12.61	12.40 ± 0.74[c]
$5d\ ^2D_{5/2} \rightarrow 6s\ ^2S_{1/2}$	~ 16.0	~ 16.0	15.78	16.86 ± 1.18[d]
				13.91 ± 3.22[e]
				16.25 ± 0.77[f]

References: [a] [15], [b] [8], [c] [41], [d] [42], [e] [43] [f] [44].

5.2.4 Transition amplitudes of $5d\ ^2D_{3/2,5/2}$ states

In the context of PNC the $6s\ ^2S_{1/2} \rightarrow 5d\ ^2D_{3/2}$ transition amplitude in the E2 channel is important as the interference of this transition amplitude and the $E1_{PNC}$ amplitude results in a light shift which can be measured [4]. The total lifetime of this state has been measured [41]. This state decays through both the M1 and E2 channel, but the E2 transition amplitude is much larger . We have calculated the reduced matrix elements from this transition through the M1 and E2 channels separately.

In table 5.11 we present the experimental reduced matrix element derived from the lifetime measurement of the $5d\ ^2D_{3/2}$ state by Yu *et al.* [41] by neglecting the small contribution from the M1 channel. This contribution we get as 0.007 in atomic unit from our calculation. We also present our results calculated using RCC theory as well as those calculated by Guet and Johnson [15] and Geetha *et al.* [8] in the same table. Also the E2 reduced matrix element involving the $5d\ ^2D_{5/2}$ state through the E2 channel for different calculations are given and compared with calculated and experimental results derived from lifetime measurements made by Nagourney *et al.* [42] and Plumelle *et al.* [43]. All the calculated results except that of Guet and Johnson [15] are in reasonable agreement with each other and also with experiment.

5.3 Discussions

As has been explained, it is not simple to generate optimal core and virtual orbitals for performing calculations of properties with different spatial dependence. Therefore, we have carried out the calculations with eight sets of basis functions with various possible combinations of active core and virtual orbitals using $\alpha_0 = 0.00525$ and $\beta = 2.73$. We generate DF orbitals for the closed-shell system Ba^{++} and then perform closed-shell RCC calculations. The DF orbitals are used to obtain the self-consistent Field (SCF) energy of the system and after closed-shell RCC calculations we compute the correlation energy. We then tabulate all these results.

To understand the dependence of various properties on different combinations of GTOs, active core and virtual orbitals, we give their results and discuss their trends. We find the basis functions which give the least average error for the properties. We then proceed with these basis functions for our PNC calculation.

Finally, we present explicitly the contributions to $E1_{PNC}$ from different RCC terms and analyze the role of electron correlation. We also investigate the relative importance of the different intermediate states by explicitly determining their individual contributions. We estimate the error in the different properties including $E1_{PNC}$ from the difference in the results of our RCC calculations with single, double as well as leading triple excitations and just single and double excitations.

We have performed calculations for two sets of GTOs given in table 5.12 (A) and (B) keeping the values of α_0 and β mentioned above fixed and varying the number of active core and virtual orbitals. Three different calculations of ionization potentials, E1 transition amplitudes and hyperfine structure constants are carried out using the first set and five different calculations of the same three quantities are carried out using the second set. The first set of GTOs did not yield accurate values of the hyperfine constants for most of the states. The second set of GTOs gave better values for these constants. The importance of exciting all the core electrons was evident by carrying out calculations with first set of GTOs. Using the second set of GTOs,

	Core orbitals	(Valence+Virtual) orbitals
A.		
GTOs	Full core	38s, 40p, 30d, 30f, 20g
RCC - I	3s, 4s, 5s, 3p, 4p, 5p, 3d, 4d	6s - 13s, 6p - 12p, 5d - 11d, 4f - 12f, 5g - 11g
RCC - II	3s, 4s, 5s, 3p, 4p, 5p, 3d, 4d	6s - 13s, 6p - 12p, 5d - 11d, 4f - 12f, 5g - 12g
RCC - III	Full core	6s - 13s, 6p - 12p, 5d - 11d, 4f - 12f, 5g - 12g
B.		
GTOs	Full core	30s, 25p, 25d, 20f, 20g
RCC - IV	Full core	6s - 13s, 6p - 12p, 5d - 11d, 4f - 12f
RCC - V	Full core	6s - 13s, 6p - 12p, 5d - 11d, 4f - 12f, 5g - 10g
RCC - VI	Full core	6s - 13s, 6p - 12p, 5d - 12d, 4f - 12f, 5g - 11g
RCC - VII	Full core	6s - 13s, 6p - 12p, 5d - 12d, 4f - 12f, 5g - 12g
RCC - VIII	Full core	6s - 13s, 6p - 13p, 5d - 13d, 4f - 13f, 5g - 13g

Table 5.12: Total basis functions used in the calculation.

we began our RCC calculations by exciting the full core and considered up to f- virtual orbitals. We then carefully added g and for the last case p virtual orbitals. Our computational resources prevented the further addition of virtual orbitals.

5.3.1 Correlation energy

In table 5.13 we give the total number of closed-shell amplitudes in the RCC calculations using the different sets of basis states that we have considered. Although we have two separate sets of GTOs, we obtain the same SCF energy up to the fifth decimal places. The correlation energies vary significantly with the total number of T- amplitudes.

	No. of T-amplitude equations	SCF energy	Correlation energy
Basis I	341071	-0.813595E+04	-1.344133
Basis II	358874	-0.813595E+04	-1.369744
Basis III	598183	-0.813595E+04	-1.672759
Basis IV	399207	-0.813595E+04	-1.496532
Basis V	508017	-0.813595E+04	-1.504341
Basis VI	570440	-0.813595E+04	-1.592781
Basis VII	598183	-0.813595E+04	-1.672998
Basis VIII	737920	-0.813595E+04	-2.056644

Table 5.13: Total basis functions used in the calculation.

We have shown graphically the total number of T- amplitude equations and correlation energies obtained using different sets of basis functions in figure 5.4. It is clear from these diagrams that the number of amplitudes increase rapidly for the RCC calculations when more active electrons are added. The magnitude of the correlation energy also increases rapidly. Adding more active orbitals from higher symmetries in the non-linear forms of the wavefunction determining equations as have been given in the previous chapters would require large computational resources.

5.3.2 Ionization Potential

The IP of the valence/virtual orbitals of Ba^{++} are calculated using the method described for open-shell CC theory. As shown in figure 5.5, we have plotted the difference between the experimental and calculated results for the 6s, $6p_{1/2}$, $6p_{3/2}$ and $5d_{3/2}$ states for different basis functions as given in table 5.12. The first three points highlight the effect of inner core electrons. It can be noted from these diagrams that p- and g- symmetry orbitals are very important for accurate calculations of IPs. For 6s, contributions from higher g- orbitals show large deviation from the experimental results. This means that the extra GTOs after this region are not able to construct the 6s wavefunction so they can be neglected in describing this state. To achieve more accurate results for d- and f- symmetry states it may also be neces-

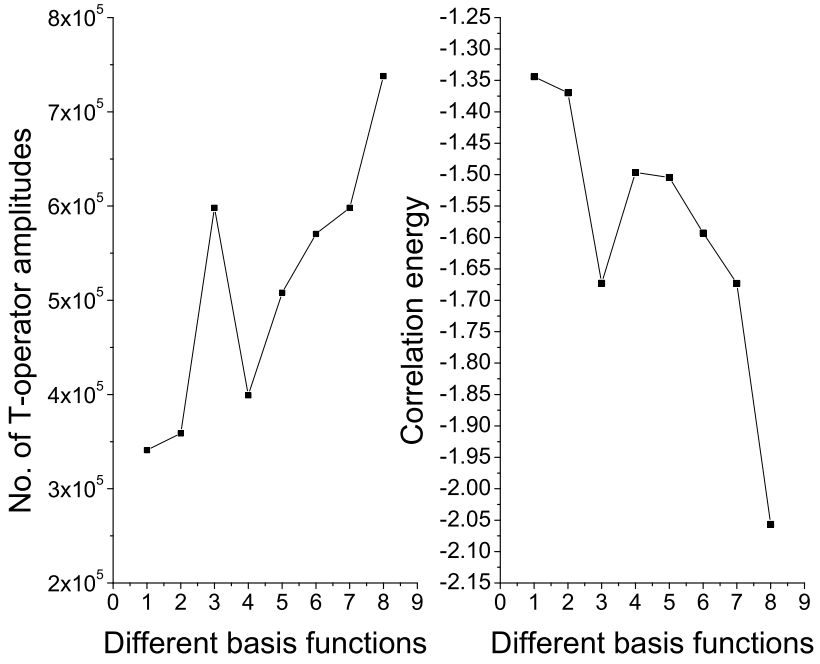

Figure 5.4: No. of T-amplitude equations and correlation energy.

sary to include higher symmetry orbitals like h and maybe even i, but in the present calculations we do not consider them.

We consider the calculated results with the least deviation from experimental values in our results table. These results are obtained from the last set of basis functions. Therefore, these basis functions would be an appropriate choice for carrying out a PNC study as has been explained earlier.

These results have also been calculated by Guet and Johnson [15], Eliav *et al.* [16], Dzuba *et al.* [17] and Geetha *et al.* [7]. Dzuba *at al.* have used a variant of all order relativistic many-body perturbation theory. Guet and Johnson had used second order relativistic MBPT theory to evaluate their

results. Both Eliav *et al.* and Geetha *et al.* used the RCC method for their calculations. The difference between these calculations and the present one is that they also considered h- symmetry orbitals in their calculations. In Geetha *et al.*'s work partial numerical orbitals from GRASP2 were also used.

We compare results obtained from various works with the corresponding experimental results by plotting them in figure 5.6. It is obvious that the RCC theory provides a significant improvement over the second order MBPT calculations. Guet and Johnson obtained an accuracy of less than 2% and the EE's around 4%. The accuracy of their 6s-$5d_{3/2}$ excitation energy calculation is misleading as it is a consequence of the cancellation of the errors from both 6s and $5d_{3/2}$ IPs. The accuracy of Eliav *et al.*'s results are less than 1% and these are compared with our calculations. In their calculations, approximate triple excitation effects are not considered, whilst they are included in both Geetha *et al.*'s and this calculation. Since Geetha *et al.*'s work and this work are calculated with different basis functions the results differ in the third decimal place. But for the 6s state this calculation is more accurate than her result.

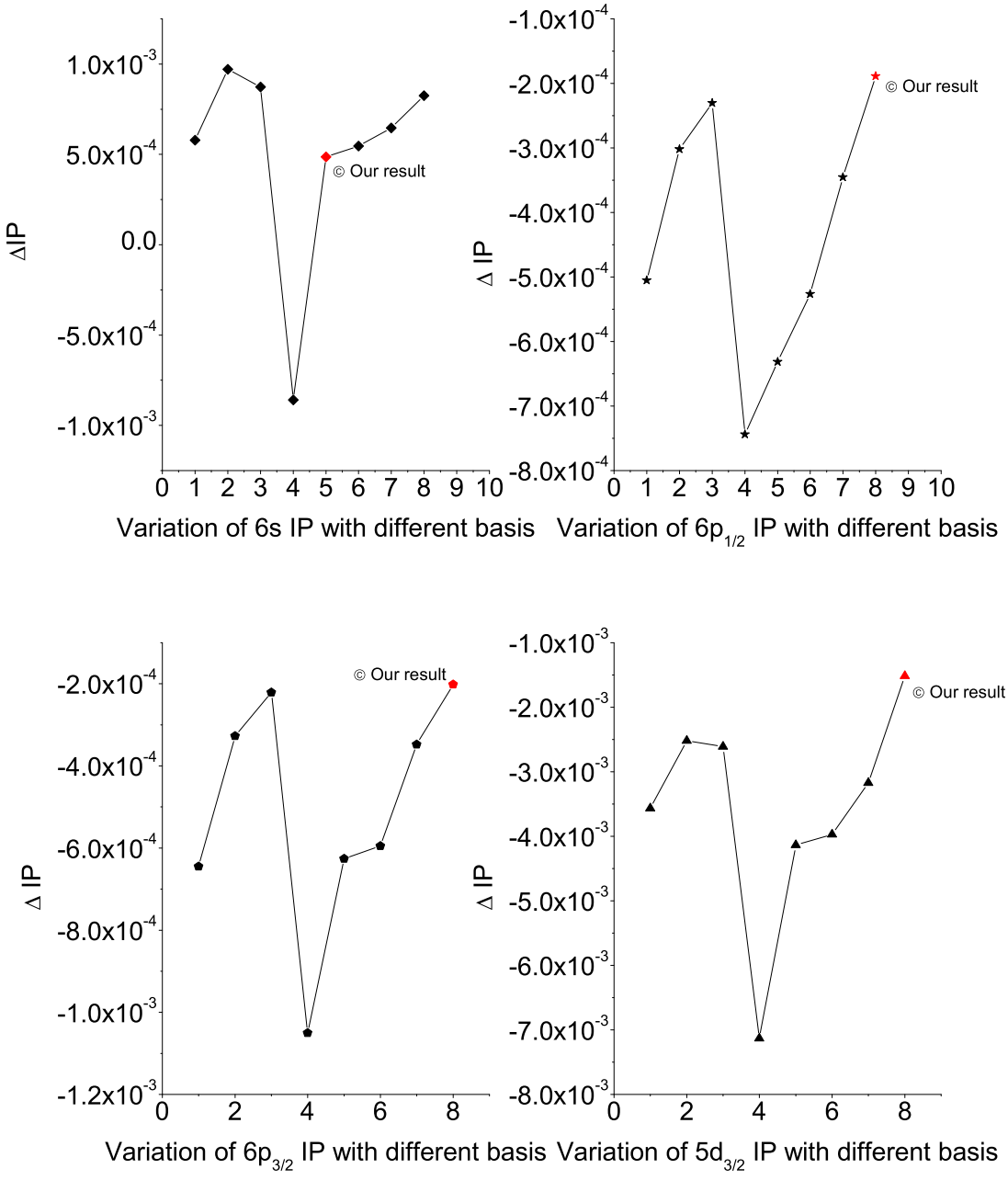

Figure 5.5: Deviation of the IP results from experimentation with different basis sets.

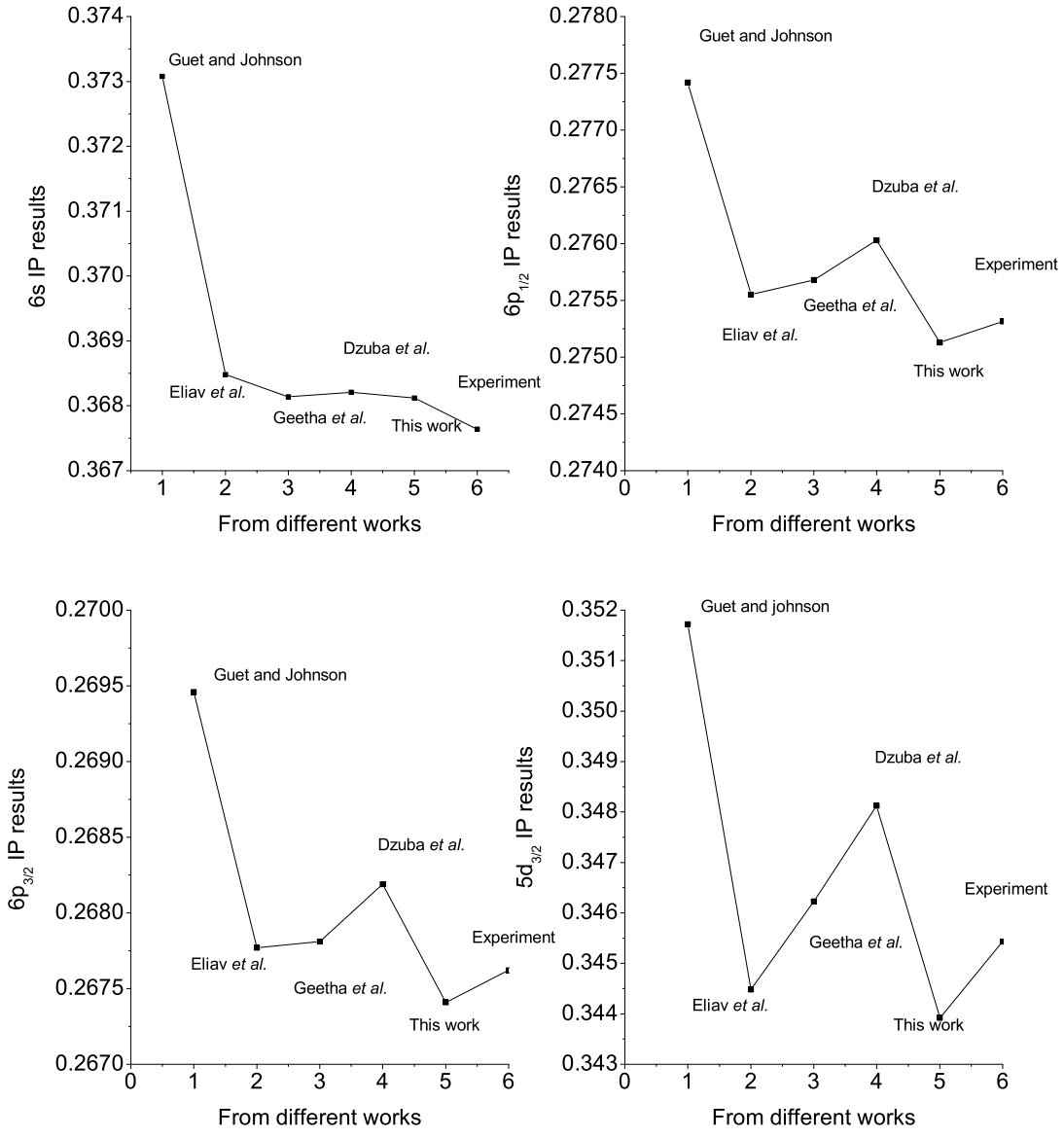

Figure 5.6: Comparison of IP results from different works.

5.3.3 E1 transition amplitudes

We have calculated E1 transition amplitudes in the length gauge and compared our results with the calculations of Guet and Johnson [15] and Geetha *et al.* [8]. Dzuba *et al.* [17] have also calculated these transition probabilities.

Three groups have measured transition probabilities for certain low-lying states of Ba^+: Gallagher *et al.* [20], Reader *et al.* [19] and Kastberg *et al.* [18]. Out of those Kastberg *et al.*'s results are the most recent, but all these results have fairly large systematic errors. We consider the central values of the experimental results which have the smallest systematic errors, to evaluate the deviation of the calculated results.

In figure 5.7, we plot the difference between the calculated and the experimental results for different basis functions given in table 5.12. From this graph it appears that it would be necessary to include more virtual orbitals of different symmetries in order to obtain accurate E1 transition amplitudes.

We also compare the reduced matrix elements of the E1 transition operator from different works along with experimental results for the 6s-$6p_{1/2}$, 6s-$6p_{3/2}$, $5d_{3/2}$-$6p_{1/2}$ and $5d_{3/2}$-$6p_{3/2}$ transitions in figure 5.8. The error bars of corresponding experimental results are also given. In all the cases, our results are well within the experimental limits. Therefore, more accurate measurements are necessary to verify the calculated results presented here. Our calculations are the most rigorous so far. Guet and Johnson have performed their calculations using only second order relativistic MBPT calculations, which are only a subset of our method. The difference between Geetha *et al.* and our method is the fact that the present calculation account contributions from the effective two-body terms $e^{T^\dagger} D e^T$, where D is the E1 operator, whereas Geetha's work does not. It seems from our results that these contributions are essential for achieving high accuracy.

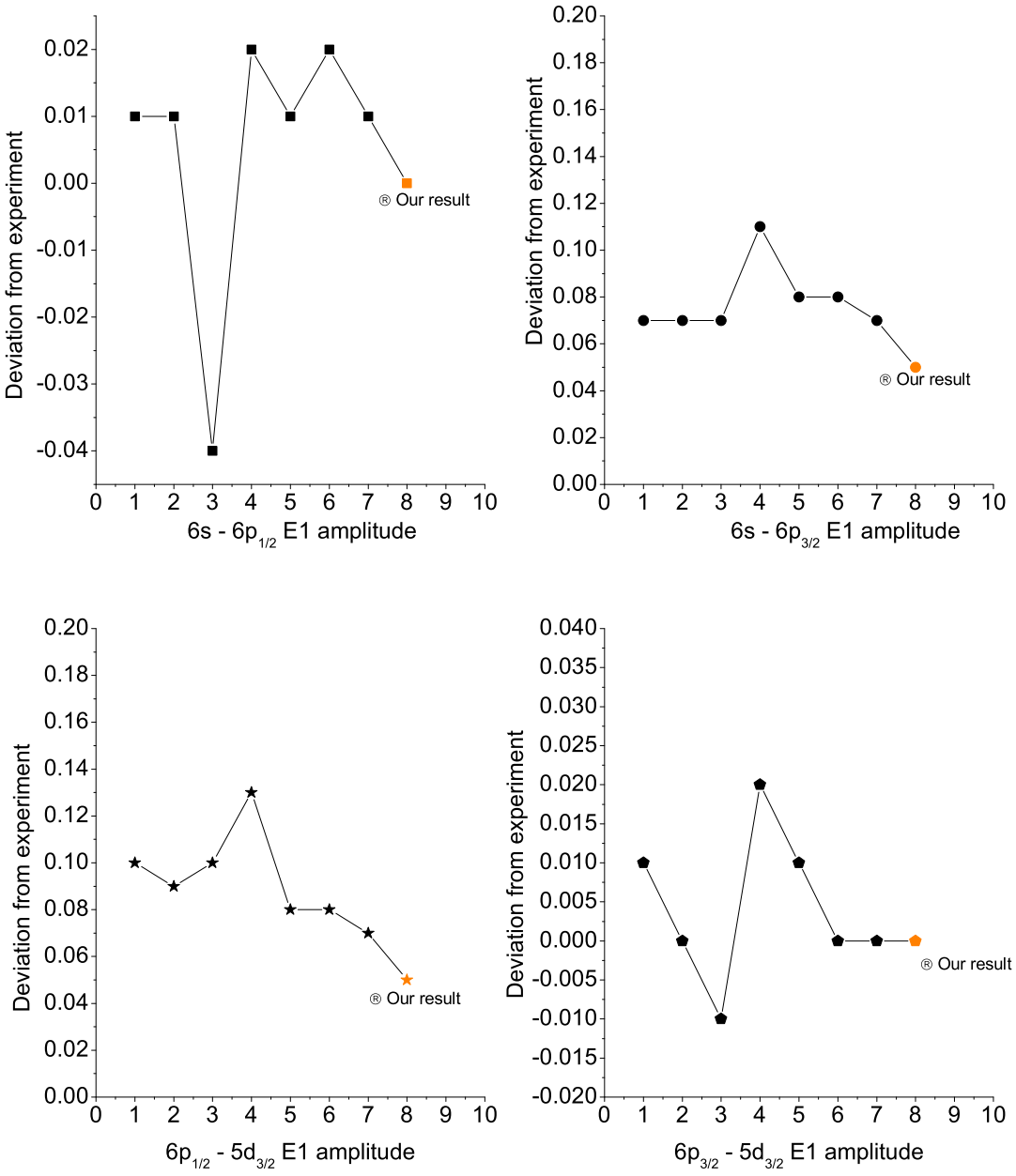

Figure 5.7: Difference between experimental results with different basis functions.

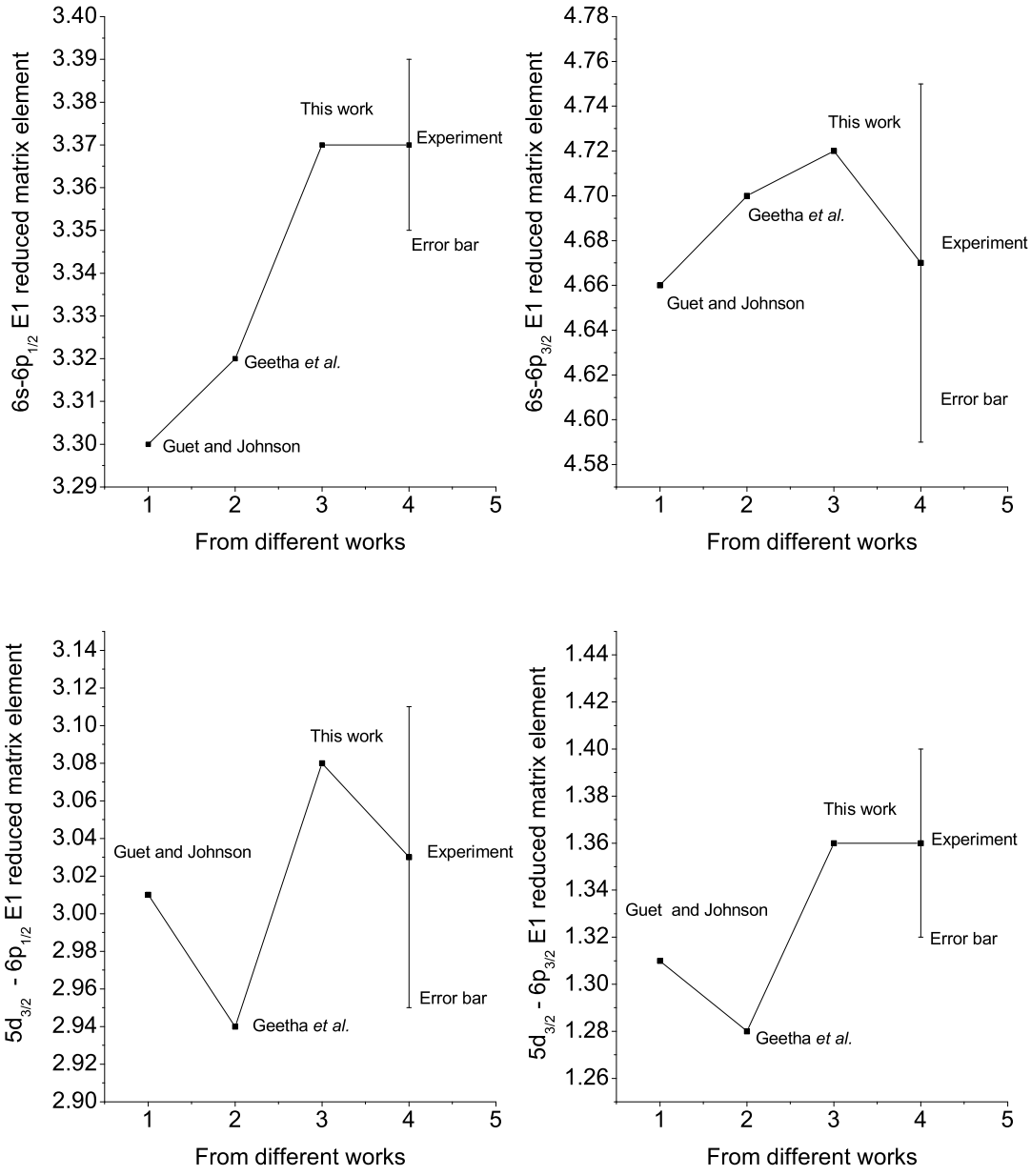

Figure 5.8: Different calculated results with experimental result.

5.3.4 Hyperfine structure

There are many experiments that have been carried out to measure the magnetic dipole (A) and electric quadrupole (B) hyperfine constants for the low lying states of Ba^+ and we have presented them earlier in this thesis. We consider only the results with relatively small error bars to compare with our calculations. Although the origin of the neutral weak and hyperfine interactions are different, the matrix elements of both these interactions depend on the overlap of single-particle wavefunctions in, or close to, the nuclear region. Therefore, the products of the square root of the A value, of the states involving PNC matrix elements, are used to determine error of the latter. These results are are sensitive to the nuclear region. Hence, it is essential to understand the role of both of the inner core as well as high lying virtual orbitals in these studies.

Only a few calculations have previously been carried out for Ba^+ hyperfine constants. Ahmad *et al.* [39] have calculated the 'A' value for the ground state using the relativistic MBPT method. Their result agrees with experiment to about 5%. Geetha *et al.* [40] have also calculated the same quantity for a few low-lying states using the same method used in this thesis. But their results differ from the present work as they have used different basis functions. As we explain later, the hyperfine studies are very sensitive to the choice of basis functions, so it is essential to consider accurate orbitals. Also in their calculations the effective two-body terms from $e^{T^\dagger} O e^T$ (where O represents hyperfine interaction operator) have not been taken into account. In an earlier work we also calculated these quantities [9], but we considered only up to f virtual orbitals. To gain better insights into our calculated results, we consider only four states: 6s, $6p_{1/2}$, $6p_{3/2}$ and $5d_{3/2}$, which are the most important states in the calculation of $E1_{PNC}$. We plot the deviation of the calculated results against the measured values in figure 5.9. This figure clearly indicates that both the inner core and high lying virtual orbitals are important for these studies. In figure 5.10, we have shown graphically contributions from different RCC terms to the A values for the above states. The difference between O and $\overline{O}$ gives an indication of the size of the core correlation effects; they are smaller than the other RCC terms. The dominant contributions to electron correlation come from the OS_1 and OS_2 terms along with their adjoints.

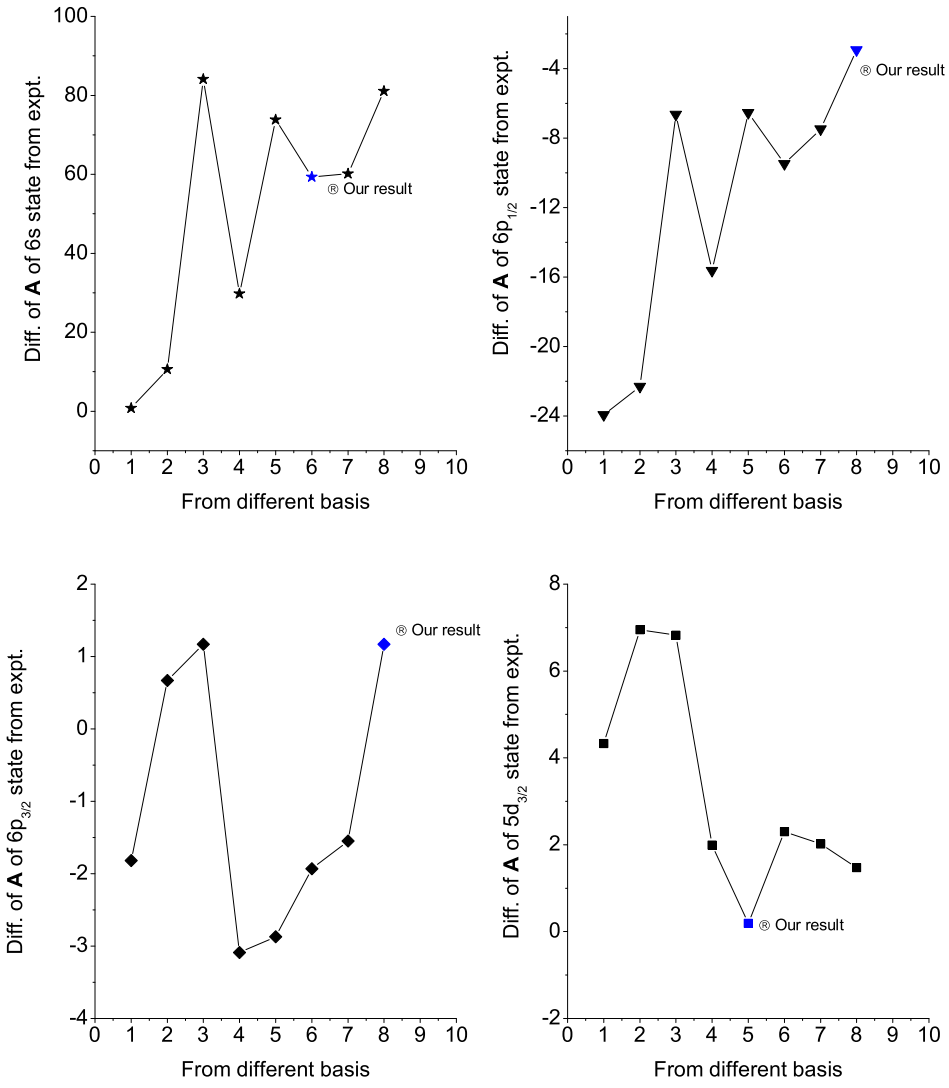

Figure 5.9: Deviation of A values from experimental results with different basis functions.

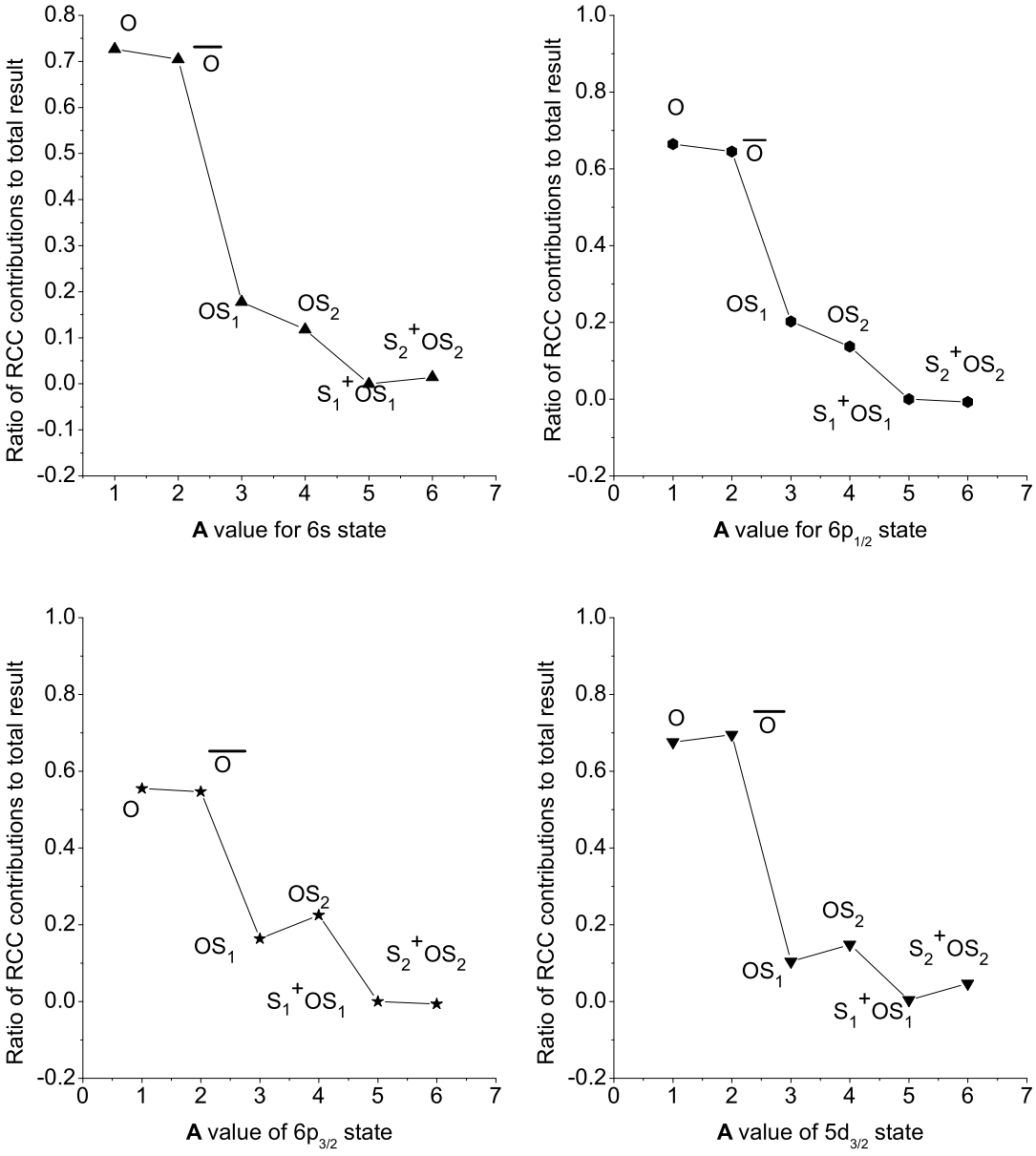

Figure 5.10: Contributions to the total magnetic dipole hyperfine structure constant from different RCC terms.

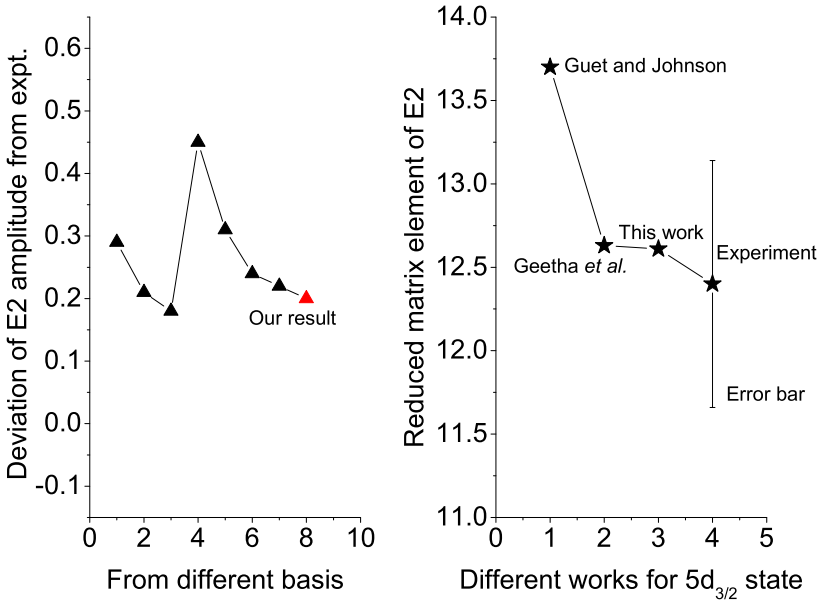

Figure 5.11: Reduced matrix element of E2 transition operator for $5d_{3/2}$ state.

5.3.5 E2 amplitude of $5d_{3/2,5/2}$ states

We present the calculated results of reduced E2 matrix element involving $5d_{3/2}$ and 6s as well as $5d_{5/2}$ and 6s states for Ba^+. The lifetimes of these d excited states have been measured, but the errors in both cases are slightly large. The decay of an electron from the $5d_{3/2}$ to the 6s ground state is possible through two channels; E2 and M1. However, through the M1 channel the transition probability is very small. From our calculation we get the reduced matrix element of the M1 transition to be 0.007 in atomic unit. If we neglect this transition, then the experimental result for the reduced matrix element for the E2 transition could be considered as 12.40±0.74, from the lifetime measurement by Yu *et al.* [41]. Since the error bar is very large in this case, we consider the calculated results which are consistent with many

basis functions.

In figure 5.11 we plot the graph of the deviation of the calculated results from the central value of the experimental result, with different basis functions. From this data, we take value of the reduced matrix element for the E2 operator of the $5d_{3/2}$ state as 12.61. The interference of $E1_{PNC}$ amplitude with E2 transition amplitude can in principle be measured . Therefore, an accurate calculation of this quantity is necessary to study the PNC amplitude in Ba^+.

In figure 5.11 we also plot results of calculations for the reduced E2 matrix element by Guet and Johnson [15], Geetha *et al.* and this work as well as experiment [41]. Both Geetha's result and the result obtained by this work match and are well within the error bounds of the experimental results. In both the calculations, RCC theory has been employed using the same approximation. Guet and Johnson have used the relativistic second order MBPT method.

In table 5.11 we also present the reduced matrix element of the E2 operator for the $5d_{5/2} \rightarrow 6s$ transition. Results obtained by Guet and Johnson [15] and Geetha *et al.* [8] are derived from their lifetime calculations for this state and these two results are in good agreement. We obtain slightly smaller values than them. This is because Guet and Johnson have calculated using the relativistic MBPT method and Geetha has not included contributions from effective two-body terms of $e^{T^\dagger} D2 e^T$, where $D2$ is the E2 operator. However, all the results are well within the experimental limits obtained by Nagourney *et al.* [42] and Plumelle *et al.* [43].

5.4 Parity non-conserving electric dipole transition amplitude

The main goal of this thesis is to obtain an accurate numerical value of the parity non-conserving electric dipole transition amplitude between the $6s\ ^2S_{1/2} \rightarrow 5d\ ^2D_{3/2}$ transition based on RCC theory. As has been mentioned before, it is necessary to test the excitation energies, E1 transition amplitudes

Table 5.14: Excitation energies (cm^{-1}), reduced E1 transition amplitudes (a.u.) and magnetic dipole hyperfine structure constants (MHz) for different low-lying states of Ba^+.

Initial state	$6s\ ^2S_{1/2}$	$6s\ ^2S_{1/2}$	$5d\ ^2D_{3/2}$	$5d\ ^2D_{3/2}$
→Final state	$6p\ ^2P_{1/2}$	$7p\ ^2P_{1/2}$	$6p\ ^2P_{3/2}$	$7p\ ^2P_{3/2}$
Excitation energy	20410	49578	16795	44884
Experiment	20262	49390	17079	45137
Initial state	$6s\ ^2S_{1/2}$	$6s\ ^2S_{1/2}$	$5d\ ^2D_{3/2}$	$5d\ ^2D_{3/2}$
→Final state	$6p\ ^2P_{1/2}$	$6p\ ^2P_{3/2}$	$6p\ ^2P_{1/2}$	$6p\ ^2P_{3/2}$
E1 transition amplitude	3.37	4.72	3.08	1.36
Experiment	3.37(2)	4.67(8)	3.03(8)	1.36(4)
Atomic state	$6s\ ^2S_{1/2}$	$6p\ ^2P_{1/2}$	$6p\ ^2P_{3/2}$	$5d\ ^2D_{3/2}$
Hyperfine constant (A)	4078.18	740.77	128.27	189.92
Experiment	4018.8708(3)	743.7(3)	127.2(2)	189.7288(6)

and magnetic dipole (A) hyperfine structure constants, in order to determine an approximate error for the PNC transition amplitude of interest. In table 5.14, we summerize the results of these properties and discuss the accuracy of each result obtained from the various calculations.

5.4.1 Accuracy of excitation energies

As has been shown in table 5.14, the agreement with experiment of the most important excitation energy ($6p\ ^2P_{1/2}$) for the calculation of $E1_{PNC}$ is better than one percent. The accuracy of the next important state ($7p\ ^2P_{1/2}$) for the initial PNC perturbed state is just 0.5%. The excitation energy of $5d\ ^2D_{3/2}$ -

$6p\ ^2P_{3/2}$ is around 1.6%. But this may not affect the $E1_{PNC}$ result very much as the $5d\ ^2D_{3/2}$ state does not contribute significantly to the PNC amplitude.

5.4.2 Accuracy of E1 transition amplitudes

All the E1 transition amplitudes given in table 5.14 are within the quoted experimental errors. This is an indication that an accurate calculation of $E1_{PNC}$ amplitude can be carried out. As we have discussed earlier, most of the other calculated results do not fall within the experimental error and are further away from the central values than ours.

5.4.3 Accuracy of PNC matrix elements

There is no direct procedure to determine the accuracy of the calculated PNC matrix elements between different states. An alternative method has been followed to calculate the error associated with this quantity, by calculating the square root of the product of the corresponding states connecting to the PNC operator as shown in [9, 45].

In table 5.15 we present the values of the square root of the product of $\sqrt{A_{6s\ ^2S_{1/2}} A_{6p\ ^2P_{1/2}}}$ and $\sqrt{A_{6p\ ^2P_{3/2}} A_{5d\ ^2D_{3/2}}}$. The accuracies of these two quantities give an indication of the accuracies of the PNC matrix elements between $6s\ ^2S_{1/2}$ and $6p\ ^2P_{1/2}$ states as well as the $6p\ ^2P_{3/2}$ and $5d\ ^2D_{3/2}$ states. Both of them are in excellent agreement with experiment, suggesting that the two leading PNC matrix elements for the $E1_{PNC}$ calculation are very accurate as shown later in this section.

5.4.4 $E1_{PNC}$ result

Our calculated results for various atomic properties that were discussed earlier, suggest that it is possible to obtain an $E1_{PNC}$ amplitude accurate to within 1%. We calculate this quantity with the last basis functions (Case VIII), with which we are able to obtain most of the calculated results accurately. As we have mentioned earlier, we apply RCC theory to calculate the first order PNC perturbed wavefunctions. Therefore, the present method

Table 5.15: Square root of the magnetic dipole hyperfine constants (MHz) and their deviations from experimental results.

	Experiment	This work	Deviation (%)
$\sqrt{A_{6s\ ^2S_{1/2}} A_{6p\ ^2P_{1/2}}}$	1728.83	1738.1	0.5
$\sqrt{A_{6p\ ^2P_{3/2}} A_{5d\ ^2D_{3/2}}}$	155.35	156.08	0.5

involves all intermediate states intrinsically. The exact procedure that had been followed to calculate them are discussed in earlier chapters.

The contributions from the different terms in the $E1_{PNC}$ amplitude calculation for the $6s\ ^2S_{1/2} \rightarrow 5d\ ^2D_{1/2}$ transition are presented in table 5.16. It is clear that the largest contribution comes from $DS_1^{(1)}$ which represents the DF term and a certain sub class of core polarization as well as pair correlation effects. This is due to the relatively large $(6s_{1/2} - 6p_{1/2})\ S_1^{(1)}$ cluster amplitude. Two different types of core polarization effects; $DT_1^{(1)}$ and $DS_2^{(1)}$ as well as its conjugate also make significant contributions. The former is mediated by the neutral weak interaction and involves the 6s valence and core electrons. Correlation effects corresponding to $S_1^{(0)\dagger} DS_1^{(1)}$ and $S_2^{(0)\dagger} DS_1^{(1)}$ are non negligible, but their signs are opposite. Contributions from other terms are comparatively small.

We consider the most important contributions given in table 5.16 and analyze them below. We also plot the magnitudes of the different contributions to $E1_{PNC}$ amplitude in figure 5.12.

5.5 Lower order MBPT contributions

We calculate the lowest order $E1_{PNC}$ amplitude for the $6s\ ^2S_{1/2} \rightarrow 5d\ ^2D_{1/2}$ transition using the MBPT method to provide insights into the different all

Table 5.16: Contributions to the E1$_{PNC}$ calculation in $\times 10^{-11} iea_0(-Q_W/N)$ using RCC calculation.

Initial pert. terms	$6s\ ^2S^{(1)}_{1/2} \rightarrow 5d\ ^2D^{(0)}_{3/2}$	Final pert. terms	$6s\ ^2S^{(0)}_{1/2} \rightarrow 5d\ ^2D^{(1)}_{3/2}$
DH^{NSI}_{PNC}	2.018	H^{NSI}_{PNC} D	-0.3 $\times 10^{-5}$
$DT^{(1)}_1$	0.0003	$T^{(1)^\dagger}D$	0.418
$\overline{D^{(0)}}S^{(1)}_{1i}$	2.634	$S^{(1)\dagger}_{1f}\overline{D^{(0)}}$	-0.179
$\overline{D^{(0)}}S^{(1)}_{2i}$	-0.242	$S^{(1)\dagger}_{2f}\overline{D^{(0)}}$	-0.166
$S^{(0)\dagger}_{1f}\overline{D^{(0)}}S^{(1)}_{1i}$	0.149	$S^{(1)\dagger}_{1f}\overline{D^{(0)}}S^{(0)}_{1i}$	0.003
$S^{(0)\dagger}_{1f}\overline{D^{(0)}}S^{(1)}_{2i}$	0.007	$S^{(1)\dagger}_{1f}\overline{D^{(0)}}S^{(0)}_{2i}$	0.008
$S^{(0)\dagger}_{2f}\overline{D^{(0)}}S^{(1)}_{1i}$	-0.116	$S^{(1)\dagger}_{2f}\overline{D^{(0)}}S^{(0)}_{1i}$	-0.009
$S^{(0)\dagger}_{2f}\overline{D^{(0)}}S^{(1)}_{2i}$	-0.001	$S^{(1)\dagger}_{2f}\overline{D^{(0)}}S^{(0)}_{2i}$	0.001
Norm.	-0.046		-0.001
Total	2.375		0.087

order RCC terms. The important MBPT diagrams are shown in figure 5.13. Contributions arising from these diagrams are given in table 5.17.

We get $E1_{PNC} = 1.98 \times (-Q_W/N)\ iea_0 \times 10^{-11}$ from this calculation. From the diagrams given in figure 5.13, it is clear that diag. (2+20+21+22+23) are the corresponding lowest order terms to the $DS^{(1)}_{1i}$ term of RCC. The pair correlation diagrams which also contribute to this term are not calculated as they are two orders in the Coulomb interaction and one order in the PNC interaction and hence their contributions are relatively small. Diagrams (22+23) are called pseudo diagrams and have been defined by Venugopal *et al.* [46]. As we have shown earlier, the contribution from $DS^{(1)}_{1i}$ is 2.634 and its lowest order diagrams yield around 2.351.

Contribution to the final perturbed state from $S_{2f}^{1\dagger}D$ mainly comes through diagram (6+8). To lowest order these results are higher than the all order contribution, -0.179.

Table 5.17: Contributions to the $E1_{PNC}$ calculation in units of $10^{-11}iea_0(-Q_W/N)$, using MBPT diagrams.

Initial pert. terms	$6s\ ^2S_{1/2}^{(1)} \rightarrow 5d\ ^2D_{3/2}^{(0)}$	Final pert. terms	$6s\ ^2S_{1/2}^{(0)} \rightarrow 5d\ ^2D_{3/2}^{(1)}$
diag. (2)	2.018	diag. (1)	-0.3 $\times 10^{-5}$
diag. (3)	-0.142	diag. (5)	0.0
diag. (4)	0.032	diag. (6)	-0.235
diag. (9)	$\sim$0.0	diag. (7)	0.0
diag. (10)	-0.006	diag. (8)	0.016
diag. (13)	$\sim$0.0	diag. (11)	$\sim$0.0
diag. (14)	-0.004	diag. (12)	-0.017
diag. (20)	0.0	diag. (15)	$\sim$0.0
diag. (21)	0.167	diag. (16)	-0.008
diag. (22)	0.0	diag. (24)	$\sim$0.0
diag. (23)	0.166	diag. (25)	$\sim$0.0
diag. (26)	$\sim$0.0	diag. (28)	$\sim$0.0
diag. (27)	0.003	diag. (29)	-0.002
diag. (17)	$\sim$0.0	diag. (30)	$\sim$0.0
diag. (31)	-0.006	diag. (32)	-0.001
Total	2.226		-0.247

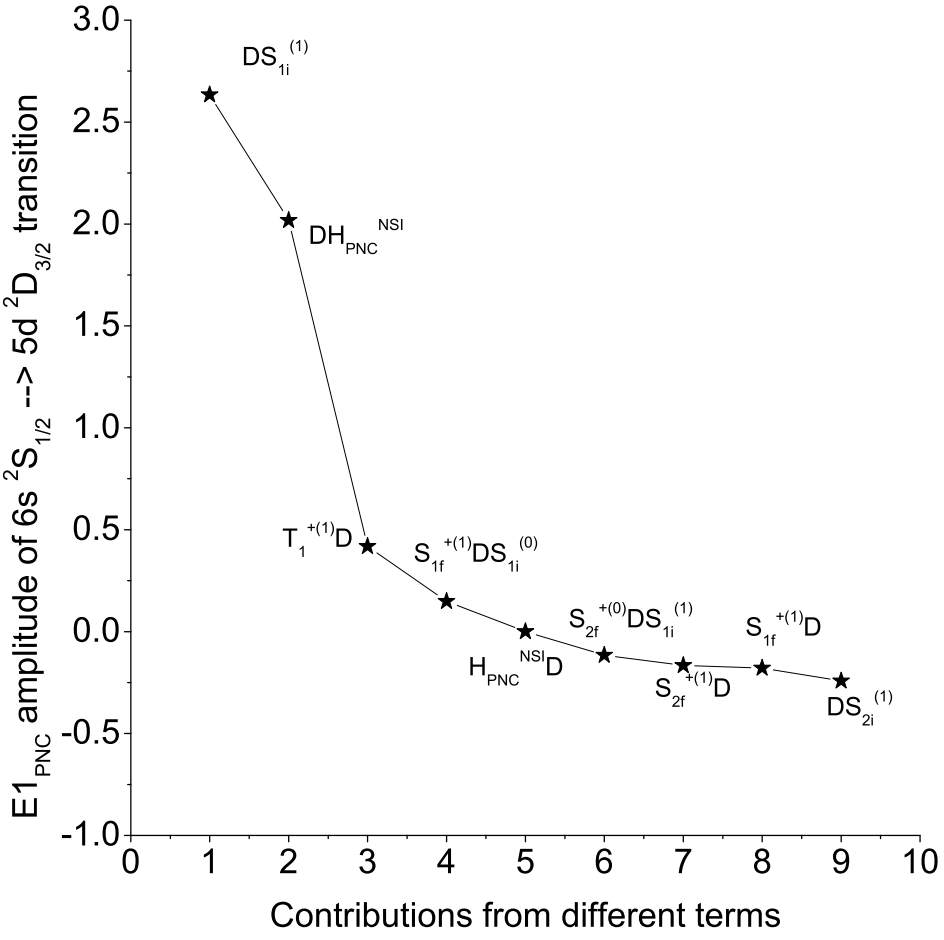

Figure 5.12: Contributions from different RCC terms to the $E1_{PNC}$ amplitude calculation in $(-Q_W/N)\ iea_0 \times 10^{-11}$.

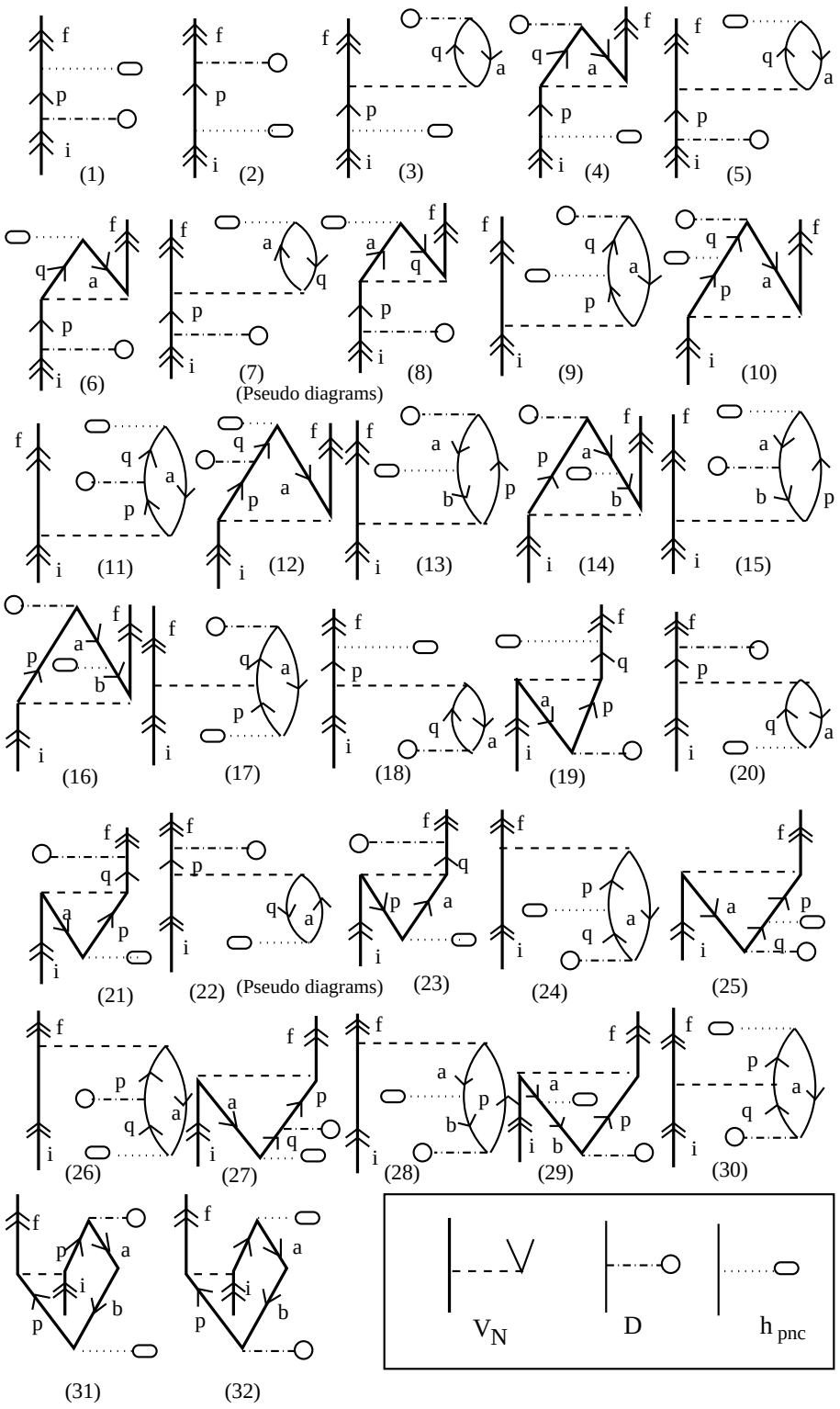

Figure 5.13: Important MBPT diagrams to calculate PNC amplitude.

5.5.1 Role of intermediate states

It is important to understand the role of different intermediate states in the calculation of the $E1_{PNC}$ amplitude of the $6s\ ^2S_{1/2} \rightarrow 5d\ ^2D_{3/2}$ transition in Ba^+. It is also possible to determine the error in this quantity by identifying important intermediate states and estimating the accuracies of the different properties of those states that are related to the PNC amplitude. As has been mentioned, in our method it is possible to include implicitly all intermediate states through the RCC theory with the PNC interaction as a first order perturbation. It is not possible to find the individual contributions from different intermediate states in this approach. However, we have made a special effort to investigate their contributions by computing the first order perturbed wavefunctions which involve summing over various intermediate states. In tables 5.18 to 5.24 we present these contributions at various levels. In table 5.17, we present the reduced E1 matrix elements for different transitions at the DF level which are used to calculate the intermediate states contributions to the above $E1_{PNC}$ amplitude.

Table 5.18: Reduced E1 matrix elements for different intermediate states.

	$\langle 5d_{3/2}\|\|D\|\|np_{1/2}\rangle_{DF}$	$\langle np_{3/2}\|\|D\|\|6s\rangle_{DF}$
$n=4$	0.75	0.07
$n=5$	1.94	0.91
$n=6$	3.73	5.48
$n=7$	0.36	0.31
$n=8$	0.19	0.18
$n=9$	0.47	0.07
$n=10$	0.23	0.08
$n=11$	0.04	0.04

Table 5.19: Contributions to the $E1_{PNC}$ calculation at Dirac-Fock level in $\times 10^{-11} iea_0(-Q_W/N)$ using RCC calculation.

	$\langle 5p_{3/2}\|D\|np_{1/2}\rangle_{DF}\times$ $\langle np_{1/2}\|H^{NSI}_{PNC}\|6s\rangle_{DF}$	$\langle 5d_{3/2}\|H^{NSI}_{PNC}\|np_{3/2}\rangle_{DF}\times$ $\langle np_{3/2}\|D\|6s\rangle_{DF}$
$n=6$	1.860	-2.6$\times 10^{-6}$
$n=7$	0.045	-2.9$\times 10^{-8}$
$n=8$	0.013	-9.5$\times 10^{-8}$
$n=9$	0.075	8.1$\times 10^{-9}$
$n=10$	0.024	5.1$\times 10^{-9}$
$n=11$	0.002	1.1$\times 10^{-9}$

Table 5.20: Contributions to the $E1_{PNC}$ calculation from core-excitation operators in $\times 10^{-11} iea_0(-Q_W/N)$ using RCC calculation.

	$\langle 5d_{3/2}\|D\|np_{1/2}\rangle_{DF}\langle np_{1/2}\|T_1^{\dagger(1)}\|6s\rangle$	$\langle 5d_{3/2}\|T_1^{(1)}\|np_{3/2}\rangle\langle np_{3/2}\|D\|6s\rangle_{DF}$
$n=4$	-0.0005	-0.00003
$n=5$	0.4188	0.0004

Table 5.21: Contributions to the $E1_{PNC}$ calculation from leading DF and pair-correlation diagrams in $\times 10^{-11} iea_0(-Q_W/N)$ using RCC calculation.

	$\langle 5d_{3/2}\|D\|np_{1/2}\rangle_{DF}\langle np_{1/2}\|S_{1i}^{(1)}\|6s\rangle$	$\langle 5d_{3/2}\|S_{1f}^{\dagger(1)}\|np_{3/2}\rangle\langle np_{3/2}\|D\|6s\rangle_{DF}$
$n=6$	2.407	-0.181
$n=7$	0.066	-0.003
$n=8$	0.019	-0.001
$n=9$	0.111	0.008
$n=10$	0.032	4×10^{-4}
$n=11$	0.003	2×10^{-5}

Table 5.22: Contributions to the E1$_{PNC}$ calculation from pair-correlation from Coulomb and PNC interactions in $\times 10^{-11} iea_0(-Q_W/N)$ using RCC calculation.

	$\langle 5d_{3/2}\|S_{1f}^{\dagger(1)}\|mp_{3/2}\rangle\times$ $\langle mp_{3/2}\|D\|ns\rangle_{DF}\times$ $\langle ns\|S_{1i}^{(0)}\|6s\rangle$		$\langle 5d_{3/2}\|S_{1f}^{\dagger(0)}\|kd_{3/2}\rangle\times$ $\langle kd_{3/2}\|D\|lp_{1/2}\rangle_{DF}\times$ $\langle lp_{1/2}\|S_{1i}^{(1)}\|6s\rangle$
$n=7$, $m=6$	0.007	$l=6$, $k=6$	0.175
$n=7$, $m=7$	-0.005	$l=7$, $k=6$	-0.089
$n=8$, $m=6$	0.001	$l=6$, $k=7$	0.024
$n=8$, $m=7$	0.002	$l=7$, $k=7$	0.349
$n=7$, $m=8$	-0.0002	$l=8$, $k=6$	-0.0004
$n=8$, $m=8$	-0.002	$l=8$, $k=7$	-0.041

Table 5.23: Contributions to the E1$_{PNC}$ calculation due to core-polarization effects from $p_{1/2}$ orbitals in $\times 10^{-11} iea_0(-Q_W/N)$ using RCC calculation.

	$\langle 5d_{3/2}mp_{1/2}\|S_{2i}^{(1)}\|ns6s\rangle$ $\times\langle mp_{1/2}\|D\|ns\rangle_{DF}$	$\langle 5d_{3/2}mp_{1/2}\|S_{2f}^{\dagger(1)}\|ns6s\rangle$ $\times\langle mp_{1/2}\|D\|ns\rangle_{DF}$
$n=4$, $m=6$	-5×10^{-5}	1.6×10^{-5}
$n=5$, $m=6$	-0.0006	0.0003
$n=4$, $m=7$	-8×10^{-6}	3×10^{-6}
$n=5$, $m=7$	-0.0002	7×10^{-5}
$n=5$, $m=8$	-0.0001	4×10^{-5}
$n=7$, $m=5$	-0.0001	4×10^{-5}
$n=8$, $m=5$	-4×10^{-6}	2×10^{-5}

Table 5.24: Contributions to the $\mathrm{E1}_{PNC}$ calculation due to core-polarization effects from $\mathrm{p}_{3/2}$ orbitals in $\times 10^{-11} iea_0(-Q_W/N)$ using RCC calculation.

	$\langle 5d_{3/2}mp_{3/2}\|S_{2i}^{(1)}\|ns6s\rangle$ $\times\langle mp_{3/2}\|D\|ns\rangle_{DF}$	$\langle 5d_{3/2}mp_{3/2}\|S_{2f}^{\dagger(1)}\|ns6s\rangle$ $\times\langle mp_{3/2}\|D\|ns\rangle_{DF}$
$n=5,\ m=6$	-9×10^{-5}	6×10^{-5}
$n=5,\ m=7$	0.0001	4×10^{-5}
$n=7,\ m=5$	-0.005	0.0005
$n=8,\ m=5$	-0.002	0.0001
$n=9,\ m=5$	-0.012	0.0009
$n=10,\ m=5$	-0.003	0.0001

Table 5.25: Contributions to the $\mathrm{E1}_{PNC}$ calculation due to core-polarization effects from higher symmetry orbitals in $\times 10^{-11} iea_0(-Q_W/N)$ using RCC calculation.

	$\langle 5d_{3/2}\phi_2\|S_{2i}^{(1)}\|\phi_1 6s\rangle$ $\times\langle\phi_2\|D\|\phi_1\rangle_{DF}$	$\langle 5d_{3/2}\phi_2\|S_{2f}^{\dagger(1)}\|\phi_1 6s\rangle$ $\times\langle\phi_2\|D\|\phi_1\rangle_{DF}$
$\|\phi_1=4p_{3/2}\rangle,\ \|\phi_2=6d_{3/2}\rangle$	-2×10^{-7}	-0.0002
$\|\phi_1=5p_{3/2}\rangle,\ \|\phi_2=6d_{3/2}\rangle$	-0.0011	-0.0005
$\|\phi_1=5p_{3/2}\rangle,\ \|\phi_2=7d_{3/2}\rangle$	-0.0004	-0.0002
$\|\phi_1=4d_{3/2}\rangle,\ \|\phi_2=6p_{3/2}\rangle$	-3×10^{-6}	-2×10^{-6}
$\|\phi_1=4d_{3/2}\rangle,\ \|\phi_2=7p_{3/2}\rangle$	-1×10^{-6}	-6×10^{-7}
$\|\phi_1=4d_{3/2}\rangle,\ \|\phi_2=4f_{5/2}\rangle$	-3×10^{-5}	-5×10^{-5}
$\|\phi_1=4d_{5/2}\rangle,\ \|\phi_2=4f_{5/2}\rangle$	-3×10^{-6}	-2×10^{-6}
$\|\phi_1=4d_{5/2}\rangle,\ \|\phi_2=4f_{7/2}\rangle$	-5×10^{-5}	-0.0001

5.6 Preliminary studies on the Breit interaction

Table 5.26: Difference between the CCSD(T) results with and without the Breit interaction for the ionization potential (cm^{-1}), E1 transition amplitudes (a.u.) and magnetic dipole hyperfine structure constant (MHz) for different low-lying states of Ba^+.

Atomic state	$6s\ ^2S_{1/2}$	$6p\ ^2P_{1/2}$	$6p\ ^2P_{3/2}$	$5d\ ^2D_{3/2}$
Ionization potential	18.82	-14.89	-32.59	24.46
Initial state	$6s\ ^2S_{1/2}$	$6s\ ^2S_{1/2}$	$5d\ ^2D_{3/2}$	$5d\ ^2D_{3/2}$
→Final state	$6p\ ^2P_{1/2}$	$6p\ ^2P_{3/2}$	$6p\ ^2P_{1/2}$	$6p\ ^2P_{3/2}$
E1 transition amplitude	0.001	-0.003	0.0006	-0.0002
Atomic state	$6s\ ^2S_{1/2}$	$6p\ ^2P_{1/2}$	$6p\ ^2P_{3/2}$	$5d\ ^2D_{3/2}$
Hyperfine constant (A)	6.05	-2.42	-0.12	0.97

We have carried out preliminary studies on the contributions from the Breit interaction to different properties for a few low-lying states that are important in determining the $E1_{PNC}$ amplitude of the $6s\ ^2S_{1/2} \rightarrow 5d\ ^2D_{3/2}$ transition in Ba^+. This contribution is less than 0.1% at the DF level, but we find that it is a little higher in the case of the RCC calculations. In table 5.26, we present the difference between the calculated results with and without the Breit interaction at the CCSD(T) level. The contribution to the $E1_{PNC}$ result is -0.003 $\times 10^{-11} ie a_0(-Q_W/N)$. Since this is the first study of the Breit interaction in Ba^+, our work should be regarded as preliminary. Therefore, we consider this contribution as an error in our calculation which has been carried out in the Dirac-Coulomb approximation.

5.7 Summary

The result of $E1_{PNC}$ for the $6s\ ^2S_{1/2} \rightarrow 5d\ ^2D_{3/2}$ transition from our calculation is $2.462 \times 10^{-11} iea_0(-Q_W/N)$. In table 5.27, we compare it with other calculations. Our result is larger in magnitude than those obtained by Dzuba *et al* [17] and Geetha [40]. The former work is based on a variant of all order many-body perturbation theory, but it has some semi-empirical features. It is carried out by using two different approaches: one of them is similar to the sum-over-states approach and the other is known as the mixed approach, where the PNC interaction explicitly mixes states of opposite parities. However, both calculations do not include contributions from certain correlation effects; i.e. structural radiation, weak correlation potential and normalization of states [17], that are included in our calculation. Their $6p\ ^2P_{1/2} \rightarrow 5d\ ^2D_{3/2}$ E1 matrix element which is important for the above mentioned PNC transition amplitude, is not as accurate as ours. Furthermore, the accuracies of their PNC matrix elements are not known, as they have not performed calculations of the hyperfine constants of the relevant states. The reason for the discrepancy between our calculation and Geetha's is that our approach implicitly includes several intermediate states; particularly doubly excited opposite parity states which her sum-over-states approach omits.

Table 5.27: Comparison of $E1_{PNC}$ results from different calculations in $\times 10^{-11} iea_0(-Q_W/N)$.

Dzuba *et al* (*mixed parity*)	[17] (*sum-over-states*)	Geetha [40]	Present work
2.17	2.34	2.35	$2.462 \pm 0.018 \pm 0.003$

The contribution from the Breit interaction, which is two orders of magnitude weaker than the Coulomb interaction, is found (-0.003 $\times 10^{-11} iea_0(-Q_W/N)$) to be around 0.1%. This can be considered as an error in our calculation at the Dirac-Coulomb level.

The error accrued in our calculation of $E1_{PNC}$ can be determined from the errors in the excitation energies, E1 transition amplitudes and hyperfine constants. We have not estimated the errors in the calculated values of these quantities by comparing with measurements, since the error bars in the E1 transition amplitudes are rather large. Instead, we have taken the differences of our RCC calculations to single, double and leading triple excitations (CCSD(T)) and also just to single and double excitations (CCSD), as the errors. We have shown the variation between different results for the important contributing intermediate states using these two methods in table 5.28. The quadrature formula used for estimating error is given below. By expressing $E1_{PNC}$ as

$$X = \frac{AB}{C}, \tag{5.1}$$

the error can be evaluated using the relationship

$$\Delta X = \sqrt{\frac{B^2}{C^2}\Delta A^2 + \frac{A^2}{C^2}\Delta B^2 + \frac{A^2B^2}{C^4}\Delta C^2}, \tag{5.2}$$

where the Δ values are the results of the differences between CCSD(T) and CCSD for the quantities given in table 5.28.

The error in $E1_{PNC}$ (0.018) has been obtained by adding the errors for the different quantities it depends on in quadrature given in the above formula, for the leading intermediate states $6p\ ^2P_{1/2}$ and $6p\ ^2P_{3/2}$ and using a scale factor to estimate the errors for the other intermediate states.

In conclusion, we have performed a sub-one percent error calculation of $E1_{PNC}$ for the $6s\ ^2S_{1/2} \rightarrow 5d\ ^2D_{3/2}$ transition in Ba^+ using the RCC method. We have included single, double as well as the leading triple excitations and highlighted the importance of various many-body effects. Given the promise that the Ba^+ PNC experiment holds, it does indeed appear that in future the result of that experiment combined with our calculation would constitute a new and an important probe of physics beyond the SM.

	$6s\ ^2S_{1/2} \rightarrow 6p\ ^2P_{1/2}$		$5d\ ^2D_{3/2} \rightarrow 6p\ ^2P_{3/2}$	
Excitation energy	CCSD(T)	CCSD(T) - CCSD	CCSD(T)	CCSD(T) - CCSD
	20410	-19.89	16795	12.45
	$6s\ ^2S_{1/2} \rightarrow 6p\ ^2P_{3/2}$		$5d\ ^2D_{3/2} \rightarrow 6p\ ^2P_{1/2}$	
E1 transition amplitude	CCSD(T)	CCSD(T) - CCSD	CCSD(T)	CCSD(T) - CCSD
	4.72	-0.004	3.08	-0.01
	$\sqrt{A_{6s\ ^2S_{1/2}} A_{6p\ ^2P_{1/2}}}$		$\sqrt{A_{6p\ ^2P_{3/2}} A_{5d\ ^2D_{3/2}}}$	
Hyperfine constant (A)	CCSD(T)	CCSD(T) - CCSD	CCSD(T)	CCSD(T) - CCSD
	1738.1	10.26	156.1	1.28

Table 5.28: Excitation energy (cm^{-1}), E1 transition amplitudes (a.u.) and magnetic dipole hyperfine structure constant (MHz) for different low-lying states of Ba^+.

Bibliography

[1] W. Marciano and J. L. Rosner, Phys. Rev. Lett. **65**, 2963 (1990)

[2] J. S. M. Ginges and V. V. Flambaum, Phys. Rep. **637**, 63 (2004)

[3] I. B. Khriplovich, *Parity Non-conservation in Atomic Phenomena*, Gordon and Breach Publication, Philadelphia (1991)

[4] N. Fortson, Phys. Rev. Lett. **70**, 2383 (1993)

[5] G. Breit, Phys. Rev. **34**, 553 (1929); **36**, 383 (1830); Phys. Rev. **39**, 616 (1932)

[6] U. Kaldor, *Microscopic Quantum Many-body Theories and their Applications*, Edited by J. Navarro and A. Polls, 71 (1998)

[7] Geetha Gopakumar, Holger Merlitz, Sonjoy Majumder, Rajat Chaudhuri, B.P. Das, U. S. Mahapatra and D. Mukherjee, Phys. Rev. A **64**, 032502 (2001)

[8] Geetha Gopakumar, Holger Merlitz, Rajat K. Chaudhuri, B. P. Das, Uttam Sinha Mahapatra and Debashis Mukherjee, Phys. Rev. A **66**, 032505 (2002)

[9] B.K. Sahoo, G. Gopakumar, R. K. Chaudhuri, B.P.Das, H. Merlitz, U.S. Mahapatra and D. Mukherjee, Phys. Rev. A **68**, 040501(R) (2003)

[10] B.K. Sahoo, R. K. Chaudhuri, B.P.Das, H. Merlitz and D. Mukherjee, Phys. Rev. A **72**, issue 3 (2005)

[11] E. Clementi, J. Chem. Phys. **40**, 1944 (1964)

[12] M. Weissmann and V. V. Tolmachev, Phys. Rev. A **3**, 1291 (1971)

[13] C. E. Moore, *Atomic Energy Levels, Natl. Bur. Standard*, Ref. Data Ser., Natl. Bur Stand. (U.S.) Circ. No. 35 (U.S. GPO, Washington, D. C., 1971)

[14] H Karlsson and U Litzén, Phys Scr **60**, 321 (1999)

[15] C. Guet and W. R. Johnson, Phys. Rev. A **44**, 1531 (1991)

[16] Ephrahim Eliav, Uzi Kaldor and Yasuyuki Ishikawa, Phys. Rev. A **53**, 3050 (1996)

[17] V. A. Dzuba, V. V. Flambaum and J. S. M. Ginges, Phys. Rev. A **63**, 062101 (2001)

[18] A. Kastberg, P. Villemoes, A. Arnesen, F. Heijkenskjöld, A. Langereis, P. Jungner and S. Linnaeus, J. Opt. Soc. Am. B **10**, 1330 (1993)

[19] J. Reader, C. H. Corliss, W. L. Wiese and G. A. Martin, *Wavelengths and Transitions Probabilities for Atoms and Atomic Ions*, Natl. Bur. Stand. (U.S.) Circ. No. 68, Vol. X, U.S. GPO, Washington, D.C. (1980)

[20] A. Gallagher, Phys. Rev. **157**, 24 (1967)

[21] I. Lindgren and J. Morrison, *Atomic Many-body Theory*, Springer, Berlin (1985)

[22] P. Raghavan, Atomic Data and Nuclear Data Tables **42**, 189 (1989)

[23] R. Blatt and G. Werth, Z. Phys. A **299**, 311 (1981)

[24] W. Becker, W. Fisher and H. Hühnermann, Z. Phys. **216**, 142 (1968)

[25] M. Van Hove, G. Borghs, P. De Bisschop and R. E. Silverans, Z. Phys. A **321**, 215 (1985)

[26] F. M. Kelly and E. Tomchuk, Can. J. Phys. **45**, 3931 (1967)

[27] R. E. Silverans, G. Borghs, G. Dumont and J.-M. Van den Cruyce, Z. Phys. **295**, 311 (1980)

[28] H. J. Andrä, *Beam foil spectroscopy* **2**, 835 New York Plenum Press (1976)

[29] A. C. G. Mitchel and M. W. Zemansky, *Resonance radiation and excited atoms*, 2nd Edn. Cambridge, Cambridge University Press (1961)

[30] J. Huenneken and A. Gallagher, Phys. Rev. A **27**, 1851 (1983)

[31] Roger E. Silverans, Gustaaf Borghs, Peter De Bisschop and Marleen Van Hove, Phys. Rev. A **33**, 2117 (1986)

[32] A. H. Arroe, Phys. Rev. **79**, 836 (1950)

[33] N. Comaniciu, V. Draganescu, N. Ionescu-Pallas and V. Tatu, Compt. Rend. Acad. Sci. Paris, Ser. B, **262**, 915 (1966)

[34] I.-J. Ma and G. Zu Putlitz, Z. Physik A **277**, 107 (1976)

[35] F. Von Sichart, H. J. Stöckmann, H. Ackermann and G. Zu Putlitz, Z. Physik **236**, 97 (1970)

[36] Petrine Villemoes, Arne Arnesen, Filip Heijkenskjöld and Anders Wan̈strom̈,J. Phys. B **26**, 4289 (1993)

[37] K. Wendt, S. A. Ahmad, F. Buchinger, A. C. Mueller, R. Neugart and E. W. Otten, Z. Phys. A **318**, 125 (1984)

[38] H. Winter and M. Galliard, J. Phys. B **10**, 2739 (1977)

[39] S. Ahmad, J. Andriessen, K. Raghunathan and T. P. Das, Phys. Rev. A **25**, 2923 (1982)

[40] K.P. Geetha, Ph.D. Thesis, Bangalore Univ.,India (2002)

[41] N. Yu, W. Nagourney and D. Dehmelt, Phys. Rev. Lett. **78**, 4898 (1997)

[42] W. Nagourney, J. Dandberg and H. Dehmelt, Phys. Rev. Lett. **56**, 2797 (1986)

[43] F. Plumelle, M. Desaintfuscien, J. L. Duchene and C. Audoin, Opt. Commun. **34**, 71 (1980)

[44] A. A. Madej and J. D. Sankey, Phys. Rev. A **41**, 2621 (1990)

[45] V. A. Dzuba, V. V. Flambaum and J. S. M. Ginges, Phys. Rev. D **66**, 076013 (2002)

[46] E. P. Venugopal, *MS thesis (unpublished)* , Utah State University (1990)

Chapter 6

Parity Non-conservation in Cesium and Electric Dipole Moment Arising from a Scalar-Pseudoscalar Interaction

6.1 Introduction

In this chapter, we present the results of preliminary calculation of parity non-conserving electric dipole ($E1_{PNC}$) amplitude for the $6s\,^2S_{1/2} \rightarrow 7s\,^2S_{1/2}$ transition in cesium by the relativistic coupled-cluster (RCC) approach developed in this thesis. This quantity as mentioned earlier has been calculated by a number of different methods [1, 2, 3]. Its current accuracy is about 0.5% [3]. It is indeed worthwhile to explore whether this accuracy can be improved.

We have also applied RCC theory and combined it with experiment to determine the scalar-pseudoscalar (S-PS) electric dipole moment (EDM) coupling constants for cesium (Cs) and thallium (Tl). The S-PS EDM Hamiltonian has a mathematical structure similar to that of nuclear spin independent (NSI) parity non-conserving Hamiltonian, although the physics underlying the two phenomena are very different. EDMs arise from violations of P and

T symmetries and can provide important information about physics beyond the Standard Model (SM) [10] of particle physics. Until 1964 it was thought that the combined operation of charge conjugation and parity (CP) was a good symmetry, but then Christenson *et al.* observed its violation in the decay of the K_0 [11]. From the CPT theorem, it is well known that the three discrete symmetries - charge conjugation (C), space inversion or parity (P) and time-reversal (T) are related [12, 13]. According to this theorem any physical system which is described by a local field theory can violate any one of these symmetries independently, but remains invariant under the combined operation of these three symmetries in any order. Therefore, CP violation for the K_0 decay implies T violation. However, this is not a direct evidence of T violation. Observation of an EDM in a non-degenerate physical system would be a direct signature of the violations T as well as P symmetries [16]. There are two main sources of an EDM in paramagnetic atoms. They are the electron EDM and the S-PS interaction between the electron and the nucleus which violates P as well as T symmetries. While the former has been dealt with extensively [14], the latter has received relatively little attention. Barr has shown that in two Higgs doublet models [15], the contribution of the S-PS interaction to an atomic EDM can exceed that due to the EDM of an electron for certain values of the model parameters.

6.2 Cs PNC

It is well known that the most accurate experimental and theoretical results for PNC studies currently available are for Cs [3, 4]. Our RCC approach to atomic PNC is novel and it is capable of including all intermediate states in the calculation of the first order perturbed wavefunctions, unlike earlier calculations by Blundell *et al.* [1]. We have carried out $E1_{PNC}$ amplitude for the $6s\ ^2S_{1/2} \rightarrow 7s\ ^2S_{1/2}$ transition in Cs and we present the result in this section. We have used a common single particle basis to calculate this transition amplitude and S-PS EDM in Cs. The details of the basis are given later while presenting the EDM results in Cs.

In table 6.1, we present the calculated results of properties which are important in evaluating the accuracy of the PNC amplitude. These results have

Table 6.1: Excitation energy (cm^{-1}), E1 elements (a.u.) and magnetic dipole hyperfine structure constant (MHz) intermediate states in cesium.

Initial state $\rightarrow$ Final state	$6s_{1/2} \rightarrow 6p_{1/2}$	$6s_{1/2} \rightarrow 7p_{1/2}$	$6p_{1/2} \rightarrow 7s_{1/2}$	$7p_{1/2} \rightarrow 7s_{1/2}$
Excitation energy	11229.38	21796.31	7307.71	3259.23
Experiment	11177.84[a,b]	21765.30[a,b]	7356.79[a,b]	3226.28[a,b]
E1 transition amplitude	4.53	0.292	4.23	10.37
Experiment	4.52(1)[c]	0.284(2)[c]	-	-
Atomic state	$6s_{1/2}$	$7s_{1/2}$	$6p_{1/2}$	$7p_{1/2}$
Hyperfine constant(A)	2292.32	545.53	284.86	94.67
Experiment	2298.16[d]	545.90(4)[e]	291.90(9)[d]	94.35(4)[d]

Reference (a): [5].
Reference (b): [6].
Reference (c): [7].
Reference (d): [8].

an accuracy of 1-2%, but can be improved further using a part numerical and part analytical basis [9]. It therefore appears that a sub 1% accuracy for Cs PNC is possible.

In table 6.2, we present the contributions of the RCC terms to the above PNC amplitude. We obtain a total of 0.902 $\times 10^{-11} iea_0(-Q_W/N)$ for our calculation. The trend in the contributions from different RCC terms differs significantly from that of the $6s\ ^2S_{1/2} \rightarrow 5d\ ^2D_{3/2}$ transition in Ba^+ presented in the previous chapter. In contrast to the case of Ba^+, the maximum contribution for Cs comes from the final PNC perturbed state, $7s\ ^2S_{1/2}$. Again, $S_1^{(0)\dagger} D S_1^{(1)}$ and $S_1^{(1)\dagger} D S_1^{(0)}$ contribute significantly to the total result.

Table 6.2: Contributions to the $E1_{PNC}$ calculation in units of $10^{-11} iea_0(-Q_W/N)$ times those obtained using the RCC calculation.

Initial pert. terms	$6s\ ^2S_{1/2}^{(1)} \rightarrow 7s\ ^2S_{1/2}^{(0)}$	Final pert. terms	$6s\ ^2S_{1/2}^{(0)} \rightarrow 7s\ ^2S_{1/2}^{(1)}$
DH_{PNC}^{NSI}	0.297	H_{PNC}^{NSI} D	-1.026
$DT_1^{(1)}$	0.039	$T^{(1)\dagger} D$	-0.037
$\overline{D^{(0)}} S_{1i}^{(1)}$	0.234	$S_{1f}^{(1)\dagger} \overline{D^{(0)}}$	-1.855
$\overline{D^{(0)}} S_{2i}^{(1)}$	0.029	$S_{2f}^{(1)\dagger} \overline{D^{(0)}}$	-0.00004
$S_{1f}^{(0)\dagger} \overline{D^{(0)}} S_{1i}^{(1)}$	0.240	$S_{1f}^{(1)\dagger} \overline{D^{(0)}} S_{1i}^{(0)}$	0.429
$S_{1f}^{(0)\dagger} \overline{D^{(0)}} S_{2i}^{(1)}$	-0.005	$S_{1f}^{(1)\dagger} \overline{D^{(0)}} S_{2i}^{(0)}$	-0.007
$S_{2f}^{(0)\dagger} \overline{D^{(0)}} S_{1i}^{(1)}$	0.034	$S_{2f}^{(1)\dagger} \overline{D^{(0)}} S_{1i}^{(0)}$	-0.004
$S_{2f}^{(0)\dagger} \overline{D^{(0)}} S_{2i}^{(1)}$	-0.011	$S_{2f}^{(1)\dagger} \overline{D^{(0)}} S_{2i}^{(0)}$	-0.001
Norm.	-0.012		0.032
Total	0.566		-1.468

We present the zeroth and first order many-body perturbation theory (MBPT) contributions in table 6.3. The corresponding diagrams for these

terms are given in figure 5.13 of the previous chapter. The importance of correlation effects are clear from the table below, particularly those arising from $DS_1^{(1)}$ and $S_1^{(0)\dagger}DS_1^{(1)}$ as well as their conjugates.

Table 6.3: Contributions to the $E1_{PNC}$ calculation in units of $10^{-11}iea_0(-Q_W/N)$, using MBPT diagrams given in figure 5.13.

Initial pert. terms	$6s\ ^2S_{1/2}^{(1)} \rightarrow 7s\ ^2S_{1/2}^{(0)}$	Final pert. terms	$6s\ ^2S_{1/2}^{(0)} \rightarrow 7s\ ^2S_{1/2}^{(1)}$
diag. (2)	-0.297	diag. (1)	1.026
diag. (3)	-0.032	diag. (5)	0.0
diag. (4)	0.005	diag. (6)	0.095
diag. (9)	$\sim$0.0	diag. (7)	0.0
diag. (10)	-0.001	diag. (8)	0.101
diag. (13)	$\sim$0.0	diag. (11)	$\sim$0.0
diag. (14)	0.001	diag. (12)	-0.001
diag. (18)	-0.006	diag. (15)	$\sim$0.0
diag. (19)	-0.004	diag. (16)	-0.001
diag. (22)	0.0	diag. (24)	$\sim$0.0
diag. (23)	-0.033	diag. (25)	$\sim$0.0
diag. (26)	$\sim$0.0	diag. (28)	$\sim$0.0
diag. (27)	0.001	diag. (29)	0.001
diag. (17)	-0.007	diag. (30)	-0.008
diag. (31)	$\sim$0.0	diag. (32)	$\sim$0.0
Total	0.817		

6.3 General Features of EDM

In general, there are various sources of atomic EDMs. They can arise from

(i) an intrinsic EDM of an electron,
(ii) an intrinsic EDM of a nucleon or T and P violating nucleon-nucleon interactions
and
(iii) T and P violating electron-nucleon interactions.

Systems with degenerate states with opposite parity can have non-zero permanent EDMs, but this is not due to T and/or P violation. Closed-shell (diamagnetic) atoms which have a non-zero nuclear spin are sensitive to CP violation in the nuclear sector and the T and P violating tensor-pseudotensor electron-nucleus interaction; while single valence electron (paramagnetic) atoms are sensitive to the electron EDM and the T and P violating S-PS electron-nucleus interaction.

Let us consider an atomic system with non-zero spin that has a permanent EDM, $\vec{D}_a$. This can be either parallel or anti-parallel to $\vec{J}$, the total angular momentum of the system [16]. Under the actions of P and T, we have

$$\Rightarrow \quad P: \quad \vec{J} \rightarrow \vec{J}, \ \vec{D}_a \rightarrow -\vec{D}_a; \tag{6.1}$$

$$\Rightarrow \quad T: \quad \vec{J} \rightarrow -\vec{J}, \ \vec{D}_a \rightarrow \vec{D}_a. \tag{6.2}$$

The above equations imply that since $\vec{D}_a$ is proportional to $\vec{J}$, T invariance gives $\vec{D}_a = 0$. Similarly, P invariance also gives $\vec{D}_a = 0$. Therefore, one concludes that P and T must be violated independently for the existence of a non-zero EDM.

Sandars first showed that an atom can have a non-zero EDM if the electron has an intrinsic EDM [17]. He performed calculations to demonstrate that Tl and Cs EDMs are two orders of magnitude larger than the EDM of the electron. A few experiments that have been carried out on these two systems [18, 19, 20]. New experiments based on laser cooling and trapping of Cs have been proposed [21, 22, 23]. Accurate atomic calculations are needed in combination with experiments to extract a variety of T violating coupling constants. A number of relativistic many-body calculations on atoms of experimental interest have been carried out in the last two decades [21, 22, 18, 19], these are discussed later. But these calculations are based on certain approximations and do not deal extensively with the electron correla-

tion effects. Our present method treats electron correlation effects rigorously and can be applied to study the T and P violating S-PS electron-nucleus interaction.

6.3.1 S-PS interaction Hamiltonian

The S-PS interaction Hamiltonian, which violates T and P, can be constructed by considering the scalar current from the nucleus and pseudoscalar current from the electron, as follows:

$$H_{EDM}^{S-PS} = \frac{iG_F}{\sqrt{2}} \int d^3r_e \int d^3r_N \sum_{i=p,n} 2[C_{si}\bar{\psi}_N\psi_N \cdot \bar{\psi}_e\gamma_\mu\gamma_5\psi_e]\delta(r_i - r_e). \quad (6.3)$$

Expanding in $\bar{\psi}$'s we obtain:

$$H_{EDM}^{S-PS} = \frac{iG_F}{2\sqrt{2}} \int d^3r_e \int d^3r_N \sum_{i=p,n} 2[C_{si}\psi_N^\dagger\gamma_0\psi_N \cdot \psi_e^\dagger\gamma_0\gamma_\mu\gamma_5\psi_e]\delta(r_i - r_e). \quad (6.4)$$

Neglecting the off-diagonal terms from the above summation over the summing index 'μ' whose contributions would be very small, this reduces to

$$H_{EDM}^{S-PS} = \frac{iG_F}{2\sqrt{2}} \int d^3r_e\psi_e^\dagger\gamma_5\psi_e \int d^3r_N \sum_{i=p,n} 2C_{si}\psi_i^\dagger\psi_i]\delta(r_i - r_e). \quad (6.5)$$

The summation over the nuclear wavefunctions yield the number densities of protons and neutrons, which, in simple nuclear models are proportional to the nuclear density which is given by

$$\begin{aligned} \sum_p \psi_p^\dagger\psi_p &= Z\rho_N(r) \\ \sum_n \psi_n^\dagger\psi_n &= N\rho_N(r) \end{aligned} \quad (6.6)$$

where Z and N denote the number of protons and neutrons, respectively, and $\rho_N(r)$ is the nucleon number density normalized so that

$$\int dr\ \rho_N 4\pi r^2 = 1. \quad (6.7)$$

In individual terms, this yields

$$H_{EDM}^{S-PS} = \frac{iG_F}{2\sqrt{2}} \int d^3r_e \psi_e^\dagger \gamma_5 \psi_e \int d^3r_N 2 \quad [\quad C_{sp}\psi_p^\dagger \psi_p]\delta(r_p - r_e) + \quad C_{sn}\psi_n^\dagger \psi_n]\delta(r_n - r_e)] \quad (6.8)$$

which over the nuclear region gives

$$\begin{aligned} H_{EDM}^{S-PS} &= \frac{iG_F}{\sqrt{2}} \int d^3r_e \psi_e^\dagger \gamma_5 \psi_e [C_{sp}Z + C_{sn}N]\rho_N(r) \\ &= \frac{iG_F}{\sqrt{2}} C_S A \gamma_5 \rho_N(r) \end{aligned} \quad (6.9)$$

where C_{sp} and C_{sn} are the proton-electron and neutron-electron S-PS coupling constants and C_S is the dimensionless S-PS constant defined by $C_S = [C_{sp}Z + C_{sn}N]/A$ and 'A' is atomic mass number of the system.

6.4 Single particle representation

Using Wigner Eckart theorem [25], the single-particle matrix element of the CP violating interaction Hamiltonian can be expressed as

$$\begin{aligned} \langle \phi_i | H_{EDM}^{S-PS} | \phi_j \rangle = iC_S A \int (P_i \chi_{\kappa_i,m_i}^\dagger - iQ_i \chi_{-\kappa_i,m_i}^\dagger) \begin{pmatrix} 0 & -I \\ -I & 0 \end{pmatrix} \\ \begin{pmatrix} P_j(r) & \chi_{\kappa_j,m_j} \\ iQ_j(r) & \chi_{-\kappa_j,m_j} \end{pmatrix} \rho_N(r) dr d\Omega \\ = (-1)^{(j_i - m_i)} \delta(\kappa_i, -\kappa_j)\delta(m_i, m_j) C_S A \int (P_i Q_j + Q_i P_j)\rho_N(r) dr, \end{aligned} \quad (6.10)$$

since

$$\int \chi_{\kappa_a,m_a}^\dagger \chi_{-\kappa_b,m_b} d\Omega = \delta(\kappa_a, -\kappa_b)\delta(m_a, m_b). \quad (6.11)$$

Hence, the reduced matrix element is given by

$$\begin{aligned} \langle \phi_i || H_{EDM}^{S-PS} || \phi_j \rangle &= \frac{G_F}{\sqrt{2}} C_S A \quad \frac{1}{\sqrt{2j_i + 1}} \delta(\kappa_i, -\kappa_j) \\ &\int_0^\infty (P_i(r)Q_j(r) + Q_i(r)P_j(r))\rho_N(r) dr. \end{aligned} \quad (6.12)$$

6.5 Method of calculation

H_{EDM}^{S-PS} is responsible for mixing states of opposite parities but with the same angular momentum. The strength of the interaction Hamiltonian is sufficiently weak for it to be considered as a first-order perturbation. Therefore, it is possible to write the atomic wavefunction as

$$|\Psi\rangle = |\Psi^{(0)}\rangle + G_F|\Psi^{(1)}\rangle. \tag{6.13}$$

We obtain $|\Psi^{(0)}\rangle$ using relativistic coupled-cluster theory (RCC) as explained in the chapter 3.

Using equation (6.20) the EDM of an atom in the ground state is given by

$$\begin{aligned} D_a(C_S) &= \frac{\langle\Psi_v|D|\Psi_v\rangle}{\langle\Psi_v|\Psi_v\rangle} \\ &= \frac{\langle\Psi_v^{(0)}|D|\Psi_v^{(1)}\rangle + \langle\Psi_v^{(1)}|D|\Psi_v^{(0)}\rangle}{\langle\Psi_v^{(0)}|\Psi_v^{(0)}\rangle} \end{aligned} \tag{6.14}$$

where terms non-linear in the perturbed wavefunctions are neglected and D is the electric dipole (E1) operator. Using the explicit expression for the first order perturbed wavefunction, we get

$$\begin{aligned} D_a(C_S) &= \frac{1}{\langle\Psi_v^{(0)}|\Psi_v^{(0)}\rangle}\{\sum_{I\neq v}\frac{\langle\Psi_v^{(0)}|D|\Psi_I^{(0)}\rangle\langle\Psi_I^{(0)}|H_{EDM}^{S-PS}|\Psi_v^{(0)}\rangle}{E_v - E_I} \\ &\quad + \sum_{I\neq v}\frac{\langle\Psi_v^{(0)}|H_{EDM}^{S-PS}|\Psi_I^{(0)}\rangle\langle\Psi_I^{(0)}|D|\Psi_v^{(0)}\rangle}{E_v - E_I}\} \end{aligned} \tag{6.15}$$

$$= \frac{2}{\langle\Psi_v^{(0)}|\Psi_v^{(0)}\rangle}\sum_{I\neq v}\frac{\langle\Psi_v^{(0)}|D|\Psi_I^{(0)}\rangle\langle\Psi_I^{(0)}|H_{EDM}^{S-PS}|\Psi_v^{(0)}\rangle}{(E_v - E_I)} \tag{6.16}$$

since both the operators are hermitian. In the above equation $|\Psi_I\rangle$ represents an intermediate state. We can express the above equation as

$$\Rightarrow D_a(C_S) = C_S X_{EDM}. \tag{6.17}$$

The accuracy of the calculation of D_a depends on the excitation energies of the different intermediate states, the matrix elements of H_{EDM}^{S-PS} and D.

Similar to the argument used for the PNC perturbed wavefunctions, we obtain the first order EDM perturbed wavefunction as the solution of the equation

$$(H^{(0)} - E^{(0)})|\Psi_v^{(1)}\rangle = (E^{(1)} - H_{EDM}^{S-PS})|\Psi_v^{(0)}\rangle \tag{6.18}$$

where $E^{(1)}$ vanishes for an odd parity first order perturbation. In this approach, $|\Psi_v^{(1)}\rangle$ implicitly contains all the intermediate states.

The perturbed cluster operators can be written as

$$\begin{aligned} T &= T^{(0)} + G_F T^{(1)}, \\ S_v &= S_v^{(0)} + G_F S_v^{(1)}, \end{aligned} \tag{6.19}$$

where $T^{(1)}$ and $S_v^{(1)}$ are the first order G_F corrections due to EDM weak interaction to the unperturbed cluster operators $T^{(0)}$ and $S_v^{(0)}$ which are discussed in chapter 3, respectively. The amplitudes of these operators are solved, keeping only linear terms in EDM perturbed amplitudes, by following equations

$$\begin{aligned} \langle \Phi_a^p | \overline{H_N^{(0)}} T^{(1)} + \overline{H_{EDM}^{S-PS}} | \Phi_0 \rangle &= 0, \\ \langle \Phi_{ab}^{pq} | \overline{H_N^{(0)}} T^{(1)} + \overline{H_{EDM}^{S-PS}} | \Phi_0 \rangle &= 0, \end{aligned} \tag{6.20}$$

and

$$\begin{aligned} \langle \Phi_v^p | \overline{H_N^{(0)}} S_v^{(1)} + (\overline{H_N^{(0)}} T^{(1)} + \overline{H_{EDM}^{S-PS}}) \{1 + S_v^{(0)}\} | \Phi_v \rangle = -\langle \Phi_v^p | S_v^{(1)} | \Phi_v \rangle IP, \\ \langle \Phi_{vb}^{pq} | \overline{H_N^{(0)}} S_v^{(1)} + (\overline{H_N^{(0)}} T^{(1)} + \overline{H_{EDM}^{S-PS}}) \{1 + S_v^{(0)}\} | \Phi_v \rangle = -\langle \Phi_{vb}^{pq} | S_v^{(1)} | \Phi_v \rangle IP. \end{aligned} \tag{6.21}$$

Where $H^{(0)}$ is the Dirac-Coulomb (DC) Hamiltonian and $\overline{H}$ is defined as $e^{-T^{(0)}} H e^{T^{(0)}}$ which is computed after determining $T^{(0)}$. IP is the ionization potential for the valence electron 'v' and the subscript N denotes the normal form of an operator. $|\Phi_v^p\rangle$ and $|\Phi_{vb}^{pq}\rangle$ are the single and double excited states, respectively, with respect to the $|\Phi_v\rangle$. Using equations (6.13), (6.15), (6.19)

and only keeping terms linear in G_F, the expression for D_a can be written as

$$\begin{aligned} D_a = G_F \quad & \frac{< \Phi_v | \{1 + S_v^{(1)^\dagger} + T^{(1)^\dagger} + S_v^{(0)^\dagger} \\ & T^{(1)^\dagger}\} e^{T^{(0)^\dagger}} D e^{T^{(0)}} \{1 + T^{(1)} + T^{(1)} S_v^{(0)} + S_v^{(1)}\} | \Phi_v >}{1 + N_v^{(0)}} \\ = G_F \quad & \frac{< \Phi_v | S_v^{(1)^\dagger} \overline{D^{(0)}} (1 + S_v^{(0)}) + (1 + S_v^{(0)^\dagger}) \overline{D^{(0)}} S_v^{(1)} + \\ & S_v^{(0)^\dagger} (T^{(1)^\dagger} \overline{D^{(0)}} + \overline{D^{(0)}} T^{(1)}) S_v^{(0)} + (T^{(1)^\dagger} \overline{D^{(0)}} + \overline{D^{(0)}} T^{(1)}) S_v^{(0)} | \Phi_v >}{1 + N_v^{(0)}}. \end{aligned} \tag{6.22}$$

In the above expression we define $\overline{D^{(0)}} = e^{T^{(0)^\dagger}} D e^{T^{(0)}}$ and $N_v^{(0)} = S_v^{(0)^\dagger} e^{T^{(0)^\dagger}} e^{T^{(0)}} S_v^{(0)}$ for the valence electron 'v' and each term is connected. This is evaluated using the procedure for calculating electric dipole transition amplitude as given in chapter 4.

6.6 Principle of Measurement

The EDM of an atom or any other neutral system is determined experimentally by applying an external static field to the atom and measuring energy shift that results from the interaction of the EDM with the electric field. Consider an atom which has a permanent EDM as well as a magnetic dipole moment. In the presence of a static electric field $\vec{E}$ and a magnetic field $\vec{B}$, the interaction Hamiltonian is given by

$$H_{int} = -\vec{D}.\vec{E} - \vec{\mu}.\vec{B} \tag{6.23}$$

where $\vec{D}$ and $\vec{\mu}$ are the electric and magnetic dipole moment operators, respectively.

The application of the external field leads to precession of the atom. The precession (Larmor) frequency is primarily due to the magnetic dipole moment, but there is also a small contribution from the EDM. The observable in an EDM experiment is the difference in the Larmor frequency corresponding to parallel and anti-parallel configurations of $\vec{E}$ and $\vec{B}$ - reversal of $\vec{E}$ relative

to $\vec{B}$. This change in frequency is

$$\Delta\omega_E = \frac{2D_a E}{\hbar} \tag{6.24}$$

$\Delta\omega_E = 10^{-6}$ Hz for $D_a \approx 10^{-25}$ e-cm and $E = 10$ KV/cm. This frequency shift corresponds to a magnetic field of 10^{-9} G for a diamagnetic atom and 10^{-12} G for a paramagnetic atom.

One of the most important systematic errors in the EDM experiment is the magnetic field that is produced by the motion of the atoms. This field to first order in $\frac{v}{c}$, in the moving frame of the atoms is given by:

$$\vec{B}_m = \frac{\vec{v}}{c} \times \vec{E}. \tag{6.25}$$

For $v = 300$ m/s and $E = 10$ KV/cm, the dynamic magnetic field $\vec{B}_m = 3 \times 10^{-5}$G. This magnetic field can give rise to a frequency shift which can mimic an EDM. In the Tl experiment, two beams propagating in opposite directions are used to minimise this effect [26]. EDM experiments using optically pumped atoms in a cell have a zero average velocity and are, therefore, not affected very much by the dynamic magnetic field [20]. Both the beam and the cell experiments have their advantages and disadvantages. While it is possible to apply large electric fields in the beam experiments, the coherence times are longer in the cell experiments. The dynamic magnetic fields often limit the sensitivity of the former, while leakage currents give rise to systematic errors in the later, which cannot be easily estimated.

6.7 Laser Cooling and Trapping Approach

EDM experiments based on laser cooled and trapped atoms in principle have the advantages of both the beam and cell experiments [23]. In these experiments, one can apply large electric fields and consider long the coherence times. The leakage current problem can be overcome using a suitable configuration for the laser trap. The systematic error due to the dynamic magnetic field is virtually non-existent because of the extremely low average velocity of the cold atoms.

The procedure of the atomic EDM measurements with cold diamagnetic atoms [24] is as follows: First, a fast atomic beam from a hot oven is slowed down by using the Zeeman-tuning method. After this pre-cooling stage, the atoms are trapped and cooled by a magneto-optical trap (MOT). A high density and large number of atoms is then loaded into the MOT within several seconds. Then the atomic beam and the magnetic field for the MOT is switched off, the detuning of the trapping laser is increased and its intensity reduced. This results in further cooling to the micro-Kelvin region by the polarization-gradient method. The next step is to perform optical pumping to polarize the nuclear spin by the application of a circularly polarized resonant light pulse after completely switching off the laser fields. Finally, a high power laser for a far blue-detuned dipole forced trap and a high static electric field for the EDM measurement are switched on. A probe laser beam will be used to measure the Larmor precession frequency. The loading and measurement procedure is repeated many times to reduce the statistical uncertainty.

Groups in the US have proposed EDM searches with laser cooled cesium atoms [21, 22].

6.8 Results and Discussions

We have taken the value of α_0 as 0.00525 and β as 2.73 for all the symmetries for both the systems. To obtain the Dirac-Fock (DF) wavefunction, we have considered $36s_{1/2}$, $34p_{1/2}$, $34p_{3/2}$, $32d_{3/2}$, $32d_{5/2}$, $30f_{5/2}$, $30f_{7/2}$, $20g_{7/2}$ and $20g_{9/2}$ GTOs in Cs and $38s_{1/2}$, $36p_{1/2}$, $36p_{3/2}$, $36d_{3/2}$, $36d_{5/2}$, $30f_{5/2}$, $30f_{7/2}$, $25g_{7/2}$ and $25g_{9/2}$ GTOs in Tl. All core (occupied) electrons are excited for both the systems.

We have presented in table 6.4 properties related to the EDM in the ground states of atomic Cs and in table 6.5 for Tl. The square root of the products of the relevant hyperfine matrix elements provide an estimate of accuracy of the EDM matrix elements. We have used nuclear $g_I = 0.7377208$ for Cs and $g_I = 3.27642922$ for Tl, respectively [28] for calculating hyperfine structure constants. The results of the various properties of Cs and Tl are

Table 6.4: Excitation energy (cm^{-1}), E1 elements (a.u.) and magnetic dipole hyperfine structure constant (MHz) of intermediate states in cesium.

Initial state → Final state	$6s_{1/2} \rightarrow 6p_{1/2}$		$6s_{1/2} \rightarrow 7p_{1/2}$
Excitation energy	11229.38		21796.31
Experiment	11177.84[a,b]		21765.30[a,b]
E1 transition amplitude	4.53		0.292
Experiment	4.52(1)[c]		0.284(2)[c]
Atomic state	$6s_{1/2}$	$6p_{1/2}$	$7p_{1/2}$
Hyperfine constant(A)	2292.32	284.86	94.67
Experiment	2298.16[d]	291.90(9)[d]	94.35(4)[d]

Reference (a): [5].
Reference (b): [6].
Reference (c): [7].
Reference (d): [8].

in most cases in very good agreement with the measured values.

We have calculated the ratio of D_a/C_S for Cs and Tl. The contributions from significant RCC terms are given in table 6.6. The leading contributions for both Cs and Tl come from $DS_{1v}^{(1)}$. These diagrams represent the DF, important pair correlations and a sub class of core-polarization effects. The DF contributions are -0.578 and 3.217 in the units given in the table for Cs and Tl, respectively. Two different types of core-polarization effects represented by the terms $DT_1^{(1)}$ and $DS_{2v}^{(1)}$ make very large contributions but with opposite signs in the case of Tl. This is primarily due to the strong Coulomb and S-PS interactions between the $6p_{1/2}$ valence and the $6s_{1/2}$ core electrons. However, these interactions are much weaker in the case of the $6s_{1/2}$ valence and core electrons for Cs. The corresponding core-polarization

Table 6.5: Excitation energy (cm^{-1}), E1 elements (a.u.) and magnetic dipole hyperfine structure constant (MHz) of intermediate states in thallium.

Initial state $\rightarrow$ Final state	$6p_{1/2} \rightarrow 7s_{1/2}$		$6p_{1/2} \rightarrow 8s_{1/2}$
Excitation energy	26038.62		10462.32
Experiment	26477.50[a]		10520.01[a]
E1 transition amplitude	1.84		0.57
Experiment	1.81(2)[b]		-
Atomic state	$6p_{1/2}$	$7s_{1/2}$	$8s_{1/2}$
Hyperfine constant(A)	21025.98	11992.11	4118.57
Experiment	21311[b]	12297[b]	
Reference (a):	[5].		
Reference (b):	[29, 30].		

contribution is, therefore, much smaller for Cs. It is interesting to note that the contributions of two other correlation effects represented by the terms $S_{1v}^{(0)\dagger} D S_{1v}^{(1)}$ and $S_{2v}^{(0)\dagger} D S_{1v}^{(1)}$ are non-negligible.

The results of previous calculations of D_a/C_S along with ours are presented in table 6.7. Bouchiat's calculation is based on an one electron potential and relativistic corrections are added to the wavefunctions. Venugopal's result is obtained using a hybrid method which combines certain important features of the MBPT and the multi-configuration Dirac-Fock (MCDF) method. Mårtensson-Pendrill and Lindroth have computed the Dirac-Fock and various types of core-polarization effects [31]. However, unlike our work they have not considered pair-correlation effects.

We have estimated the error in D_a/C_S by taking the difference of our RCC calculations with single, double and leading triple excitations and just

Table 6.6: Contributions from important RCC terms for D_a/C_S calculations of $6s\ ^2S_{1/2}$ and $6p\ ^2P_{1/2}$ states for cesium and thallium, respectively in $10^{-18}e-cm$.

Important terms	Cesium $6s\ ^2S^{(1)}_{1/2}$	Thallium $6p\ ^2P^{(1)}_{1/2}$
Contributions from DF		
$DH^{S-PS}_{EDM} + H^{S-PS}_{EDM}D$	-0.578	3.217
Contributions from RCC		
$DT^{(1)}_1 + T^{(1)^\dagger}D$	-0.035	3.056
$\overline{D^{(0)}}S^{(1)}_{1v} + S^{(1)\dagger}_{1v}\overline{D^{(0)}}$	-0.878	4.453
$\overline{D^{(0)}}S^{(1)}_{2v} + S^{(1)\dagger}_{2v}\overline{D^{(0)}}$	0.043	-3.835
$S^{(0)\dagger}_{1v}\overline{D^{(0)}}S^{(1)}_{1v} + S^{(1)\dagger}_{1v}\overline{D^{(0)}}S^{(0)}_{1v}$	0.015	-0.304
$S^{(0)\dagger}_{2v}\overline{D^{(0)}}S^{(1)}_{1v} + S^{(1)\dagger}_{1v}\overline{D^{(0)}}S^{(0)}_{2v}$	0.041	0.174
$S^{(0)\dagger}_{1v}\overline{D^{(0)}}S^{(1)}_{2v} + S^{(1)\dagger}_{2v}\overline{D^{(0)}}S^{(0)}_{1v}$	0.004	0.023
$S^{(0)\dagger}_{2v}\overline{D^{(0)}}S^{(1)}_{2v} + S^{(1)\dagger}_{2v}\overline{D^{(0)}}S^{(0)}_{2v}$	-0.008	-0.036
Norm.	0.019	-0.032
Total	-0.801	4.056

Table 6.7: Comparison of D_a/C_S results with others in $\times 10^{18} e-cm$.

	Cesium D_a/C_S	Thallium D_a/C_S
Mårtensson-Pendrill and Lindroth [31]	-0.72(1±0.03)	7±2
Bouchiat [32]	-0.689	-
Venugopal [33]	-0.805	-
Present	-0.801(±0.004)	4.056(±0.137)

single and double excitations. We consider measured values $D_a = (-1.8 \pm 8.5) \times 10^{-24}\ e-cm$ for Cs by Murthy *et al.* [18] and $D_a = (-4.036 \pm 4.329) \times 10^{-25}\ e-cm$ for Tl by Regan *et al.* [26] and obtained new limits for C_S as $(2.247 \pm 6.809 \pm 0.011) \times 10^{-6}$ and $(0.995 \pm 1.756 \pm 0.033) \times 10^{-7}$ for cesium and thallium, respectively. In these results the first uncertainty comes from the errors associated with the measurements and secondly from the calculations. Our new limit for Tl is a significant improvement over the previous limit $(2 \pm 7) \times 10^{-7}$ [31].

Bibliography

[1] S. A. Blundell, W. R. Johnson and J. Sapirstein, Phys. Rev. Lett. **65**, 1411 (1990)

[2] S. A. Blundell, J. Sapirstein and W. R. Johnson, Phys. Rev. D **45**, 1602 (1992)

[3] V. A. Dzuba, V. V. Flambaum and J. S. M. Ginges, Phys. Rev. D **66**, 076013 (2002)

[4] C. S. Wood, S. C. Bennet, D. Cho, B. P. Masterson, J. L. Roberts, C. E. Tanner and C. E. Wieman, Science **275**, 1759 (1997)

[5] C. E. Moore, *Atomic Energy Levels*, Natl. Bul. Stand. (U.S.) **35** (1971)

[6] K. -H. Weber and C. J. Sansonetti, Phys. Rev. A **35**, 4650 (1987)

[7] L. Shabanove, Yu. Monkayov and A. Khlyustalov, Opt. Spektrosk. **47**, 3 (1979); Opt. Spectrosc. (USSR) **47** 1 (1979)

[8] E. Arimondo, M. Inguscio and P. Violino, Rev. Mod. Phys. **49**, 31 (1977)

[9] S. Majumder, K.P. Geetha, H. Merlitz and B.P. Das, *J. Phys. B*, **34**, 2841 (2001)

[10] S. M. Barr, Int. J. Mod. Phys. A **8**, 209 (1993)

[11] J. H. Christenson, J. W. Cronin, V. L. Fitch and R. Turlay, Phys. Rev. Lett. **13**, 138 (1964)

[12] F. Halzen and A. D. Martin, *Quarks and Leptons: An Introductory Course in Modern Particle Physics*, John Willey & Sons., New York (1984)

[13] G. Lüders, Ann. Phys. **2**, 1 (1957)

[14] W. Berrether and M. Suzuki, Rev. Mod. Phys. **63**, 313 (1991)

[15] S. M. Barr, Phys. Rev. D **47**, 2025 (1993); Phys. Rev. Lett. **68**, 1822 (1992); Phys. Rev. D **45**, 4148 (1992)

[16] P. G. H. Sandars, J. Phys. B **1**, 511 (1968)

[17] P. G. H. Sandars, Phys. Lett. **14**, 194 (1965); **22**, 290 (1966)

[18] S. A. Murthy, D. Krause Jr., Z. L. Li and L. R. Hunter, Phys. Rev. Lett. **63** , 965 (1989)

[19] E. D. Commins, S. B. Ross, D. DeMille and B. C. Regan, Phys. Rev. A **50**, 2960 (1994)

[20] J. P. Jacobs, W. M. Klipstein, S. K. Lamoreux, B. R. Heckel and E. N. Fortson, Phys. Rev. A **52**, 3521 (1995)

[21] D. S. Weiss, F. Fang and J. B. Chen, BAPS/APR03, J1.008 (2003)

[22] D. Heinzen, *Private communication* (2005)

[23] M. Bijlsma, J. Verhaar and D. Heinzen, Phys. Rev. A **49**, R4285 (1994)

[24] Y. Takahashi, M. Fujimoto, T. Yabuzaki, A. D. Singh, M. K. Samal and B. P. Das, *Proceedings of CP violation and its origin*, edited by K. Hagiwava (KEK Report, Tsukuba, 1997)

[25] I. Lindgren and J. Morrison, *Atomic Many-Body Theory*, edited by G. Ecker, P. Lambropoulos, and H. Walther (Springer-Verlag, Berlin, 1985)

[26] B. C. Regan, E. D. Commins, C. J. Schmidt and D. DeMille, Phys. Rev. Lett. **88**, 071805 (2002)

[27] W. Fischler, S. Paban and S. Thomas, Phys. Lett. B **289**, 373 (1992)

[28] P. Raghavan, Atomic Data and Nuclear Data Tables **42**, 189 (1989)

[29] J. C. Hsieh and J. C. Baird, Phys. Rev. A **6**, 141 (1972)

[30] A. Gallagher and A. Lurio, Phys. Rev. **136**, A87 (1964)

[31] A.-M. Mårtensson-Pendrill and E. Lindroth, Eur. Phys. Lett. **15**, 155 (1991)

[32] C. Bouchiat, Phys. Letts. B **57**, 284 (1975)

[33] Eswara Prasad Venugopal, *MS thesis (unpublished)* , Utah State University (1990)

Chapter 7

Conclusion and Outlook

7.1 Conclusion

Parity non-conservation (PNC) in atoms arising from neutral weak currents has the potential to test the Standard Model (SM) of particle physics [1, 2]. Accurate theoretical calculation of parity non-conserving electric dipole ($E1_{PNC}$) amplitude and high precision measurements [2] are required for this purpose. The most accurate data on atomic PNC currently comes from the $6s\ ^2S_{1/2} \rightarrow 7s\ ^2S_{1/2}$ transition in cesium (Cs), where the claimed experimental [3] and theoretical [4] accuracies are 0.35% and 0.5%, respectively, and the deviation from the SM is about 1σ [4]. An experiment to observe parity non-conservation in trapped and laser cooled singly ionised barium ($^{137}Ba^+$) [5, 6, 7] has been proposed.

The most important achievement of this thesis is the successful completion of a sub one percent calculation of the $E1_{PNC}$ amplitude for $6s\ ^2S_{1/2} \rightarrow 5d\ ^2D_{3/2}$ in Ba^+ using the relativistic coupled-cluster (RCC) theory. This is important for the following two reasons:

(i) If the accuracy of this calculation can be matched by that of experiment, which seems very probable in the not-too-distant future, then PNC in Ba^+ would be a second independent atomic probe of physics beyond the Standard

Model (SM).

(ii) It is the first application of RCC theory to atomic PNC and therefore advances the field of relativistic many-body theory.

A significant feature of our work is that it is concerned with two different fundamental interactions (electromagnetic and weak) and their interplay. It would certainly be of interest to theorists in different areas of many-body physics. Furthermore, it would be of great interest to particle physicists as it addresses the issue of new physics beyond the Standard Model (SM). As mentioned, if our sub one percent calculation of Ba^+ PNC can be matched by the proposed experiment on this ion, then the combination of the two results would provide an independent test of the SM of the particle physics.

As mentioned in chapter 3, we apply the full fledged RCC theory which incorporates all the single, double and leading triple excitations to calculate atomic wavefunctions. Blundell *et al.* had earlier used the linearized approximation to this theory to calculate the $E1_{PNC}$ amplitude of the $6s\ ^2S_{1/2} \rightarrow 7s\ ^2S_{1/2}$ transition in Cs [8, 9]. As mentioned in chapter 4, our approach implicitly takes into account all the intermediate states in the PNC perturbed wavefunctions. Our present calculation of the $E1_{PNC}$ amplitude for the $6s\ ^2S_{1/2} \rightarrow 5d\ ^2D_{3/2}$ transition in Ba^+ is more accurate than the previous calculations by Dzuba *et al.* [4] and Geetha [10] since it includes larger range of physical effects.

Our method of evaluating the error in the calculation of the $E1_{PNC}$ amplitude is more rigorous than those used in the previous calculations [8, 9]. The difference between the calculations for different properties related to $E1_{PNC}$ based on the single, double and leading triple excitations and just the single and double excitations have been computed and added in quadrature to determine the error bars for $E1_{PNC}$. We have also carried out preliminary calculations of the Breit interaction and its contribution is taken as one of the errors (0.1%) in the Dirac-Coulomb approximation.

We have also carried out preliminary studies of the $E1_{PNC}$ amplitude for the $6s\ ^2S_{1/2} \rightarrow 7s\ ^2S_{1/2}$ transition in Cs as well as related properties. The errors in the various quantities are about 1-2%. As in the case of Ba^+ PNC,

non-linear clusters have been included in the calculation of Cs PNC and the first order perturbed wavefunction takes into account all the intermediate states in an implicit way.

We have calculated the ratios of the atomic electric dipole moment (D_a) to the scalar-pseudoscalar coupling constant (C_S) for cesium and thallium (Tl) using RCC theory with accuracies of 0.5% and 3.3%, respectively. Many-body effects were found to be of crucial importance, particularly for Tl. Our calculated value of this quantity for Tl in combination with the experimental result of the electric dipole moment (EDM) for the same atom gives the most accurate limit for the scalar-pseudoscalar (S-PS) coupling constant to date. It would be possible to improve this limit even further if the new generation of EDM experiments using cold cesium atoms reach their expected levels of accuracies [11, 12, 13, 14]. The results of these experiments could then be combined with our calculation of D_a/C_S for Cs (0.5% accuracy) to yield this new limit.

7.2 Outlook

Although the precision we have achieved in our $E1_{PNC}$ and EDM calculations are better than the existing results for these quantities, it may be necessary to improve them even further in order to test the SM of the particle physics. This is an extremely challenging task as it would require improving the quality of the single particle basis wavefunctions and the RCC theory used in this thesis. It would indeed be worthwhile to explore different methods for optimizing the basis wavefunctions. The simplest step in this direction would be to use a part numerical and part analytical basis [15]. Going beyond RCC with single, double and leading triple excitations calls for a reformulation of the computational techniques in calculating the cluster amplitudes. The work of Kallay which makes the solution of the coupled-cluster (CC) equations at any level of excitation more tractable than before deserves special mention [16]. It would be desirable to first apply this approach with full single, double and triple excitations to PNC in Ba^+ and Cs as well as EDM in Cs. A simpler solution to this problem would be to use the unitary coupled-cluster (UCC) method [17] which has certain advantages over the ordinary

CC method. The important thing is that at a given level of approximation UCC contains certain higher order excitations that are not present in CC. For example, at level of the singles and doubles, UCC has some important triple and even quadrupole excitations.

Beyond the Dirac-Coulomb approximation, it is necessary to include the Breit and important quantum electrodynamics (QED) corrections as accurately as possible. The accuracies of the nuclear structure corrections which contribute at the level of 0.2% in Cs PNC [18] and 0.3% in Ba^+ PNC [19] must be improved.

One can indeed expect exciting new theoretical developments in atomic parity non-conservation and electric dipole moments in the years to come.

Bibliography

[1] W. Marciano and J. L. Rosner, Phys. Rev. Lett. **65**, 2963 (1990)

[2] G. S. M. Ginges and V. V. Flambaum, Phys. Re. **637**, 63 (2004)

[3] C. S. Wood, S. C. Bennett, D. Cho, B. P. Masterson, J. L. Roberts, C. E. Tanner and C. E. Wieman, Science **275**, 1759 (1997)

[4] V. A. Dzuba, V. V. Flambaum and J. S. M. Ginges, Phys. Rev. D **66**, 076013 92002)

[5] N. Fortson, Phys. Rev. Lett. **70**, 2383 (1993)

[6] T. W. Koerber, M. H. Schacht, K. Hendrickson, W. Nagourney and E. N. Fortson, Phys. Rev. Lett. **88**, 143002 (2002)

[7] T. W. Koerber, M. H. Schacht, W. Nagourney and E. N. Fortson, Phys. Rev. Lett., J. Phys. B **36**, 637 (2003)

[8] S. A. Blundell, W. R. Johnson and J. Sapirstein, Phys. Rev. Lett. **65**, 1411 (1990)

[9] S. A. Blundell, J. Sapirstein and W. R. Johnson, Phys. Rev. D **45**, 1602 (1992)

[10] K. P. Geetha, Ph. D. Thesis, Bangalore University, India (2002)

[11] C. Chin, Véronique Leiber, V. Vuletić, A. J. Kerman and S. Chu, Phys. Rev. A **63**, 033401 (2001)

[12] D. S. Weiss, F. Fang and J. B. Chen, BAPS/APR03, J1.008 (2003)

[13] M. Bijlsma, B. J. Verhaar and D. J. Heinzen, Phys. Rev. A **49**, R4285 (1994)

[14] D. Heinzen, *Private communication* (2005)

[15] S. Majumder, K.P. Geetha, H. Merlitz and B.P. Das, *J. Phys. B*, **34**, 2841 (2001)

[16] Mihály Kállay and Péter R. Surján, J. Chem. Phys. **115**, 2945 (2001)

[17] C. Sur, R. K. Chaudhuri, B. P. Das, B. P. Das and D. Mukherjee, Submitted to Phys. Rev. Lett., arXiv:physics/0502033 (2005)

[18] P. K. Panda and B. P. Das, Phys. Rev. C **62**, 065501 (2000)

[19] P. K. Panda and B. P. Das, *private communication*, Submitted to Phys. Rev. C, arXiv:physics/0508187 (2005)

Appendix:A

JLV theorems

We present a series of theorems developed by Jucys, Lenson and Vanagas in 1962 which are known as JLV theorems. These theorems provides formulas to simplify complex angular factors represented by angular momentum diagrams in the many-electron matrix element calculations. The basic principle of this theorem is, " *if a complex angular momentum diagram can be divided into a closed part with any number of open lines then simpler angular factors can be found out using the following rules which are known as JLV theorems*".

Let us consider an angular momentum diagram such that it has a closed part represented by $\overline{\alpha}$ and an open part represented by β as shown by Fig. (i). Using the orthogonality relationships given by Fig.s (ii) and (iii), one could arrive the simpler form of angular momentum diagrams with one, two, three, four etc. open lines using the formulas given by Fig.s (iv), (v), (vi), (vii) etc., respectively.

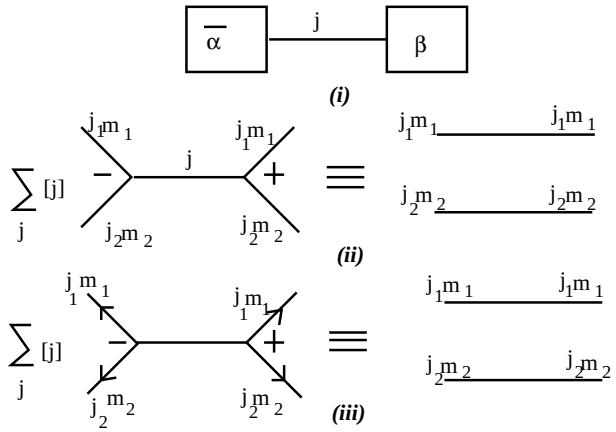

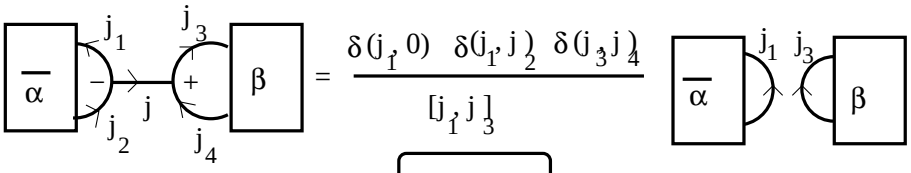

(iv)

JLV 1

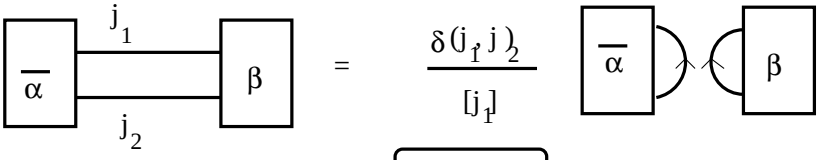

(v)

JLV 2

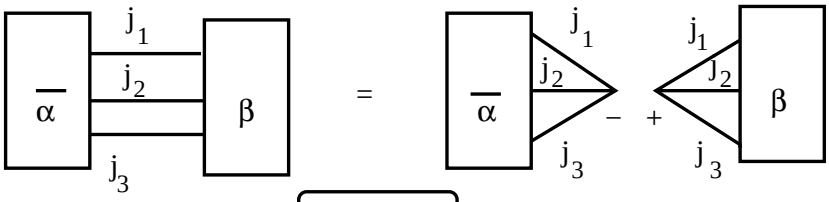

(vi)

JLV 3

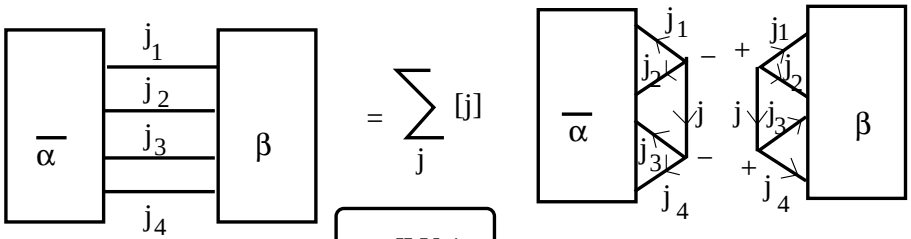

(vii)

JLV 4

where [j] = 2j+1

Appendix:B

Generalized Wick's Theorem

B.1 Normal order

A string of creation and annihilation operators are said to be in normal order if $a_a^\dagger$ *and* a_p *always appear to the right of* a_b *and* $a_q^\dagger$, where a, b and p, q represent for holes and particles, respectively.

The expectation value with respect to the Fermi vacuum of any operator string in normal order is zero, since

$$a_a^\dagger|\Phi\rangle = 0$$

and

$$a_p|\Phi\rangle = 0. \tag{B.1}$$

It is therefore possible to express an operator $\hat{O}$ as

$$\hat{O} = O_N + \langle\Phi|O|\Phi\rangle \tag{B.2}$$

where O_N represents normal order of the operator $\hat{O}$ which is sometime denoted by ordinary curly bracket (e.g. {O}) and $\langle\Phi|O|\Phi\rangle$ as the vacuum expectation value, where $|\Phi\rangle$ is the Dirac-Fock (DF) wavefunction.

B.2 Wick's theorem

Let A, B, C,$\cdots$ represent a string of creation and annihilation operators. As per the notation, a normal ordered operator made of A, B, C $\cdots$ can be written as $\{ABC\cdots\}$. Hence any normal order operator taken between the reference state denoted as $|\Phi\rangle$ is equal to zero. i.e.,

$$\langle\Phi|\{ABC\cdots\}|\Phi\rangle = 0. \tag{B.3}$$

We define the contraction of two creation/absorption operator as follows: if x and y are arbitrary creation and absorption operators, then the contraction of x and y is defined as the difference between the ordinary and the normal product of the operators. i.e.,

$$\widehat{xy} = xy - \{xy\}. \tag{B.4}$$

These creation and absorption operators obey the anti-commutation rules given by

$$\begin{aligned} \{a_i, a_j\} &= 0. \\ \{a_i^+, a_j^+\} &= 0. \\ \{a_i, a_j^+\} &= 0. \end{aligned}$$

Consider the four different cases where x and y being core or virtual orbitals.

Case I: x and y being core $(a_b a_a^+)$

$$\widehat{a_b a_a^+} = a_b a_a^+ - \{a_b a_a^+\}. \tag{B.5}$$

Using the normal order property, $\{a_b a_a^+\} = a_b a_a^+$. Therefore,

$$\widehat{a_b a_a^+} = 0. \tag{B.6}$$

Case II: x and y being core $(a_a^+ a_b)$

$$\widehat{a_a^+ a_b} = a_a^+ a_b - \{a_a^+ a_b\}. \tag{B.7}$$

Using the normal order property, $\{a_a^+ a_b\} = -a_b a_a^+$. Therefore,

$$\widehat{a_a^+ a_b} = \delta_{ab}. \tag{B.8}$$

Case III: x and y being virtual $(a_r a_s^+)$

$$\widehat{a_r a_s^+} = a_r a_s^+ - \{a_r a_s^+\}. \tag{B.9}$$

Using the normal order property, $\{a_r a_s^+\} = -a_s^+ a_r$. Therefore

$$\widehat{a_r a_s^+} = \delta_{rs} \tag{B.10}$$

Case IV: x and y being virtual $(a_s^+ a_r)$

$$\widehat{a_s^+ a_r} = a_s^+ a_r - \{a_s^+ a_r\} \tag{B.11}$$

Using the normal order property, $\{a_s^+ a_r\} = a_s^+ a_r$. Therefore,

$$\widehat{a_s^+ a_r} = 0. \tag{B.12}$$

From the above four cases we can infer that the contraction is non vanishing only for the combination $a_r a_s^+$ and $a_a^+ a_b$. This rule will be used in the construction of Goldstone diagrams for the further calculations. *Wick's theorem* can be formulated as follows:

If A is a product of creation and absorption operators, then

$$A = \{A\} + \{\widehat{A}\} \tag{B.13}$$

where $\{A\}$ represents the normal form of A and $\{\widehat{A}\}$ represents the sum of the normal-ordered terms obtained by making all possible single, double, $\cdots$ contractions within A.

B.3 Generalized Wick's theorem

The above theorem can be generalized for products of normal ordered operators and this leads to the *generalized Wicks's theorem* given by

$$\begin{aligned}
\{ABC\}\{DE\}\{FGH\}... &= \{ABCDEFGH\} \\
&+ \sum_{singlecontractions} \overbrace{\{\overbrace{ABC}\}\{\overbrace{DE}\}}\{FGH\} \\
&+ \sum_{doublecontractions} \overbrace{\{\overbrace{ABC}\}\{\overbrace{DE}\}\{FGH\}}+... \\
&+ \sum_{fullycontracted} \{ABC\}\{DE\}\{FGH\}
\end{aligned} \tag{B.14}$$

The graphical interpretation of Wick's theorem goes like this. If A and B are two operators in normal form represented by Goldstone diagrams, then the

graphical representation of the operator product AB is the sum of diagrams obtained by joining zero, one, two,... lines at the bottom of the diagram A with lines at the top of the diagram of B in all possible ways so that the direction of the arrows is continuous.

Let us introduce the concept of an object. An arbitrary operator containing the same number of creation and annihilation operators standing inside a normal product is called an object.

Let A and B be two different objects. By generalized Wick's theorem we can write

$$AB = \{AB\} + \{\widehat{AB}\} \tag{B.15}$$

$$BA = \{BA\} + \{\widehat{BA}\} \tag{B.16}$$

Since A and B are composed of an even number of creation and annihilation operators, we have

$$\{AB\} = \{BA\} \tag{B.17}$$

Therefore,

$$AB - BA = [A, B] = \{\widehat{AB}\} - \{\widehat{BA}\} \tag{B.18}$$

Thus any commutation of two objects contains only contracted terms. This simple result can be interpreted also in the diagrammatic formalism. In terms of a diagrammatic interpretation, the commutation $[A, B]$ is equal to the sum of all possible non-equivalent connected diagrams that are composed of A and B vertices with at least, one hole or particle internal line (contraction), the closed elementary loops are strictly forbidden.

B.4 Brillouin's theorem

If 'a' represents an occupied orbital of an atomic system and a discrepancy causes a small admixtures of virtual orbitals 'r' to this occupied orbital, i.e.

$$|a\rangle \rightarrow |a\rangle + \eta|r\rangle \tag{B.19}$$

where η is very small and a real number, then the multi-electron Dirac-Fock statefunction with occupied electrons ($|\Phi\rangle$) will lead to an admixture of single substations $|\Phi_a^r\rangle$

$$|\Phi\rangle \rightarrow |\Phi\rangle + |\Phi_a^r\rangle \tag{B.20}$$

and the Dirac-Fock energy shifts to the value

$$E_{DF} = \langle\Phi|H|\Phi\rangle \rightarrow \langle\Phi|H|\Phi\rangle + \eta(\langle\Phi_a^r|H|\Phi\rangle + \langle\Phi|H|\Phi_a^r\rangle) \tag{B.21}$$

neglecting higher order in η.

To minimize the effect in the shift of the energy, one obtains

$$\langle\Phi_a^r|H|\Phi\rangle = 0 \tag{B.22}$$

This is known as *Brillouin's theorem.*

Following this fact for the single particle (Dirac-)Fock Hamiltonian as given in chapter 2 satisfies the relationship

$$\langle\Phi_a^r|H_0|\Phi\rangle = \langle r|h_0|a\rangle = 0 \tag{B.23}$$

This condition is called as *Brillouin's condition.*

Appendix:C

The Goldstone Evaluation Rules

C.1 Goldstone Diagrams

To assign various factors to Goldstone diagrams we prescribe the following rules

(i) *A creation (absorption) operator for each free outgoing (incoming) orbital line. These are written in normal form*

$$\{a_i^\dagger a_j^\dagger a_k^\dagger \cdots a_{k'} a_{j'} a_{i'} \}$$

where $a_i^\dagger$, $a_{i'}$ *etc., originate from the same vertex or from vertices connected by orbital lines.*

(ii) *A matrix element for each interaction line.*

(iii) *A summation over all internal orbital lines.*

(iv) *A phase factor equal to* $(-1)^{h+l}$*, where 'h' is the number of internal lines representing core (hole) orbitals and 'l' the number of closed loops of orbital lines.*
(Closed loop of a diagram is calculated by considering a closed path which flows continuously from a starting point and returns back to it. This definition is followed from I. Lindgren, but sometime it changes by other authors. Effectively all the signs are accounted same by these rules and the definition is immaterial.

(v) *A factor 1/2 for each two-particle interaction and an equivalence factor equal to the number of topological equivalent diagrams.*

(vi) *A factor of 1/2 for each symmetry operation – like reflection in a vertical plane or interchange of the vertices of an interaction line – which transforms the diagram into itself or to any other diagram appearing in the expansion.*

C.2 The Linked-diagram Theorem

We define a diagram as *closed* if it has no free orbital lines and a digram is *unlinked* if it has a disconnected closed diagram. According to *linked-diagram theorem*:

"*Discard all the unlinked diagrams from the calculations*".

C.3 Angular Momentum Diagrams

We discuss here the rules to extract angular momentum diagrams from the corresponding Goldstone diagrams. The rules are:

(a) *Remove all single particle potential interaction lines.*

(b) *Replace each orbital line by the corresponding angular-momentum line and add an arrow on outgoing lines from each interaction.*

(c) *Replace each Coulomb and/or Breit interaction line by a directed angular momentum line with an appropriate rank 'k'.*

Appendix:D

Hausdorff Expansion

Let us consider $e^{-T}Ae^{T}$, where A is an object and T is the excitation operator. The Hausdorff Expansion formula for this expression is

$$e^{-T}Ae^{T} = \sum_{n=0}^{\infty} \frac{1}{n!}[A,T]^{(n)} \tag{D.1}$$

Proof:

Let us define

$$A'(\lambda) = e^{-\lambda T}Ae^{\lambda T} \tag{D.2}$$

Taking the first derivative of the above expression with λ, we get

$$\frac{d}{d\lambda}A'(\lambda) = e^{-\lambda T}[A,T]e^{\lambda T} \tag{D.3}$$

Taking the second derivative of it, we get

$$\frac{d^2}{d\lambda^2}A'(\lambda) = e^{-\lambda T}\left[[A,T],T\right]e^{\lambda T} \tag{D.4}$$

et cetera. Therefore,

$$A'(\lambda) = A'(0) + \lambda\frac{d}{d\lambda}A'(0) + \frac{1}{2!}\lambda^2\frac{d^2}{d\lambda^2}A'(0) + \cdots \tag{D.5}$$

which is nothing but

$$A'(\lambda) = A + \lambda[A,T] + \frac{1}{2!}\lambda^2[[A,T],T] + \cdots \tag{D.6}$$

For $\lambda = 1$,

$$\begin{aligned} e^{-T}Ae^{T} &= A + [A,T] + \frac{1}{2!}[[A,T],T] + \cdots \\ &= \sum_{n=0}^{\infty}\frac{1}{n!}[A,T]^{(n)} \end{aligned} \tag{D.7}$$

Hence proved.

List of Figures

List of Tables

Abbreviation and notations

C	Charge conjugation	P	Parity
T	Time-reversal	SCF	Self consistent field
V	Vector	A	Axial Vector
S	Scalar	PS	Pseudo scalar
PNC	Parity non-conservation	$E1_{PNC}$	E1 amplitude by PNC
LH	Left Handed	RH	Right Handed
SM	Standard Model	QED	Quantum Electrodynamics
GUT	Grant Unification Theory	SUSY	Super Symmetry
DC	Dirac-Coulomb	DCB	Dirac-Coulomb-Breit
HF	Hartree-Fock	C_S	S-PS coupling constant
DF	Dirac-Fock	DFB	Dirac-Fock-Breit
CI	Configuration Interaction	CC	Coupled-cluster
MCDF	Multiconfiguration DF	LCC	Linearised CC
MBPT	Many Body Perturbation Theory	RCC	Relativistic CC
NSI	Nuclear spin independent	NSD	Nuclear spin dependent
RMBPT	Relativistic MBPT	RCI	Relativistic CI
CCSD	CC with singles and doubles	LCCSD	Linearised CCSD
GTO	Gaussian Type Orbitals	EDM	Electric Dipole Moment
IP	Ionisation Potential	EE	Excitation Energy
p	Proton	n	Neutron
Q_W	Weak charge	Z	Atomic number
N	Nucleon number	$\sin^2\theta_W$	Weinberg mixing angle
GRASP	General Relativistic Atomic Structure Program	CCSD(T)	CCSD method with approximated triples
CPU	Central Processor Unit	MPI	Message Passing Interface
UCC	Unitary coupled-cluster	CCSD(T)	CCSD with partial triples

Fundamental Constants, Units and Conversions

Conversions:
1 electron mass $= 5.4857990 \times 10^{-4}$ a.u. $= 9.1093897 \times 10^{-31}$ Kg
$a_0 = \frac{\hbar^2}{m_e e^2} = 0.529177249 \times 10^{-8}cm= 0.50.529177249\mathring{A}$
1 fm $= 10^{-13}$cm$= 1.88973 \times 10^{-5}$ bohr
1 $a.u.$ of time $= \frac{\hbar}{E_h} = 2.4188843265 \times 10^{-17}$s
Compton wavelength $\lambda_e = 2.4263 \times 10^{-10}$cm
Electric field $E = \frac{e^2}{a_0} = 0.51422082 \times 10^{12}$ V/m
Magnetic field $B = \frac{E_h}{e a_0 \alpha c} = 2.350518 \times 10^5$ tesla $= 2.350518 \times 10^9$ Gauss

Energy:
1 cal $= 4.184$ J
1 Debye $= 0.393456$ a.u.
1 Hartree $(1a.u.) = \frac{e^2}{a_0} = 4.3597438110 \times 10^{-18}$ J $= 27.2113961$ eV $= 219474.63068$ cm^{-1} $= 627.50956$ kcal/mol
1 eV $= 3.67493260(14) \times 10^{-2} a.u. = 1.6022 \times 10^{-19}$ J
1 K $= 3.1668153(55) \times 10^{-6} a.u.$, (K $\rightarrow$ Kelvin)
1 $a.u.$ $= 6.579683920735(50) \times 10^{15}$ Hz $(= \nu)$
1 cm^{-1} $= 4.556335252750(35) \times 10^{-6} a.u. = 1.4387752$ K
1 Kaysers $= 1$ cm^{-1}

Constants:
1 Avogadro's no. $= 6.0221367 \times 10^{23}$
1 Rydberg $= 0.5 a.u.$

Transition rates: $S = 1/\tau$
$1eV/\hbar = 1.6022 \times 10^{-19}$ J$/\hbar = 1.5192 \times 10^{15}$ sec^{-1} $= 3.6748 \times 10^{-2} (a.u.)^{-1}$

Wavelength:
λ (A^0) $= a_0 \frac{2\pi c}{\Delta E(a.u.)} \times 10^8 = \frac{455.634}{\Delta E(a.u.)}$
λ (nm) $= a_0 \frac{45.5634}{\Delta E(a.u.)}$
λ (cm^{-1}) $= \frac{1}{a_0} \frac{1}{2\pi c} \Delta E(a.u.) = 219474.63068 \Delta E(a.u.)$, $\Delta E \rightarrow$ Excitation energy

Physical constants

Physical quantity	Symbol	Numerical value
speed of light in vacuum	c	299 792 458 m s^{-1}
Boltzman's constant	k_B	1.380 6503 $\times 10^{-23}$ J/K
Plank's constant	$\hbar$	1.054 57266 (63) $\times 10^{-34}$ J s
		6.582 122 0 (20) $\times 10^{-16}$ eV s
elementary charge	e	1.602 177 33 (49) $\times 10^{-19}$ C
electron mass	m_e	9.109 389 7 (54) $\times 10^{-31}$ kg
proton mass	M_p	1.672 623 1 (10) $\times 10^{-27}$ kg
atomic mass unit	u	1.660 540 2 (10) $\times 10^{-27}$ kg
classical electron radius	r_0	2.817 940 92 (38) $\times 10^{-15}$ m
Bohr radius	a_0	5.291 772 49 (24) $\times 10^{-11}$ m
inverse fine-structure constant	$1/\alpha$	137.035 989 5 (61)
Hartree energy	E_h	27.211 396 1 (81) eV
		8065.540 320 7 (81) Kaysers

Atomic units:	$\hbar = 1$	$m_e = 1, e = 1$
unit of length	$a_0 = \hbar^2/m_e e^2$	5.291 772 49 $\times 10^4$ fm
unit of time	$\hbar^3/m_e e^4$	2.418884 3 $\times 10^{-17}$ fm
unit of velocity	$e^2/\hbar = \alpha c$	2.187 691 4 $\times 10^6$ m s^{-1}
unit of energy	$e^2/a_0 = m_e e^4/\hbar^2$	27.211 396 1 eV
unit of electric charge	e	1.602 177 33 $\times 10^{-19}$ C
unit of electric potential	e/a_0	27.211 396 1 eV
unit of electric field	e/a_0^2	5.142 208 24 $\times 10^{-4}$ V/fm

List of Publications

1. **B. K. Sahoo**, S. Majumder, R. K. Chaudhuri, B. P. Das and D. Mukherjee, *Influence of correlation effects on the magnetic dipole hyperfine interaction in the low-lying states of* Ca^+, J. Phys. B.: At. Mol. Opt. Phys. **36**, 1899-1906 (2003)

2. **B. K. Sahoo**, G. Gopakumar, H. Merlitz, R. K. Chaudhuri, B. P. Das, U. S. Mahapatra and D. Mukherjee, *Magnetic dipole hyperfine interactions in* $^{137}Ba^+$ *and the accuracies of the neutral weak interaction matrix elements*, Rapid Communication PRA **68**, 040501(R) (2003)

3. R. K. Chaudhuri, **B. K. Sahoo**, B. P. Das, U. S. Mahapatra and D. Mukherjee, *Relativistic coupled cluster calculations of the energies for Rubidium and Cesium atoms*, J. Chem. Phys. **119**, 10633 (2003)

4. C. Sur, **B. K. Sahoo**, R. K. Chaudhuri, B. P. Das and D. Mukherjee, *Comparative studies of the magnetic dipole and electric quadrupole hyperfine constants for the ground and low lying excited states of* $^{25}Mg^+$, Eur. Phys. J. D **32**, 25 (2005)

5. **B. K. Sahoo**, S. Majumder, R. K. Chaudhuri, B. P. Das and D. Mukherjee, *Ab initio determination of the lifetime of the* $6^2P_{3/2}$ *state for* $^{207}Pb^+$ *by relativistic many-body theory*, J. Phys. B **37**, 3409 (2004)

6. B. P. Das, K. V. P. Latha, **B. K. Sahoo**, C. Sur, R. K. Chaudhuri and D. Mukherjee, *Relativistic and correlation effects in atoms*, J. Comp. Chemistry (Ed.) (2004)

7. **B. K. Sahoo**, R. K. Chaudhuri, B. P. Das, H. Merlitz and D. Mukherjee, *Application of Relativistic Coupled-cluster Theory to Heavy Atomic System with Strongly Interacting Configuration: Hyperfine Interactions in* $^{207}Pb^+$, Phys. Rev. A **72**, 032507 (2005)

8. C. Sur, R. K. Chaudhuri, **B. K. Sahoo**, B. P. Das and D. Mukherjee, *Relativistic unitary coupled-cluster theory and applications* (Submitted to PRL)

arXiv:physics/0502033 (2005)

9. **B. K. Sahoo**, R. K. Chaudhuri, B. P. Das and D. Mukherjee, *Relativistic Coupled-Cluster Theory of Atomic Parity Non-conservation: Application to* $^{137}Ba^{+}$ (Submitted to PRL) arXiv:physics/0509130 (2005)

10. **B. K. Sahoo**, R. K. Chaudhuri, B. P. Das, D. Mukherjee and E. P. Venugopal, *A New Limit for the Coupling Constant of the Parity and Time Reversal Violating Scalar-Pseudoscalar Interaction* (Submitted to PRL) arXiv:physics/0509070 (2005)

11. **B. K. Sahoo**, Thomas Beier, B. P. Das, R. K. Chaudhuri and Debashis Mukherjee, *Electron Correlation Effects in Hyperfine Interactions in* ^{45}Sc *and* ^{89}Y (Submitted to J. Phys. B) arXiv:physics/0506011 (2005)

12. **B. K. Sahoo**, S. Majumder, H. Merlitz, R. K. Chaudhuri, B. P. Das and D. Mukherjee, *Electric Dipole Transition Amplitudes for* $^{205}Pb^{+}$ (Submitted to J. Phys. B) (2005)